Lecture Notes in Electrical Engineering 989

Koushik Guha
Gorachand Dutta
Arindam Biswas
K. Srinivasa Rao *Editors*

MEMS and Microfluidics in Healthcare

Devices and Applications Perspectives

Springer

Lecture Notes in Electrical Engineering

Volume 989

Series Editors

Leopoldo Angrisani, Department of Electrical and Information Technologies Engineering, University of Napoli Federico II, Naples, Italy
Marco Arteaga, Departament de Control y Robótica, Universidad Nacional Autónoma de México, Coyoacán, Mexico
Bijaya Ketan Panigrahi, Electrical Engineering, Indian Institute of Technology Delhi, New Delhi, Delhi, India
Samarjit Chakraborty, Fakultät für Elektrotechnik und Informationstechnik, TU München, Munich, Germany
Jiming Chen, Zhejiang University, Hangzhou, Zhejiang, China
Shanben Chen, Materials Science and Engineering, Shanghai Jiao Tong University, Shanghai, China
Tan Kay Chen, Department of Electrical and Computer Engineering, National University of Singapore, Singapore, Singapore
Rüdiger Dillmann, Humanoids and Intelligent Systems Laboratory, Karlsruhe Institute for Technology, Karlsruhe, Germany
Haibin Duan, Beijing University of Aeronautics and Astronautics, Beijing, China
Gianluigi Ferrari, Università di Parma, Parma, Italy
Manuel Ferre, Centre for Automation and Robotics CAR (UPM-CSIC), Universidad Politécnica de Madrid, Madrid, Spain
Sandra Hirche, Department of Electrical Engineering and Information Science, Technische Universität München, Munich, Germany
Faryar Jabbari, Department of Mechanical and Aerospace Engineering, University of California, Irvine, CA, USA
Limin Jia, State Key Laboratory of Rail Traffic Control and Safety, Beijing Jiaotong University, Beijing, China
Janusz Kacprzyk, Systems Research Institute, Polish Academy of Sciences, Warsaw, Poland
Alaa Khamis, German University in Egypt El Tagamoa El Khames, New Cairo City, Egypt
Torsten Kroeger, Stanford University, Stanford, CA, USA
Yong Li, Hunan University, Changsha, Hunan, China
Qilian Liang, Department of Electrical Engineering, University of Texas at Arlington, Arlington, TX, USA
Ferran Martín, Departament d'Enginyeria Electrònica, Universitat Autònoma de Barcelona, Bellaterra, Barcelona, Spain
Tan Cher Ming, College of Engineering, Nanyang Technological University, Singapore, Singapore
Wolfgang Minker, Institute of Information Technology, University of Ulm, Ulm, Germany
Pradeep Misra, Department of Electrical Engineering, Wright State University, Dayton, OH, USA
Sebastian Möller, Quality and Usability Laboratory, TU Berlin, Berlin, Germany
Subhas Mukhopadhyay, School of Engineering and Advanced Technology, Massey University, Palmerston North, Manawatu-Wanganui, New Zealand
Cun-Zheng Ning, Electrical Engineering, Arizona State University, Tempe, AZ, USA
Toyoaki Nishida, Graduate School of Informatics, Kyoto University, Kyoto, Japan
Luca Oneto, Department of Informatics, BioEngineering, Robotics and Systems Engineering, University of Genova, Genova, Genova, Italy
Federica Pascucci, Dipartimento di Ingegneria, Università degli Studi "Roma Tre", Rome, Italy
Yong Qin, State Key Laboratory of Rail Traffic Control and Safety, Beijing Jiaotong University, Beijing, China
Gan Woon Seng, School of Electrical and Electronic Engineering, Nanyang Technological University, Singapore, Singapore
Joachim Speidel, Institute of Telecommunications, Universität Stuttgart, Stuttgart, Germany
Germano Veiga, Campus da FEUP, INESC Porto, Porto, Portugal
Haitao Wu, Academy of Opto-electronics, Chinese Academy of Sciences, Beijing, China
Walter Zamboni, DIEM—Università degli studi di Salerno, Fisciano, Salerno, Italy
Junjie James Zhang, Charlotte, NC, USA

The book series *Lecture Notes in Electrical Engineering* (LNEE) publishes the latest developments in Electrical Engineering—quickly, informally and in high quality. While original research reported in proceedings and monographs has traditionally formed the core of LNEE, we also encourage authors to submit books devoted to supporting student education and professional training in the various fields and applications areas of electrical engineering. The series cover classical and emerging topics concerning:

- Communication Engineering, Information Theory and Networks
- Electronics Engineering and Microelectronics
- Signal, Image and Speech Processing
- Wireless and Mobile Communication
- Circuits and Systems
- Energy Systems, Power Electronics and Electrical Machines
- Electro-optical Engineering
- Instrumentation Engineering
- Avionics Engineering
- Control Systems
- Internet-of-Things and Cybersecurity
- Biomedical Devices, MEMS and NEMS

For general information about this book series, comments or suggestions, please contact leontina.dicecco@springer.com.

To submit a proposal or request further information, please contact the Publishing Editor in your country:

China

Jasmine Dou, Editor (jasmine.dou@springer.com)

India, Japan, Rest of Asia

Swati Meherishi, Editorial Director (Swati.Meherishi@springer.com)

Southeast Asia, Australia, New Zealand

Ramesh Nath Premnath, Editor (ramesh.premnath@springernature.com)

USA, Canada

Michael Luby, Senior Editor (michael.luby@springer.com)

All other Countries

Leontina Di Cecco, Senior Editor (leontina.dicecco@springer.com)

**** This series is indexed by EI Compendex and Scopus databases. ****

Koushik Guha · Gorachand Dutta ·
Arindam Biswas · K. Srinivasa Rao
Editors

MEMS and Microfluidics in Healthcare

Devices and Applications Perspectives

Springer

Editors
Koushik Guha
Department of Electronics
and Communication Engineering
National Institute of Technology Silchar
Silchar, Assam, India

Arindam Biswas
School of Mines and Metallurgy
Kazi Nazrul University
Asansol, West Bengal, India

Gorachand Dutta
School of Medical Science and Technology
Indian Institute of Technology Kharagpur
Kharagpur, West Bengal, India

K. Srinivasa Rao
Department of Electronics
and Communication Engineering
KL University
Guntur, Andhra Pradesh, India

ISSN 1876-1100 ISSN 1876-1119 (electronic)
Lecture Notes in Electrical Engineering
ISBN 978-981-19-8713-7 ISBN 978-981-19-8714-4 (eBook)
https://doi.org/10.1007/978-981-19-8714-4

© The Editor(s) (if applicable) and The Author(s), under exclusive license to Springer Nature Singapore Pte Ltd. 2023
This work is subject to copyright. All rights are solely and exclusively licensed by the Publisher, whether the whole or part of the material is concerned, specifically the rights of translation, reprinting, reuse of illustrations, recitation, broadcasting, reproduction on microfilms or in any other physical way, and transmission or information storage and retrieval, electronic adaptation, computer software, or by similar or dissimilar methodology now known or hereafter developed.
The use of general descriptive names, registered names, trademarks, service marks, etc. in this publication does not imply, even in the absence of a specific statement, that such names are exempt from the relevant protective laws and regulations and therefore free for general use.
The publisher, the authors, and the editors are safe to assume that the advice and information in this book are believed to be true and accurate at the date of publication. Neither the publisher nor the authors or the editors give a warranty, expressed or implied, with respect to the material contained herein or for any errors or omissions that may have been made. The publisher remains neutral with regard to jurisdictional claims in published maps and institutional affiliations.

This Springer imprint is published by the registered company Springer Nature Singapore Pte Ltd.
The registered company address is: 152 Beach Road, #21-01/04 Gateway East, Singapore 189721, Singapore

Preface

The significance of medical MEMS is increasing exponentially from past two decades. There exist numerous MEMS diagnostic devices for detection of blood pressure, glucose, TB, Hepatitis, etc. This is possible due to the multi-disciplinary fields fusing together to make a potent solution for the existing problems. MEMS has proven to be capable of paving bridge between medicine and engineering field, which helps in developing medical instruments. The controllability of sample volume, response time, and size of these devices is satisfactory. The research on the biomaterials to realize such medical devices has a huge scope in future. Furthermore, the book is aimed to study different microfluidic devices. The microfluidics technology has vast number of medical applications ranging from μTAS, drug delivery, DNA sequencing, cancer and COVID-19 detection, and organ on chip. Presently, organ-on-chip technology is prevailing in the scientific community, it can be expected that within a decade there will be marketed microphysiological devices. Microfluidics is capable of regenerating any organ functional physiology and pathophysiology which can be useful in disease diagnosis and organ replacement as well. The present book focuses on the past developments and future research directions in MEMS and microfluidic medical device field, the research available currently on these instruments is intriguing. Though there were plenty of marketed devices, MEMS technology has not yet been explored to its potential. This book primarily focuses on the reader's enlightenment on MEMS medical devices by introducing all the diagnostic devices and treatment tools at one place. The book covers in-depth technical works and general introductions to the devices such that the book can reach technical and general audience as well. In addition, the fabrication techniques of bio-MEMS and bio-microfluidic devices will also be elaborated, which makes the book a complete guide from device development to fabrication stages.

Therefore, in this text, all the above mentioned are covered through chapters spanning from 1 to 12. The first chapter "N/MEMS Biosensors: An Introduction" covering Introduction to N/MEMS Biosensors and the second chapter "Lab-On-A-Chip Technology in Health Care" explains Lab-on-a-Chip Technology in Health Care. The third chapter "A Review on Recent Trends in the Segregation of Red Blood Cells Using Microfluidic Devices" presents recent trends in the segregation of red blood cells using microfluidic devices. The fourth chapter "A Road Map to Paper-Based Microfluidics Towards Affordable Disease Detection" deals with paper-based microfluidics and its journey toward affordable disease diagnosis and the fifth chapter "Critical Review and Exploration on Micro-pumps for Microfluidic Delivery" presents a critical review and exploration on micro-pumps for microfluidic delivery. The sixth chapter "Fabrication Techniques and Materials for Bio-MEMS" introduces fabrication techniques and materials for bio-MEMS. The seventh chapter "In-silico Analysis of Expandable Radiofrequency Electrode for Ablation of Hepatic Tumors" proposes an in-silico analysis of expandable radiofrequency electrode for ablation of hepatic tumors and the eighth chapter "Lab-On-Chip Electrochemical Biosensor for Rheumatoid Arthritis" describes a work on lab-on-chip electrochemical biosensor for rheumatoid arthritis. The ninth chapter "Transdermal Injection with Microneedle Devices in Healthcare Sector: Materials, Challenging Fabrication Methodologies, and its Limitations" indulges with transdermal injection with microneedle devices in healthcare sector: materials, challenging fabrication methodologies, and its limitations. The work on an economical and efficient method for the fabrication of spiral micromixer is presented in the tenth chapter "An Economical and Efficient Method for the Fabrication of Spiral Micromixer". The eleventh chapter "Damping Estimation and Analysis for High Performance Inertial MEMS for Early Detection of Neurological Disorders During Pregnancy" is all about damping estimation and analysis for high-performance inertial MEMS for early detection of neurological disorders during pregnancy. Finally, the last chapter "Affinity Biosensing: Modeling of Adsorption Kinetics and Fluctuation Dynamics" presents the concept of affinity biosensing: modeling of adsorption kinetics and fluctuation dynamics.

Silchar, India — Dr. Koushik Guha
Kharagpur, India — Gorachand Dutta
Asansol, India — Arindam Biswas
Guntur, India — K. Srinivasa Rao

Contents

Editors and Contributors

About the Editors

Koushik Guha is awarded Distinguished Faculty Award 2021 by NIT Silchar for his outstanding performance in teaching and research. Recently, he has been awarded IETE R S Khandpur award 2022 for his achievements and outstanding contribution at national and international level in the field of ‘Medical Instrumentation’ covering education, research, design, development, and production. Dr. Guha is also awarded Institute of Smart Structures and Systems Young Scientist award (ISSS, IISc Bangalore) 2021 for his contribution in MEMS/NEMS sensors and actuators. He is Optimistic Researcher and Associate Professor in the Department of Electronics and Communication Engineering, National Institute of Technology Silchar, India. He is now Associate Dean of Academic Affairs and Former Assoc. Dean of Students Welfare in NIT Silchar. Dr. Guha is awarded five international patents and one national patent. He has been nominated Fellow of Institution of Electronics and Telecommunication Engineers (IETE) and Institute of Scholars (InSc) Government of India. He has been Active and Regular Reviewer of (SCI/SCIE journals) and various IEEE hosted/sponsored conferences.

Gorachand Dutta Ph.D., is Assistant Professor with the School of Medical Science and Technology, Indian Institute of Technology Kharagpur. He received his Ph.D. in Biosensor and Electrochemistry from Pusan National University, South Korea, Postdoctoral fellowships in the Department of Mechanical Engineering, Michigan State University, USA, and Department of Electronic and Electrical Engineering at University of Bath, UK. He has expertise on electrochemical biosensors.

Arindam Biswas received M.Tech. degree in Radio Physics and Electronics from University of Calcutta, India, in 2010 and Ph.D. from NIT Durgapur in 2013. He has worked as Postdoctoral Researcher at Pusan National University, South Korea. Dr. Biswas has received DST-JSPS Invitation Fellow at RIE, Japan, DST-ASEAN Invitation Fellow at Duy Tan University, Vietnam and Taylors University, Malaysia, and Visiting Fellow to Department of Electrical and Computer Engineering, National University Singapore. He has worked as Specially Appointed Associate Professor (Visiting) at Research Institute of Electronics, Shizouka University, Japan. He has been selected for IE (I) Young Engineer Award: 2019–2020; KNU Best Researcher Award (Engineering and Technology): 2021; and KNU Best Faculty Award-2022 (Faculty of Science and Technology). Presently, Dr. Biswas is working as Associate Professor in School of Mines and Metallurgy at Kazi Nazrul University, West Bengal, India, where he has been actively engaged in teaching, research, and administration. He has 53 technical papers in different journals and 55 conference proceedings and 8 authored books, 18 edited volumes, and 10 chapters with international repute. Dr. Biswas has produced six Ph.D. students till date. His research interest is in carrier transport in low-dimensional system and electronic device, nonlinear optical communication, THz semiconductor source, IoT, and optimization.

K. Srinivasa Rao was born in Andhra Pradesh, India. He received Master's and Ph.D. degree from Central University. He is presently working as Professor and Head of Microelectronics Research Group, Department of Electronics and Communication Engineering in Koneru Lakshmaiah Education Foundation (Deemed to be University), Guntur, Andhra Pradesh, India. His current research areas are MEMS-based Reconfigurable Antenna's actuators, Bio-MEMS, RF MEMS Switches, RF MEMS Filters, MOSFET, FinFETs, etc. He received Young Scientist Award from Department of Science and Technology, Government of India, in 2011. He also received UGC Major Research Project in 2012. He received early career research Award from SERB, Government of India, in 2016. Presently, he is working on MEMS project worth of 40 Lakhs funded by SERB, Government of India. He has published more than 140+ international research publications and presented more than 55 conference technical papers around the world. He is Member of IETE, ISTE, and IEEE.

Contributors

Valanukonda Bhavya Bhargavi Department of Electronics and Communication Engineering, Velagapudi Ramakrishna Siddhartha Engineering College, Kanuru, Vijayawada, Andhra Pradesh, India

Moushumi Biswas Silchar Medical College and Hospital, Silchar, India

Sonali Biswas Jorhat Engineering College, Assam Science and Technology University, Jorhat, India

Ashish. B. Deoghare Department of Mechanical Engineering, National Institute of Technology Silchar, Assam, India

Nanda Sai Donepudi Siddhartha Government College and Hospital, Vijayawada, India

Gorachand Dutta NanoBiosensors and Biodevices Lab, School of Medical Sciences and Technology, Indian Institute of Technology, Kharagpur, West Bengal, India

Nirmita Dutta NanoBiosensors and Biodevices Lab, School of Medical Sciences and Technology, Indian Institute of Technology, Kharagpur, West Bengal, India

Sudhanshu Dwivedi S.S. Jain Subodh P.G. (Autonomous) College, Jaipur, India

Anup Kumar Gogoi Indian Institute of Technology Guwahati, Amingaon, Guwahati, India

A. Gowthami Materials and MEMS Laboratory, Department of Electronics and Communication Engineering, Sri Sivasubramaniya Nadar College of Engineering, Chennai, Tamilnadu, India

Koushik Guha Department of Electronics and Communication Engineering, National Institute of Technology Silchar, Assam, India

Olga Jakšić Center of Microelectronic Technologies, Institute of Chemistry, Technology and Metallurgy, National Institute of the Republic of Serbia, University of Belgrade, Beograd, Serbia

C. Joshitha Department of Electronics and Communiction Engineering, Koneru Lakshmaiah Education Foundation, Hyderabad, Telangana, India

Neha Mishra Indian Institute of Technology, Bombay, India

Mareedu Nagavalli Department of Electronics and Communication Engineering, Velagapudi Ramakrishna Siddhartha Engineering College, Kanuru, Vijayawada, Andhra Pradesh, India

Naga Nikhila Nandam Department of Electronics and Communication Engineering, Velagapudi Ramakrishna Siddhartha Engineering College, Kanuru, Vijayawada, Andhra Pradesh, India

Vinayak Pachkawade VPACHKAWADE Research Center, Nagpur, India

Sukumar Pati Department of Mechanical Engineering, National Institute of Technology Silchar, Silchar, Assam, India

Promod Kumar Patowari Department of Mechanical Engineering, National Institute of Technology Silchar, Silchar, Assam, India

J. Prithvi Department of Electronics and Communication Engineering, Sri Sivasubramaniya Nadar College of Engineering, Chennai, Tamil Nadu, India

S. Radha Materials and MEMS Laboratory, Department of Electronics and Communication Engineering, Sri Sivasubramaniya Nadar College of Engineering, Chennai, Tamilnadu, India

Rahul Kumar Ram NanoBiosensors and Biodevices Lab, School of Medical Sciences and Technology, Indian Institute of Technology, Kharagpur, West Bengal, India

Vuyyuru Dinesh Kumar Reddy Department of Electronics and Communication Engineering, Velagapudi Ramakrishna Siddhartha Engineering College, Kanuru, Vijayawada, Andhra Pradesh, India

Shaik Sadikbasha Department of Mechanical Engineering, National Institute of Technology Silchar, Assam, India

Pallab Sarmah Department of Mechanical Engineering, National Institute of Technology Silchar, Silchar, Assam, India

Jasti Sateesh Department of Electronics and Communication Engineering, Velagapudi Ramakrishna Siddhartha Engineering College, Kanuru, Vijayawada, Andhra Pradesh, India

Tatineni Sharmila Swaroopa Department of Electronics and Communication Engineering, Velagapudi Ramakrishna Siddhartha Engineering College, Kanuru, Vijayawada, Andhra Pradesh, India

Jai Shukla NanoBiosensors and Biodevices Lab, School of Medical Sciences and Technology, Indian Institute of Technology, Kharagpur, West Bengal, India

B. S. Sreeja Department of Electronics and Communication Engineering, Sri Sivasubramaniya Nadar College of Engineering, Chennai, Tamil Nadu, India;
Materials and MEMS Laboratory, Department of Electronics and Communication Engineering, Sri Sivasubramaniya Nadar College of Engineering, Chennai, Tamilnadu, India

Pannangi Sri Vidya Gayathri Department of Electronics and Communication Engineering, Velagapudi Ramakrishna Siddhartha Engineering College, Kanuru, Vijayawada, Andhra Pradesh, India

Shahed Baba Syed Department of Electronics and Communication Engineering, Velagapudi Ramakrishna Siddhartha Engineering College, Kanuru, Vijayawada, Andhra Pradesh, India

Ekta Tripathi Department of Mechanical Engineering, National Institute of Technology Silchar, Silchar, Assam, India

Subhash Turaka Department of Electronics and Communication Engineering, Velagapudi Ramakrishna Siddhartha Engineering College, Kanuru, Vijayawada, Andhra Pradesh, India

Dhanya Yalamanchili Siddhartha Government College and Hospital, Vijayawada, India

N/MEMS Biosensors: An Introduction

Vinayak Pachkawade

Abstract In the twenty-first century, biosensors have gathered much wider attention than ever before, irrespective of the technology that promises to bring them forward. With the recent COVID-19 outbreak, the concern and efforts to restore global health and well-being are rising at an unprecedented rate. A requirement to develop precise, fast, point-of-care, reliable, easily disposable/reproducible and low-cost diagnostic tools has ascended. Biosensors form a primary element of hand-held medical kits, tools, products, and/or instruments. They have a very wide range of applications such as nearby environmental checks, detecting the onset of a disease, food quality, drug discovery, medicine dose control, and many more. This chapter explains how Nano/Micro-Electro-Mechanical Systems (N/MEMS) can be enabling technology toward a sustainable, scalable, ultra-miniaturized, easy-to-use, energy-efficient, and integrated bio/chemical sensing system. This study provides a deeper insight into the fundamentals, recent advances, and potential end applications of N/MEMS sensors and integrated systems to detect and measure the concentration of biological and/or chemical analytes. Transduction principle/s, materials, efficient designs, including readout technique, and sensor performance are explained. This is followed by a discussion on how N/MEMS biosensors continue to evolve. The challenges and possible opportunities are also discussed.

Keywords Biosensors · N/MEMS · Health and well-being · BioMEMS · Applications

1 Introduction

Biosensors are playing a crucial role in today's biomedical science and technology [1]. Biosensors allow the sensitive and precise detection of a range of biological or chemical contaminants [1–5]. It is a device that measures biological or chemical reactions and generates an output signal in proportion to the concentration of a target

---

V. Pachkawade (✉)
VPACHKAWADE Research Center, 440032, Nagpur, India
e-mail: vinayak@vpachkawade.com; vinayakp@ieee.org

K. Guha et al. (eds.), *MEMS and Microfluidics in Healthcare*, Lecture Notes in Electrical Engineering 989, https://doi.org/10.1007/978-981-19-8714-4_1

analyte in the reaction. Typical elements of a biosensor are shown in Fig. 1. It consists of the following elements: (1) a small inlet/channel (μfluidic) to collect/navigate the sample/solution to the sensing system. A sample may be in the form of a solid, liquid, gas, or combination thereof. A sample in solid form may contain dust, dirt, soot, or smoke particles. Samples in the gaseous form include air with a mixture of oxygen, nitrogen, carbon dioxide, or other hazardous gas elements. A liquid sample may include bodily fluids, for example, nasal swabs, saliva, blood, semen, sweat, urine, etc. Analyte/s in the samples are a target substance to be detected. For example, particulate matter (PM) is an analyte whose concentration in the surrounding air is to be measured. Triglyceride is an analyte whose concentration in the blood is to be measured. In clinical applications, analytes of interest are glucose, vitamins, hemoglobin, molecules, proteins, amino acids, urea, bodily gases, toxins, specific biomarkers (to detect chronic disease), living cells, and pathogens (viruses and bacteria). (2) Next element is called bioreceptors (see Fig. 1). Bioreceptors are a group of molecules that are deposited/immobilized (as a thin film/layer) onto the surface of a transducer. Bioreceptors interact with the sample/solution to precisely recognize the target analyte/antigen. Such interaction between the bioreceptor molecules and target analyte is termed biorecognition. The output of a biorecognition event may result in a change in mass, light, color, temperature, pH level, etc. (3) A sensor converts this form of energy into a measurable signal in either optical or electrical form (conductance/impedance, charge/current, potential/voltage, frequency/phase, etc.). Here, we use the words transducer and sensor interchangeably. (4) A sustaining electronics in the biodevice/module can process the sensor output by further amplification, filtering, analog-to-digital (A/D) conversion, and microprocessor/memory storage. Eventually, the module shows the reading on the computer or an embedded display in real time. A wireless data transmission may also be added to the unit.

Figure 2 shows the information on the potential areas of applications of biosensors. Biosensors are widely being deployed for environmental check (to detect hazardous gas elements), to detect the onset of the existing/future disease, monitoring the quality of food and beverages at places where these are stored, on farms to inspect soil quality, in medicine dose control, and many other.

2 Characteristics of a Biosensor

In the biosensing development platform, the following parameters are of the most importance. Researchers are continuously finding ways to improve the following features (see Fig. 3).

Sensitivity/Resolution: It is defined as the smallest possible change in the physical/biological/chemical properties of a transducer that can be resolved after the biomass/target analyte/s are adsorbed/absorbed by the sensor surface (i.e., after the reaction occurs). Sensitivity (also expressed in %) can be given as the ratio of change in the sensor output per unit change in the input. It is also called the detection limit.

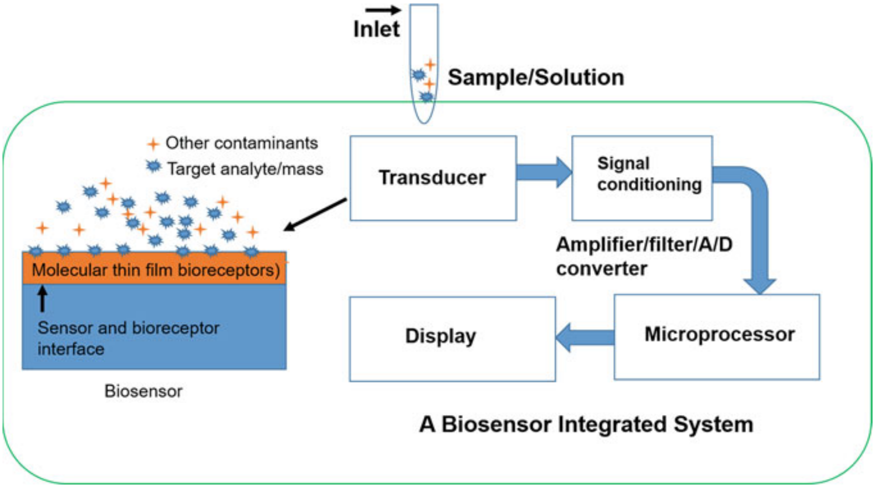

Fig. 1 A typical bio/chemical sensing platform. Bioreceptors enable the selective detection of a target analyte in the sample. A transducer's job is to convert the biorecognition process into measurable output. Such measurable output is then correlated to the detection and concentration of a target analyte

Fig. 2 A diagram showing potential application areas where biosensors are used. There are many other areas where biosensors are primarily used

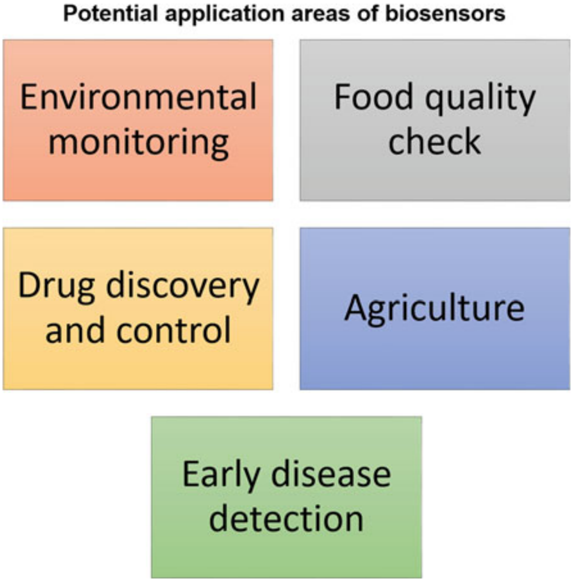

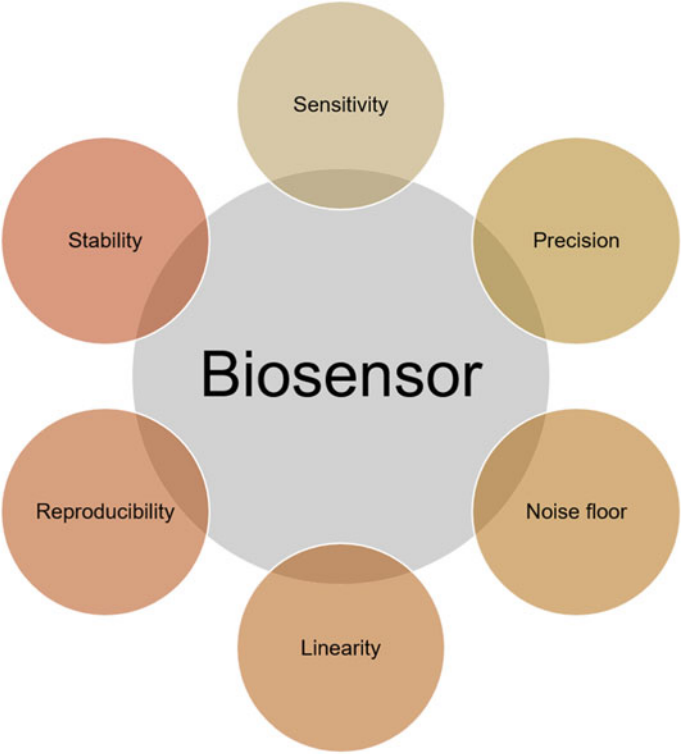

Fig. 3 Performance parameters in biosensor development

A mass sensor, for example, can show resolution up to fg/ml to record the concentration of analyte traces in a liquid sample. Measuring a lowest possible concentration of a specific analyte/s (for example, antigen) can be associated with an underlying medical condition for which doctors can prescribe a test.

Precision: Precision is an important feature of a biosensor. Precision/selectivity/specificity indicates the ability of a bioreceptor thin film molecule to detect/recognize a specific analyte within a mixture of other contaminants in a sample under test (see Fig. 1). An example of precision is the contact of an antigen with the antibody. Typically, antibodies act as bioreceptors and are immobilized on the surface of the transducer. A solution/sample that contains the antigen is exposed to the transducer, where antibodies should interact specifically with the antigens. To develop a biosensor, precision is the key characteristic.

Stability: The stability of a sensor is the characteristic to avoid responding to changes in the environmental conditions (i.e., temperature, humidity, vibrations, pressure, etc.), thereby preventing a false output. To address this issue, a provision is made in the embedded electronics to compensate for environmental drifts in the sensor output. Such common-mode signals can be canceled using a differential sensor readout.

Reproducibility: Reproducibility is the capability of the biosensor module to produce the same output when the experiment/test is repeated. It implies that the sensor provides an average value close to the correct value when a sample is measured several times. Reproducible sensor output indicates the high consistency and robustness of a biosensor.

Noise floor: This parameter provides the baseline above which a sensor output can reliably be detected/measured. Noise in the sensing system stems from i) the intrinsic noise in the sensing element and ii) electronics. Therefore, a sensor is designed to reduce the overall noise. Lower the noise floor, better the sensor signal-to-noise ratio (S/N), or say sensitivity/resolution.

Linearity and Dynamic range: A sensor can show linear changes in the output per unit change in the input. The output of a sensor should produce a linear response to different concentrations being measured. This characteristic is also often represented by the % nonlinearity in the sensor output. Linear dynamic range (expressed in dB) is the ratio of the maximum to the minimum sensor output.

3 N/MEMS Biosensor (BioMEMS)

N/MEMS features scalability, ultra-high sensitivity, energy efficiency, and compatibility to easily integrate with microelectronics[6–8]. N/MEMS offers outstanding precision in the detection and measurement of ultra-small elements. This advantage comes with the miniaturization N/MEMS offers. For example, a nominal mass of N/MEMS can scale down to nanograms or even smaller. It is therefore possible to detect and measure things at 10^{-15}, 10^{-18}, or even lower scale. Miniaturization also means a small footprint, weight, energy, and Internet of sensors (IoS), all at reduced system-level cost. With N/MEMS, it is possible to precisely detect the target analyte and measure its concentration. This is achieved through precisely recording even the minutest shift in the sensor output [4, 9, 10]. Transduction principles such as piezoelectricity, piezo-resistivity, electro-static, electro-magnetic, electro-thermal, optical, etc. are popularly used in the development of the N/MEMS-enabled bio/chemical sensors.

3.1 Mass Accumulation

N/MEMS devices are operated by the principle of gravimetric sensing [7, 11]. Mass accumulation is characterized by the adsorption/absorption (biorecognition) of the mass of a particle or target element in a biological/chemical sample. N/MEMS transducer is a mechanical cantilever/tuning-fork/plate/disk/bar/membrane. This transducer is set in a static or a dynamic mode (vibrate at a particular frequency called a natural resonant frequency). Figure 4 shows a schematic illustration of an N/MEMS

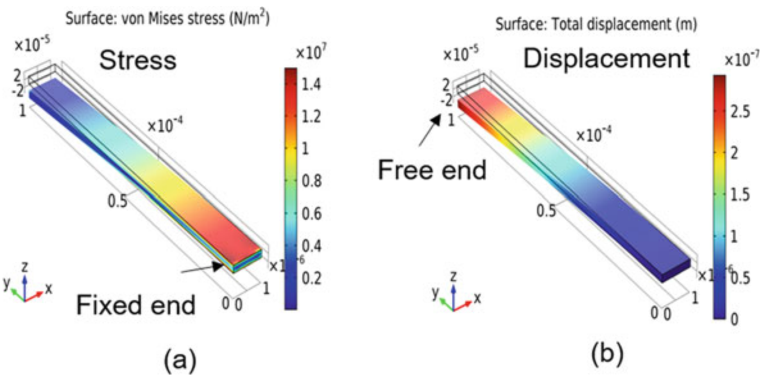

Fig. 4 A static N/MEMS transducer that can be used to sense and quantify target bio/chemical contaminants in a sample. Part **a** shows a stress profile of a structure that can be used to use piezoresistive transduction. Part **b** shows a displacement profile of a structure that can be used to use capacitive transduction

transducer that can be used as a primary element in a typical N/MEMS biosensing platform. As seen in Fig. 4, a transducer (cantilever in this case) in a static form is used for sensing purposes. A transducer surface is functionalized to attract specific molecules. The functionalization takes place by depositing/loading nanoparticles (for example, gold nanoparticles) onto the surface of a cantilever. After this, target molecules are attached to the nanoparticles. Such mass accumulation leads to the gradient in (i) the surface stress (σ) (see Fig. 4a), (ii) surface strain, and (iii) a position/displacement of a cantilever (see Fig. 4b). In other words, the transducer is actuated by the component of the force exerted by the bio/chemical reaction that occurs at the surface of a transducer.

For the sensing part, a set of resistors (forming a Wheatstone bridge electronic circuit) is embedded at the other end of a cantilever, where it is fixed/anchored (see Fig. 4). At this end, the stress is maximum. Another viable method of sensing is to monitor a change in the parallel plate capacitance at the free end of a cantilever. At this end, displacement is maximum. A bottom electrode placed beneath the free end of the cantilever can be used to detect the capacitive gradient when the cantilever moves.

3.2 Materials

Usually, silicon/polysilicon is used to construct such a transducer. In recent years, piezoelectric materials (for example, aluminum nitride (AlN) and quartz) have become a popular choice in realizing several potential applications in BioMEMS [4]. However, materials such as silicon, piezo, etc. are suited only for non-invasive applications, a procedure that does not require inserting an instrument through the skin or into a body. Such materials can be a part of N/MEMS-enabled biosensors. These sensors can then be used for monitoring environmental parameters, lab-on-chip, laboratory tests, wearable gadgets, etc. Given the biocompatibility issue, materials such as Polydimethylsiloxane (PDMS) and other polymers are also widely used for biosensing [12]. Another application of PDMS is that a transducer can be embedded into the μ channels made by PDMS for lab-on-chip fluid testing applications.

3.3 N/MEMS Resonators for Ultra-Precise Bio/Chemical Sensing

N/MEMS resonators are one of the most promising candidates to develop a wide range of applications in medical diagnostic and instrumentation [1, 4, 8, 13–16]. N/MEMS resonators offer extremely high-quality factors (Q) and high frequency. These two parameters result in exceptionally high parametric sensitivity. Additionally, the N/MEMS resonant sensing platform provides good output stability. Due to their highly precise output, N/MEMS resonators are extremely useful to sense environmental, physical, biological, and chemical quantities. They can detect multiple analytes in parallel, and offer immunity toward a false output. Being a primary component in many commercial applications, N/MEMS resonators are today a popular choice to develop low-cost, miniaturized, reliable, reproducible, and precise sensing solutions. Possible areas of applications are point-of-care/remote monitoring of target parameters in the environment, agriculture, medicine, health, and well-being, thus democratizing sensing across the globe. N/MEMS resonators operate on the principle of gravimetric sensing. The N/MEMS mass sensor is reported to detect particle concentration as low as attogram (ag) or even zeptogram (zg). Figure 5 shows a representative example of a N/MEMS resonator that can be used to detect and quantify the concentration of a target contaminant in a biological/chemical sample. Upon adsorption/absorption of a target trace/particle, a shift in the resonant frequency of a transducer can be accurately recorded (in real time). These shifts can be correlated to the concentration of the contaminant/s. The essential assumption is that adsorption/absorption of a mass, Δm is much smaller than the nominal mass, M of the resonant transducer ($\Delta m << M$).

3.4 Multiple Analyte Detection Using N/MEMS

Figure 6 shows a platform parallel processing using N/MEMS sensors. As seen, $C_1 - C_n$ are the cantilevers arranged as an array. These sensors are attached to a common base. Each of the cantilevers is coated/immobilized/functionalized with a *specific* bioreceptor thin film to attract the target molecules/particles. Such a sensing platform is highly useful for the fast testing of multiple parameters in bio/chemical

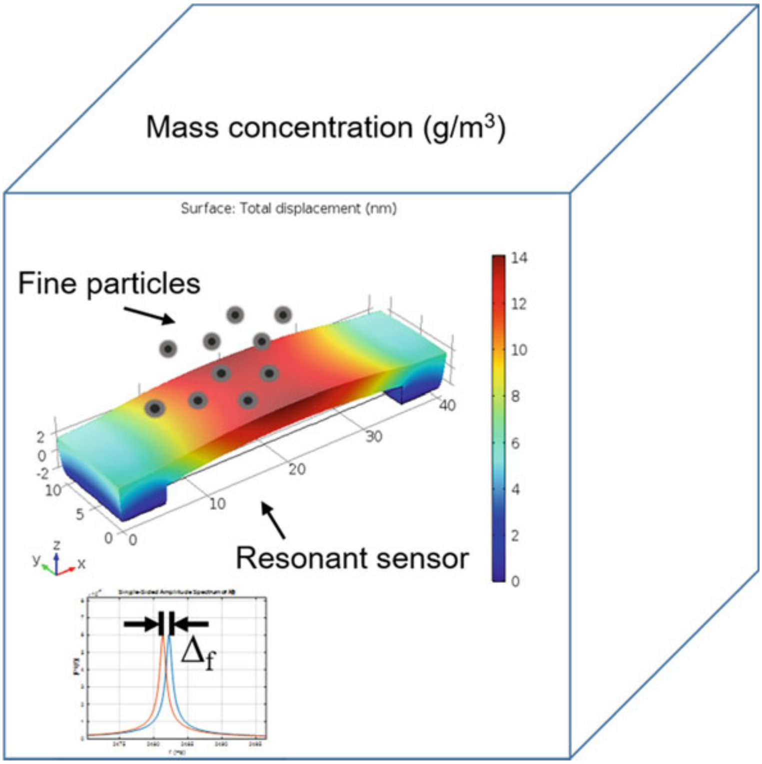

Fig. 5 A representative example schematic of a resonant mass sensor for particle detection and concentration measurement of a target analyte. Δf indicates the shift in the resonant frequency, i.e., transducer output

samples. Due to simultaneous testing and processing, the overall cost is low. Such a platform is compact and efficient. However, a specific coating of *n* number of sensing units in an array is required. Such a requirement may be a trade-off with the advantages in terms of cost and time.

4 Summary, Outlook, and Conclusion

This chapter introduced the basics of biosensors and how N/MEMS sensors can be used in several bio/chemical applications. The chapter started by providing an overview of a typical N/MEMS-enabled bio/chemical sensing platform. The N/MEMS sensors can be used to detect and precisely quantify several biological and chemical contaminants. This scientific area requires expertise, experience, and collaborations across the multi-domains (mechanics, optics, biology, chemistry, physics, and microelectronics). A static mode N/MEMS can be used to monitor

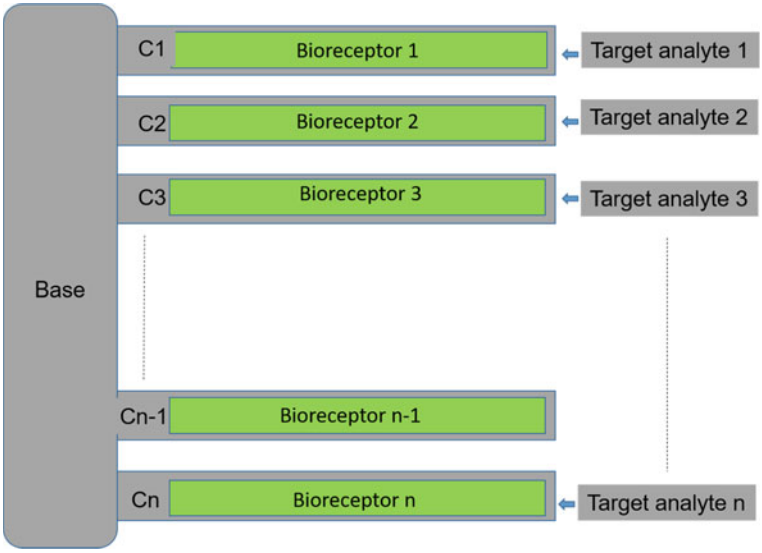

Fig. 6 An array of N/MEMS sensors to specifically detect and measure the concentration of a target analyte in a sample. A parallel test and processing of multiple analytes in the sample are useful in terms of cost and time

the surface stress, strain, or displacement when the mass of a target particle/analyte is attached to the sensor. An electro/optical sensing mechanism or a combination thereof can then be used to read and correlate the sensor output to the presence and concentration of the target element/s in a sample. A dynamic (resonant) mode N/NEMS is also used as a high-sensitivity transducer in biological and chemical applications. Here, a transducer element is set to vibrate at the designed frequency. When the mass of a target particle/analyte is adsorbed/absorbed on the chemically functionalized surface of a transducer, a change in the effective mass of the resonant transducer results in a change in the frequency.

N/MEMS-enabled hand-held biosensor modules can be employed for many applications. These applications are health care, surgery, drug discovery/dose control, recognition of pollutants, detection of micro-organisms responsible for causing a disease, and markers to indicate disease in bodily liquids/fluids (blood, urine, saliva, semen, sweat, etc.). Typical applications of BioMEMS also include sensors measuring intravascular blood pressure, therapeutics applications (e.g., drug delivery actuators, disease monitors), pacemakers, and defibrillators. Biosensors can be implantable or wearable. These are also part of sensing systems for real-time monitoring of several body parameters such as pulse rate, blood pressure, oxygen, and neurological activities.

References

1. Haleem A, Javaid M, Singh RP, Suman R, Rab S (2021) Biosensors applications in medical field: A brief review
2. Mohankumar P, Ajayan J, Mohanraj T, Yasodharan R (2021) Recent developments in biosensors for healthcare and biomedical applications: A review. Meas J Int Meas Confed 167. https://doi.org/10.1016/j.measurement.2020.108293
3. Choi JR (2020) Development of point-of-care biosensors for COVID-19
4. Pachkawade V, Tse Z (2022) MEMS sensor for detection and measurement of ultra-fine particles. Eng Res Express 4:022002. https://doi.org/10.1088/2631-8695/ac743a
5. Pachkawade V, Tse Z (2021) MEMS sensor for detection and measurement of ultra-fine particles: A review
6. Pachkawade V, Li CSC-S, Li SSS-S (2012) A fully-differential CMOS-MEMS resonator integrated with an on-chip amplifier. In: Proceedings of IEEE sensors
7. Pachkawade V (2021) State-of-the-art in mode-localized MEMS coupled resonant sensors: A comprehensive review. IEEE Sens J. https://doi.org/10.1109/JSEN.2021.3051240
8. Leïchlé, T., Nicu, L., Alava, T.: MEMS Biosensors and COVID-19: Missed Opportunity, (2020)
9. Timurdogan E, Alaca BE, Kavakli IH, Urey H (2011) MEMS biosensor for detection of Hepatitis A and C viruses in serum. Biosens Bioelectron 28. https://doi.org/10.1016/j.bios.2011.07.014
10. Erdil K, Akcan G, Gül Ö, Gökdel YD (2022) A disposable MEMS biosensor for aflatoxin M1 molecule detection. Sens Actuators Phys 338. https://doi.org/10.1016/j.sna.2022.113438
11. Wang Y, Zhao C, Wang C, Cerica D, Baijot M, Pachkawade et al (2017) A reversible method to characterize the mass sensitivity of a 3-Dof mode localized coupled resonator under atmospheric pressure. Proceedings 1: 493. https://doi.org/10.3390/proceedings1040493
12. Liu CF, Wang MH, Jang LS (2018) Microfluidics-based hairpin resonator biosensor for biological cell detection. Sens Actuators, B Chem 263. https://doi.org/10.1016/j.snb.2018.01.234
13. Keegan N, Hedley J, Hu ZX, Spoors JA, Waugh W et al (2012) Piezoelectrically actuated circular diaphragm resonator mass sensors. In: 2012 7th IEEE International conference on nano/micro engineered and molecular systems, NEMS 2012
14. Lee C, Yee ASP, Perera JLJ, Chen et al (2008) Design of nanobiophotonics resonators for biomolecules detection. In: 3rd IEEE International conference on nano/micro engineered and molecular systems, NEMS)
15. Ducloux O, Park JW, Tiercelin N, Pernod P, Preobrazhensky V, Hamon M et al (2009) MEMS resonators actuated by TbCo/FeCo nanostructured magnetostrictive multilayers in a liquid environment. In: TRANSDUCERS 2009—15th International conference on solid-state sensors, actuators, and microsystems
16. Li DJ, Chen HY, Liu CR, Fan K, Wang GF (2021) A review on MEMS/NEMS-based biosensor

Lab-On-A-Chip Technology in Health Care

Neha Mishra

Abstract In the current era when early disease diagnosis is a need of the hour for the proper cure, LOC devices are the most reliable and promising solution. Lab-on-a-chip (LoC) devices are used for point-of-care diagnostics as they are compact, cost-effective, integrable, and multiple diagnostics can be performed on a single chip. For this reason, there are different diagnostic techniques used for LOC devices such as optical detection, PCR, qPCR, paper-based assays, and lab-on-a-chip using microfluidic platforms. The main focus of the aforesaid technique is the simplification of device design with multiplexed processes and the availability of automation to make LOC devices user-friendly. In this chapter, different techniques and processes are discussed which are used in diagnostic and healthcare applications.

Keywords Microfabrication · Biosensor · Microfludic channel · Optical detection

1 Introduction

A microfluidic platform consists of a group of precisely defined, fabricated microfluidic operating components. Miniaturization, automating, and parallelizing chemical processes [1, 2] are made possible by lab-on-a-chip (LOC) technologies. Because they employ less chemical reagent in modularly constructed, miniaturized devices, LOC devices have a lower cost advantage. The ability to operate quickly in a small space is another significant benefit of LOC devices; this is made possible by the parallelization of response chambers. The throughput and automation of analytical systems are also increased by LOC technology. To regulate fluidics at the micro- and nanoscales, LOC devices can be created (Fig. 1), and depending on the scale difference, these devices are sometimes referred to as microfluidics and nano-fluidics. Micro-channels or nano-channels in LOC technology offer control of fluids in minuscule quantities to enable biological processes in incredibly small volumes.

N. Mishra (✉)
Indian Institute of Technology, Bombay, India
e-mail: nehamishra1308@gmail.com

K. Guha et al. (eds.), *MEMS and Microfluidics in Healthcare*, Lecture Notes
in Electrical Engineering 989, https://doi.org/10.1007/978-981-19-8714-4_2

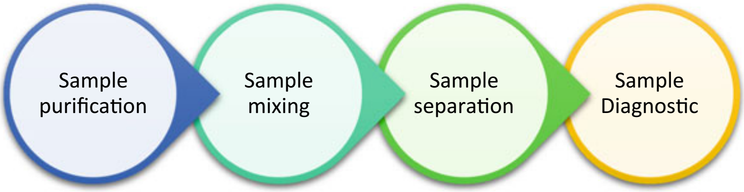

Fig. 1 Basic component of lab-on-a-chip technology

Utilizing the photolithography process, integrated circuits and microchannels can have fluid control components and routes created. For LOC to become a comprehensive system, it also needs the integration of micro-pumps, valves, micro-electrodes, electrical fields, and micro-electronics [3].

Smaller and faster electronic devices are produced as a result of advances in integrated circuit technology and wafer fabrication facilities. Silicon or glass and polymers are the foundation of microfluidic manufacturing. Despite having well-controlled mechanical and chemical qualities, silicon and glass require more expensive manufacturing processes. One mould can be used as a master for fabricating multiple devices in the case of polymers, however, using soft lithography or hot embossing. This makes it possible to produce disposable goods in large quantities. In contrast, polymers' mechanical and chemical properties have reliability issues, which necessitate surface modification for reliable device functionality [4]. In many cases, PoC diagnostics involve lateral flow assays. These assays include moving a liquid sample that contains the target analyte through various zones of polymeric strips that have immobilized capture probes that can interact with the analyte as shown in Fig. 2 [5, 6]. Commercially available pregnancy tests for the detection of human chorionic gonadotropin hormone present in bio-analyte (urine) are widely used for lateral flow assays. These tests use a sandwich-based immunoassay to detect the target protein, which is realized by a colour shift that can be seen with the unaided eye [5–8]. The key benefits of lateral flow tests include their affordability, convenience of use, simplicity, and extended shelf life. However, multiplexing and flow rate control are difficult with lateral flow assays since they call for a lot of chemicals and relatively significant volumes of material [5–8]. By offering fine flow control through various microfluidic channel geometry, microfluidic technology has been used to overcome these restrictions [8, 9]. Figure 2 illustrates the basic schematic diagram of the lateral flow assay, which explains how the process works. A small amount (generally in microliters) of the analyte is placed into the sample pad and then the analyte will go slowly to the probe pad through capillary action. The target analyte is beholden by tagged detection probes. It will take to the detection membrane, and then be captured on a line where capture probes are immobilized [5]. For proof-of-concept diagnostics of several analytes, capillary-driven microfluidic chips have been employed [6, 10–13]. For instance, a triage system is commercially available, which consists of a disposable protein chip and a portable analyzing device, that attempts to identify a wide range of medical disorders [14, 15] (Table 1).

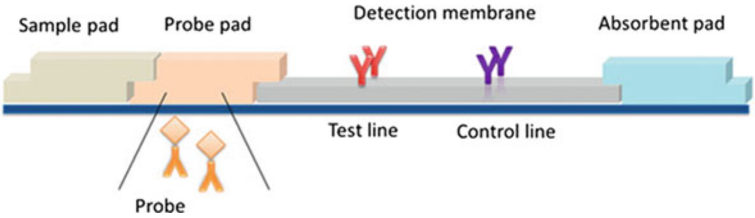

Fig. 2 Schematic diagram of lateral flow assay strip. *Reproduced with permission from Anfossi* et al., *Biosensors 9(1):2 (2018)*[5]

Table 1 LOC Technologies in healthcare [2]

LOC area	LOC application	Products	References
Diagnostics	PoC, PCR, qPCR, DNA isolation, electrophoresis, sequencing, Colorimetric detection, Optical absorbance, Amperometric sensor	Fluidigm, biomark HD, Agilent lab chip, Elvesys system	[16–25]
Genomics	Microarray for next-generation sequencing	Nanopore, Illumina hiseq, PasificBio, Ion torrent	[26–28]
Biochemical Assays	Immunological assays, Pregnancy kit, glucose Monitoring	Dexcom G5, Preganews	[29–31]
Proteomics	MS, SDS-PAGE	908 Devices zip chip	[32, 33]
Biosensors	Optical biosensors-based devices, Bio-affinity and bio-catalytic devices, Antigen–antibody-based devices	IST AG IV4 biosensor	[34–36]
Cell research	Flow cytometers, cell culturing and monitoring	Fluidigm helios	[37]

One of the major fields of application of lab-on-a-chip is molecular biology; it includes biochemical, research related to cell and proteomic, biosensors, and is further used for drug design and development. Diagnostic and genomic analyses are the primary uses for LOC. There are numerous molecular biology studies present which include PCR, DNA isolation, qPCR, sequencing, and electrophoresis by using LOC. It has enormous scope to develop PCR microfluidics devices that can be used for speeding up the amplification of DNA and RNA. LOC PCR devices provide quick viral and bacterial identification during any pandemic to prevent infection. Different genetic diagnostic mechanisms are laboratory-independent and there are used for the detection of HIV and HBV infection. These methodologies are made possible because LOC technologies have reduced the size of diagnostic devices.

These emerging LOC devices can also be utilized to identify the biomarkers of diseases with a genetic base. LOC devices are also used in the food industry for the detection of pathogens present in food. Earlier for this purpose DNA sequencing was used which was a time-consuming and costly process.

It took 15 years to complete the first human genome project. Today, a human genome can be sequenced using LOC devices in a matter of hours, which is faster than traditional methods. Next-generation sequencing devices are mostly used in laboratories for reading millions of DNA fragments on a single chip using LOC technologies. Nanopore Technologies is one of these companies and has produced the smallest and fastest platform that is now awaiting commercialization. Mass spectrometry (MS) analysis, cell extraction, electrophoresis, blotting, and digestion are all components of protein analysis. LOC combines every phase of protein analysis onto a single chip [2]. The integrating steps speed up the analysis by several minutes. In LOC systems, the crystallization process can be parallelized and accelerated to better understand its structure. Immunoassays are another LOC use that can decrease the reaction time in comparison to the standard method. The best platform for cell research is LOC microchannels; microfluidics allows for the control of cell flow, tagged antibody staining and imaging, cell differentiation, cell sorting, and cytometry in cell biology experiments [2].

1.1 Diagnostics

LOCs are used in a variety of chemical and molecular diagnostic procedures, including heavy metal ion detection [18, 20, 35], biological analyte present in biological fluid [15, 19, 21, 22, 24] antigen–antibody interaction, DNA extraction, PCR, qPCR, electrophoresis, DNA purification, molecular detection, and others.

1.1.1 Optical Detection Techniques for the Detection of the Analyte Using a Microfluidic Channel

There are various methods currently used for the sensing and detection of relevant biological and chemical analytes present in biological as well as water samples. For this purpose, optical absorbances, as well as evanescent-based optical techniques, are used [18, 19, 21, 22, 35].

1.1.2 LOC Devices Used for the Extraction and Purification of DNA

For diagnostic tests, nucleic acid from biological cells must be purified. The two main processes in the extraction of DNA are cell lysis (disruption of the cell membrane and nucleus membrane) and DNA purification (removal of undesirable RNA, membrane lipids, and proteins). Devices for lysing LOC cells can use a variety of lysis techniques, including chemical, thermal, ultrasonic, electrical, mechanical, etc. Most macroscale DNA purification methods employed in extraction columns, which rely on DNA adsorption on silica beads in particular buffer conditions, are portable to microfluidic techniques. Therefore, silica beads can either be inhibited during the washing and elution phases of LOC devices by mechanical barriers or by silica-coated magnetic beads which can be easily stopped by a magnet [17].

1.1.3 Molecular, qPCR, and PCR Detection Using LOC Devices

PCR is the next most popular analysis following DNA extraction. Numerous PCR uses are similar to sequencing techniques both directly and indirectly. Undoubtedly, one of the applications of direct PCR is the amplification of DNA sequences that aids in the observation of minuscule amounts of DNA (e.g., for the detection of different pathogen such as viruses, fungi, and bacteria). The creation of multiple LOC PCR machines is impacted by the significance of PCR in genetic analysis. Rapid thermal transfer for quick and coupled PCR is caused by the miniaturization of volume and increased surface-to-volume ratio. To merge PCR and electrophoresis on-chip, PCR additionally needs a post-analysis to allow for the size identification of amplicons by electrophoresis [38].

Originally, gels comprised primarily of agarose (for longer DNA) and polyacrylamides were used for electrophoresis (for shorter DNA). DNA electrophoresis was one of the first molecular processes that could be incorporated into a chip with the development of LOCs [39]. This miniaturization made it possible to speed up the electrophoresis process, even more, use fewer reagents, and assemble other previously described DNA manufacturing steps on a chip. Another method that has been tailored for LOC devices is qPCR, which has the advantages of being quicker (automatic detection during PCR), more sensitive, and long-lasting. The below Fig. 3 shows the basic process flow of the micro-PCR system.

A device is being developed by Elvesys, which is an ultra-fast qPCR microfluidic system for the molecular analysis of numerous diseases, including ebola and anthrax. Using an ultra-fast pressure controller, fluorescence reader, and depending on ultra-fast temperature control, it takes only a fraction of a minute and also has detection efficiency comparable to the commercial system [40].

Another newly-emerging field is digital microfluidics which deals with emulsions and droplets inside LOC devices. Droplets can collect extremely small amounts of DNA, and limits can be raised by detecting one copy numbers using LOC droplet qPCR as shown in Fig. 3 [25].

1.2 Genomic Application

Due to the results of sequencing initiatives like the Human Genome Project, the discipline of genomics has experienced a remarkable expansion in recent years. Sequencing-related projects help advance the field's technology. Analyzing DNA sequences to determine their nucleotide order is known as sequencing. The Sanger

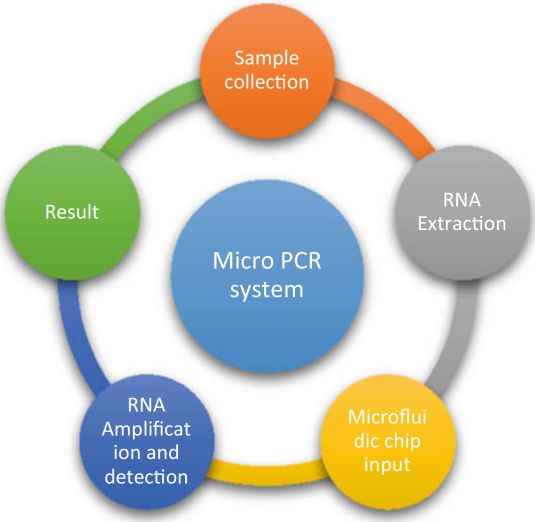

Fig. 3 Microfluidic RT-PCR assay

method, on which the initial sequencing was based, produces DNA fragments of various lengths with fluorophores that correspond to various nucleotide ends. By substituting a tiny capillary filled with gel for the polyacrylamide gel slab used in conventional DNA sequencing, miniaturization of the process was made possible. The volume of the necessary DNA sample was reduced by the capillaries' modest size [41].

The next-generation sequencing technologies for ultra-fast DNA sequencing currently developed are Sequencing-by-hybridization (SBH), nano-pore sequencing, and sequencing-by-synthesis (SBS). High-throughput sequencing's cost and duration can be significantly decreased by using the LOC method for these technologies [27].

1.3 Microarray

Multiple biosensors must be integrated in conjunction with DNA microarrays for the investigation of complicated DNA sample expression. Miniaturization, speed, and precision are the key characteristics of lab-on-a-chip devices. Rapid multiplex analysis of nucleic acid samples using this technology has enormous potential for applications such as forensic investigation, drug screening, infectious agent identification, differential gene expression measures, and the diagnosis of genetic illnesses. Numerous elements of genetic study are being revolutionized by this usage of DNA microarrays [28].

1.4 Biochemical Applications

The LOC technology can be coupled with immunological and enzymatic assays on a single microfluidic platform, as in the case of monitoring glucose and insulin simultaneously. The availability of a LOC that can track both glucose and insulin simultaneously holds enormous promise for better diabetic management.

The incorporation of pertinent sample pre-treatment/clean-up processes necessary for whole-blood analysis is critical for the proper and effective realization of such glucose monitoring. The assembling of additional tests and analyte handling steps can be done using the new LOC technique, which is desirable for developing miniature clinical devices [31].

1.5 Proteomics

One of the serious challenges affecting science in the post-genome era is proteomics. Proteome profiling, the most fundamental form of proteomics, is a difficult task that involves identifying all the proteins identified in each sample. Owing to its broad range of concentrations, diversity of molecules, and capacity to bind to solid surfaces, the proteome presents special analytical challenges. LOC devices help create creative solutions to challenging analytical challenges like proteome profiling. The four areas of this application where LOC devices are advanced are chemical processing, sample pre-concentration and clean-up, chemical separations, and interfaces with mass spectrometry [42]. LOC is a small device for protein separation and detection that takes minimal reagents is simple to operate and completes tests relatively quickly. LOC protein devices can manufacture a wide range of data points, allowing for the extraction of the most information from each sample. Another benefit is that it is simple to compare information from LOC devices to data collected using 2D-PAGE [32].

LOC proteins sodium dodecyl sulphate polyacrylamide gel electrophoresis (SDS-PAGE) isolation with UV spectrophotometry is the most frequently used approach for sorting and quantifying protein combinations. SDS-PAGE frequently takes a lot of work and time. LOC devices hasten separation and pave the way for protein sizing automation [33]. LOC MS protein profiling is one technique for measuring proteins. These devices are utilized for indirect infusion into the mass spectrometer during Capillary Electrophoresis (CE) segregation, on-chip processing of the sample, and infusion of CE before MS analysis, it was claimed. The goal of the project is to use electrospray ionization MS to provide an interconnection between both the spectrometer and the LOC [33].

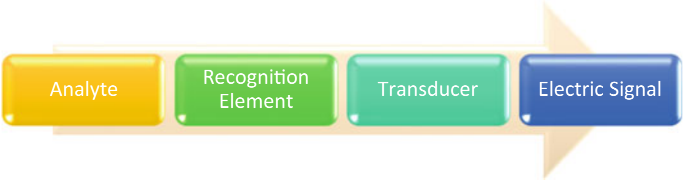

Fig. 4 Basic element of biosensors

1.6 Biosensors

Lab-on-a-chip biosensors, which are small and biologically active devices, are used to find the target analytes. Such systems directly couple a biorecognition element (direct interaction with the intended analyte) with a physical transducer, which transforms the biorecognition process into electric signals as illustrated in Fig. 4. Bio-catalytic and bio-affinity devices are the two categories of LOC biosensors. Devices that use bio-affinity are based on the target analyte binding selectively to a partner ligand that is encapsulated on the surface (e.g., antibody, oligonucleotide).

Single-stranded (ss) DNA probes, for instance, are fixed on the transducer surface in hybridization biosensors. The attachment of an adequate hybridization indication after binding allows for the detection of duplex formation. But in bio-catalytic devices, the target substrate is recognized by an immobilized enzyme. For instance, glucose oxidase immobilized sensor strips for diabetes monitoring [36]. The biosensors are also used for the detection of certain biomarkers for the detection of chronic diseases like cancer. Monitoring of cancer cell biomarkers is a need of the hour. For this purpose SPR and LSPR-based biosensors are prominently used [43].

1.7 Cell Research

A study into a single cell may be carried out on a very small scale thanks to the employment of LOC devices. Single-cell handling and manipulation are typically necessary because, after being positioned inside the microchannel, the single cell must also be put or trapped at a certain location. It should be possible for the microsystem to carry out minimal analyte present in the sample fluid. LOC systems also made it possible to control the surrounding environment of a cell using different methodologies such as controlling the physical or chemical nature of the surface to which the cell attaches, surrounding temperature, and pH. It is possible to use several, frequently intricate fluid-handling components when the cell is to be subjected to diverse kinds of stimuli. These concepts suggest that cell location and chemical stimulation must be combined. To prevent sample wastage, which might happen if multiple devices will be used, a single platform is used for cell lysis and analysis [44, 45].

Flow Cytometry is one of the most commonly and successfully developed and used lab-on-a-chip devices. LOC flow cytometer systems have advanced quickly over the past ten years as a result of the growing need for data on cellular analysis that is of higher quality and broader scope as well as the complexity involved and availability of microfabrication technologies. As a result of increasing technological capabilities and expanding needs, microfluidics in the flow cytometric examination of cells and particles has experienced several exciting advancements [37].

1.8 Organ-On-A-Chip

The term “organ-on-a-chip” (OOC) refers to a microfluidic cell culture system that has constantly perfused chambers colonized by a variety of cell types to mimic the physiology of different tissue and organ types. OOC has the potential to be a valuable tool in the application of drug research and development by accurately recapturing levels of tissue and organ functionality. The different components of organ-on-a-chip are shown in Fig. 5 [46].

Fig. 5 Basic components of an organ on a chip. Reproduced with permission from Peng Zhang Elsevier, (181–198), 2022

1.9 Drug Design and Development

To help guide the emergence of new pharmaceuticals, the industry needs new tools, especially ones that can predict how potential new treatments might behave in humans based on how well they operate in cells and animals [34]. Even though some analytical applications of Lab-on-a-chip systems in the innovation and use of biopharmaceuticals seem simple (like analytical techniques to measure and enhance the yield of protein drugs like therapeutic antibodies), others, like assays based on primary human cells, are technically more challenging but are still possible, at least in some circumstances. In any setting, the LOC platform could be used repeatedly in a highly flexible and reproducible way [44].

2 Conclusion and Future Directions

A recent field termed LOC deals with the miniaturization of laboratory devices into micro dimension devices. The major advantage of LOC devices is that they are cost-effective, user-friendly, multiple processes can be performed at the same time sensitive and speedy device. Aforesaid devices conclude that they are used for advanced diagnostic purposes shortly by taking a look at commercialized LOC equipment like RT-PCR, pregnancy kit, DNA sequencing, and glucose monitoring. In future, more goods created with LOC technology will be available in the market. Day by day, the industry will produce LOC devices more affordably. LOC development has a direct impact on molecular-based inventions that are employed in daily life.

References

1. Mark D, Haeberle S, Roth G, von Stetten F, Zengerle R (2010) Microfluidic lab-on-a-chip platforms: requirements, characteristics, and applications. Chem Soc Rev 39 (3), 11531182. Available from https://doi.org/10.1039/b820557b.
2. Yılmaz B, Yılmaz F (2018) Chapter 8—Lab-on-a-chip technology and its applications. In: Barh D, Azevedo V (eds) Omics technologies and bio-engineering. Academic Press, pp 145–153. ISBN 9780128046593. https://doi.org/10.1016/B978-0-12-804659-3.00008-7
3. Casquillas G, TimotheˊE H (2015) Introduction to lab-on-a-chip 2015: review, history, and future. Retrieved from http://www.elveflow.com/microfluidic-tutorials/microfluidic-reviews-and-tutorials/introduction-to-lab-on-achip-2015-review-history-and-future/
4. Neuzi P, Giselbrecht S, Lange K, Huang TJ, Manz A (2012) Revisiting lab-on-a-chip technology for drug discovery. Nat Rev Drug Discov 11 (8):620632. Available from https://doi.org/10.1038/nrd3799
5. Koczula KM, Gallotta A (2016) Lateral flow assays. Essays Biochem 60(1):111–120
6. Anfossi L, Di Nardo F, Cavalera S, Giovannoli C, Baggiani C (2018) Multiplex lateral flow immunoassay: an overview of strategies towards high-throughput point-of-need testing. Biosensors 9(1):2

7. Hemmig E, Temiz Y, Gökçe O, Lovchik RD, Delamarche E (2020) Transposing lateral flow immunoassays to capillary-driven microfluidics using self-coalescence modules and capillary assembled receptor carriers. Anal Chem 92(1):940–946
8. Carrell C, Kava A, Nguyen M, Menger R, Munshi Z, Call Z et al (2019) Beyond the lateral flow assay: a review of paper-based microfluidics. Microelectron Eng 206:45–54
9. Yetisen AK, Akram MS, Lowe CR (2013) Paper-based microfluidic point-of-care diagnostic devices. Lab Chip 13(12):2210–2251
10. Gong MM, Sinton D (2017) Turning the page: advancing paper-based microfluidics for broad diagnostic application. Chem Rev 117(12):8447–8480
11. Channon RB, Nguyen MP, Scorzelli AG, Henry EM, Volckens J, Dandy DS et al (2018) Rapid flow in multilayer microfluidic paper-based analytical devices. Lab Chip 18(5):793–802
12. Magro L, Escadafal C, Garneret P, Jacquelin B, Kwasiborski A, Manuguerra J-C et al (2017) Paper microfluidics for nucleic acid amplification testing (NAAT) of infectious diseases. Lab Chip 17(14):2347–2371
13. Tian T, Bi Y, Xu X, Zhu Z, Yang C (2018) Integrated paper-based microfluidic devices for point-of-care testing. Anal Methods 10(29):3567–3581
14. Gervais L, de Rooij N, Delamarche E (2011) Microfluidic chips for point-of-care immunodiagnostics. Adv Mater 23(24): H151–HH76
15. Song Y, Lin B, Tian T, Xu X, Wang W, Ruan Q et al (2019) Recent progress in microfluidics-based biosensing. Anal Chem 91(1):388–404
16. Apple FS, Christenson RH, Valdes R Jr, Andriak AJ, Berg A, Duh S-H et al (2020) Simultaneous rapid measurement of whole blood myoglobin, creatine kinase MB, and cardiac troponin I by the triage cardiac panel for detection of myocardial infarction. Clin Chem 45(2):199–205
17. Clark TJ, McPherson PH, Buechler KF (2002) The triage cardiac panel: cardiac markers for the triage system. Point Care 1(1):42–46
18. Arshavsky-Graham, S., Segal, E. (2020). Lab-on-a-Chip Devices for Point-of-Care Medical Diagnostics. In: Advances in Biochemical Engineering/Biotechnology Springer, Berlin, Heidelberg. https://doi.org/10.1007/10_2020_127
19. Timothe´e H (2015b) Microfluidics for DNA analysis. Retrieved from http://www.elveflow.com/microfluidictutorials/microfluidic-reviews-andtutorials/microfluidics-for-dna-analysis-pcr/
20. Mishra N, Dhwaj A ,Verma D, Prabhakar A (2022) Cost-effective microabsorbance detection based nanoparticle immobilized microfluidic system for potential investigation of diverse chemical contaminants present in drinking water. Anal Chim Acta 1205:339734, ISSN 0003-2670. https://doi.org/10.1016/j.aca.2022.339734
21. Mishra N, Dwivedi P, Trivedi R (2021) Non-invasive portable uric acid sensor for biomedical and healthcare application. Mater Today: Proc. ISSN 2214–7853. https://doi.org/10.1016/j.matpr.2021.05.626.
22. Mishra N, Dhwaj A, Vishwakarma R, Prabhakar A (2018) PDMS bonding via A portable, low-cost corona system, for microfluidic chip fabrication. Int J Adv Sci Eng Technol 6 (1). ISSN(p): 2321 e8991, ISSN(e): 2321 e9009
23. Prabhakar A, Agrawal M, Mishra N, Roy N, Jaiswar A, Verma D, Dhwaj A (2020) Cost-effective smart microfluidic device with immobilized silver nanoparticles and embedded UV-light sources for synergistic water disinfection effect. RSC Adv 10:17479
24. Prabhakar A, Mishra N, Verma D, Mukherji S (2018) Investigation of dual bend - serpentine/spiral waveguides, coupled to microchannel system, for competent, evanescent wave absorption based, on-chip, biological/chemical sensing applications. RSC Adv 8:35539e35550
25. Kaigala GV, Behnam M, Bidulock ACE, Bargen C, Johnstone RW, Elliott DG et al. (2010) A scalable and modular lab-on-a-chip genetic analysis instrument. Analyst 135 (7), 16061617. Available from https://doi.org/10.1039/b925
26. Prabhakar A, Mishra N, Mukherji S (2017) A comprehensive investigation of a microfabricated U-bend polymer waveguide With Analyte micro-reservoir for versatile on-chip sensing applications. J Microelectromech Sys 26 (4):935e945

27. Beer NR, Hindson BJ, Wheeler EK, Hall SB, Rose KA, Kennedy IM, et al. (2007) On-chip, real-time, single-copy polymerase chain reaction in picoliter droplets. Anal Chem 79 (22):84718475. Available from https://doi.org/10.1021/ac701809w
28. Zhang Y, Ge S, Yu J (2016) Chemical and biochemical analysis on lab-on-a-chip devices fabricated using three-dimensional printing. TrAC Trends Anal Chem 85, Part C: 166–180. ISSN 0165–9936. https://doi.org/10.1016/j.trac.2016.09.008
29. Metzker ML (2005) Emerging technologies in DNA sequencing. Genome Res 15 (12):17671776. Available from https://doi.org/10.1101/gr.3770505
30. Wang J, Ahmad H, Ma C, Shi Q, Vermesh O, Vermesh U et al (2010) A self-powered, one-step chip for rapid, quantitative and multiplexed detection of proteins from pinpricks of whole blood. Lab Chip 10(22):3157–3162
31. Sengupta P, Khanra K, Chowdhury AR, Datta P (2019) 4—Lab-on-a-chip sensing devices for biomedical applications. In: Pal K, Kraatz HB, Khasnobish A, Bag S, Banerjee I, Kuruganti U (eds) Woodhead publishing series in electronic and optical materials, bioelectronics and medical devices. Woodhead Publishing, pp 47–95. ISBN 9780081024201. https://doi.org/10.1016/B978-0-08-102420-1.00004-2
32. Malic L, Brassard D, Veres T, Tabrizian M (2010) Integration and detection of biochemical assays in digital microfluidic LOC devices. Lab Chip 10:418–431. https://doi.org/10.1039/B917668C
33. Wang J, Ibanez A, Chatrathi MP (2003) On-chip integration of enzyme and immunoassays: simultaneous measurements of insulin and glucose. J Am Chem Soc 125 (28):84448445. Available from https://doi.org/10.1021/ja036067e
34. Schasfoort RBM (2004) Proteomics-on-a-chip: the challenge to couple lab-on-a-chip unit operations. Expert Rev Proteomics 1 (1):123132. Available from https://doi.org/10.1586/14789450.1.1.123
35. Mouradian S (2002) Lab-on-a-chip: applications in proteomics. Curr Opin Chem Biol 6 (1):5156. Available from https://doi.org/10.1016/S1367-5931(01)00280-0
36. Ma Z, Li B, Peng J, Gao D (2022) Recent development of drug delivery systems through microfluidics: from synthesis to evaluation. Pharmaceutics 14(2):434. https://doi.org/10.3390/pharmaceutics14020434
37. Mishra N, Mishra M, Prabhakar A (2021) Design and fabrication of bio-mems device for detection of heavy metalion present in potable water. In: 2021 International conference on advances in electrical, computing, communication and sustainable technologies (ICAECT). pp 1–3. https://doi.org/10.1109/ICAECT49130.2021.9392388
38. Wang J (2000) From DNA biosensors to gene chips. Nucleic Acid Res 28 (16): 30113016. Available from https://doi.org/10.1093/nar/28.16.3011
39. Huh D, Gu W, Kamotani Y, Grotberg JB, Takayama S (2005) Microfluidics for flow cytometric analysis of cells and particles. Physiol Meas 26 (3):R73R98. Available from https://doi.org/10.1088/0967-3334/26/3/R02
40. Timothe´e H (2015a) Microfluidic PCR, qPCR, RT-PCR & qRT-PCR. Retrieved from http://www.elveflow.com/microfluidic-tutorials/microfluidic-reviews-and-tutorials/microfluidic-pcr-qpcr-rtpcr/
41. Curtis Saunders D, Holst GL, Phaneuf CR, Pak N, Marchese M, Sondej N et al. (2013) Rapid, quantitative, reverse transcription PCR in a polymer microfluidicchip. Biosens Bioelectron 44:222228. Available from https://doi.org/10.1016/j.bios.2013.01.019
42. Ramalingam N, Rui Z, Liu HB, Dai CC, Kaushik R, Ratnaharika B, et al. (2010) Real-time PCR-based microfluidic array chip for simultaneous detection of multiple waterborne pathogens. Sens Actuat B Chem 145 (1):543552. Available from https://doi.org/10.1016/j.snb.2009.11.025
43. Figeys D, Pinto D (2000) Lab-on-a-chip: a revolution in biological and medical sciences. Anal Chem 72 (9):330A335A. Available from https://doi.org/10.1021/ac002800y
44. Freire SLS, Wheeler AR (2006) Proteome-on-a-chip: mirage, or on the horizon? lab chip 6 (11), 1415. Available from: https://doi.org/10.1039/b609871a

45. Azzouz A, Hejji L, Kim KH, Kukkar D, Souhail B, Bhardwaj N, Brown RJC, Zhang W (2022) Advances in surface plasmon resonance–based biosensor technologies for cancer biomarker detection. Biosens Bioelectron 197:113767. ISSN 0956-5663. https://doi.org/10.1016/j.bios.2021.113767
46. Sedgwick H, Caron F, Monaghan PB, Kolch W, Cooper J.M., 2008. Lab-on-a-chip technologies for proteomic analysis from isolated cells. J R Soc Interface 5 (Suppl 2), S123S130. Available from: https://doi.org/10.1098/rsif.2008.0169
47. Whitesides GM (2006) The origins and the future of microfluidics. Nature 442 (7101):368373. Available from https://doi.org/10.1038/nature05058
48. Zhang P (2022) Chapter 6—Organ-on-a-chip. In: Li XJ, Yang C, Li PCH. Multidisciplinary microfluidic and nanofluidic lab-on-a-chip. Elsevier, pp 181–198. ISBN 9780444594327. https://doi.org/10.1016/B978-0-444-59432-7.00007-8

A Review on Recent Trends in the Segregation of Red Blood Cells Using Microfluidic Devices

Subhash Turaka, Valanukonda Bhavya Bhargavi, Naga Nikhila Nandam, Shahed Baba Syed, Nanda Sai Donepudi, Dhanya Yalamanchili, Koushik Guha, and Jasti Sateesh

Abstract The isolation of Red Blood Cells (RBCs) has become a broad area of research in recent times. The early segregation of RBCs from the blood prevents them from lysis. The segregation of RBCs using traditional techniques like centrifugation has become outdated due to the usage of bulky equipment. This paper reviews the functions of RBCs, the age-old techniques that were practically used to distinguish RBCs, and their drawbacks. The assessment of microfluidic devices which are prevalently used in present-day diagnostics that are promised to replace the bottlenecks posed by the traditional methods is also presented. This review aims to project the recent advancements in microfluidics, their applications, and the segregation of microfluidic particles using them. The modern approaches that can separate RBCs virtually using electroosmotic phenomena like di-electrophoresis are also reviewed. The present scenarios for the separation of RBCs with a FEM tool computer-aided design for virtual analysis are also discussed.

Keywords Isolation · Red Blood Cells · Centrifugation · Microfluidics · Di-electrophoresis

1 Introduction

The human body resembles a very complex and technological machine. It functions as a single entity, although it is made up of numerous interconnected systems. Each system is linked to a certain function that is generally required for an individual's

---

S. Turaka · V. B. Bhargavi · N. N. Nandam · S. B. Syed · J. Sateesh (✉)
Department of Electronics and Communication Engineering, Velagapudi Ramakrishna Siddhartha Engineering College, Kanuru, Vijayawada, Andhra Pradesh 520007, India
e-mail: jastisateesh@vrsiddhartha.ac.in

N. S. Donepudi · D. Yalamanchili
Siddhartha Government College and Hospital, Vijayawada 520008, India

K. Guha
Department of Electronics and Communication Engineering, National Institute of Technology Silchar, Assam 780010, India

K. Guha et al. (eds.), *MEMS and Microfluidics in Healthcare*, Lecture Notes in Electrical Engineering 989, https://doi.org/10.1007/978-981-19-8714-4_3

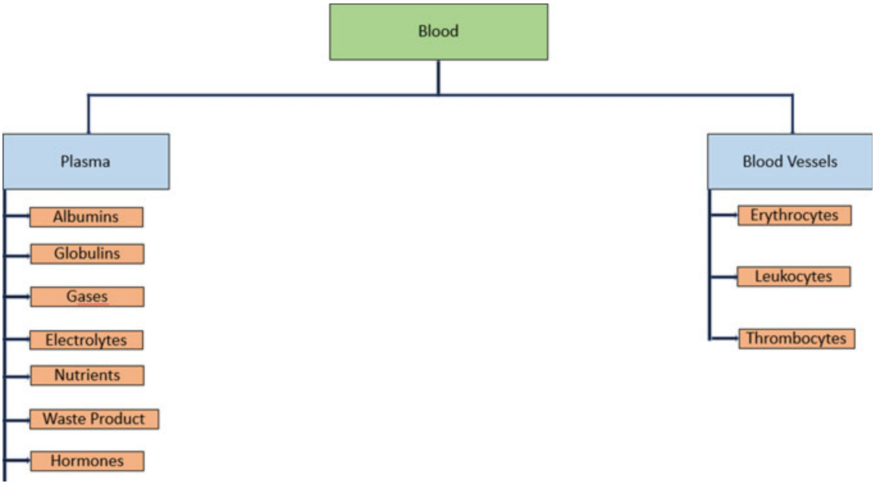

Fig. 1 The figure illustrates the classification of blood in the human body

well-being. The ability of the body systems to function together assures survival. As a result, both the composition and working of the human body are obscured [1]. Among all the body systems, transport systems that consist of the blood, cardiovascular, and lymphatic systems guarantee that all body cells have insight into different nutrients necessary to sustain them and offer a way of eliminating waste. The blood exports substances throughout the body using a network of blood vessels. The main functions of blood are respiratory, transportation, temperature regulation, excretory functions, immunity, acid–base balance, etc [2]. Blood can be categorized into two parts: plasma and blood cells. Plasma consists of 95% water with a wide range of substances and proteins like albumins, globulins, electrolytes, nutrients, waste products, hormones, and gases as shown in Fig. 1. Blood cells can be classified into erythrocytes, leukocytes, and thrombocytes as shown in Fig. 1 to perform functions of gaseous exchange, protection, and blood clotting. Red Blood Cells (RBCs) constitute 99% of blood cells [1].

2 Red Blood Cells and Their Functions

Erythrocytes are hollowed disks without nuclei which are around 7 μm in circumference [1]. Their primitive function is to transport gases, primarily oxygen, although they also transport carbon dioxide. Their distinctive form is well adapted to their function; the concavity improves the surface area available for gas exchange, while the core portion's thinness allows for quick gas entrance and escape. The cells are elastic, allowing them to pass through tiny holes, and they lack intramolecular structures, enabling hemoglobin, a large colored protein involved in gas transport, to occupy a wider area. In clinical practice, measurements of red cell counts, volume, and hemoglobin concentration are helpful measures.

RBCs do not split as they lack nuclei, so they should be restored regularly by parent cells from the red bone marrow, which may be observed at the extremities of bones. Before being absorbed into circulation, RBCs experience a number of stages during their development. In circulation, erythrocytes have a lifespan of roughly 120 days in adults and 70 days in infants [3]. In the typical healthy body, there are roughly 30 trillion RBCs, about 25% of the overall cell count, and 1% of these, mostly older cells, are removed and destroyed every day [1]. Since the bone marrow generates erythrocytes at the same rate as they are destroyed, red cell levels stay relatively constant. A homeostatic negative feedback system is responsible for the regeneration of RBCs [4]. Erythropoietin, a hormone generated mostly by the kidney, controls red blood cell formation [5]. When erythropoietin concentrations are low, red cell production is inhibited, resulting in anemia.

Phagocytic reticuloendothelial cells do hemolysis or blood degradation [6]. These cells can be found in different organs, but the spleen, bone marrow, and liver are the most common sites of hemolysis. The cell membranes of erythrocytes grow weaker as they age, making them more prone to hemolysis. The iron produced by hemolysis is stored in the body and utilized to make new hemoglobin molecules in the bone marrow. The hem component of hemoglobin is used to make biliverdin [7]. It is nearly completely converted to the yellow color bilirubin before being linked to plasma globulin and transmitted to the liver. It is transformed in the liver from a fat-soluble to a water-soluble state and then excreted as component bile. As a result, RBCs must be separated from the blood to be protected against hemolysis.

3 Laboratory Techniques for the Segregation of RBCs

The conventional laboratory approach for the separation of RBCs is centrifugation which is based on the density and volume of particles [8]. The other techniques that are practiced for the isolation of RBCs are density gradient centrifugation, agglutination, and phase partitioning as shown in Fig. 2 [9–15]. The principle involved in every technique has been discussed further.

3.1 Centrifugation

Centrifugation is a methodology that utilizes centrifugal force to remove blends or particulates from a solution. The major components required for centrifugation are centrifuge and centrifuge rotors. When rotating swiftly, the centrifuge rotor forces the heavier molecules to the narrow end and the milder particles to the upper end. The centrifuge rotors play a crucial role in the segregation process. The centrifuge rotor can be categorized into three types: swinging-bucket rotors, vertical rotors, and

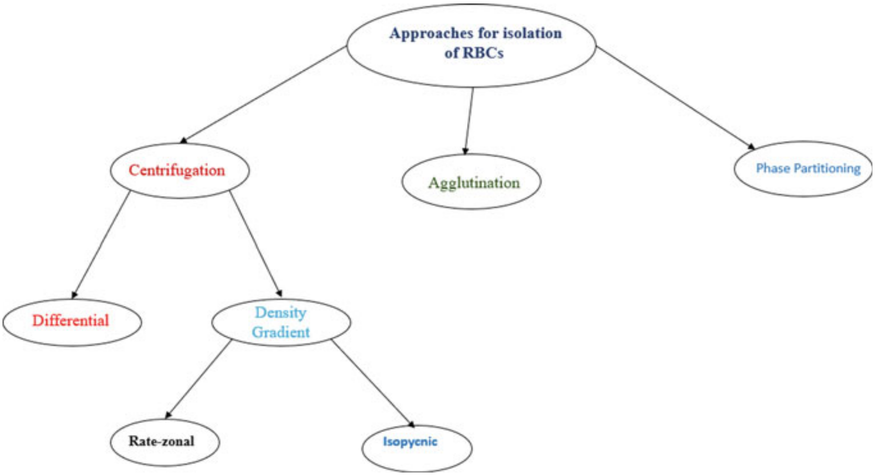

Fig. 2 The figure illustrates different laboratory techniques that are in practice for the segregation of RBCs

fixed-angle rotors which are used to determine the type, speed, and range of the volume. Depending on the type of rotor used, centrifugation can be classified into two types: differential and density gradient as shown in Fig. 2. Density gradient can further be classified into rate-zonal and isopycnic.

As the rotor rotates in a centrifuge under the influence of centrifugal force, the blood particles in the solution residues at a rate that is in correlation with the applied centrifugal force. Buoyant and frictional forces oppose the centrifugal force operating on blood particles. As a result, the blood particles migrate from the point of rotation. When the induced centrifugal force is greater than the two opposing forces the blood particles precipitate at a constant rate as shown in Fig. 3. In Fig. 3, RBCs are at the lower end as they have low density, whereas plasma is at the upper end due to its high density. The middle layer in Fig. 2 is a buffy coat which is a combination of platelets and white blood cells (WBCs).

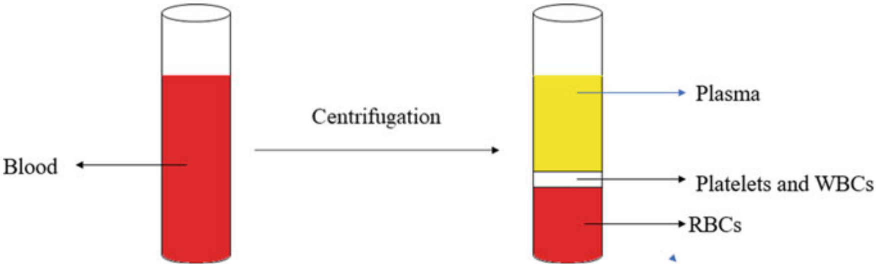

Fig. 3 The figure depicts the isolation of blood particles under the influence of centrifugal force

The factors that affect the centrifugation process are the density of the sample and solution, viscosity, temperature, and rotation speed. However, the significant drawbacks of this process are its bulky equipment, the transformation of cell structure when subjected to high gravity, salts present in the blood that can cause corrosion to the equipment, requires costly infrastructure for continuous centrifuges [16]. Moreover, the centrifugation technique is based on the size of the blood particles which alters as they age in circulation. To overcome this effect, density gradient centrifugation came into the picture which is based on the density of particles.

3.2 Density Gradient Centrifugation (DSC)

In hematology, difficulties such as partitioning erythrocytes into age-dependent fractions and preparing blood samples rich in reticulocytes are of major interest. The frequently utilized approach for the separation of RBCs is density gradient centrifugation [10–12]. Density gradient centrifugation is almost similar to that of the conventional centrifugation process but is based on density rather than size. In DSC, each particle has a unique collection of physical traits or biological features, that may be utilized to separate and isolate it. The focus of density gradient centrifugation is on two factors: size and density. The amount of time needed for this treatment is determined by the particle size. Tiny particles take longer to cross through the bigger particulate region and accept the position deeper in the gradient, whereas larger particles reach their point of stability sooner.

DSC uses subsidiary materials like bovine serum albumin, gum acacia, etc., which the reader may refer to [9, 11, 17–21]. The reagent in DSC is a substance that aids in the isolation or separation of cells. These items can not only speed up the process, but they can also improve purity and throughput. The reagents can considerably enhance the accuracy of DSC by preventing particles from aggregating, generating a set divider, or removing remaining red blood cells. But these reagents can cause various types of cancer which are not desirable. Hence, there is a need for another separation technique that does not require reagents. Differential centrifugation (DC) is a technique that does not use reagents but segregates particles based on their mass. DC is sometimes seen to be a more straightforward method of centrifugation. Cells and organelles are separated using it, while molecules and particles are separated using density gradient centrifugation. The sort of physical qualities on which the two centrifugation processes are based is the fundamental distinction between them. Although differential centrifugation is simpler, density gradient centrifugation may separate considerably smaller particles. But the physical properties of blood alter as they age in circulation. A comparative study has been drafted about the aging of blood by researchers using agglutination.

3.3 Agglutination

Antibodies can cluster cells or particles in a process termed agglutination, in addition to precipitating soluble molecules and flocculating molecules in suspension. The existence of immunoglobulin against microbial species or erythrocytes can be detected through agglutination. On a glass plate or a microtiter plate, agglutination experiments are typically rapid and simple to perform. The process of agglutination can be performed by direct and indirect Coomb's test. In the direct Coomb's test, first, a sample of blood is extracted with hemolytic anemia and antibodies attached to RBCs. Coomb's reagent is blended with the collected blood sample then clumping (agglutination) is observed after the cross-linkage of antibodies. In the indirect method, patient serum containing antibodies is drawn and donor blood is mixed with the collected serum. As a result, the patient's antibodies bind to donor RBCs. After adding a few drops of Coomb's reagent agglutination reaction is observed. When RBCs are subjected to agglutination it is observed that the younger RBCs have more negative charge when compared to older RBCs [22].

3.4 Phase Partitioning

The topology of microvascular networks is complicated, with many bifurcating vessels. At diverging bifurcations, phase partitioning of RBCs (which contains various enzymes) occurs, resulting in a diverse RBC distribution that impacts the oxygen supply to living tissues [23]. T-butanol and ammonium sulphate are used in three-phase partitioning (TPP) to extract important nucleoids from aqueous solutions. The approach may be used upstream as well as downstream with basic steps that can be scaled up. Various laboratories have isolated around 25 lipids and proteins using TPP–t-butanol [24]. When enough salts, like ammonium sulphate, are added to tertiary butanol, the blood distinguishes into two stages: a higher t-butanol stage and a lower hydrated stage. If RBCs are observed in the initial hydrated stage, they may divide into a third stage, midway between the lower hydrated and higher t-butanol stages, based on the quantity of ammonium sulphate added. This is the foundation of the technical term "three-phase partitioning," or TPP, for isolating and concentrating proteins.

The above-mentioned approaches for the separation of RBCs depend on the physical and chemical properties of blood. The properties of blood alter as they age in circulation. Furthermore, these approaches require reagents like polyethylene glycol and phthalates which can cause life-threatening diseases. Moreover, the laboratory techniques require bulky equipment, huge laboratory, and human intervention. To overcome these, microfluidic devices have been developed for the separation of RBCs.

4 Microfluidics and Applications

Microfluidics has the potential to impact a large assortment of fields, which includes biological analysis, optics, and information technology [25]. As a variety of innovative components and techniques for injecting, blending, regulating, and preserving fluids in microfluidic channels have been developed and applied, the range of applications of microfluidics in genetics and numerical biochemistry has risen [26]. Despite fast advancement, some issues remain addressed, including sample preparation and introduction, connecting microlevel channels with human intervention, dealing with a variety of testable quantities, and mobility.

Microfluidics can change how biology is currently handled [27]. Microfluidic systems enable the isolation, manipulation, and examination of tiny groups of cells, or even single cells [28–30]. The capabilities of microfluidic devices relevant to chemurgy are miniaturization, small volume, large surface area, scaling out, automation, etc. For personalized care, microfluidic devices can gather factors such as proteomic, metagenomic, and genetic data [31, 32].

Microfluidic systems are emerging in a large assortment of applications, making them impossible to assess all within a given amount of time. Some of the applications are arrays (interaction of a large number of molecules), gradients, microfilters, droplets, etc.

5 Physics of Microfluidics

To comprehend and deal with microfluidics, it is necessary to first comprehend the physics that prevails at the micro range. Other microfluidic reviews are available [33–37], but none of them includes a thorough examination of the quantum mechanics of the microlevel and how it enables particular devices. The physics of microfluidics is addressed in this section, with pointers to more comprehensive studies.

At the microscale, factors that are not present in ordinary life become prominent [38]. Because of scaling, it’s generally detrimental to downsize existing big devices and expect them to work well at the microscale [39]. Designs must be developed to take benefit of microscale forces. Laminar flow, diffusion, Reynolds number, surface area to volume ratio, and surface tension are some of the factors which are prevalent in microfluidics.

5.1 Laminar Flow

A phenomenon in which the motion of particulate in a liquid medium is not a stochastic phenomenon of time is known as laminar flow. The microchannel stream is usually laminar because of its limited size [40]. The major consequence of laminar flow is that two or more streams running nearby will not mix unless they do so through diffusion. For conducting experiments and sorting particles by size, diffusion across laminar flows in a microfluidic device has been employed [41, 42]. Another approach made possible by the laminar stream is the formation of fluid particles, barring eccentric influences on both sides, which remain reasonably well-formed. These particulates may be transported about in an organized fashion, allowing a wide range of cellular investigation options.

5.2 Diffusion

Diffusion is the phenomenon by which a dense concentration of molecules in an area spreads radially outward owing to random motion, resulting in a constant average particle concentration across the volume. $D^2 = 2dt$ may be used to accomplish one-dimensional diffusion, where D is the particle's distance traveled in time period t and d is the diffusion parameter. Because displacement alters from the square power on the microlevel, diffusion evolves even more essential.

5.3 Reynolds Number

A fluid flow's Reynolds number (Re) indicates whether the flow is laminar or turbulent. Below is a detailed description of the laminar flow. Turbulent flow is erratic as well as uncertain. The Reynolds number may be determined using the following formula:

$$\mathrm{Re} = \frac{\rho \mathrm{v} \mathrm{d_h}}{\mu} \tag{1}$$

where ρ is the density of the fluid, v is the fluid velocity, d_h is the circumference of the hydraulic, and μ is the viscosity of the fluid.

The value of Re 2300, as computed by the formula, implies a laminar flow. The liquid starts to exhibit indications of turbulence when Re approaches 2300, and when Re exceeds 2300, the flow is deemed turbulent [27].

5.4 Surface Area to Volume Ratio

The component which is essential in the micro range is the surface area to volume ratio (SAV). Capillary electrophoresis (CE) in microchannels is more efficient when the SAV ratio is high because surplus heat is removed more quickly. Unfortunately, when utilizing electrokinetic flow to transfer fluids, the high SAV ratio permits macroparticles to readily absorb and bind to channel surfaces, lowering the performance.

5.5 *Surface Tension*

Adhesion among molecules of a solution at the fluid/gas interface causes surface tension. The solvent surface-free energy is the amount that shows how much tension is present on its surface. The height at which liquid can pass through a capillary is proportional to the liquid surface energy and conversely to the capillary radius. The distances that solvents will migrate solely on capillary pressure are substantial when microchannels with sizes in the range of microns are employed.

The Young–Laplace equation may be used to compute the pressure created by a surface of the liquid with orthogonal radii of curvature R1 and R2 and is given by

$$\Delta \mathrm{P} = \gamma\left(\frac{1}{\mathrm{R}_1} + \frac{1}{\mathrm{R}_2}\right) \tag{2}$$

where γ is the solution surface energy, The height of the wall is defined by R, which extends to infinity, and the equation is reduced to

$$\Delta \mathrm{P} = \frac{\gamma}{\mathrm{R}} \tag{3}$$

It calculates the pressure at the liquid border linking two cosmic long plates isolated by 2R. If R1 = R2 and the region is spherical, the equation becomes

$$\Delta \mathrm{P} = \frac{2\gamma}{\mathrm{R}} \tag{4}$$

6 Modeling of Microfluidic Devices for Medical Applications

Microfluidics, a branch of biomedical research, has shown to be a profitable sector for replacing regular assessments and detection procedures, conducting basic botanical investigations in cells and disorders. Microfluidics investigations have enabled the development of a variety of assuring biomedical applications, including biosensing elements, point-of-care medical diagnostics, drug tests, content providers, innate medical gadgets, unique biomimetics, artificial tissues, and unicellular studies, among others [43]. Different micro- or nanotechnology methods are employed and can be chosen based on the eventual use of the microdevice.

In the application, material selection is also critical. The typical materials used are silicon, glass, thermoplastics, and elastomers [44]. Out of these elastomers like Polydimethylsiloxane (PDMS) has moderate protein crystallization, porosity, and droplet formation. It also provides good permeability, bio-culture, and disposable device use.

The connection and/or merging of components for the applications for which the device is being created is another key part of microfluidic device construction. Micro heaters, injectors, detectors, electroosmotic liquid taps, and readout electronics, may be integrated to create full microfluidic systems with impressive capabilities [45].

7 Microfluidic Cell Separation and Sorting Techniques

Despite product evolution into microdevices, the downsizing of lab-on-a-chip (LOC) devices persists as a hedge. The mixing, pumping, isolation, and management of liquids at the microscopic level are constrained by minimal testing quantities and stream velocity requisite for biomimetic assessment, as well as the microscale features of the systems. At the microscale, the primary physical and chemical processes differ from those at the macroscale, resulting in greater complexity in the glide and migration process. To counter these restrictions, many experiments have been conducted to improve the modeling of microfluidic devices and isolation equipment which may be implemented on LOC systems while tackling the quasi behavior of bulky corporeal fluids [46–50].

Microfluidic equipment may incorporate several cell sorting methods based on physical factors, offering a precise interface for manipulating cellular components and extracting forces in a range of methods, as well as allowing for the entire sovereign assessment of phenomenal components [51]. In particular, cell sorting approaches have evolved specifically for cell absorption; claret endowment; blood fractionation; cell categorizing (separation of cells by type); and cell eliminator, which can act as cell segregator [52]. Active technologies, such as di-electrophoresis, magnetophoresis, acoustophoresis, and optical tweezers, are based on microelectromechanical systems and increase fluid control by employing mobile components or external mechanical forces [53]. The recent electrokinetic phenomenon used for the segregation of RBCs is di-electrophoresis [8, 54]. When polarizable particles floating in a liquid are exposed to a quasi-electric field, di-electrophoresis is induced, and it is often employed to manipulate bio-particles, including cells in microfluidic devices [55–59].

Electrical charges are stimulated on the cell/medium junction when a polarisable particle, such as a cell, is introduced to an electric field. When dipoles are oriented parallelly, electrical stress is formed by the induced charges. When a homogeneous electric field is provided, the coulombic forces experienced by either side of the dipole are equal, resulting in equivalent and neutralizing forces exerted on the cell. In a quasi-electric field, the imposed coulombic forces are uneven, providing a resultant force on the cell. Based on its comparable polarizability about the surrounding medium, the cell can be lured to or driven from regions of the intense electric field. If cells have a spherical form, they are subjected to a DEP force, which may be stated as follows:

$$\mathrm{F_{DEP}} = 4\pi\varepsilon_{\mathrm{m}}\mathrm{r}^3\mathrm{Re}\left\{\frac{\varepsilon_p^*(\omega) - \varepsilon_m^*(\omega)}{\varepsilon_p^*(\omega) + 2\varepsilon_m^*(\omega)}\right\} \cdot \nabla \mathrm{E}^2 \tag{5}$$

where ε_m and ε_p are the permittivities of the medium and particle, r is the radius of the sphere, and E is the induced electric field.

Because red blood cells have a more intricate structure, comprising a cytosolic core encased inside a plasma membrane, the single-shell spherical model is frequently used to compute the Real part of Clausius Mossotti's (CM) factor. The CM factor obtained for RBCs is negative, and hence RBCs follow negative di-electrophoresis as shown in Fig. 4. Whereas the negative DEP response of cells is somewhat lower at 100 MHz than at 100 kHz, the chosen frequency of 100 MHz guarantees that the thermal stress delivered to the blood owing to the Joule heating effect is kept to a minimum.

Bharat et al. [54] constructed a microfluidic device to separate RBCs using di-electrophoresis. The platelet is split by the induced electric field (n-DEP), which results in separation. Using di-electrophoresis field flow fractionation, a modified solution is used to isolate thrombocytes from blood. The microfluidic system is used to pre-focus and fractionation features to capture cells in contrast to regions relying on their area. By establishing a nonuniform electric field and placing alternating polarity electrodes, the particle trajectories are also varied. This sorting mechanism might be used with a system that sorts cells according to their "opacity." Variations of the design specifications, such as the applied separating voltage, frequency, pressure, and flow inlet rates, were tested using the 2D finite element model as shown in Fig. 5. An electric potential of 5 V is applied and the materials used are silicon, germanium, and copper.

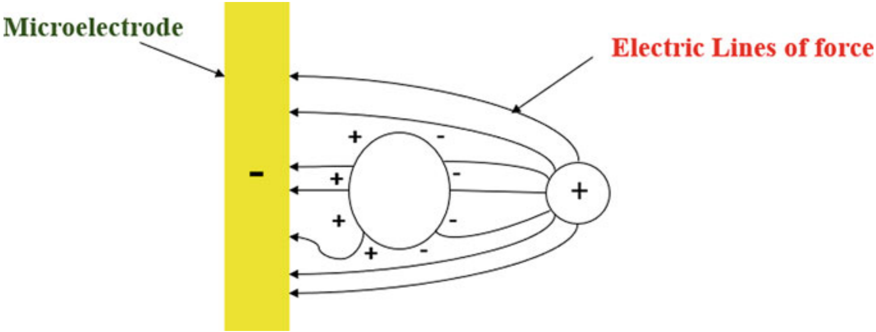

Fig. 4 The figure illustrates the mechanism of negative di-electrophoresis

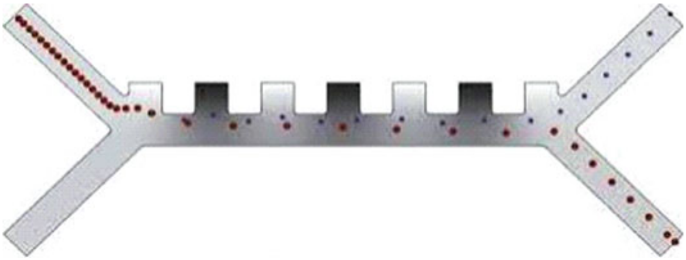

Fig. 5 The microfluidic device with applied voltage, outlet velocity, pressure and outlet velocity [56]

The lower inlet's velocity is substantially higher (853 m/s) than the top inlet's (134 m/s) to concentrate all of the infused particulates toward the upper output, as seen in Fig. 5. The velocity differential between the separation (highest velocity) and collection (lowest velocity) regions allows particles to quickly approach the collecting zone when an electric field is supplied with an initial frequency of 100 kHz. The maximum potential is determined to be 1.45 × 10–3 mV.

Mitra et al. [8] designed a microfluidic device that uses di-electrophoresis for the isolation of RBCs with dimensions 3, 5, and 8 μm diameters as shown in Fig. 6. The dimensions of the design are 820 × 320 μm with two inlets and two outlets. Blood is first injected into the inlet, then into the microscale, which encounters a quasi-electric field, causing blood cells to separate. During the filtering process, Newton's law of motion is employed as the primitive expression to define the particle orientation, which incorporates drag force, Brownian force, and DEP force. The finite element approach is used to solve the governing equation (FEM). Up to 3 s of transient analysis have been performed. Three different voltages (3, 5, and 7 V) were employed, with red blood cell diameters ranging from 3, 5, and 8 μm. The work concluded that the RBCs with a 5 μm diameter and an applied voltage of 5 V produced an efficient segregation process.

Fig. 6 Particle trajectory during filtering for various RBC diameters at t = 3 s with a 5 V applied voltage. (The red hue denotes RBCs, whereas the blue tint denotes Platelets) [8]

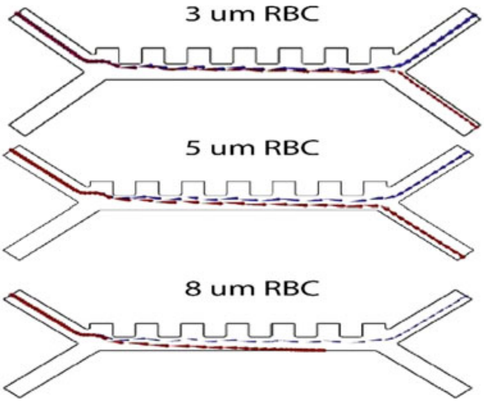

Sahin et al. utilized microfluidic technology to obtain RBCs from B-lymphocytes (B-Cells). Di-electrophoresis is a method to handle and isolate micron-scaled substances. RBCs and B-Cells with circumferences of 8.8 m and 10.3 m are subjected to dielectrophoretic manipulation. A microdevice with a side electrode is simulated and the results are exhibited. RBCs and B-Cells could be separated with a magnitude of 10 kHz and a stream rate of 1.5 L/s. RBCs and B-Cells could be separated with 98 percent efficiency using an induced electric potential of 0.06 V [60].

Salahi et al. showed the use of RBCs as heterogeneous particles with carefully controlled subcellular electrodiagnosis with related fluorescence intensity is described in this paper. Each customized RBC form could recognize unicellular sensitivity relying on phenomenological resistance indicators which are equipped with electrical designs to quantify rheological statistics employing glutaraldehyde fusion to alter membrane capability and membrane resealing beyond electrolyte invasion to transform inner cytosolic conductivity and fluorescence in a congruent fashion as shown in Fig. 7. Mono cell resistance data from unfamiliar erythrocyte variants can be mapped against these models, allowing for the quick assessment of subcellular physical and biological data and DEP sorting circumstances unaccompanied by the use of tedious algorithms with unfamiliar parameters [61].

The computer-aided design modeling of a microfluidic channel capable of isolating thrombocytes and erythrocytes from other blood cells is presented by Praveen et al. [62] as shown in Fig. 8. The use of negative dielectrophoretic (n-DEP) force in combination with drag force allows for separation based on their sizes. Within the microchannel, a 38° angled electrode array separated by 70 μm is developed and studied for quasi-electric field distribution. The projectile trajectories module simulates particle motion inside the microchannel under an induced electric field to show separation. The CM factor, n-DEP force, and drag forces are calculated using numerical research. The work concluded that the electrode with an applied electric potential of 5 V, electrode array angle of 38°, and a displacement of 70 μm can be used for the efficient separation of RBCs from blood platelets.

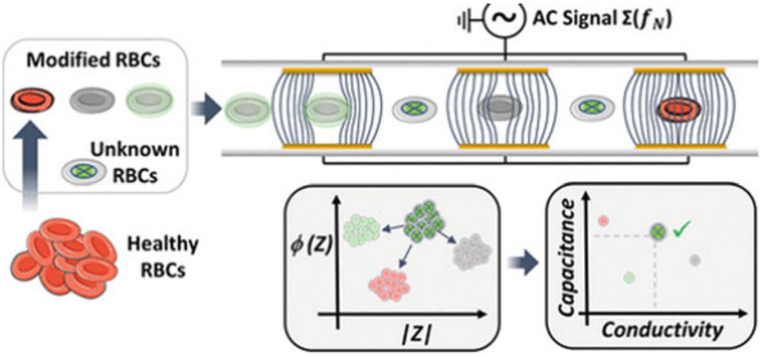

Fig. 7 Subcellular electrical prediction of RBCs with relevance to fluorescence intensity [61]

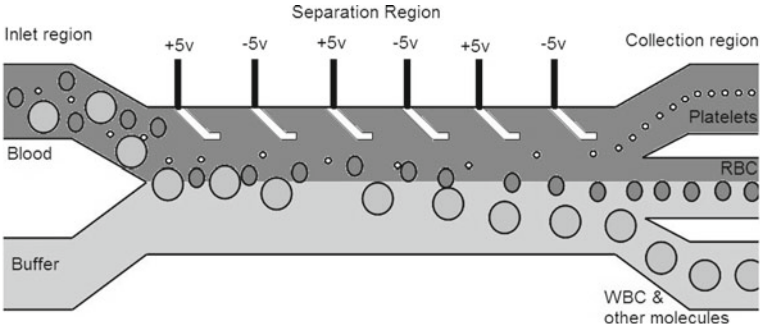

Fig. 8 The figure depicts the behavior of distinct blood molecules under a 5 V applied voltage of a di-electrophoretic-based microfluidic channel

Shirmohammadli et al. constructed a microfluidic device for the analysis of divergent electrodes in a DEP-based microfluidic device for cell segregation as shown in Fig. 9 [63]. This study eliminates the need for initial RBC lysis by separating MCF-7 tumor cells from leukocytes and erythrocytes. The differential electrodes not only successfully suppressed the requirement for high applied voltages via dc di-electrophoresis but also reduced the joule heating effects, according to numerical simulation findings. Aside from that, the configuration of the divergent electrodes was shown to have a significant impact on separation performance. Designing the outputs, as well as altering the electrode voltage, has made it possible for the gadget to be tunable for a variety of cancer cells with varying radii. More importantly, the device's capacity to deflect waste cells (WBCs and RBCs) out of the porous channel before cancer cells has been shown to improve separation efficiency and purity. The suggested system was capable of discerning distinct cells with grab purity and accuracy of more than 83 percent and 100 percent, respectively, using varied diameters.

Amir et al. designed a trapezoidal microfluidic device for cell segregation of blood by acoustic force [64]. Unlike prior research in which the stream was rectangular, the channel in this article is trapezoidal to improve the dissolution rate. WBC's position from the axis will change when the trapezoidal leg tilt changes. A Bio-MEMS channel with two inlets for sheath flow and blood particulates, a trapezoidal main conduit, and three exits was created as shown in Fig. 10. On the LiNbO3 substrate, there are two aluminum interdigital transducers. We used alternating voltage on transducers to generate the acoustic force. Because of the positive acoustic distinction factor, blood particles will be pushed toward the acoustic nodes. Because acoustic radiation force is proportional to particle size and compressibility, cells may be sorted by diameter and compressibility, terminating in particle separation. The work modified the trapezoidal channel tilt, the input signal, and the fluid velocity to optimize the device.

Zhao et al. demonstrated how to separate nano/microparticles using a high-performance, detachable acoustofluidic platform as shown in Fig. 11. The

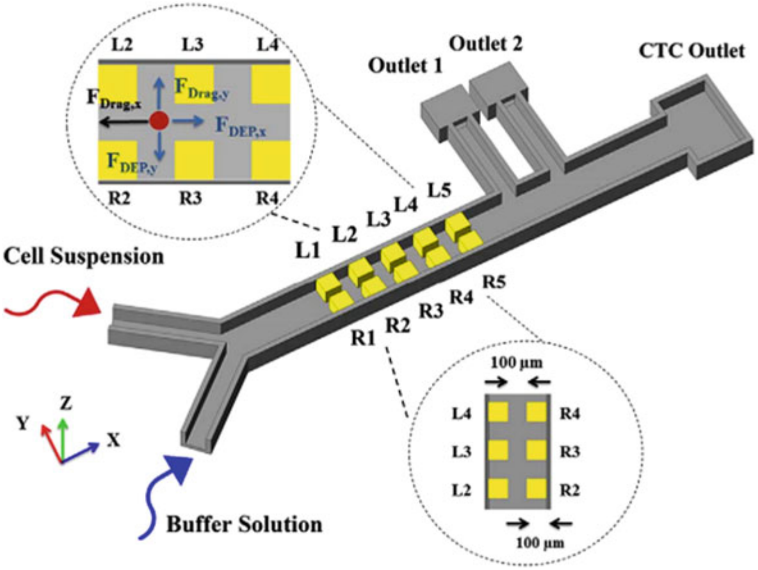

Fig. 9 The figure illustrates the proposed device for cell separation with two inlets for buffer and cell suspension. The WBCs and RBCs will flow to outlets 1 and 2 with MCF-7 cells flowing directly to the CTC outlet [63]

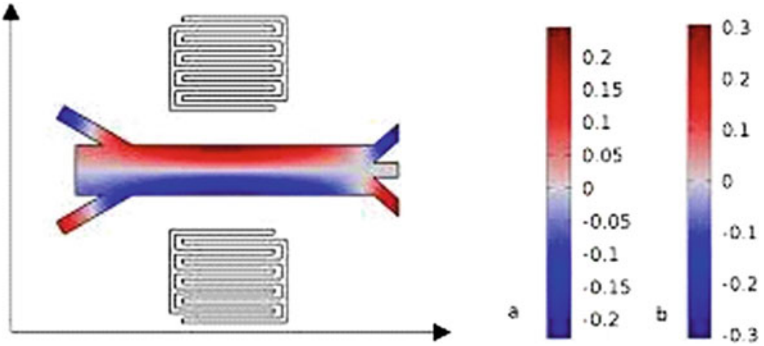

Fig. 10 Top view of the device with tilt angle = π/20 [66]

proposed expendable acoustofluidic devices accomplish acoustic radiation forces similar to those engendered by emerging permanently bound, non-disposable devices by utilizing unidirectional interdental transducers (IDTs), a blended path design with hard/soft materials, and tilted-angle standing SAWs (taSSAWs). Not only microparticles, but even nanoparticles may be separated using our disposable instruments. Furthermore, they can distinguish pathogens from human erythrocytes with up to 96 percent purity. Overall, we created a disposable acoustofluidic platform based

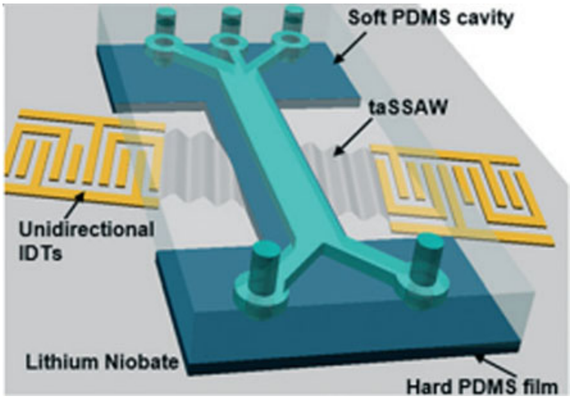

Fig. 11 Proposed design of detachable acoustofluidic isolation chip utilizing a single direction IDT-based design [65]

on unidirectional IDT for micro/nanoparticle separation that has good separation efficiency, adaptability, and biocompatibility [65].

Mantegazza et al. proved that in a sophisticated in vitro network with homogeneous bifurcations and 176 microchannels, quantifiable data for phase separation was acquired. The investigations revealed that hematocrit is heterogeneously distributed, confirming the traditional finding that the branch with the highest blood fraction also had the highest RBC fraction (classical partitioning). In the event of a distorted hematocrit pattern in the parental vessels of bifurcations, a reversal of this traditional phase transition (reverse partitioning) was found [23]. They constructed a microfluidic device with an inlet and outlet that comprises 49 hexagon components as shown in Fig. 12. The flow was generally going from left to right. The microchannels were 10 μm wide, 8 μm in height, and 85 μm long. A conventional microscopic field of view of 512 × 512 pixels is represented by the picture at the bottom right. The work concluded that the RBC flux fractions were frequently over proportional in branches with larger blood flow fractions.

Zhang et al. proposed a microfluidic device for the segregation of RBCs from platelets. The study offers a particle separation di-electrophoresis microfluidic device that exploits dielectric characteristics to size-based fractionate red blood cells and platelets. Using COMSOL Multiphysics, the propagation of the electron beam in the device and the trajectory of the particulates in the capillary are estimated for various electrode geometries, voltages, and chip exit configurations based on the control variables. Negative di-electrophoresis, which uses an AC signal of 100 kHz, affects both erythrocytes and platelets. The platelets flow out of the left nozzle under the joint effect of fluid force and DEP force, whereas the bigger RBCs are subjected to a higher DEP force and are skewed toward the right outlet as shown in Fig. 13. On this premise, a more optimized microfluidic chip capable of properly separating particles is eventually selected via statistical analysis [66].

Eugen et al. designed a microfluidic device for the isolation of CTCs (Circulating tumor cells) from RBCs using DEP. The device is modeled in a way that it has one inlet and three outlets. The interdigital electrodes provide a quasi-alternate electric field

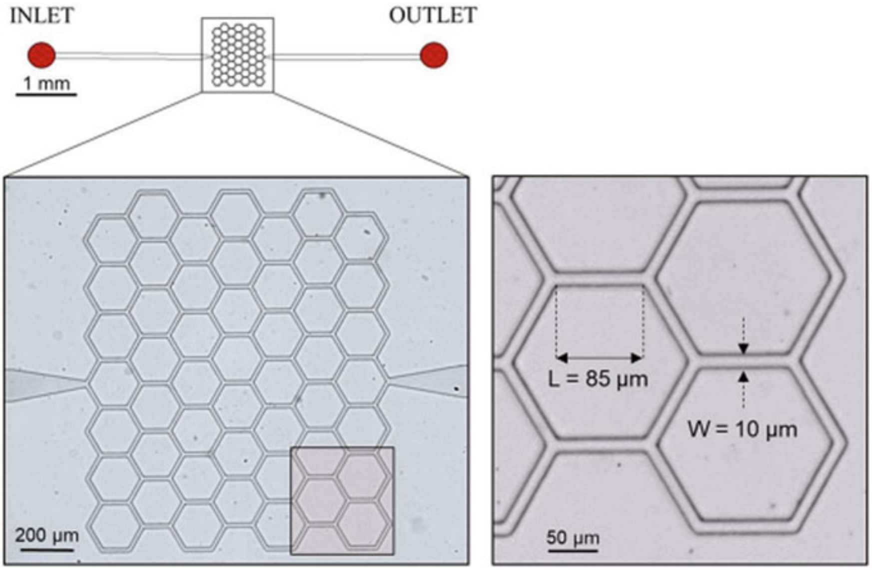

Fig. 12 The figure depicts the top view of an enlarged microfluidic device with a mono inlet and outlet

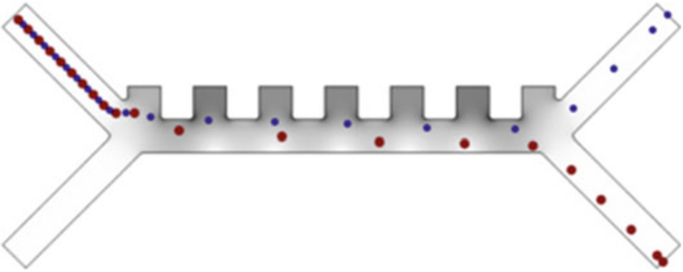

Fig. 13 The figure encapsulates the separation of RBCs from platelets using DEP force [66]

that isolates the biological particles within the device from the appropriate terminal as shown in Fig. 14. Simulations were carried out with COMSOL Multiphysics. In the simulation, the CTCs and RBCs are modeled as spheres with afferent attributes. The work concluded that the RBCs move through the first zone of strong electric field contours and toward the outlet with negative electric potential due to its initial momentum. While the CTC particle attaches directly to the electrodes and proceeds over the high electric field gradient zone, propelled by its initial velocity. The particle, however, remains connected to the electrodes in this situation and does not meet the predicted exit, as in Fig. 15 [67]. This research might be expanded to include testing numerous CTC lines at different flow rates and electric field frequencies.

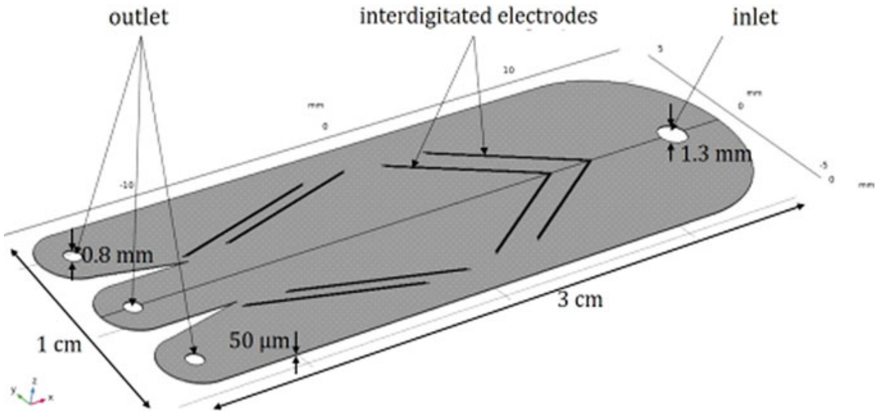

Fig. 14 The figure illustrates the proposed DEP device for the segregation of CTCs from RBCs

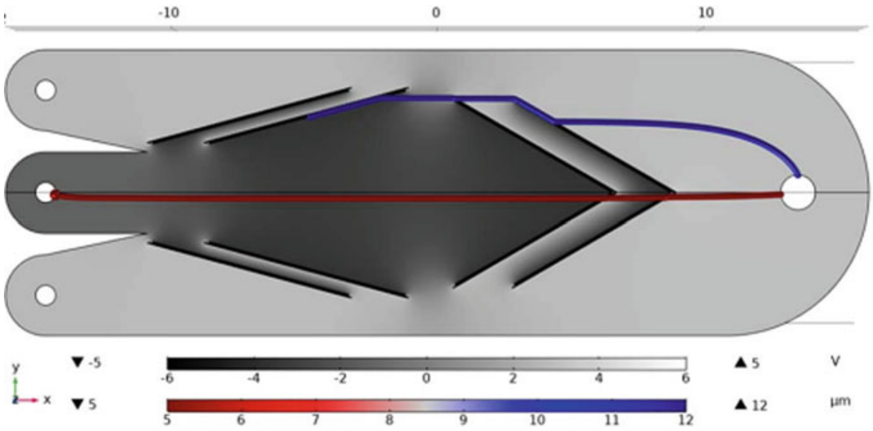

Fig. 15 Figure depicts particle trajectories at t = 300 s, CTC: blue, RBCs: red, and electric potential: greyscale

8 Conclusion

The review focused on the microfluidic devices and old approaches that were utilized to separate RBCs and their limitations. Red blood cell separation is used to identify sickle cells. The RBCs in the blood have a big volume and can be easily separated by centrifugation. However, centrifugation necessitates the use of bulky equipment and large samples. The bottleneck of the traditional approaches can be overcome by microfluidic devices. Microfluidics is a well-known technology with unique characteristics that have the potential to revolutionize illness detection and treatment. It has been well established for micron-sized particle sorting because it provides a comparatively simple, low-cost, and continuous particle separation technique.

Microfluidic devices are subtle in the areas of biomedical applications. Moreover, this technique demonstrates a new concept for particle-sorting applications in medical biology for its simplicity and efficiency. Microfluidic devices use techniques like di-electrophoresis for cell sorting. In the fields of biomedical and biosensors, the DEP force has numerous uses which are used to separate RBCs utilizing microfluidics have been discussed in this review. RBC separation using DEP demonstrates how RBCs can be selectively filtered from a blood sample. RBCs, which seem to be larger than other blood cells, are exposed to a greater force and are therefore deflected more. But the short come of DEP force is that it fails for large-size RBC particles [8]. Furthermore, the recent microfluidic devices that are used to isolate RBCs occupy a large area and have high power consumption [8, 23, 54, 60–67]. Hence, future works will focus on novel approaches for RBC particle isolation that is independent of size, optimization of the device, affordability, and low power consumption.

Acknowledgements The authors would like to thank the Department of Electronics and Communication Engineering, Velagapudi Ramakrishna Siddhartha Engineering College for providing the necessary infrastructure.

References

1. Waugh A, Grant A (2014) Ross & Wilson anatomy and physiology in health and illness E-book. Elsevier Health Sciences
2. Pal GK, Pal P, Nanda N (2016) Comprehensive textbook of medical physiology-two volume set. JP Medical Ltd
3. Pearson HA (1967) Life-span of the fetal red blood cell. J Pediatr 70(2):166–171
4. Turrigiano G (2007) Homeostatic signaling: the positive side of negative feedback. Curr Opin Neurobiol 17(3):318–324
5. Bunn HF (2013) Erythropoietin. Cold Spring Harb Perspect Med 3(3):a011619
6. Saba TM (2018) Fibronectin: role in phagocytic host defense and lung vascular integrity. In: Fibronectin in Health and Disease. pp 49–68
7. Weaver L, Hamoud AR, Stec DE, Hinds TD Jr (2018) Biliverdin reductase and bilirubin in hepatic disease. Am J Physiol Gastrointest Liver Physiol 314(6):G668–G676
8. Mitra S, Rahman MH, Prince HA, Rozin EH (2020) Numerical investigation on dielectrophoresis blood cell separation for different applied voltage and red blood cell size. In: 2020 IEEE Region 10 Symposium (TENSYMP). IEEE, pp 730–733
9. Danon D, Marikovsky Y (1964) Determination of density distribution of red cell population. J Lab Clin Med 64(4):668–674
10. Piomelli S, Lurinsky G, Wasserman LR (1967) The mechanism of red cell aging. I. Relationship between cell age and specific gravity evaluated by ultracentrifugation in a discontinuous density gradient. J Lab Clin Med 69(4):659–674
11. Corash LM, Piomelli S, Chen HC, Seaman C, Gross E (1974) Separation of erythrocytes according to age on a simplified density gradient. J Lab Clin Med 84(1):147–151
12. Vettore L, De Matteis MC, Zampini P (1980) A new density gradient system for the separation of human red blood cells. Am J Hematol 8(3):291–297
13. Marikovsky Y, Danon D (1971) Agglutination of young and old human red cells by blood group antibodies. Vox Sang 20(2):174–177
14. Bartos HR, Desforges JF (1967) Enzymes as erythrocyte age reference standards. Am J Med Sci 254(6):862–865

15. Walter H, Krob EJ, Garza R (1968) Factors in the partition of red blood cells in aqueous dextran-polyethylene glycol two-phase systems. Biochim Biophys Acta (BBA)-Gen Subj 165(3):507–514
16. Costa JAV, de Morais MG (2014) An open pond system for microalgal cultivation. In: Biofuels from algae. Elsevier, pp 1–22
17. Rigas DA, Koler RD (1961) Ultracentrifugal fractionation of human erythrocytes on the basis of cell age. J Lab Clin Med 58:242–246
18. Boyd EM, Thomas DR, Horton BF, Huisman THJ (1967) The quantities of various minor hemoglobin components in old and young human red blood cells. Clin Chim Acta 16(3):333–341
19. Pertoft H, Bäck O, Lindahl-Kiessling K (1968) Separation of various blood cells in colloidal silica-polyvinylpyrrolidone gradients. Exp Cell Res 50(2):355–368
20. Desimone J, Kleve L, Shaeffer J (1974) Isolation of a reticulocyte-rich fraction from normal human blood on renografin gradients. J Lab Clin Med 84(4):517–524
21. Goebel KM, Goebel FD, Schubotz R, Schneider J (1977) Red cell metabolic and membrane features in haemolytic anaemia of alcoholic liver disease (Zieve's syndrome). Br J Haematol 35(4):573–585
22. Danon D, Marikovsky Y (1961) Difference de charge electrique de surface entre erythrocytes jeunes et ages. Comptes Rendus Hebd Seances L Acad Sci 253(12):1271
23. Mantegazza A, Clavica F, Obrist D (2020) In vitro investigations of red blood cell phase separation in a complex microchannel network. Biomicrofluidics 14(1):014101
24. Dennison C, Lovrien R (1997) Three phase partitioning: concentration and purification of proteins. Protein Expr Purif 11(2):149–161
25. Whitesides GM (2006) The origins and the future of microfluidics. Nature 442(7101):368–373
26. Weibel DB, Whitesides GM (2006) Applications of microfluidics in chemical biology. Curr Opin Chem Biol 10(6):584–591
27. Beebe DJ, Mensing GA, Walker GM (2002) Physics and applications of microfluidics in biology. Annu Rev Biomed Eng 4(1):261–286
28. Groisman A, Lobo C, Cho H, Campbell JK, Dufour YS, Stevens AM, Levchenko A (2005) A microfluidic chemostat for experiments with bacterial and yeast cells. Nat Methods 2(9):685–689
29. Balagaddé FK, You L, Hansen CL, Arnold FH, Quake SR (2005) Long-term monitoring of bacteria undergoing programmed population control in a microchemostat. Science 309(5731):137–140
30. Lee H, Purdon AM, Chu V, Westervelt RM (2004) Controlled assembly of magnetic nanoparticles from magnetotactic bacteria using microelectromagnets arrays. Nano Lett 4(5):995–998
31. Weston AD, Hood L (2004) Systems biology, proteomics, and the future of health care: toward predictive, preventative, and personalized medicine. J Proteome Res 3(2):179–196
32. Reyes DR, Iossifidis D, Auroux PA, Manz A (2002) Micro total analysis systems. 1. Introduction, theory, and technology. Anal Chem 74(12):2623–2636
33. Gravesen P, Branebjerg J, Jensen OS (1993) Microfluidics-a review. J Micromech Microeng 3(4):168
34. Whitesides G, Stroock A (2001) Flexible methods for microfluidics. Phys Today 54:42–48
35. Jakeway SC, de Mello AJ, Russell EL (2000) Miniaturized total analysis systems for biological analysis. Fresenius J Anal Chem 366(6):525–539
36. Ho CM, Tai YC (1998) Micro-electro-mechanical-systems (MEMS) and fluid flows. Annu Rev Fluid Mech 30:579–612
37. Becker H, Gärtner C (2000) Polymer microfabrication methods for microfluidic analytical applications. ELECTROPHORESIS Int J 21(1):12–26
38. Brody JP, Yager P, Goldstein RE, Austin RH (1996) Biotechnology at low Reynolds numbers. Biophys J 71(6):3430–3441
39. Purcell EM (1977) Life at low Reynolds number. Am J Phys 45(1):3–11
40. Flow VF (1991) Frank M. White

41. Brody JP, Yager P (1997) Diffusion-based extraction in a microfabricated device. Sens Actuat A 58(1):13–18
42. Hatch A, Kamholz AE, Hawkins KR, Munson MS, Schilling EA, Weigl BH, Yager P (2001) A rapid diffusion immunoassay in a T-sensor. Nat Biotechnol 19(5):461–465
43. Yeo LY, Chang HC, Chan PP, Friend JR (2011) Microfluidic devices for bioapplications. Small 7(1):12–48
44. Ren K, Zhou J, Wu H (2013) Materials for microfluidic chip fabrication. Acc Chem Res 46(11):2396–2406
45. Friend J, Yeo L (2010) Fabrication of microfluidic devices using polydimethylsiloxane. Biomicrofluidics 4(2):026502
46. Catarino SO, Rodrigues RO, Pinho D, Miranda JM, Minas G, Lima R (2019) Blood cells separation and sorting techniques of passive microfluidic devices: from fabrication to applications. Micromachines 10(9):593
47. Haeberle S, Zengerle R (2007) Microfluidic platforms for lab-on-a-chip applications. Lab Chip 7(9):1094–1110
48. Rife JC, Bell MI, Horwitz JS, Kabler MN, Auyeung RCY, Kim WJ (2000) Miniature valveless ultrasonic pumps and mixers. Sens Actuat A 86(1–2):135–140
49. Yc F (1997) Biomechanics: circulation
50. Roselli RJ, Diller KR (2011) Biotransport: principles and applications. Springer, New York, p 139
51. Mohamed H (2012) Use of microfluidic technology for cell separation. In: Blood cell-an overview of studies in hematology, pp 195–226
52. Shields CW IV, Reyes CD, López GP (2015) Microfluidic cell sorting: a review of the advances in the separation of cells from debulking to rare cell isolation. Lab Chip 15(5):1230–1249
53. Kersaudy-Kerhoas M, Sollier E (2013) Micro-scale blood plasma separation: from acoustophoresis to egg-beaters. Lab Chip 13(17):3323–3346
54. Bharat et al (2020) Modelling of dielectrophoretic separation platelets from red blood cells. ISSN 2394–5125
55. Pethig R (2010) Dielectrophoresis: Status of the theory, technology, and applications. Biomicrofluidics 4(2):022811
56. Khoshmanesh K, Nahavandi S, Baratchi S, Mitchell A, Kalantar-zadeh K (2011) Dielectrophoretic platforms for bio-microfluidic systems. Biosens Bioelectron 26(5):1800–1814
57. Demircan Y, Özgür E, Külah H (2013) Dielectrophoresis: applications and future outlook in point of care. Electrophoresis 34(7):1008–1027
58. Li M, Li WH, Zhang J, Alici G, Wen W (2014) A review of microfabrication techniques and dielectrophoretic microdevices for particle manipulation and separation. J Phys D Appl Phys 47(6):063001
59. Jubery TZ, Srivastava SK, Dutta P (2014) Dielectrophoretic separation of bioparticles in microdevices: a review. Electrophoresis 35(5):691–713
60. Sahin O, Kosar A, Yapici MK (2021) Modeling the dielectrophoretic separation of red blood cells (RBCs) from B-Lymphocytes (B-Cells). In: 2021 43rd annual international conference of the IEEE engineering in medicine & biology society (EMBC). IEEE, pp 1238–1241
61. Salahi A, Honrado C, Rane A, Caselli F, Swami NS (2022) Modified red blood cells as multimodal standards for benchmarking single-cell cytometry and separation based on electrical physiology. Anal Chem 94(6):2865–2872
62. Praveenkumar S, Srigitha SN, Dinesh RG, Ramesh R (2020) Computational modeling of dielectrophoretic microfluidic channel for simultaneous separation of red blood cells and platelets. Curr Signal Transduct Ther 15(3):243–251
63. Shirmohammadli V, Manavizadeh N (2019) Application of differential electrodes in a dielectrophoresis-based device for cell separation. IEEE Trans Electron Devices 66(9):4075–4080
64. Shamloo A, Parast FY (2019) Simulation of blood particle separation in a trapezoidal microfluidic device by acoustic force. IEEE Trans Electron Devices 66(3):1495–1503

65. Zhao S, Wu M, Yang S, Wu Y, Gu Y, Chen C, Huang TJ (2020) A disposable acoustofluidic chip for nano/microparticle separation using unidirectional acoustic transducers. Lab Chip 20(7):1298–1308
66. Zhang Y, Chen X (2020) Dielectrophoretic microfluidic device for separation of red blood cells and platelets: a model-based study. J Braz Soc Mech Sci Eng 42(2):1–11
67. Chiriac E, Avram M, Bălan C (2020) Dielectrophoretic separation of circulating tumor cells and red blood cells in a microfluidic device. In: 2020 International semiconductor conference (CAS). IEEE, pp 211–214

A Road Map to Paper-Based Microfluidics Towards Affordable Disease Detection

Mareedu Nagavalli, Tatineni Sharmila Swaroopa, Pannangi Sri Vidya Gayathri, Vuyyuru Dinesh Kumar Reddy, Nanda Sai Donepudi, Dhanya Yalamanchili, Koushik Guha, and Jasti Sateesh

Abstract Microfluidic technology (µF) is an approach in managing very small volumes of fluids through patterned tiny channels. The present chapter focuses on the importance of designing microfluidic systems, their capabilities, and their applications. As microfluidic diagnostics are complex and unaffordable, paper-based microfluidic technology has become viable for low-cost disease diagnosis. The branch of microfluidics that manages very small amounts of fluids through capillary action and are made of paper and porous materials are termed paper-based microfluidics (PBM). This review chapter mainly illustrates the significance of PBM devices and their capabilities, applications, and advantages over microfluidics. Diagnostic applications in the detection of chronic diseases, cancer, dengue, glucose, and tuberculosis with µF and µPAD are also reviewed to the finest level in this review. In the current scenario, Artificial Intelligence (AI) and Internet of Things have become an integral part of every technology. Integration of µF and µPAD with IoT and AI aids to produce better design considerations, which are also covered in this review.

Keywords Microfluidics · Paper-based microfluidics · Disease diagnosis · And affordable diagnostics

---

M. Nagavalli · T. Sharmila Swaroopa · P. Sri Vidya Gayathri · V. D. K. Reddy · J. Sateesh (✉)
Department of Electronics and Communication Engineering, Velagapudi Ramakrishna Siddhartha Engineering College, Kanuru, Vijayawada, Andhra Pradesh 520007, India
e-mail: jastisateesh@vrsiddhartha.ac.in

N. S. Donepudi · D. Yalamanchili
Siddhartha Government College and Hospital, Vijayawada 520008, India

K. Guha
Deparment of Electronics and Communication Engineering, National Institute of Technology Silchar, Assam 780010, India

K. Guha et al. (eds.), *MEMS and Microfluidics in Healthcare*, Lecture Notes in Electrical Engineering 989, https://doi.org/10.1007/978-981-19-8714-4_4

1 Microfluidics

1.1 Introduction to Microfluidics

Life-threatening diseases such as cancer, dengue, and TB cannot be rapidly diagnosed using various microscopy techniques. Microfluidics plays a vital role in such micro-level disease detection by utilizing channels with dimensions of 0.1 times micro meters [1]. The main objective of microfluidic technology is to provide a single platform from the input of samples to the disclosure of diagnostic results. Other technologies used for the diagnosis of a disease cannot produce rapid response, so microfluidic systems are also denominated as μTAS (micro-total analysis systems), LOC (Lab-On-Chip), and biochip devices [2]. In macroscopic systems, performing single-cell assays and parallelized experiments is very difficult. Miniaturization of microfluidics became the only solution for all those drawbacks and has numerous advantages which include reduced utilization of sample and reagents, minimized cost of reagent, narrowing the risk of contamination, decreasing the cost of analysis, and increasing throughput [1]. With numerous proven and pertinent applications within the areas of biological sciences, engineering sciences, genomics, chemical sciences, proteomics, and biodefence, microfluidics evolved as the dominant technology [3]. During the early days of microfluidics, most of the devices are fabricated using silicon material. Later, silicon is replaced with polymer materials like Polymethylmethacrylate (PMMA) [4], Polystyrene (PS) [5], Polycarbonate (PC) [6], and Polydimethylsiloxane (PDMS) [7]. Among all these polymer materials, PDMS is currently used for fabricating microfluidic devices in laboratories due to its easy cloning, transparency, biocompatibility, and low cost [5]. Microfluidic devices fabricated with PDMS have various biomedical applications, namely DNA analysis, immunochemical assays, and cell-based assays [8–19].

1.2 Applications of Microfluidics

Microfluidics has expanded applications in the areas of molecular and clinical diagnostics [21], neuronal studies [22], biological sciences such as chemical biology [23, 24], quantitative biology [25], stem cell biology [26], and fluid mechanics. One of the widely used applications is the LOC devices. A LOC device integrates one or more operations on a single integrated circuit as shown in Fig. 1.

This device performs various operations and processing steps that include sample separation viz. electrophoresis, molecular exclusion, and liquid chromatography. Applications of microfluidic devices in biological systems include the delivery of drugs, microscopic sensors, namely cellular-level quantum dots, and nano-scaled electrodes [29–36]. Furthermore, there exist a few other applications of microfluidics including C. elegans immobilization [37], pH control [37], drug administering [37],

Fig. 1 A microfabricated system for aligning miniature molecules with intracellular resolution [24]. Reproduced with permission from Weibel, Douglas B., and George M. Whitesides. *Current opinion in chemical biology* 10.6 (2006): 584–591

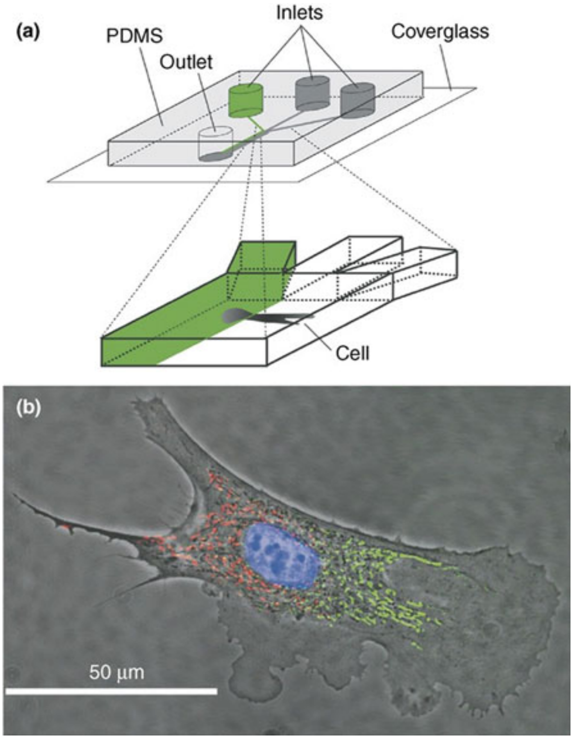

gradients generation [37], point-of-care devices [37], and cell analysis [37]. Applications of microfluidics also stretch in chemical biology which includes microdilution, gel structures, droplets, cell painting, and the study of single cells [24]. Stem cell biology using microfluidics has extended its wings widely for a decade that includes high throughput screening and regeneration of stem cell physiological environment such as differentiation and isolation [26]. In microfluidic devices, molecular diagnostics are extensively used in pathogen detection. This technique also helps in the detection of cancer and diagnosis of diseases caused by bacteria and viruses such as HIV, Cholera, and Syphilis [21].

1.3 Capabilities of Microfluidics

All the microfluidic devices designed for diagnosis are aimed at the detection of a single disease. However, diagnostic devices have to be capable of detecting multiple diseases to satisfy market needs [21]. In today's world, 95% of mortality is due to inadequate diagnostics and lack of treatment-providing centres for many infectious diseases like HIV, COVID-19, AIDS, TB, etc. [27]. To date, epidemics like the 2009 H1N1 influenza and 2019 COVID have highlighted the necessity of rapid diagnostic tools to restrain transmittable diseases [28]. The critical analysis of the physiological and pharmacological responses at one-cell level can be achieved by microfluidic platforms [22]. Microfluidics can minimize monotonous operations; increase sensitivity, specificity, and reliability, and reduce the time of analysis [1]. They can also diagnose and segregate the molecular components when analytical devices require high resolution and smaller footprints. Microfluidics has the capability of regulating the concentration of molecules in analytical devices.

2 Paper-Based Microfluidics

2.1 Introduction to Paper-Based Microfluidics

Paper-based microfluidics is the sub-division of microfluidic technology, where the devices are made using paper to manage a small quantity of fluids via capillary forces [39]. PBM is also termed lab-on-paper or μPAD [38]. For decades, analytical chemistry uses paper as the basic platform, and various forms of highly engineered paper with various distinct properties are also used [44]. Paper became an attractive substrate because of the following reasons: (1) easy availability, (2) very cheap cellulose material, (3) transports tiny amounts of fluids with capillary forces, and (4) biocompatibility [38]. Capillary pressure generates the flow that results in capillary formation in the material by cellulose fibre wetting. In paper devices, capillary flow rate, thickness, size, and permeability (porosity) are some of the factors determining fluidic flow. There are microchannels that are built on the paper substrate so that fluid flows in a controlled manner [38] as shown in Fig. 2. In Fig. 2 below is a paper-based microfluidic (PBM) device fabricated by photolithography; urine is given as a sample to that device. Fabrication of μPAD involves the patterning of hydrophobic barriers on paper to generate hydrophilic microchannels. In Fig. 3, using a wax pencil a microchannel is patterned on laboratory paper and a kitchen towel. Microchannel is patterned on one side of the laboratory paper in one case and in the next case, it is patterned on either side, and in the other it is patterned on the kitchen towel. On single-sided laboratory paper, fluid leakage can be observed and on double-sided laboratory paper smooth flow can be observed whereas on kitchen towel incomplete wax diffusion occurs so fluid leakage can be observed [41].

Paper-based microfluidics has various applications that include testing of food quality, environment monitoring, and health diagnostics and have potential advantages like minimal cost, speed detection, user friendliness, biocompatibility, sensitivity, specificity, etc.

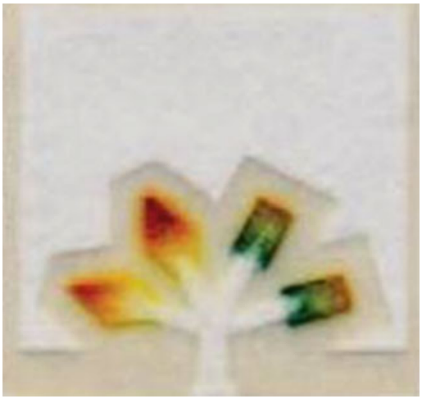

Fig. 2 Paper-based analytical microfluidic device schematics that can detect glucose and protein in urine simultaneously [40]. Reproduced with permission from Journal of biological engineering 5.1 (2011): 1–22

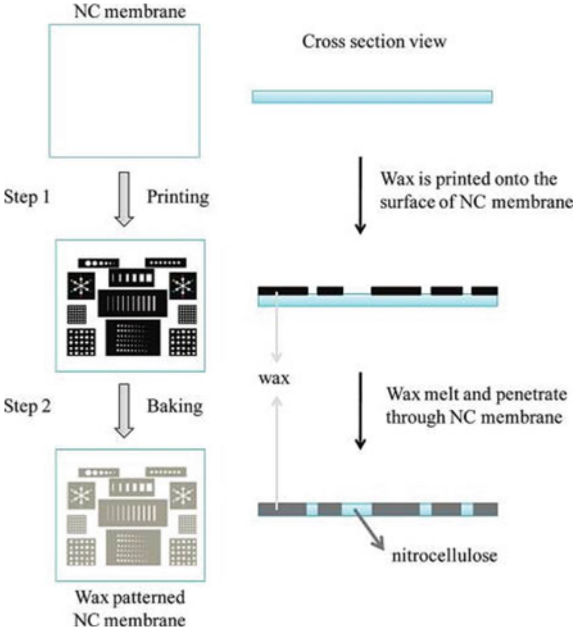

Fig. 3 To design a paper-based microfluidic device in a Nitro Cellulose (NC) membrane using wax printing [41]. Reproduced with permission from Lu, Y., Shi, W., Qin, J., & Lin, B. (2010). *Analytical Chemistry, 82(1), 329–335*

2.2 *Advantages of Microfluidics*

In comparison with other microfluidic devices, paper-based devices are sensitive and affordable and fit themselves into point-of-care (POC) testing because of natural disposability, situational flexibility, and capability to store and analyse the target at the site of requirement. The main reason for choosing paper as starting material for fabricating micro-analytical devices is that it wicks aqueous fluids. The fabricated paper-based device is used for numerous purposes such as recognition of dyes and pigments, and urine tests [43]. The wicking of liquid makes passive transport of fluids without active pumping on μPADs. In addition, paper has several other crucial advantages such as high bioavailability, being inexpensive, biodegradable, and biocompatible representing an alternate material for making diagnostic devices.

2.3 Capabilities

PBM is used for robust diagnostics which require less volume of fluid for testing. The paper which is made up of cellulose or polymers of cellulose controls the movement of fluids by slow capillary actions via pores without the help of any external actuation or pumps [45]. PBM can detect nucleic acid which helps in disease detection such as cancer [48]. Open channel microfluidics can be created with the help of paper microfluidics which enables water–oil emulsification by controlling the speed of fluids. It also creates a preferable size of the emulsion particle such that it can be integrated into a drug or tablet [49]. In the delivery of the drug to the target site at the correct times, paper-based microfluidics plays a crucial role [51]. PBM also helps to manage the rate of flow of drugs and studies the effectiveness of drug and their side effects at different concentrations [50, 51]. Long channels can be created through a micropatterning technique by wax printing in PBM [53]. Micropatterning leads to the creation of POC testing which diagnoses the condition of patients at their location [54]. To improve the diagnosis of disease at an earlier stage of the development, an amplification strategy under isothermal conditions is required such as Loop Mediated Isothermal Amplification (LAMP) which is highly compatible with POC analysis. The use of LAMP-based technology along with paper-based microfluidics results in the development of portable POC nucleic acid assays that can amplify the DNA/RNA which enables in the detection of diseases like malaria, pneumonia, Ziko virus, and food pathogens [57].

3 Paper and Its Materials

Paper is a thin sheet obtained by chemical and mechanical treatment of cellulose fibres. Several sources of cellulose fibres such as cotton, bamboo, grass, and wood have been used for obtaining μPADs [58]. The finest quality of cotton which contains 98% of α-cellulose is used for the manufacturing of chromatography and filter papers [59]. The chromatography paper helps to identify the amino acids, bases, proteins, and low concentrations of DNA/RNA [46]. In Fig. 4, a PBM device is fabricated to measure the least functioning hydrophilic channel that has Grade 1 Chromatography paper as substrate [53].

Paper which is made from pure cotton is widely used for diagnostic purposes. Whatman chromatography paper, nitrocellulose membrane/paper, Whatman filter paper, and Whatman 105 lens paper are the most commonly used papers for the

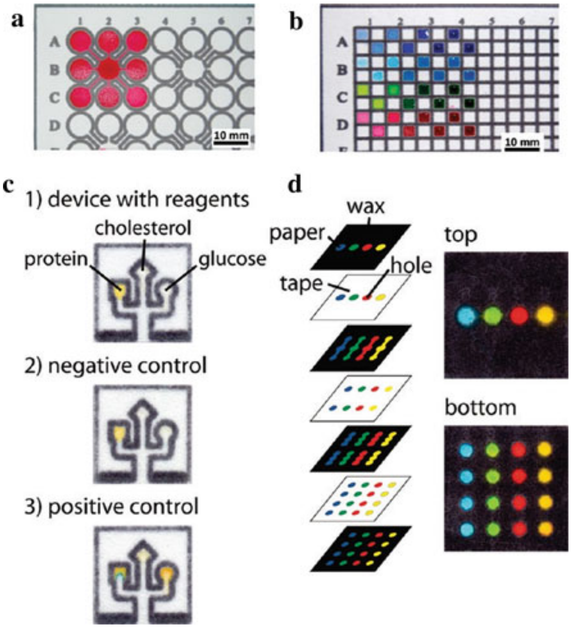

Fig. 4 Examples of wax-printed Micro Paper-based Analytical Devices (μPADs) [53]. Reproduced with permission from Carrilho, E., Martinez, A. W., & Whitesides, G. M. (2009). Analytical Chemistry, 81(16), 7091–7095

fabrication of PBM [38, 39, 60–65]. Nitrocellulose membrane/paper is a 3D porous structure that is ideal for protein immobilization and is made out of pure cellulose nitrate [61]. It has a smooth surface, homogeneous pore size (0.45 µm), and stable flow of liquid [38]. Hence, nitrocellulose membrane is used in numerous applications like western blotting, test strips based on gold nanoparticles, dot ELISA, DNA immobilization, protein immobilization, and cell immobilization [62, 65–70]. Whatman chromatography paper and Whatman filter paper belong to the family of cellulose-based paper [38]. Despite its hydrophilic nature, cellulose paper is widely used due to its affordability and rapid penetration of liquid [71]. Whatman filter is the most famous cellulose paper due to particle withholding capability, well-categorized rate of flow, and permeability. In 2007, the Whiteside group patterned Whatman filter paper was fabricated using the photolithography technique for colourimetric analyses of urine and protein pH [69]. Whatman filter and chromatography papers are categorized into four grades (Grades 1–4) depending on the pore size. Cellulose paper containing the maximum percentage of alpha-cellulose is used for making Whatman chromatography paper. Whatman filter paper is incompatible with normal filter paper in many ways. In comparison with normal filter paper, the Whatman filter paper is worthy and best for conducting qualitative analysis. Qualitative filter papers like Whatman filter paper are majorly based on diverse properties which include thickness, retention, and weight. In everyday applications, Grade 1 filter paper is the most commonly used filter paper for clarifying liquids. With an analogous increase in filtration time, Grade 2 filter paper is slightly more retentive than Grade 1. As Grade 3 filter paper is double the thickness of Grade 1, it can hold more precipitate without clogging and has improved wet strength that is well suited for sample transport after collection. For the retention of coarse particles and gelatinous precipitates, such as aluminium hydroxide, a fast filter material is used known as Grade 4 filter paper. Grade 5 filter paper provides the equivalent slow rate of flow. Whatman filter No 1 is a kind of filter paper whose pore size is 11 μm and allows medium flow rates [62]. Whatman filter No 4 also belongs to the Whatman filter paper family; it has a greater pore size (22–25 μm) and is ideal for etch printing fabrication techniques [65]. Whiteside patterned the Whatman chromatography paper with SU8 photoresist through photolithography for the detection of glucose and proteins simultaneously [69].

4 Applications

4.1 *Chronic Diseases*

Nowadays, diagnosis and monitoring of chronic diseases is a major challenge that requires established laboratory infrastructure and specialized instrumentation. The Most Common Chronic Diseases (CD) are chronic respiratory diseases (CRD), diabetes, and chronic kidney diseases (CKD) [72]. The diseases of the airways and other structures of the lung lead to chronic respiratory diseases (CRD). Some of the most common CRDs are pulmonary hypertension, chronic obstructive pulmonary disease (COPD), minor respiratory infections frequently, and asthma. For a person affected with CKD, their kidney gradually loses the filtering capacity of blood to eliminate wastes and also has several adverse effects like premature birth, kidney failure, cardiovascular disease, and, ultimately, death. The main causes of the most common chronic disease diabetes are insufficient insulin produced by the pancreas and the body’s inefficiency to properly utilize the produced insulin. Levels of blood sugar are regulated by the insulin hormone. Diabetes or diabetes mellitus (DM) is a metabolic disorder that has very high levels of blood sugar over a long period [73]. Nowadays, monitoring and diagnosis of chronic disease (CD) is a major challenge that requires established laboratory infrastructure and specialized instrumentation.

The moratorium on CD diagnosis leads to a significantly increased economic burden [74]. Among the existing laboratory clinical approaches, microfluidic technology gained increased engrossment over the past few decades due to the miniaturization of bioanalytical assays for improving diagnostic performance. In microfluidic technology, the prognosis, diagnosis, and monitoring of chronic disease require the measurement of biomarkers effectively [75–82]. Hepatitis C virus (HCV) belongs to the family of Flaviviridae, which is an RNA virus that accounts for acute infection. HCV is the primary basis of hepatocellular carcinoma and liver cirrhosis, causing a large number of deaths worldwide. The immunoassays of HCV are classified into 3

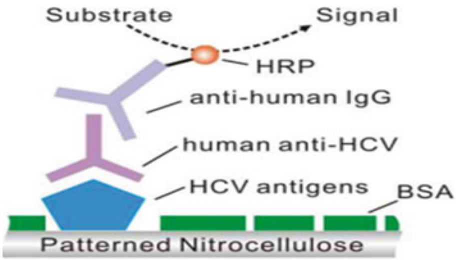

Fig. 5 For diagnosis and detection of anti-HCV using paper-based immunoassay [83]. Reproduced with permission from Mu, Xuan, et al. Analytical chemistry 86.11 (2014): 5338–5344

sub-divisions, targeting core antigen detection of HCV, antibody detection of anti-HCV, and multiple HCV antigen detection. Biomarker detection uses some conventional methods like mass spectrometry (MS), enzyme-linked immunosorbent assay (ELISA), polymerase chain reaction (PCR) chromatography, and gel electrophoresis [74–82]. It is expected that these contemporary approaches will be soon embraced and deployed in point-of-care (POC) settings leading to betterment in the patient's life quality.

In Fig. 5, ELISA Indirect is performed on patterned NC (nitro-cellulose) for detecting quantitative analysis of IgG. ELISA Indirect is considered as a two-step binding process that contains 1st antibody (primary) and enzyme-linked 2nd antibody (secondary) that is complementary to the primary. Incubation of 1st antibody with antigen is followed by 2nd antibody. Horseradish peroxidase (HRP) could catalyse substrate and produce a signal like colour precipitate or chemiluminescence as shown in Fig. 6.

4.2 Dengue

Dengue virus (DENV) is the most commonly encountered infection worldwide. Approximately 200 million people are infected every year due to DENV [84, 85]. DENV belongs to the family of flavivirus genus and people are exposed to dengue by Aedes mosquitoes. Four serotypes of DENV, i.e., DENV 1–4 are known. Dengvaxia and CYD-TDV are the WHO recommended Dengue vaccines for all 4 serotypes. Fever, rashes, and musculoskeletal pain are commonly experienced symptoms of DENV [86]. Numerous laboratory diagnostic tests exist for DENV detection which include hemagglutination-inhibition test, 50% plaque reduction neutralization test, viral isolation, enzyme-linked immunosorbent assay (ELISA), and molecular assays [87–93]. IgG (Immunoglobulin G), IgM (Immunoglobulin M), and NS1 (Non-structural protein 1) are the DENV markers; this simplifies the Paper Analytical Devices (PADs). IgG/IgM and NS1 diagnosis using lateral flow assays produce

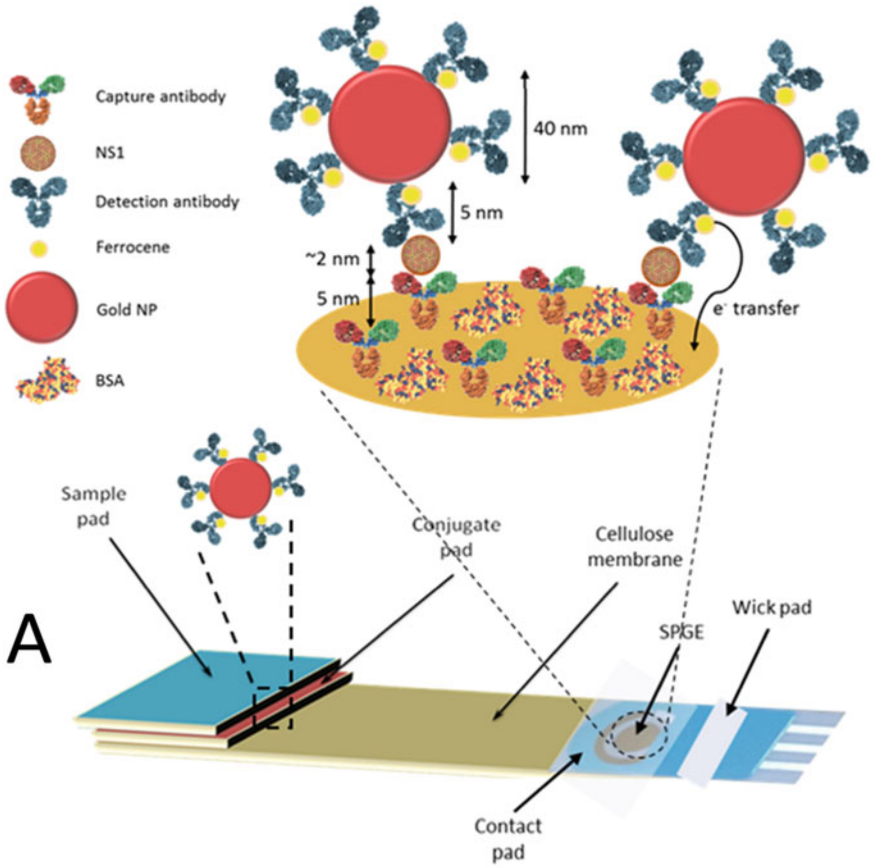

Fig. 6 Procedure of diagnosis of dengue in paediatric serum using paper-based microfluidics [86]. Reproduced with permission from Choi, Jane Ru, et al. *Biosensors and Bioelectronics* 74 (2015): 427–439

qualitative results [93–95]. Paper-based analytical microfluidic devices for diagnosis of DENV markers are fabricated using sandwich immunoassay on Grade 2 chromatography paper patterned with wax activated with antibodies of anti-dengue NS 1 monoclonal for the POC testing of NS1 dengue marker [86].

DEN-NS1-PAD (Paper Analytical Devices): Fig. 7 consists of four major areas of detection of DENV; those are sample, detection, conjugate, and absorbent areas. These areas are allied by a single channel which is bounded by a hydrophobic barrier patterned with wax. The sample given to the sample area absorbs over the channel. In the conjugate area, sample interacts with Gold Nanoparticle–Antibody Conjugates (AuNPs-Ab) and in the detection area sample interacts with anti-NS1antibody that shows dengue NS1 positive results; meanwhile, at the control spot AuNPs-Ab interacts with the captured antibody. Red colour generated at the test and control spots indicates that the given sample is dengue positive and that is observed by a scanner,

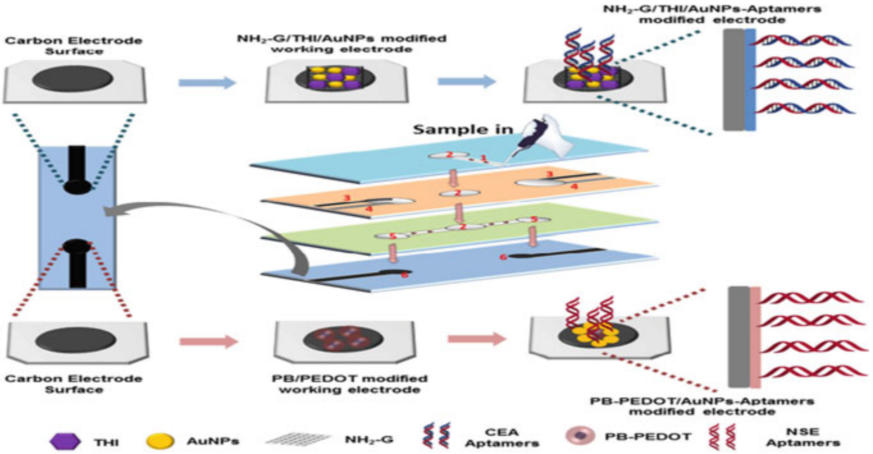

Fig. 7 Modification and fabrication procedure of electrochemical paper-based aptasensors [98]. Reproduced with permission from Wang, Yang. Biosensors and Bioelectronics 136 (2019): 84–90

smartphone, and even the naked eye, Fig. 6. Early detection of dengue is not geared up to a crowing point; the researchers may investigate it.

4.3 Cancer

Cancer is a frightening disease or set of diseases which is the preeminent cause of death worldwide [96]. Cancer is stated as the cells of uncontrolled growth. These cells might be formed as abnormal cells. The mutilation cells do not die and become cancer cells owing to uncontrolled growth. These destruction cells are transferable easily through the blood into several body organs. The indexes of cancer are elicited from the genre of cancer, and certain patients don't show indexes or markers until it reaches distant advanced stages.

The cancer disease affects and progresses in three steps: (1) Initiation, (2) Promotion, and (3) Progression. Currently, we have several sorts of treatments for cancer, i.e., (1) Surgery, the surgeon cuts the cancer tumour; (2) Radiation therapy, which uses immense shots of radiation to eradicate tumour cells; (3) Chemotherapy, used to eliminate cancer cells using drugs, etc. Through wax and screen printing, PBM was fabricated and it enables sample filtration and injection functionalities. The authors opted for the label-free electrochemical method which enables rapid testing and designed a simple PBM that involves an inlet hole sample, filter hole, counter electrode screen printing, reference electrode screen printing, diagnosis zone, and working electrode screen printing as shown in Fig. 7. This PBM can diagnose two biomarkers from a single sample that are integrated onto a single device.

4.4 Glucose

Glucose is an important medical analyte and also an important metabolic intermediator [99, 100]. It acts as an indicator for several diseases which includes glucose metabolism disorders and islet cell carcinoma [99–102]. Detection of concentration levels of glucose helps to regulate insulin levels in order to avoid diabetes complications. Colourimetric and electrochemical μPAD are familiar in the detection of glucose levels [101].

Figure 8 shows the procedure for fabricating dumbbell-shaped Electrochemical Paper-Based Analytical Devices (ePADs) using the wax dipping technique: (a) Iron mould designing, (b) Alignment of Whatman No 1 paper and blood separation paper, (c) ePADs assembly construction steps, and (d) Blood separation ePADs [105]. Noiphung, Julaluk, et al. designed μPAD to measure the glucose level from a blood sample using plasma isolation methods [105]. In this, electrochemical dumbbell-shaped paper-based analytical devices (ePADs) were used to obtain uniform plasma isolation. The blood sample was given to the separation zone of ePADs, and in 4 min plasma separation takes place. Isolated plasma from the separation zone transmits to the detection zone. Glucose oxidase immobilized in the middle of the paper device in the detection zone detects the glucose in isolated plasma. Hydrogen peroxide is generated when the reaction between glucose and enzyme is passed through Prussian blue modified screen-printed electrodes (PB-SPEs). Chronoamperometry is used to measure the currents at the optimal detecting potential for H_2O_2 (Hydrogen peroxide) where glucose concentrations in whole blood are proportional [105].

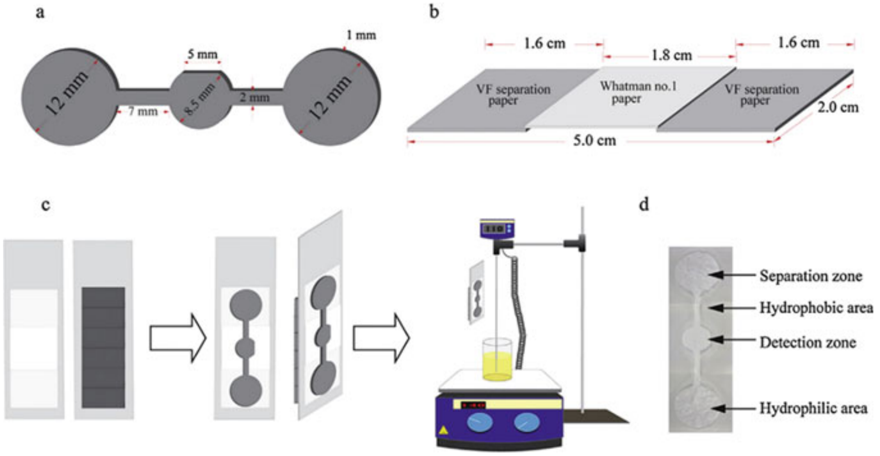

Fig. 8 Wax dipping technique for identification of Glucose [105]. Reproduced with permission from Noiphung, Julaluk, Analyticachimicaacta 788 (2013): 39–45

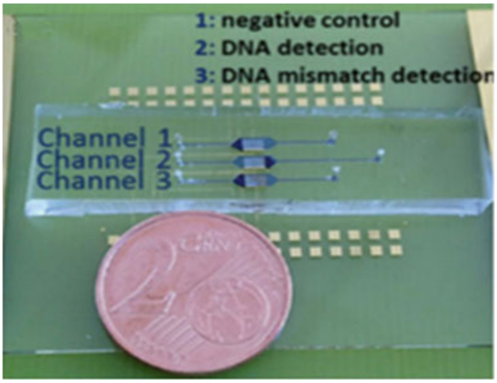

Fig. 9 Represents label-free electrochemical μPAD using carbon/ferrocene nanotubes for detection of mycobacterium tuberculosis DNA [104]. Reproduced with permission from Wu, Jiandong, NPJ digital medicine 1.1 (2018): 1–11

4.5 Tuberculosis

Tuberculosis is a very serious infective disease which mainly deteriorates lungs' health. In 2020, an estimated 10 million people developed active TB, resulting in 1.5 million deaths, making it the second leading cause of death from an infectious disease after COVID-19 [106]. Mycobacterium tuberculosis (MTB) bacteria causes Tuberculosis (TB). Generally, TB not only affects the lungs but also affects other parts of the body [106]. Chronic cough with blood-containing mucus, fever, night sweats, and weight loss are typical symptoms of active TB. TB is a communicable disease; the spreading happens through air when the infected person coughs, spits, speaks, or sneezes [106]. The current routine diagnostic tests for TB are chest X-ray, tissue culture, tuberculin skin test (TST), and acid-fast staining. These diagnostic tests are time-consuming, and require laboratory equipment and well-trained technician (Fig. 9).

5 Integration of MF and PμF with AI and IoT

Electronic devices, sensors, and software collectively form a network that can communicate with each other. This network is termed Internet of Things (IoT). Large volumes of data can be generated by the networks, sensors, and users which assists in gaining knowledge and developing applications with the help of Artificial Intelligence (AI) approaches. The combination of AI and IoT facilitates the advancement of public safety, education, health care, transportation, and various such domains offering valuable services. Over the last decade, the phenomenon of μF and Paper-Based Microfluidics are coupled with Artificial Intelligence (AI) and Internet of Things (IoT). It utilizes nano-functionalized materials that have been identified as the economical and sustainable tool for point-of-care-testing (POCT) for the diagnosis of various diseases. The aim of designing these devices is to provide cost-effective, eco-friendly, rapid, and accurate results [107]. Traditional hospital management systems contain problems like work overload for doctors and nurses, loads of paperwork, and many more. Integration of IoT into the hospital environment can avoid all these drawbacks and replace the voluminous paperwork with a centralized and automated database. Artificial Intelligence (AI) and Machine Learning (ML) are proven as better tools to predict the result through analysis of available data in a database.

6 Conclusion

An accurate disease diagnosis is crucial for successful treatment. The diagnostic equipment available are costly, bulky, and time-consuming, which necessitates the need for new and innovative techniques. The field of microfluidics and its branch paper-based microfluidics have great potential in revolutionizing diagnostic equipment. Their applications are becoming more apposite in molecular diagnostics and life sciences. The success of microfluidics and paper-based microfluidics is attributed to the distinct chemical and physical features of fluids at micron size. The advantages of μF and μPAD are cost-effective, easy to use, biocompatible, and easily disposable. The μF and μPAD are capable of implementing many functions within them that include flow control components such as valves and pumps. The COVID-19 pandemic has highlighted the spotlight on the necessity of μF and μPAD for rapid diagnostics. The paper-based diagnostics are relatively simple, fast, and cost-effective; the reason for such advantages is clearly described in the paper. Future researchers should focus on improving the reliability and accuracy of the device. It would be a major breakthrough if a single paper-based device for multiple disease detection. Further, the integration of μF and μPAD with IoT and AI will allow the device to quickly reach the hands of users.

References

1. Whitesides GM (2006) The origins and the future of microfluidics. Nature 442(7101):368–373
2. Lei KF (2018) Introduction: the origin, current status, and future of microfluidics. In: Microfluidics: fundamental, devices and applications: fundamentals and applications. pp 1–18
3. Tian W-C, Finehout E (2008) Introduction to microfluidics. In: Microfluidics for biological applications. Springer, Boston, MA, pp 1–34
4. Xia Y, et al (1996) Complex optical surfaces formed by replica molding against elastomeric masters. Science 273(5273):347–349
5. Xia Y, Whitesides GM (1998) Soft lithography. Annu Rev Mater Sci 28(1):153–184
6. Unger MA, et al (2000) Monolithic microfabricated valves and pumps by multilayer soft lithography. Science 288(5463):113–116
7. Wu, H, et al (2003) Fabrication of complex three-dimensional microchannel systems in PDMS. J Am Chem Soc 125(2):554–559

8. Erickson D, et al (2004) Electrokinetically controlled DNA hybridization microfluidic chip enabling rapid target analysis. Anal Chem 76(24):7269–7277
9. Zhang Y, Jiang H-R (2016) A review on continuous-flow microfluidic PCR in droplets: advances, challenges and future. Anal Chim Acta 914:7–16
10. Zhang Y, Ozdemir P (2009) Microfluidic DNA amplification—a review. Anal Chim Acta 638(2):115–125
11. Burns, Mark A., et al. An integrated nanoliter DNA analysis device. Science 282(5388):484–487
12. Lei KF, et al (2015) Electrokinetic acceleration of DNA hybridization in microsystems. Talanta 138:149–154
13. He Y, et al (2011) Gate manipulation of DNA capture into nanopores. Acs Nano 5(10):8391–8397
14. Diercks AH, et al (2009) A microfluidic device for multiplexed protein detection in nano-liter volumes. Anal Biochem 386(1):30–35
15. Herr AE, et al (2007) Microfluidic immunoassays as rapid saliva-based clinical diagnostics. Proc Natl Acad Sci 104(13):5268–5273
16. Bhattacharyya A, Klapperich CM (2007) Design and testing of a disposable microfluidic chemiluminescent immunoassay for disease biomarkers in human serum samples. Biomed Microdevice 9(2):245–251
17. Yang D, et al (2008) Electrospunnanofibrous membranes: a novel solid substrate for microfluidic immunoassays for HIV. Adv Mater 20(24):4770–4775
18. van den Brink FTG, et al (2011) Parallel single-cell analysis microfluidic platform. Electrophoresis 32(22):3094–3100
19. Lei KF, Wu Z-M, Huang C-H (2015) Impedimetric quantification of the formation process and the chemosensitivity of cancer cell colonies suspended in 3D environment. Biosens Bioelectron 74:878–885
20. Ballerini DR, Li X, Shen W (2012) Patterned paper and alternative materials as substrates for low-cost microfluidic diagnostics. Microfluid Nanofluid 13(5):769–787
21. Jayamohan H, Sant HJ, Gale BK (2013) Applications of microfluidics for molecular diagnostics. Microfluidic Diagn 305–334
22. Gross PG, et al (2007) Applications of microfluidics for neuronal studies. J Neurol Sci 252(2):135–143
23. Beebe DJ, Mensing GA, Walker GM (2002) Physics and applications of microfluidics in biology. Annu Rev Biomed Eng 4(1):261–286
24. Weibel DB, Whitesides GM (2006) Applications of microfluidics in chemical biology. Curr Opin Chem Biol 10(6):584–591
25. Bai Y, et al (2018) Applications of microfluidics in quantitative biology. Biotechnol J 13(5):1700170
26. Zhang Q, Austin RH (2012) Applications of microfluidics in stem cell biology. BioNanoScience 2(4):277–286
27. Yager P, Domingo GJ, Gerdes J (2008) Point-of-care diagnostics for global health. Annu Rev Biomed Eng 10:107–144
28. Kiechle FL, Holland CA (2009) Point-of-care testing and molecular diagnostics: miniaturization required. Clin Lab Med 29(3):555–560
29. Yokoyama M (2005) Drug targeting with nano-sized carrier systems. J Artif Organs 8(2):77–84
30. Moshfeghi AA, Peyman GA (2005) Micro-and nanoparticulates. Adv Drug Deliv Rev 57(14):2047–2052
31. Rosi NL, et al (2006) Oligonucleotide-modified gold nanoparticles for intracellular gene regulation. Science 312(5776):1027–1030
32. Winter JO, et al (2001) Recognition molecule directed interfacing between semiconductor quantum dots and nerve cells. Adv Mater 13(22):1673–1677
33. Vu TQ, et al (2005) Peptide-conjugated quantum dots activate neuronal receptors and initiate downstream signaling of neurite growth. Nano Lett 5(4):603–607

34. Michalet X, et al (2005) Quantum dots for live cells, in vivo imaging, and diagnostics. Science 307(5709):538–544
35. Pinaud F, et al (2006) Advances in fluorescence imaging with quantum dot bio-probes. Biomaterials 27(9):1679–1687
36. Esplandiu MJ, et al (2004) Nanoelectrode scanning probes from fluorocarbon-coated single-walled carbon nanotubes. Nano Lett 4(10):1873–1879
37. Minella W (2021) C. elegans immobilization via microfluidics: a short review. Elveflow
38. Li X, Ballerini DR, Shen W (2012) A perspective on paper-based microfluidics: Current status and future trends. Biomicrofluidics 6(1):011301
39. Nishat S, et al (2021) based microfluidics: Simplified fabrication and assay methods. Sens Actuat B Chem 336:129681
40. Sin MLY, et al (2011) System integration-a major step toward lab on a chip. J Biol Eng 5(1):1–22
41. Lu Y, Shi W, Qin J, Lin B (2010) Fabrication and Characterization of Paper-Based Microfluidics Prepared in Nitrocellulose Membrane By Wax Printing. Anal Chem 82(1):329–335
42. Muller R, Clegg D (1949) SCIENTIFIC COMMUNICATIONS Automatic Paper Chromatography. Anal Chem 21(1):192–192
43. Weil H, Williams, TI (1951) Early history of chromatography. Nature 167(4257):906–907
44. Giddings JC (ed) (1976) Advances in chromatography, vol 14. CRC Press
45. Yang Y, et al (2017) based microfluidic devices: emerging themes and applications. Anal Chem 89(1):71–91
46. Mao K, et al (2020) based microfluidics for rapid diagnostics and drug delivery. J Control Release 322:187–199
47. Reid MS, Le XC, Zhang H (2018) Exponential isothermal amplification of nucleic acids and assays for proteins, cells, small molecules, and enzyme activities: an EXPAR example. Angew Chem Int Ed 57(37):11856–11866
48. Duncan R, et al (2016) Advances in multiplex nucleic acid diagnostics for blood-borne pathogens: promises and pitfalls. Expert Rev Mol Diagn 16(1):83–95
49. Li C, Boban M, Tuteja A (2017) Open-channel, water-in-oil emulsification in paper-based microfluidic devices. Lab Chip 17(8):1436–1441
50. Sanjay ST, et al (2018) Recent advances of controlled drug delivery using microfluidic platforms. Adv Drug Deliv Rev 128:3–28
51. Barrett TH (2011) The woman who invented notepaper: towards a comparative historiography of paper and print. J R Asiat Soc 21(2):199–210
52. Hong B, et al (2016) A concentration gradient generator on a paper-based microfluidic chip coupled with cell culture microarray for high-throughput drug screening. Biomed Microdev 18(1):1–8
53. Carrilho E, Martinez AW, Whitesides GM (2009) Understanding wax printing: a simple micropatterning process for paper-based microfluidics. Anal Chem 81(16):7091–7095
54. Li H, Steckl AJ (2018) Paper microfluidics for point-of-care blood-based analysis and diagnostics. Anal Chem 91(1):352–371
55. Zhang H, et al (2019) LAMP-on-a-chip: revising microfluidic platforms for loop-mediated DNA amplification. TrAC Trends Anal Chem 113:44–53
56. Xu G, et al (2016) Paper-origami-based multiplexed malaria diagnostics from whole blood. AngewandteChemie 128(49):15476–15479
57. Kaarj K, Akarapipad P, Yoon J-Y (2018) Simpler, faster, and sensitive Zika virus assay using smartphone detection of loop-mediated isothermal amplification on paper microfluidic chips. Sci Rep 8(1):1–11
58. Vinatier C, et al (2009) Cartilage engineering: a crucial combination of cells, biomaterials and biofactors. Trends Biotechnol 27(5):307–314
59. Zhong ZW, Wang ZP, Huang GXD (2012) Investigation of wax and paper materials for the fabrication of paper-based microfluidic devices. Microsyst Technol 18(5):649–659
60. Martinez AW, et al (2008) FLASH: a rapid method for prototyping paper-based microfluidic devices. Lab on a Chip 8(12):2146–2150

61. Roberts BP (1996) Understanding the rates of hydrogen-atom abstraction reactions: empirical, semi-empirical and ab initio approaches. J Chem Soc Perkin Trans 2(12):2719–2725
62. Lu Y, et al (2010) Fabrication and characterization of paper-based microfluidics prepared in nitrocellulose membrane by wax printing. Anal Chem 82(1):329–335
63. (2012): Ballerini DR, Li X, W Shen (2012) Patterned paper and alternative materials as substrates for low-cost microfluidic diagnostics. MicrofluidNanofluid 13(5):769–787
64. Mu X, Zhang YS (2017) Fabrication and applications of paper-based microfluidics. In: Diagnostic devices with microfluidics. CRC Press, pp 45–64
65. Cretich M, et al (2010) Coating of nitrocellulose for colorimetric DNA microarrays. Anal Biochem 397(1):84–88
66. Lisa M et al (2009) Gold nanoparticles based dipstick immunoassay for the rapid detection of dichlorodiphenyltrichloroethane: an organochlorine pesticide. Biosens Bioelectron 25(1):224–227
67. Hou S-Y, et al (2007) Development of Zeptomole and Attomolar detection sensitivity of biotin–peptide using a dot−blot goldnanoparticle immunoassay. Anal Chem 79(3):980–985
68. Dou M, et al (2015) Low-cost bioanalysis on paper-based and its hybrid microfluidic platforms. Talanta 145:43–54
69. Martinez AW, et al (2008) Simple telemedicine for developing regions: camera phones and paper-based microfluidic devices for real-time, off-site diagnosis. Anal Chem 80(10):3699–3707
70. Hawkes R, Niday E, Gordon J (1982) A dot-immunobinding assay for monoclonal and other antibodies. Anal Biochem 119(1):142–147
71. Apilux A, et al (2010) Lab-on-paper with dual electrochemical/colorimetric detection for simultaneous determination of gold and iron. Anal Chem 82(5):1727–1732
72. Li X, et al (2010) Fabrication of paper-based microfluidic sensors by printing. Coll Surf B Biointerf 76(2):564–570
73. World Health Organization (2009) 2008–2013 action plan for the global strategy for the prevention and control of noncommunicable diseases: prevent and control cardiovascular diseases, cancers, chronic respiratory diseases and diabetes
74. World Health Organization (2016) World Health Organization global report on diabetes. World Health Organization, Geneva
75. Bleakley H, Lange F (2009) Chronic disease burden and the interaction of education, fertility, and growth. Rev Econ Stat 91(1):52–65
76. Mishra SK, Kumar D, Biradar AM (2012) Electrochemical impedance spectroscopy characterization of mercaptopropionic acid capped ZnS nanocrystal based bioelectrode for the detection of the cardiac biomarker—myoglobin. Bioelectrochemistry 88:118–126
77. de Ávila BE-F, et al (2018) Disposable amperometricmagnetoimmunosensor for the sensitive detection of the cardiac biomarker amino-terminal pro-B-type natriuretic peptide in human serum. AnalyticaChimicaActa 784:18–24
78. De La Rica R, Stevens MM (2012) Plasmonic ELISA for the ultrasensitive detection of disease biomarkers with the naked eye. Nat Nanotechnol 7(12):821–824
79. Diamandis EP (2004) Mass spectrometry as a diagnostic and a cancer biomarker discovery tool: opportunities and potential limitations. Mol Cell Proteom 3(4):367–378
80. Li NJ, et al (2010) Plasma metabolic profiling of Alzheimer's disease by liquid chromatography/mass spectrometry. Clin Biochem 43(12):992–997
81. Jones MB, et al (2002) Proteomic analysis and identification of new biomarkers and therapeutic targets for invasive ovarian cancer. PROTEOMICS 2(1):76–84
82. Loonen AJM, Schuurman R, Van Den Brule AJ (2012) Highlights from the 7th European meeting on molecular diagnostics. Expert Rev Mol Diagn 12(1):17–19
83. Nahavandi S, et al (2014) Microfluidic platforms for biomarker analysis. Lab on a Chip 14(9):1496–1514
84. Mu X, et al (2014) Multiplex microfluidic paper-based immunoassay for the diagnosis of hepatitis C virus infection. Anal Chem 86(11):5338–5344

85. Choi JR, et al (2015) based sample-to-answer molecular diagnostic platform for point-of-care diagnostics. Biosens Bioelectron 74:427–439
86. Sinawang PD, Rai V, Ionescu RE, Marks RS (2016) Electrochemical lateral flow immunosensor for detection and quantification of dengue NS1 protein. Biosens Bioelectron 77:400–408
87. Prabowo MH, et al (2020) Dengue NS1 detection in pediatric serum using microfluidic paper-based analytical devices. Anal Bioanalytic Chem 412(12):2915–2925
88. World Health Organization, et al. (2009) Dengue: guidelines for diagnosis, treatment, prevention and control. World Health Organization
89. Guzman MG, et al (2010) Dengue: a continuing global threat. Nat Rev Microbiol 8(12):S7–S16
90. Thomas SJ, et al (2008) Dengue plaque reduction neutralization test (PRNT) in primary and secondary dengue virus infections: How alterations in assay conditions impact performance. Am J Trop Med Hyg 81(5):825
91. Salje H, et al (2014) Variability in dengue titer estimates from plaque reduction neutralization tests poses a challenge to epidemiological studies and vaccine development. PLoS Negl Trop Dis 8(6):e2952
92. Pal S, et al (2014) Evaluation of dengue NS1 antigen rapid tests and ELISA kits using clinical samples. PLoS One 9(11):e113411
93. Lanciotti RS, et al (1992) Rapid detection and typing of dengue viruses from clinical samples by using reverse transcriptase-polymerase chain reaction. J Clin Microbiol 30(3):545–551
94. Kumar S, et al (2018) Tapered lateral flow immunoassay based point-of-care diagnostic device for ultrasensitive colorimetric detection of dengue NS1. Biomicrofluidics 12(3):034104
95. Sinawang PD, et al (2016) Electrochemical lateral flow immunosensor for detection and quantification of dengue NS1 protein. Biosens Bioelectron 77:400–408
96. Wang R, et al (2019) Rapid diagnostic platform for colorimetric differential detection of dengue and Chikungunya viral infections. Anal Chem 91(8):5415–5423
97. Cokkinides V, et al (2005) American cancer society: cancer facts and figures. American Cancer Society, Atlanta
98. Fern LA, et al (2011) How frequently do young people with potential cancer symptoms present in primary care? Br J Gen Pract 61(586):e223–e230
99. Wang Y, et al (2019) Label-free microfluidic paper-based electrochemical aptasensor for ultrasensitive and simultaneous multiplexed detection of cancer biomarkers. Biosens Bioelectron 136:84–90
100. Kaefer M, et al (2010) Association between ischemia modified albumin, inflammation and hyperglycemia in type 2 diabetes mellitus. Clin Biochem 43(4–5):450–454
101. Lu J et al (2011) Comparable efficacy of self-monitoring of quantitative urine glucose with self-monitoring of blood glucose on glycaemic control in non-insulin-treated type 2 diabetes. Diabetes Res Clin Pract 93(2):179–186
102. Chen X, et al (2012) Determination of glucose and uric acid with bienzyme colorimetry on microfluidic paper-based analysis devices. Biosens Bioelectron 35(1):363–368
103. Si P, et al (2011) Highly stable and sensitive glucose biosensor based on covalently assembled high density Au nanostructures. Biosens Bioelectron 26(9):3845–3851
104. Liu S, Wenqiong S, Ding X (2016) A review on microfluidic paper-based analytical devices for glucose detection. Sensors 16(12):2086
105. Wu J, et al (2018) Lab-on-chip technology for chronic disease diagnosis. NPJ Dig Med 1(1):1–11
106. Noiphung J, et al (2013) Electrochemical detection of glucose from whole blood using paper-based microfluidic devices. Analyticachimicaacta 788:39–45
107. Chakaya J, et al (2021) Global tuberculosis report 2020–reflections on the global TB burden, treatment and prevention efforts. Int J Infect Dis 113:S7–S12
108. Gopinath SCB, et al (2016) Aptamer-based 'point-of-care testing'. Biotechnol Adv 34(3):198–208

Critical Review and Exploration on Micro-pumps for Microfluidic Delivery

J. Prithvi, B. S. Sreeja, S. Radha, C. Joshitha, and A. Gowthami

Abstract This review covers various types of micro-pumps designs, and the design aspects of an IPMC actuator-based micro-pump are much focused on flow rate as the primary objective while maintaining a low power consumption. A detailed comparison of various diaphragm micro-pump types and pump structures is discussed. The need for durability led to the choice of valve-less micro-pump over their active counterparts. Choice of PEGDA (Polyethyleneglycoldiacrylate) as the membrane material for actuation has been proposed due to the ease of curing and biocompatibility aspect. In addition to the review, a 2D simulation of IPMC membrane has been performed for obtaining corresponding values of membrane displacement in COMSOL Mutliphysics. The valve-less nozzle/diffuser configuration with a conical angle of 4–6° allows the pump to provide the desired flow rate. The simulation results show the relationship between applied voltage, frequency, dimensions and displacement of actuator and the flow rate and accumulated flow volume for various cone angles of valve. Further, the backflow rates for conical and tesla valves have been observed at various pressures. Tesla valve exhibits a much lesser backflow rate of 240 µl/s at an inlet pressure of 130 Pa.

Keywords Micro pumps · Low power · IPMC membrane · Flowrate

1 Introduction

Microfluidics deals with the study of fluid flow in extremely small amounts typically in the nano-liter to typically a few microliters range in a miniaturized system of the milli-order. The main functions performed are sample preparation, purification, transport, biosensing, and detection. The physics of fluid flow is no longer in terms of

---

J. Prithvi · B. S. Sreeja (✉) · S. Radha · A. Gowthami
Department of Electronics and Communication Engineering, Sri Sivasubramaniya Nadar College of Engineering, Chennai, Tamil Nadu 603110, India
e-mail: sreejabs@ssn.edu.in

C. Joshitha
Department of Electronics and Communiction Engineering, Koneru Lakshmaiah Education Foundation, Hyderabad, Telangana 500075, India

K. Guha et al. (eds.), *MEMS and Microfluidics in Healthcare*, Lecture Notes in Electrical Engineering 989, https://doi.org/10.1007/978-981-19-8714-4_5

conventional models and negligent parameters such as surface tension become dominant characteristics. Keeping these difficulties in mind, the research into MEMS and NEMS has been rapidly increasing in recent years for biomedical applications. Due to availability of technologies with the potential to revolutionize the current manufacturing processes, such as laser micromachining and 3D printing, the prototyping phase has been substantially reduced. In recent years, the most important advancement of MEMS and NEMS in biomedicine is microfluidic transdermal drug delivery (TDD) systems. TDD systems are involved in the movement of pharmaceutical drugs through the skin for subsequent distribution in the human body. TDD system consists of micro-pumps, micro-needles, reservoir, micro-flow sensor, blood pressure sensor, and required electronic circuit for necessary operations. A schematic of a sample TDD system is shown in Fig. 1.

The micro-pump is the main component of the TDD system that performs the actuation process required to transport the drugs from a reservoir at specific volumes. The main performance metrics are the flow rate desired in the system, the power consumption, and the efficiency of electrical energy conversion to mechanical energy. They can be of two types—Mechanical and Non-mechanical based on the type of actuation. Mechanical micro-pumps need moving parts to perform the actuation like diaphragm and check valves, whereas the non-mechanical counterparts use electrical, chemical, or magnetic energy to produce kinetic momentum.

Some types of mechanical micro-pumps are Electrostatic [1, 2], Piezoelectric [3–9], Thermo-pneumatic [10–13], Bimetallic, Shape Memory Alloy (SMA) [14], Ion Conductive Polymer Film (ICPF) [15–22], MEMS-based pumps [47, 48, 50], Electromagnetic, and Phase-Change Type pumps. Some types of non-mechanical pumps

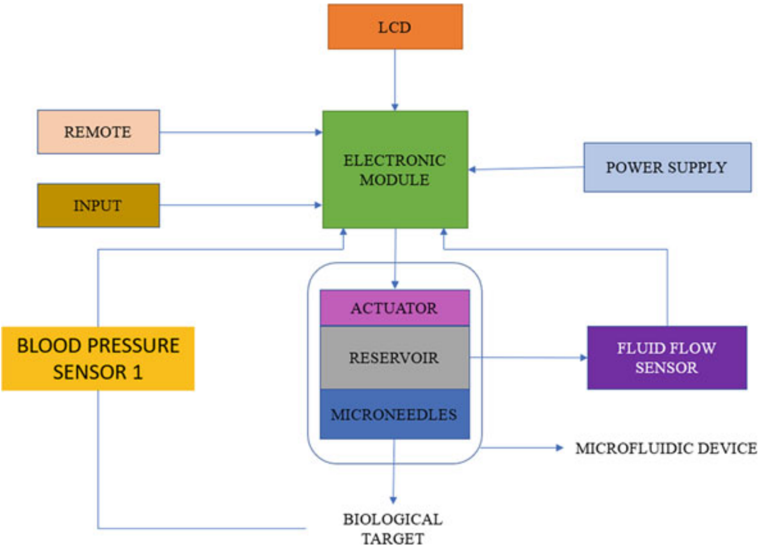

Fig. 1 Schematic of sample TDD system

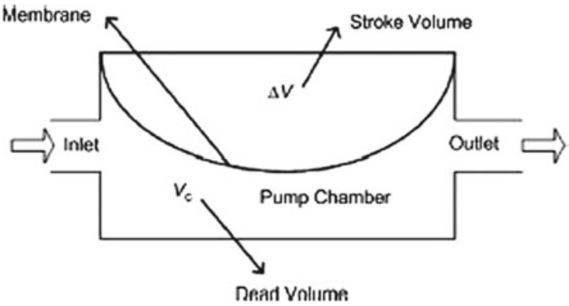

Fig. 2 Schematic of mechanical diaphragm type micro-pump

are Magnetohydrodynamic (MHD), Electrohydrodynamic (EHD), Electro-osmotic, Electrowetting, Bubble-type, Flexural Planar Wave (FPW), Electrochemical, and Evaporation type pumps. Since insulin is the primary focus of this work and it does not exhibit any significant magnetic or chemical properties that can be utilized for actuation, and to reduce design complexity, mechanical pumps have been chosen for micro-pump design (Fig. 2).

A typical diaphragm type mechanical micro-pump consists of a membrane that takes energy in the form of electricity, heat, liquid pressure, air pressure and converts it into some form of mechanical energy. Fluid flow is achieved by oscillatory movement of the diaphragm which creates a difference in pressure. When low pressure is created, fluid flows into the chamber through the inlet valve and during high pressure, fluid is pushed out through the outlet valve. The pressure generated inside the chamber is a function of stroke volume (ΔV) produced by the actuator which must contend with dead volume of the chamber (V0).

Pumps can either consist of single chamber or multiple chambers placed sequentially in series or parallel. Such pumps are called peristaltic micro-pumps that transfer fluid through the alternating oscillation of the diaphragms in different chambers. This could lead to better control of volume transfer as well as better pump efficiency.

Micro-valves are used to regulate fluid flow at inlets and outlets basing on pumping motion. They can be of two types—active or passive. Active micro-valves use an actuating force similar to the main diaphragm and improve efficiency but are limited by design complexity and fabrication cost. Electrostatic, Thermo-pneumatic, and Piezoelectric are some of the mechanisms that have been reported for active valves. Passive valves, on the other hand, obtain the valving effect as a difference of pressure between the inlet and outlet valve.

A third type are valve-less micro-pumps which don't use check valves but rely on nozzle/diffuser action for flow rectification. Figure 3 shows the schematic representation of the setup. The flow is directed in such a way that more fluid enters the chamber through the inlet than exits the outlet in supply mode. The reverse occurs during pump mode. Predominant research has been conducted in cone-shaped valveless nozzle/diffuser setup but there exists another specially shaped valve called the tesla valve as shown in Fig. 4. Like conical valves, they offer minimum resistance to flow of fluid in one direction indicated by the blue lines, whereas resistance is increased in the opposite direction by looping back the fluid on itself as indicated by the red lines thus arresting the fluid flow. The ease of fabrication of tesla valves makes it an important alternative to conical valves.

Biocompatibility of MEMS-based micro-pumps is becoming increasingly important and is being regarded as a key requirement for drug delivery systems. As there is the possibility of implanting micro-pumps inside the human body, the materials used for fabrication are required to fulfill rigorous biocompatibility and biostability constraints. Further, the implanted pump should be able to withstand long-term physiological exposure of surrounding tissues. In line with these conditions, there is a recent trend in usage of polymers as a substrate material since they are widely used in medicine and are suitable for human implantation. Polymer materials such as Polymethylmethacrylate (PMMA) [49], Polydimethylsiloxane (PDMS), and Polyethyleneglycoldiacrylate (PEGDA) are being used in fabrication of MEMS micro-pumps.

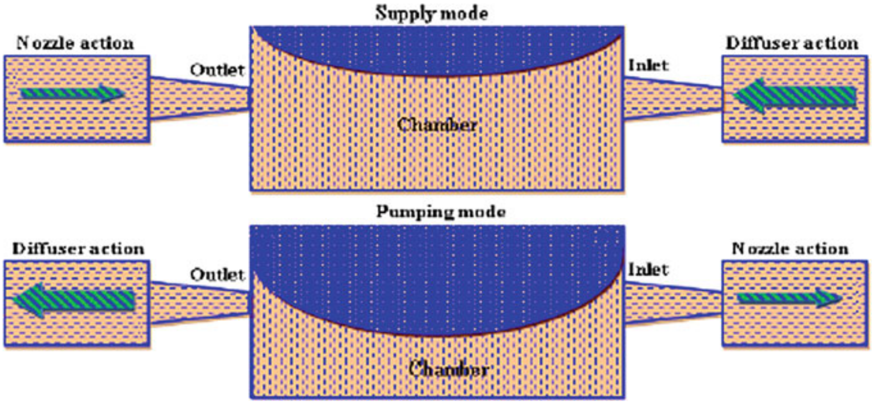

Fig. 3 Schematic of valve-less micro-pump

Fig. 4 Schematic of tesla valve. **a** Flow in the blocking direction, part of the fluid is turned around and interferes with the forward flow. **b** Flow in the unhindered direction [U.S. Patent 1,329,559 "Valvular Conduit"]

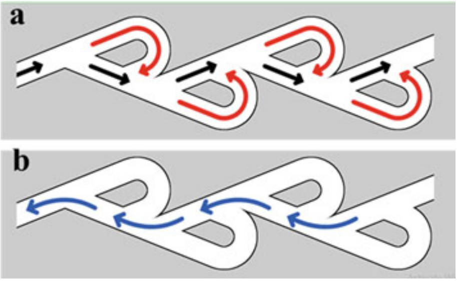

2 Background Study

Piezoelectric micro-pumps function by the application of electrical energy to a piezoelectric crystal whose structure is altered due to net polarization at the surface, leading to mechanical stress and thereby actuation. These actuators have large actuation and fast response time but are difficult to fabricate. They also exhibit small stroke volumes at high voltages. Figure 5 exhibits the representation of piezoelectric micro-pump.

Liu et al. have proposed a disposable, high-performance piezoelectric micro-pump with four chambers in serial connection for closed-loop insulin therapy system [23]. Outflow resolution of 6.23×10^{-5} ml/pulse was observed. The maximum backpressure of 22 kPa was reported at applied voltage 36 Vpp and 200 Hz frequency.

Electrostatic micro-pumps involve actuation by electrostatic form of attraction and repulsion between two plates separated by a small distance. The plate attached to the membrane performs supply and pumping respectively is depicted in Fig. 6. The fabrication is easy, power consumption is low and response times are fast, but it provides very low stroke volume. Lee et al. fabricated and tested a peristaltic electrostatic gas micro-pump that employed fluidic resonance for high flow rate [24]. The micro-pump presented pressure ranges from 3.3 to 7.3 kPa and flow rates from 0.07 to 0.29 sccm.

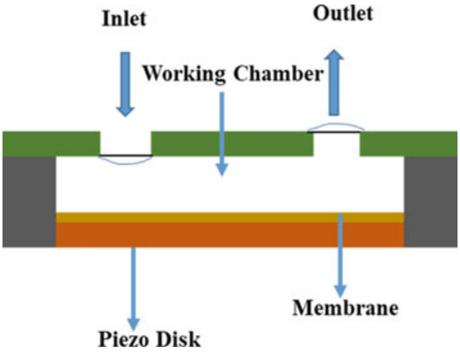

Fig. 5 Piezoelectric micro-pump

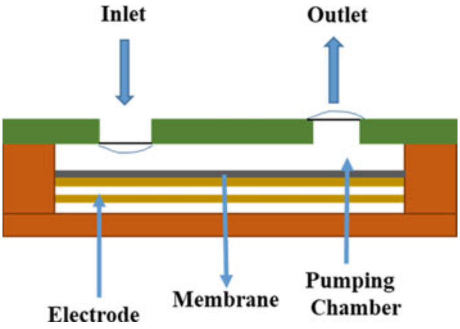

Fig. 6 Electrostatic micro-pump

Thermo-pneumatic micro-pumps function on thermal expansion for actuation where a chamber above the membrane is filled with air which is then heated and cooled to provide expansion and compression using a heater and cooler respectively is shown in Fig. 7. This type of pump generates strong pressure and displacement of membrane; however, the driving power is constantly held high.

Kim et al. proposed a thermo-pneumatic micro-pump with a glass layer, indium tin oxide heater, polydimethylsiloxane (PDMS) chamber, PDMS membrane, and PDMS cavity [25]. The flow rate of 0.078 μL/min was achieved at applied voltage of 55 V with frequency of 6 Hz. Chia et al. proposed a novel thermo-pneumatic peristaltic micro-pump comprised of two separate zones for air heating and fluid squeezing [10]. The temperature elevation of 2.0 K was reported on the fluid pumping area. Tan et al. fabricated a peristaltic micro-pump by bonding a PDMS part with micro-channels to the PDMS/PMMA (polymethylmethacrylate) part where PDMS/adhesive membrane worked like a pneumatic actuator [27]. The maximum flow rate of 96 l μL/min was achieved.

Electromagnetic actuation is large and covers a longer distance as compared to electrostatic actuation. It needs low voltage, but an external source is required for actuation such as a permanent magnet is depicted in Fig. 8. On small scale, this type

Fig. 7 Thermo-pneumatic micro-pump

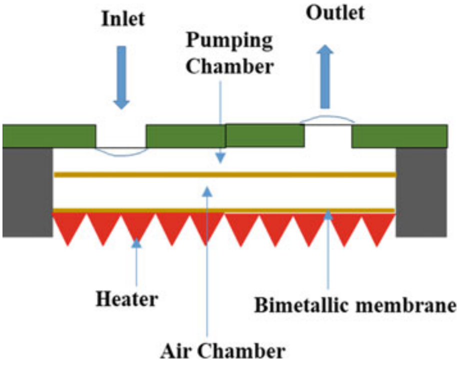

Fig. 8 Electromagnetic micro-pump

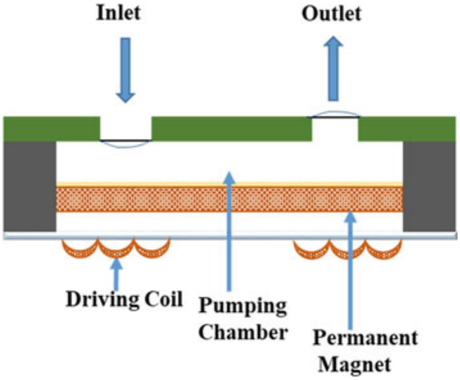

of actuation has no benefit because it is reduced by the cube of scaling factor. The driving coils or permanent magnets bond directly with the membrane and provide a magnetic field. However, at the same time, the size is compromised. Usually, electromagnetic micro-pumps have high power consumption and heat dissipation.

Yamahata et al. fabricated and characterized a reciprocating PMMA ball valve micro-pump with electromagnetic actuation. The micro-pump showed a backpressure of 35 kPa and flow rate of 6 mL/min at 2 W electromagnetic actuation power with 20 Hz resonant frequency [28]. Halhouli et al. worked on the design of a novel electromagnetic pump that is based on the rotation of two hard magnets kept in channel, with opposing polarity [29]. The maximum flow rate of 13.7 mL/min at 200 rpm and a pressure of 785 Pa at 136 rpm were observed.

Bimetal refers to an object that is composed of two different metals jointed together as in Fig. 9. The thermal expansion coefficients of these metals are different. The deflection of a diaphragm made of bimetallic materials is induced against thermal alternation if the two chosen materials possess adequately discriminative thermal expansion factors.

Zou et al. [30] designed a micro-pump that operated on both bimetallic thermal actuation and thermal pneumatic actuation mechanisms. When the bimetallic actuator made of Al/Si membrane was heated, the membrane deformed in downward direction. At the same time, the gas in the air chamber expended due to the heat to support bimetallic actuation. The flow rate of 336 μL/min was achieved when the open pressure was 0.5 kPa.

ICPF actuator shows high speed response. However, the positioning control is difficult. Physically it looks like a—sandwich diaphragm between two thin films of metallic or electro-active polymers that are placed on both sides of the polymer. These two films have high electrical conductivity. Both ends of the diaphragm are fixed in case of rectangular diaphragm or the outer edge in case of circular diaphragm, and the ICPF diaphragm can be controlled by bending in the direction of either upside or downside if an appropriate pair of voltages is applied at the electrodes as shown in Fig. 10. The ICPF actuator is commonly called an artificial muscle because of the large bending displacement, low actuation voltage, and biocompatibility. Fang and Tan [26] proposed a control-oriented model to envisage the deformation of diaphragm and the flow rate. Experimental results of the polypyrrole (PPy) actuated micro-pump

Fig. 9 Bimetallic micro-pump

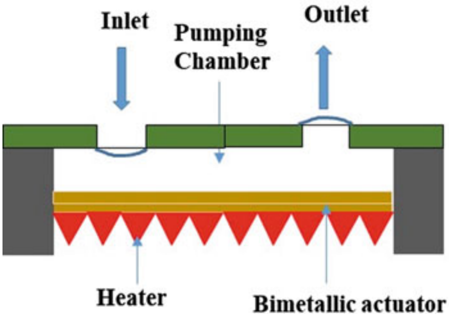

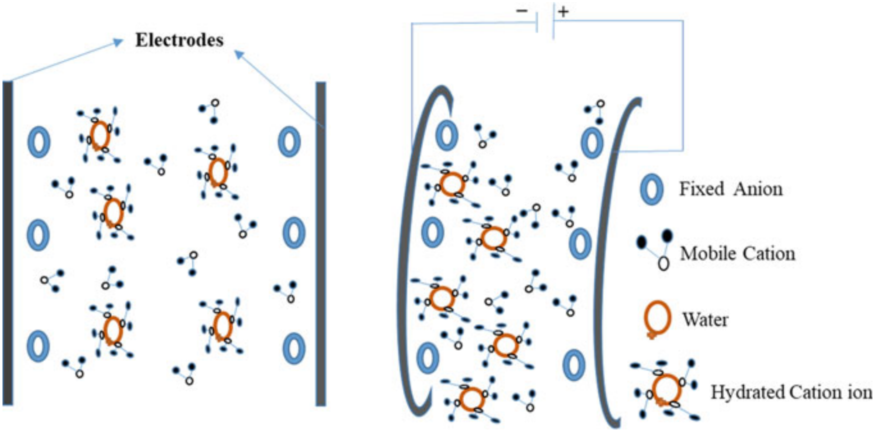

Fig. 10 ICPF micro-pump

showed that the maximum flow rate of 1260 μL/min was observed at the voltage of 4 V.

The basic principle used in phase-change type actuators and micro-pumps is the vaporization and condensation phenomenon. In vaporization, the phase transition occurs from liquid phase to vapor phase. While in condensation, the change of the physical state occurs from gaseous phase to liquid phase. The phase-change type micro-pump consists of a heater, diaphragm, and working fluid chamber.

Sim et al. [31] proposed a phase-change type micro-pump consisting of a pair of Al flap valves and a phase-change type actuator. The actuator comprised of a heater, working fluid chamber, and silicone rubber diaphragm as shown in Fig. 11. The diaphragm was actuated by the vaporization and the condensation of the working fluid in the chamber of the pump. The maximum flow rate of 6.1 μL/min was achieved at applied voltage of 10 V with 0.5 Hz frequency and 60% duty ratio for zero pressure difference.

SMA are the metals which exhibit two unique properties such as pseudo elasticity and the shape memory (SM) effect. They have the capability of changing their shapes

Fig. 11 Phase-Change micro-pump

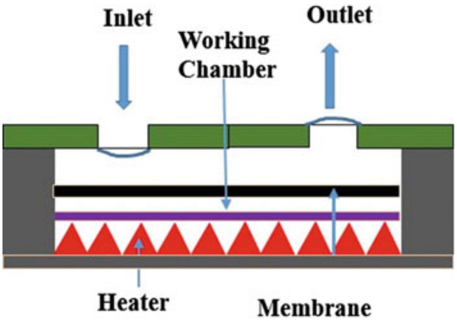

upon application of an external stimulus. The SM effect involves a phase transformation between two solid phases. At high temperature the phase is called austenite and at low temperature the phase is called martensite. SMA starts in martensite phase and transforms into austenite phase after being heated. This property of materials is useful to make SMA micro-pump. SMA have many attractive properties like high force to volume ratio, ability to recover large transformation stress and strain upon heating and cooling processes, high damping capacity, chemical resistance, and biocompatibility. Usually, the deformation of SMA cannot be precisely controlled and investigated due to temperature sensitivity.

Zhang and Qiu [32] reported a Ti/Ni/Copper (Cu) shape memory thin film micro-pump comprised of a TiNiCu/Si driving membrane, pump chamber and two inlet and outlet check valves. The hysteresis width ΔT of 9 °C was observed. Setiawan [14] reported the performance assessment of SMA spring as actuator for gripping manipulation. The SMA actuator was a TiNi tensile spring with diameter of 50 mm wire and 350 g hanging mass.

From the available options, ICPF, Electromagnetic, and Thermo-pneumatic have desirable characteristics but however owing to size and voltage supplied, ICPF have the necessary trade-off required to satisfy the key parameters expected in a TDD system micro-pump. Literature has been studied to cover the various design configurations adapted for ICPF micro-pumps.

Pak et al. [33] presented a micro-pump which combined Poly Dimethylsiloxane (PDMS) micro-channel and ICPF actuator. In the micro-channel, there is a nozzle, diffuser structure which controls fluid flow from inlet to outlet. The recorded flow rate was 9.97 μl/min in response to 8Vp-p and 0.5 Hz input voltage. The membrane was fabricated using commercial Nafion 112 conductive polymer polypyrrole as electrode where in order to have best performance, and it needed to have 17–19 μm thick electrode.

Lee and Kim [34] tried to model ICPF disk as a micro-pump diaphragm. Low cost and ease of manufacturing were the key factors considered when trying this method as opposed to other technologies. A finite element analysis (FEA) was used to find the shape of IPMC diaphragm and its electrodes and the estimation of its stroke volumes (ΔV). Based on the optimum designed nozzle/diffuser structure and the estimated stroke volume of the IPMC diaphragm, the flow rate of the IPMC-based micro-pump was estimated at a low Reynolds number (about 50) and it means that this IPMC-based micro-pump is an appropriate choice for microfluidic devices because in microfluidic devices we face with low Reynolds number fluids. The assumed IPMC for this model had a Nafion membrane with Pt electrodes and based on the calculated results for the IPMC diaphragm, the optimum center displacement (the best result to have maximum pumping rate) was 0.966 mm, in which the radius of the electrode was 8.5 mm. Based on the numerical result of this study, in response to a 2 V and 0.1 Hz input voltage, the flow rate of this micro-pump is 8.2 μl/s (492 μl/min).

Nguyen et al. [35, 36] presented a flap valve-based IPMC micro-pump. In this device, a multilayered IPMC has been fabricated with a consecutive recasting method, which consists of a Nafion/modified silica layer as a membrane sandwiched between two thin layers containing Nafion, layered silicate, and conductive material particles (Ag Nanopowder) as electrodes. The developed modified multilayered IPMC has better blocking force without making any constraint and problem for its bending displacement. The main material using in the flap valve was PDMS (due to its flexibility and solving the sealing problem), but the whole of micro-pump is a composition of several PMMA (Poly(methyl methacrylate)) layers that is equipped with IPMC diaphragm and PDMS flap valve. Its flow rate is 760 μl/min in response to a 3 V and 3 Hz input voltage.

Santos et al. [37] presented a micro-pump with two different types of diaphragms proposed by the way in which voltage was applied to them. As shown in Fig. 12, the second diaphragm has four additional branches in comparison with the first diaphragm where we can apply a voltage to the IPMC by two thin copper rings attached to these branches as shown in Fig. 13 while in diaphragm 1, two copper wires are soldered to the center of the Pt electrodes in both sides as shown in Fig. 14. The IPMC diaphragm of second diaphragm is more practical and durable and hence the micro-pump has been fabricated by this diaphragm. The proposed micro-pump is a four layers nozzle/diffuser pump as depicted in Fig. 15 with two acrylic layers on top and down, with a layer of IPMC diaphragm covered by a layer of Teflon. This pump was fabricated and the stroke volume of both IPMC diaphragms was tested with different values of supplied electric current. The results showed an asymmetric behavior of upward and downward displacements for both diaphragms. Stroke volumes up to 80 μl were measured and in response to a 0.1 Hz input voltage (amplitude was not reported), the flow rate of the fabricated micro-pump with second diaphragm is reported to be about 8.02 μl/s (481.2 μl/min).

Guo and Wei [38] presented a micro-pump with an improved diaphragm was presented to overcome the limitation of a single disk shaped diaphragm. This kind of ICPF disk is clamped at all edges, which makes an obstacle for ICPF deformation,

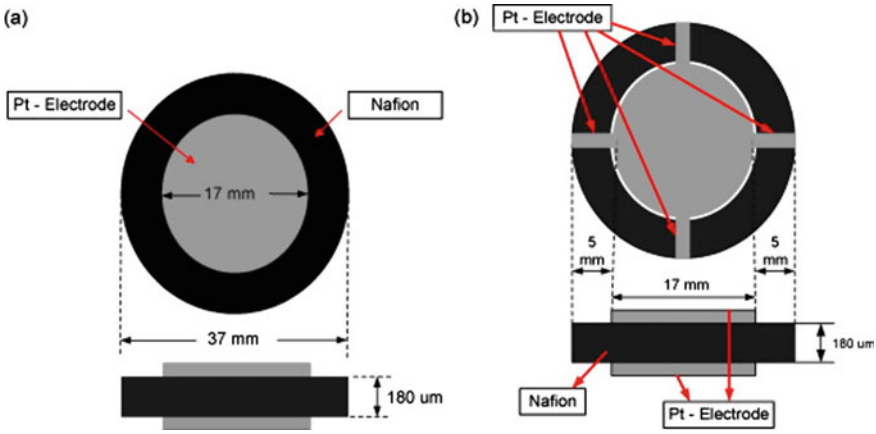

Fig. 12 **a** First diaphragm. **b** Second diaphragm [37]

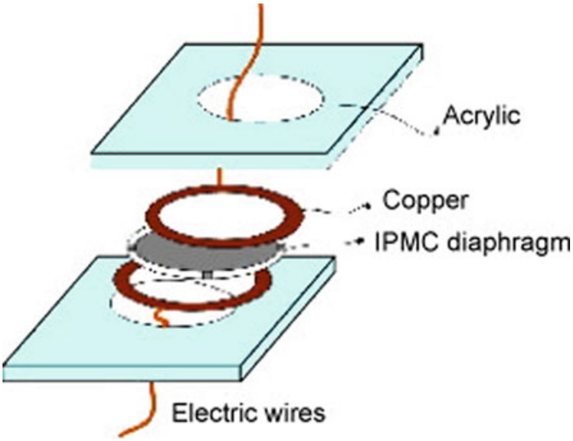

Fig. 13 Voltage application corresponding to second diaphragm [37]

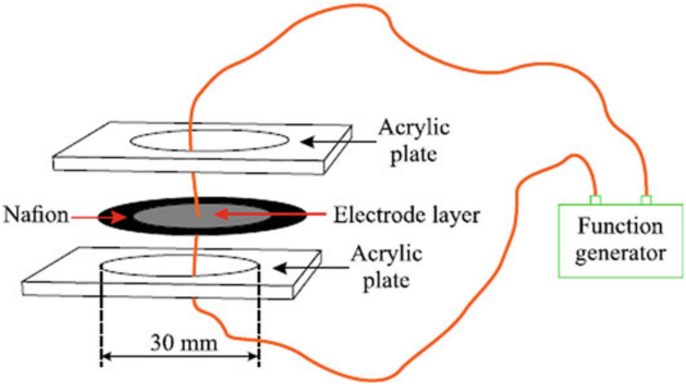

Fig. 14 Voltage application corresponding to first diaphragm [37]

i.e., it decreases the ICPF bending, and consequently, the pumping ability of ICPF-based micro-pump will be decreased significantly. In order to solve this problem and increasing the deformation and pumping ability of the micro-pump, Guo presented a new form of ICPF diaphragm using four pieces petal-shaped ICPF actuator instead of a disk-shaped one. This petal-shaped structure has been depicted in Fig. 16 where four quarter-disk-shaped ICPF actuators are attached on a thin PDMS diaphragm. In this structure, the ICPFs are only clamped on one edge, and they are freer to bend and make an up-down movement in the PDMS diaphragm so that the pumping operation occurs. The 3D schematic of micro-pump consists of a petal-shaped ICPF actuator in a sealed actuating chamber, and two check valves with a PDMS diaphragm attached to the ICPF actuator. Under applying voltage, the ICPF and then PDMS diaphragm will be moved up and down. Thus, this movement makes the pumping pressure,

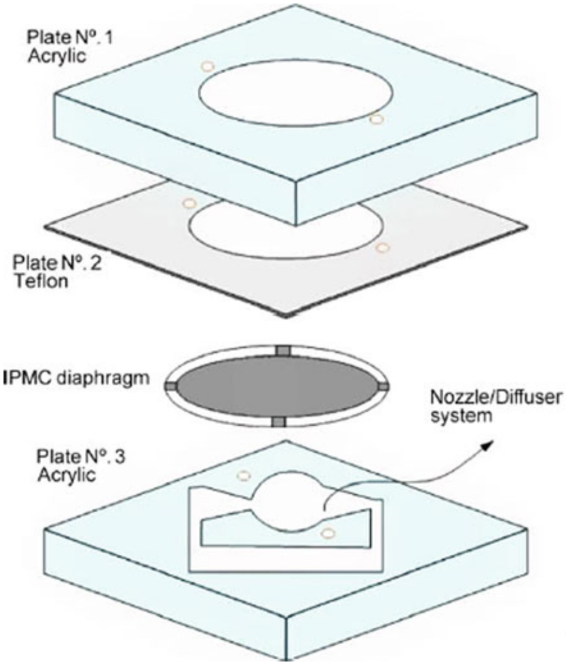

Fig. 15 Exploded view of the micro-pump structure [37]

and the fluid will be pumped from the inlet to the outlet. The functionality of the micro-valves of this micro-pump is keeping the directional flow during the pumping process. The micro-valves are fabricated using PDMS diaphragms. The working principle and duties of these valves are as follows:

1. When pressure is applied from the bottom, the outlet diaphragm will be lifted to allow the fluid flow out through the outlet.
2. When pressure is applied from the top, the inlet diaphragm will be pushed down and allows the fluid flow into the pump through the inlet.

The proposed micro-pump has been made in the form of a cube with the size of 30 mm × 30 mm and 27 mm (height). A petal-shaped IPMC actuator is used as the active element of the pump with a PDMS diaphragm and under experimental tests, this IPMC-based micro-pump was able to pump the fluids by 202 μl/min flow rate in response to a 5-V 2-Hz applied voltage.

In all the previous ICPF-based micro-pumps, a disk-shaped or petal-shaped IPMC was used as diaphragm or active element of the micro-pump, but McDaid et al. [39] presented a new version of IPMC-based micro-pump using the ICPF in its standard cantilever form. The authors believe the major issue in integrating ICPF in microfluidic devices is its control in order to have a reliable and durable actuation over a long period and many cycles. In the proposed structure, there is no diaphragm, and the pumping actuator is an IPMC in its cantilever beam form. The device has

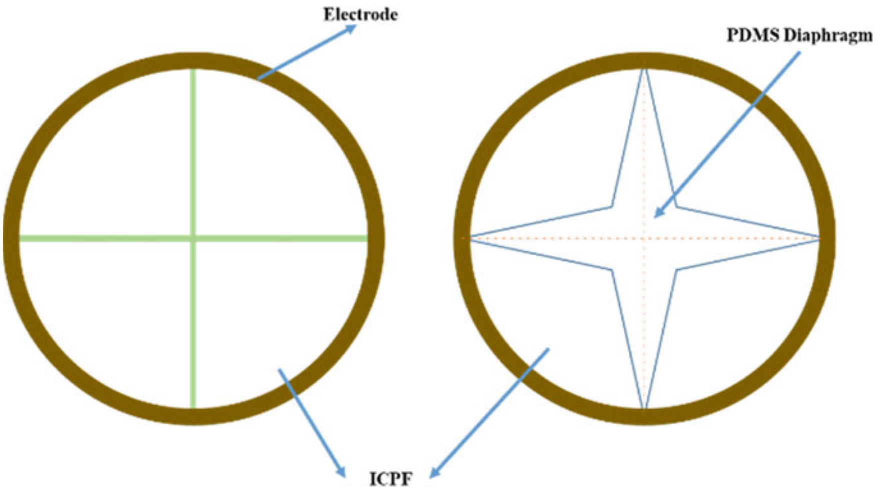

Fig. 16 Petal-shaped diaphragm before (left) and after (right) application of voltage

been fabricated by four layers of Perspex (Poly methyl methacrylate) for making the inlet channel, the outlet channel, the pump chamber where the ICPF actuator is embedded in it, and the bottom layer as the tank that allows the IPMC remains hydrated throughout all experiments and hence it can work durable over a long time. A thin layer of latex also has been attached to the bottom of the pump chamber, so when the IPMC is deforming, the volume of the pump chamber also will be changed. Hence, pressure is produced, and pumping of the fluid is obtained. In order to have a continuous pumping actuation, a sinusoid IPMC displacement is needed. By an open loop test, the optimum frequency to have the highest pumping rate was obtained around 0.1 Hz. Of course, the high pumping rate is not the desire of all applications. For example, in some drug delivery microfluidic chips, the lower pumping rates are needed. Hence the proposed controller can work by lower frequencies too, for example, 0.05 Hz.

Rajapaksha et al. [40] demonstrated a high-performance actuator based on cross-linked poly(ethylene glycol) diacrylate (PEGDA) modified with Thiosiloxane (TS) and ionic liquid (1-hexyl-3-methylimidazolium hexafluorophosphate) placed between 2 μm thick poly(3,4-etylenedioxythiophene) polystyrene sulfonate (PEDOT: PSS) electrodes. The maximum observed displacement was 2.5 mm at a sinusoidal voltage of 3 V at 0.5 Hz. The displacement reduces exponentially with increasing frequency for a polymer formed using 50% ionic liquid and 50% PEGDA/TS composite. At the same composition, the ICPF shows fastest switching time of 2 s which enables faster actuation speeds if required [43, 44].

Lastly, the literature relevant to conical valves has been explored to identify a suitable design that can be incorporated in the fabrication process. Schabmueller et al. [41] developed a valve-less piezoelectric pump with cone-shaped tubes. The tubes had a moderate cone angle of 35.3° etched in the 111 plane on a single crystal

Table 1 Summary of ICPF-based micro-pumps

Reference	Voltage/frequency	Device material	Electrode material	Shape	Main measurement index
Pak et al.	8 V/0.5 Hz	PDMS	Ppy	Square	FR: 9.97 µl/min
Lee and Kim	2 V/0.1 Hz	Unknown	Platinum	Disk	FR: 492 µl/min
Ngugen et al.	3 V/3 Hz	PDMS, PMMA	Silver nanopowder	Disk	FR: 760 µl/min
Santos et al.	Unknown/0.1 Hz	Acrylic, Teflon, Copper	Platinum	Disk	FR: 481.2 µl/min
Guo and Wei	5 V/2 Hz	Unknown	Gold	Petal	FR: 202 µl/min
Mc Daid et al.	Unknown/0.1 Hz	Persperex, Latex	Platinum	Cantilever	Diaphragm Displacement ~300 µm

silicon. A liquid pump rate of 1500 µl/min and a gas pumping rate of 690 µl/min were achieved using PZT actuator (Table 1).

Pun et al. [30] developed cone-shaped tubes laterally placed using Hot Embossing Technique as opposed to DRIE or Advanced Silicon Etching (ASE). This resulted in a preformed structure within the mold and internal stress was avoided. In addition, inserting sacrificial layer in order to obtain the fluidic cavity wasn't necessary, thus simplifying the fabrication process. The final structure with a cone angle of 7° is obtained.

Huang et al. [42] designed a single nozzle valve-less micro-pump using layers of PMMA and adhesives. Carbon dioxide laser etching is used to create the pump chamber, which consists of a circular chamber and an exponentially curved nozzle as shown in Fig. 17. A peak flow rate of 0.4 ml/min was achieved at 20 V voltage at a frequency of 70 Hz. A PZT piezoelectric disk attached to brass sheets in direct contact with the chamber was used for actuation.

He et al. [5] developed conical valve micro-pump with a cone angle of 7°. The paper shows extensive relationship between frequency of operation of a PZT-based piezoelectric actuator and cone angles. For frequencies lesser than or equal to 100 Hz, the efficiency is independent of frequency, between 100 and 1000 Hz the efficiency increases and beyond that efficiency decreases for a cone angle less than 20°. For cone angles greater than 40°, efficiency increases beyond 1000 Hz. The optimal angle for lesser than 1000 Hz is ten degrees. The pump design is shown in Fig. 18. All the

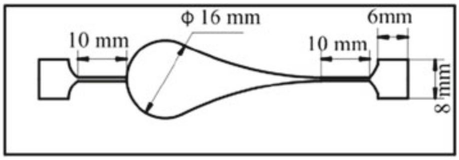

Fig. 17 Schematic of single nozzle rain drop shaped micro-pump [42]

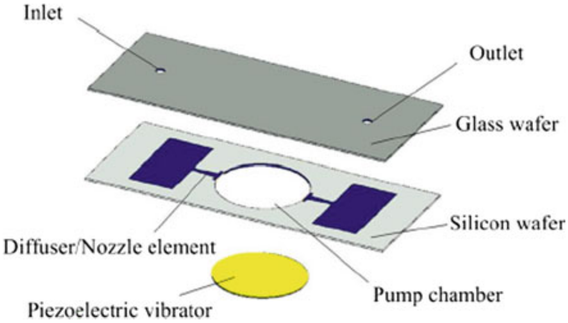

Fig. 18 Schematic of 7° conical valve micro-pump [5]

above micro-pumps are much useful for biomedical applications and drug delivery systems [51–59].

3 Modeling IPMC Membrane and Nozzle/Diffusor Valve in COMSOL Multiphysics

There are three basic phenomena which define the characteristics of the physical model of IPCF actuators: (1) electric field change inside the polymer due to distribution of mobile cations and the applied electric potential at the electrodes (2) Mass transfer using diffusion and migration transport (3) Occurrence of stress and strain due to redistribution of ions and water inside the polymer membrane. The IPMC is made of ICPF sandwiched between two metal electrodes [45, 46]. When voltage is applied to the electrodes, cation flux or ionic current is induced by the imposed electric field. In case of water-based IPMC, migrating cations drag the water molecules along, causing osmotic pressure changes and therefore swelling of the polymer near the cathode and contraction near the anode. This in turn results in bending of material towards the anode.

3.1 Governing Equations

The ionic current in the polymer is calculated with the Nernst-Planck equation:

$$\frac{\partial C}{\partial t} + \nabla.(-D\nabla C - z\mu FC\nabla\varphi - \mu C\Delta V\nabla P) = 0 \tag{1}$$

where C is the cation concentration, μ is the mobility of cations, D is the diffusion constant, F is the Faraday constant, z is the charge number, ΔV is molar volume that quantifies the cation hydrophilicity, P is solvent pressure, and φ is the electric potential in the polymer. Mobility can be expressed as

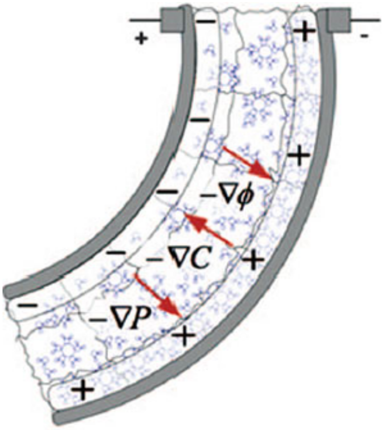

Fig. 19 Conceptual model of IPMC with gradients [45]

$$\mu = \frac{D}{RT} \tag{2}$$

where R is gas constant and T is absolute temperature. Equation (1) is the main governing equation for describing the transduction phenomena in IPMC materials. There are three gradients present namely the potential gradient ∇φ, the concentration gradient ∇C, and solvent pressure gradient ∇V. Conceptual model of IPMC along with gradients is shown in Fig. 19.

The potential φ is defined by Poisson's equation:

$$-\nabla^2\varphi = \frac{\rho}{\varepsilon} \tag{3}$$

where ρ is the charge density and is defined as

$$\rho = F(C - C_a) \tag{4}$$

where Ca is the major anion concentration. The variable ε is the effective dielectric permittivity that can be explicitly written as

$$\varepsilon = \varepsilon_o\varepsilon_r \tag{5}$$

where ε0 is the dielectric permittivity in vacuum. While cation concentration is governed by Eq. (1), anion concentration is related to the local volumetric strain as

$$dV = \nabla.u \tag{6}$$

where u is the local displacement vector. A positive value of the volumetric strain means an increase in local volume and vice versa. The volume changes affect the local polymer anion concentration as they are part of the polymer backbone. Hence the anion concentration is expressed as:

$$C_a = C_o(1 - dV) \tag{7}$$

where C_0 is the initial anion concentration. It must be noted that for most practical calculations it is reasonable to approximate anion concentration to C_0. The solvent pressure is caused by local strain in the polymer matrix, forcing the solvent from the concave side to the convex side of IPMC. Effective cation transport due to this term is governed by the pressure gradient ∇P and molar volume constant ΔV in the ionic flux term in Eq. (1). Pressure P is the solvent pressure caused by the strain in the polymer. According to the momentum conservation, the solvent pressure and the pressure of the polymer p are related as follows:

$$\nabla(P + p) = 0 \tag{8}$$

It has been shown that

$$p(dV) = \frac{E(1-v)}{(1+v)(1-2v)}dV \tag{9}$$

where E is Young's modulus of the material and v is Poisson's ratio. By knowing these constants, Navier's equations can be constructed for displacements:

$$-\nabla.\sigma = \mathbf{F} \tag{10}$$

where F is the force per unit volume. Body force F is defined as a function of charge density ρ:

$$\mathbf{F} = f(\rho) \tag{11}$$

3.2 Boundary Conditions

This section presents the boundary conditions that are used to solve the governing equations described in the previous section. Figure 20 represents the polymer domain, electrode domains, and boundaries of the actuator model. Equations (1) and (3) are solved in the polymer domain δ and the domains ψ1 and ψ2 are used for electrodes which are used to apply electric potential.

For Eq. (1) for domain δ at the boundaries $\partial\delta_{1\text{-}4}$:

$$-D\frac{\partial C}{\partial n} - z\mu FC\frac{\partial\varphi}{\partial n} = 0 \tag{12}$$

For Eq. (3) which is used to solve potential inside the polymer:

At boundary $\partial\ \delta_2$ and $\partial\delta_4$:

$$\varphi_{\partial\delta 4} = \varphi_{\partial\delta 2} = V \tag{13}$$

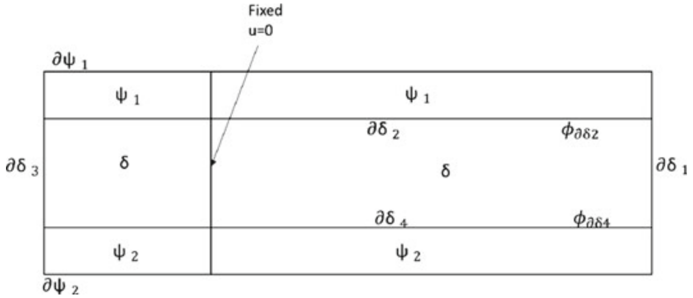

Fig. 20 2D model of actuator with all boundaries and domains

At boundary $\partial\delta1$ and $\partial\delta3$:

$$\frac{\partial\varphi_{\partial\delta3}}{\partial n} = \frac{\partial\varphi_{\partial\delta1}}{\partial n} = 0 \tag{14}$$

For Ohm's law in electrode domain $\psi1$ and $\psi2$:

$$\mathrm{V}_{\partial\Psi_1} = \mathrm{V}_{\mathrm{pos}}, \mathrm{V}_{\Psi_2} = \mathrm{V}_{\mathrm{neg}} \tag{15}$$

where Vpos and Vneg are applied electric potentials. The input applied signal is a sinusoidal wave set at a specific amplitude and specific frequency for positive terminal and ground at negative terminal.

3.3 Nozzle/Diffuser

In most pumps, mechanical check valves were used for the inlet and outlet ports, either with membranes or flaps. The process of designing and fabricating this type of valve is very complex. The pump itself may suffer from problems such as high pressure drop across the valves. Some crucial properties like backward flow and switching speed have to be controlled precisely in order to achieve a working miniature pump. Moreover, wear and fatigue can be critical issues, especially in polymer-fabricated devices. This may result in reduced lifetimes and reliabilities. There is also the risk of valve blocking by even small particles, which instantly degrade the pumping performance or cause damage to sensitive fluids. This limits the application range of most valve-based miniature pumps to filtered media. Therefore, there was a need for miniature pumps with no movable parts.

Valve-less miniature pumps can eliminate these problems. The diffuser/nozzle setup provides flow-rectifying properties like a check valve. Literature shows a maximum achievable forward–backward flow ratio of 2.23 for this type of valve which is sufficient for a pump. A diffuser is a diverging duct, and nozzle is a converging duct. These ducts are designed to have lower pressure loss in the diffuser direction than in the nozzle direction for the same flow velocity. When chamber volume increases (the supply mode), the inlet element acts as a diffuser with a lower flow restriction than the outlet element, which acts as a nozzle. Therefore, a larger volume is transported through the inlet into the chamber than through the outlet. On the other hand, during decreasing chamber volume (the pump mode), the outlet element acts as a diffuser with a lower flow restriction than the inlet element, which acts as a nozzle. This means that a larger volume is transported through the outlet out of the chamber than through the input. As a result, a net volume is transported (i.e., pumped) from the inlet side to the outlet side. Therefore, a complete pump cycle is achieved, even though the fluid traveled in both directions of the diffuse/nozzle element.

The dimensions that decide the flow rate of the ducts are the smaller diameter, larger diameter, height of the cone, and the angle of inclination of cone with side wall which is an optimum of 5° when dynamic fluid resistance is minimum. The inlet pressure and fluid density are other deciding factors for the pressure distribution flow velocity across the ducts.

3.4 Pump Designs for Fabrication

The following pump designs were proposed for fabrication of micro-pump: single chamber as shown in Fig. 21 with left-hand side inlet and right-hand side outlet, dual chamber with 180° out of phase pumping using conical valves as shown in Fig. 22 with right-hand side inlet and left-hand side outlet and single chamber pump with tesla valve as shown in Fig. 24 with right-hand side inlet and left-hand side outlet. Rectangular inlet and outlet chambers have been provided in double chamber design for increased pumping efficiency by promoting fluid pumping in alternate chambers whereas in single chamber design, cylindrical chambers have been provided to prevent excess backflow (Fig. 23).

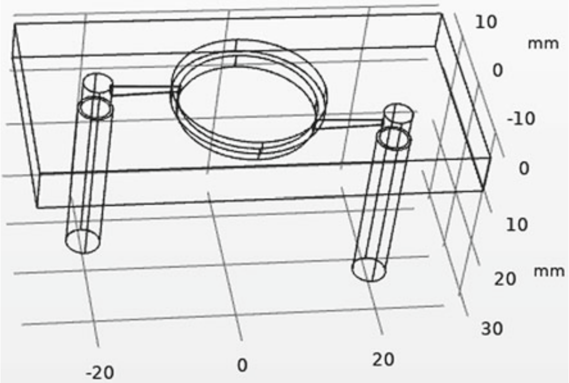

Fig. 21 Single chamber conical valve-less micro-pump

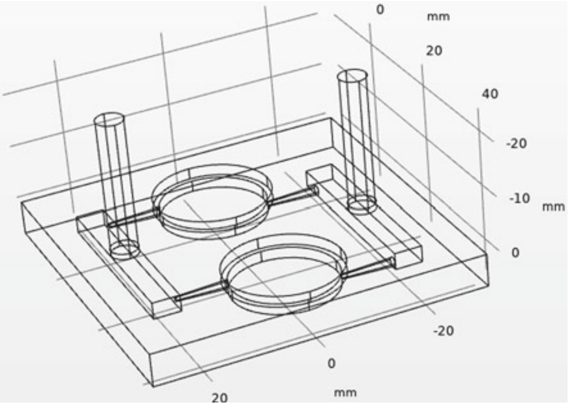

Fig. 22 Dual chamber conical valve-less micro-pump

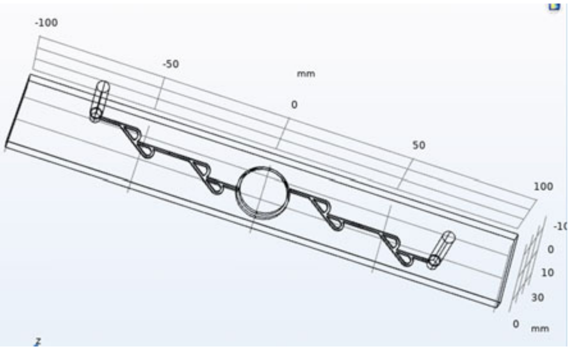

Fig. 23 Single chamber tesla valve-less micro-pump

The pumps were being tested with the existing, popular piezoelectric buzzer-based actuation as well as the proposed PEGDA-based ICPF membrane-based actuation. The pump chamber was proposed to be fabricated using impression molding using PDMS polymer (Tables 2 and 3).

Table 2 Specifications of single chamber conical valve-less pump

Part	Dimensions
Main block	30 × 60 × 6 mm
Diaphragm holder radius	21 mm
Pumping chamber radius	19 mm
Nozzle/diffuser base diameter	1.8 mm
Nozzle/diffuser base height	10 mm
Nozzle/diffuser angle	5°
Fluid receiving chamber diameter	4 mm
Tube fitting pipe diameter	4.8 mm

Table 3 Specifications of dual chamber conical valve-less micro-pump

Part	Dimensions
Main block	60 × 60 × 6 mm
Diaphragm holder radius	21 mm
Pumping chamber radius	19 mm
Nozzle/diffuser base diameter	1.8 mm
Nozzle/diffuser base height	10 mm
Nozzle/diffuser angle	5°
Fluid receiving chamber diameter	35 × 5 × 3 mm
Tube fitting pipe diameter	4.8 mm

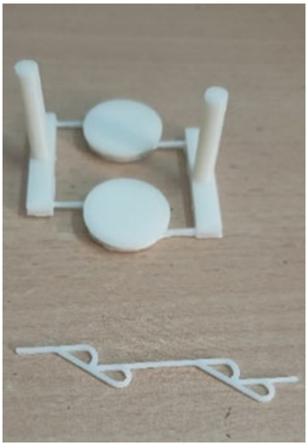

Fig. 24 Inverse 3D print of double chamber conical valve micro-pump and tesla valve

4 Simulation Results

4.1 IPMC Actuator

The model is designed as shown in Fig. 25. The modules used in COMSOL Multiphysics to implement the IPMC model in 2D are Transport of Diluted Species (tds) which is responsible for Eq. (1) and boundary condition Eq. (12), Electric currents (ec) which is used to provide potential and boundary conditions corresponding to Eqs. (13), (14) and (15), Solid mechanics (solid) to implement Eq. (9) and boundary condition is implemented using Dirichlet boundary for Eq. (10), General Form PDE (g) to implement Eqs. (3), (4), (5) and the various constants needed to solve the system of equations is provided in Fig. 26. The applied voltage at the top is Vpos = 0.5*sin(2*pi*t) V at a frequency of 1 Hz and at the bottom is Vneg = 0 V. The width of the IPMC is modeled as coming out of the plane and approximated to 2D calculations. The deformation plot is shown in Fig. 27 where the scale shows the minimum and maximum value of stress across the 2D domain. The displacement plot of the mid-point of the actuator where the displacement is highest at any given point of time is shown in Fig. 28.

Parametric studies were performed by varying the length of the IPMC actuator and the frequency of the sine voltage provided to perform the actuation. It can be observed that the displacement steadily increases with increase in length however at a length of 71.07 mm, the displacement drops to a really low value as seen in Fig. 29. This can be attributed to poor charge distribution and low control of the actuator when the actuator is excessively long. The frequency of input sine wave voltage was varied from 0 to 3 Hz with step increments of 0.5 Hz is displayed in Fig. 30. The maximum displacement which is nearly 20 mm is observed at 0.5 Hz which drops sharply with increasing frequency. This observation can be attributed to poor response time of ionic current flow within the polymer with higher frequencies.

Fig. 25 IPMC model

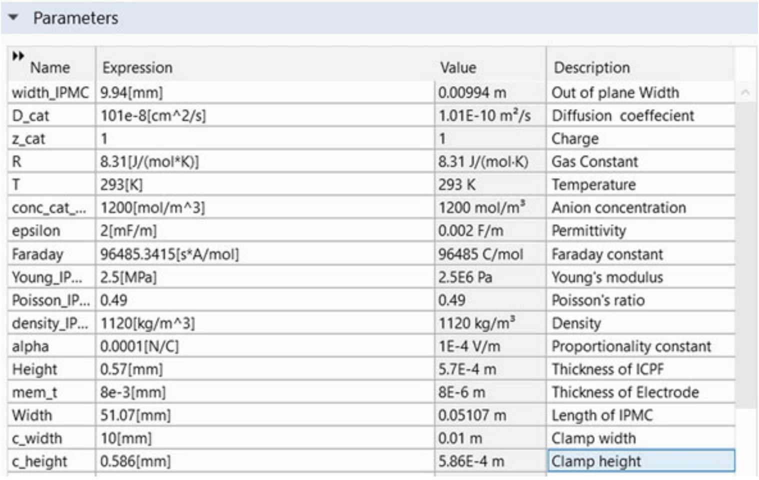

▾ Parameters

Name	Expression	Value	Description
width_IPMC	9.94[mm]	0.00994 m	Out of plane Width
D_cat	101e-8[cm^2/s]	1.01E-10 m²/s	Diffusion coeffecient
z_cat	1	1	Charge
R	8.31[J/(mol*K)]	8.31 J/(mol·K)	Gas Constant
T	293[K]	293 K	Temperature
conc_cat_...	1200[mol/m^3]	1200 mol/m³	Anion concentration
epsilon	2[mF/m]	0.002 F/m	Permittivity
Faraday	96485.3415[s*A/mol]	96485 C/mol	Faraday constant
Young_IP...	2.5[MPa]	2.5E6 Pa	Young's modulus
Poisson_IP...	0.49	0.49	Poisson's ratio
density_IP...	1120[kg/m^3]	1120 kg/m³	Density
alpha	0.0001[N/C]	1E-4 V/m	Proportionality constant
Height	0.57[mm]	5.7E-4 m	Thickness of ICPF
mem_t	8e-3[mm]	8E-6 m	Thickness of Electrode
Width	51.07[mm]	0.05107 m	Length of IPMC
c_width	10[mm]	0.01 m	Clamp width
c_height	0.586[mm]	5.86E-4 m	Clamp height

Fig. 26 Parametric constants for IPMC model

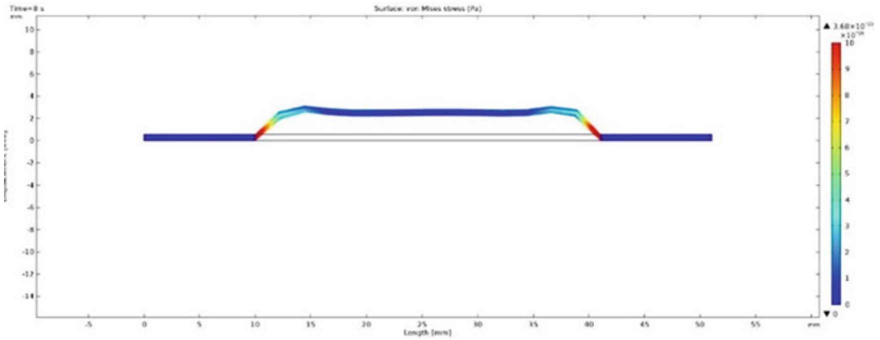

Fig. 27 Surface stress (Pa) with length (mm) of IPMC along x-axis and displacement (mm) along y-axis

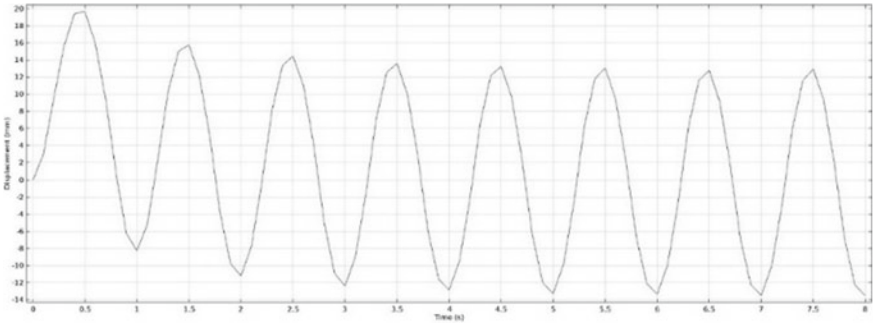

Fig. 28 Displacement (mm) versus time (s) of IPMC actuator of length 51.07 mm, thickness 0.57 mm actuated at 0.5 V, 1 Hz

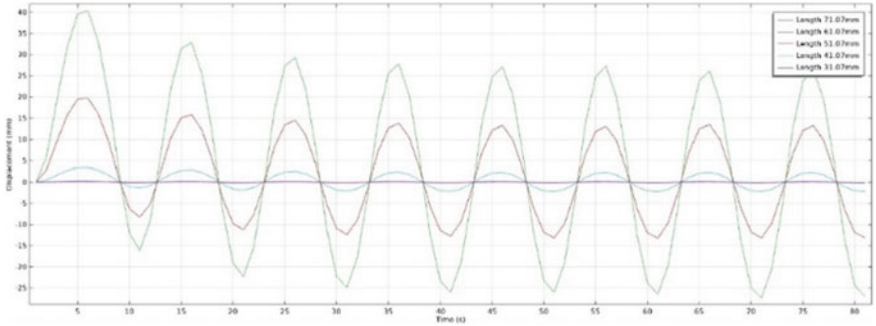

Fig. 29 Displacement (mm) versus time (s) of varying IPMC actuator lengths at 0.5 V, 1 Hz

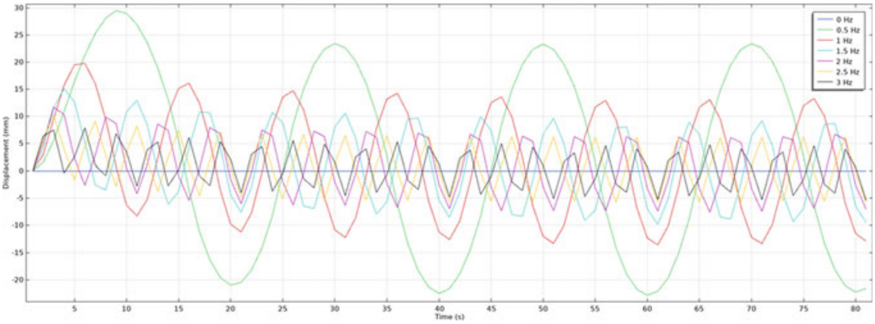

Fig. 30 Displacement (mm) versus time (s) of varying voltage frequencies at 0.5 V

4.2 Nozzle/Diffuser

In order to analyze the effectiveness of a passive valve, an existing model of a piezoelectric pump was used so that the results generated could be attributed to solely the study of the nozzle/diffuser setup. The modules used in COMSOL Multiphysics to achieve this study are Solid mechanics (solid), Laminar flow. The parametric constants required are shown in Fig. 31. Due to computational difficulty of IPMC actuator in 3D, passive valve characterization has been performed using a piezoelectric pump with a 12 V, 60 Hz supply voltage.

The volume of pump chamber used is 4.5 ml with dimensions 30 mm × 30 mm × 10 mm. The valves are symmetrically placed equidistant from the edge of the pump at the bottom. The height of valve is 10 mm, the larger diameter of inlet and

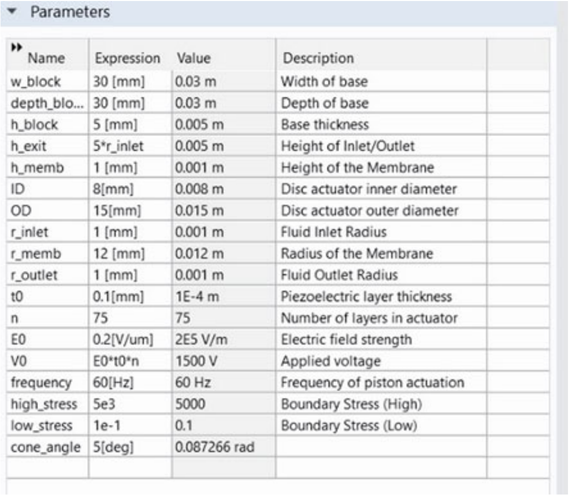

Name	Expression	Value	Description
w_block	30 [mm]	0.03 m	Width of base
depth_blo...	30 [mm]	0.03 m	Depth of base
h_block	5 [mm]	0.005 m	Base thickness
h_exit	5*r_inlet	0.005 m	Height of Inlet/Outlet
h_memb	1 [mm]	0.001 m	Height of the Membrane
ID	8[mm]	0.008 m	Disc actuator inner diameter
OD	15[mm]	0.015 m	Disc actuator outer diameter
r_inlet	1 [mm]	0.001 m	Fluid Inlet Radius
r_memb	12 [mm]	0.012 m	Radius of the Membrane
r_outlet	1 [mm]	0.001 m	Fluid Outlet Radius
t0	0.1[mm]	1E-4 m	Piezoelectric layer thickness
n	75	75	Number of layers in actuator
E0	0.2[V/um]	2E5 V/m	Electric field strength
V0	E0*t0*n	1500 V	Applied voltage
frequency	60[Hz]	60 Hz	Frequency of piston actuation
high_stress	5e3	5000	Boundary Stress (High)
low_stress	1e-1	0.1	Boundary Stress (Low)
cone_angle	5[deg]	0.087266 rad	

Fig. 31 Parametric constants for valve simulations

outlet is 3 mm while the smaller diameter is controlled by cone angle which is at 5° corresponding to roughly 1.06 mm radius. The volume of the valves is approximately 52 µl. The model designed is shown in Fig. 32. The model has been bisected along the x–z plane to reduce computational complexity since the pump is symmetric in nature. The flow rate is calculated as the spatial integral of the volume of liquid passing through the inlet and outlet. The flow rate was found as shown in Fig. 33 which is 2.4 ml/min at steady state. The flows below 0 represent backward flow which is less than 10 µl/min.

The flow rate for different cone angles was plotted as shown in Fig. 34 and as expected with shrinking diameters of the smaller end the flow rate changes accordingly. However, there is no major change in variation of flow rate between various angles. The maximum outflow at every angle is shown in Fig. 35 which is a better representation of the variation.

The above results show that valve-less model for micro-pumps is a suitable alternative to their active counterparts. Not only do they save on power, but also the manufacturing difficulty is overcome, and wear and tear associated is reduced. Figure 33 illustrates acceptable backflow values that can be fine-tuned by varying the cone angle as observed in Figs. 31 and 35. Since the effective height of valve was kept constant, the flow rate doesn't seem to improve with different angles and could have been limited by the smaller diameter of the valve. Additionally, the overall volumetric out flow varies nearly linearly with time which implies that fluid is transported efficiently with minimum delay as shown in Fig. 36. The response times of active valves could be prone to slow response due to the actuation mechanism in case of dual valve type micro pump. Additional study has to be conducted to verify if usage of multiple valves with greater backflow resistance can improve efficiency and flow control and if variation of sidewall curvature has any effect on flow rate control.

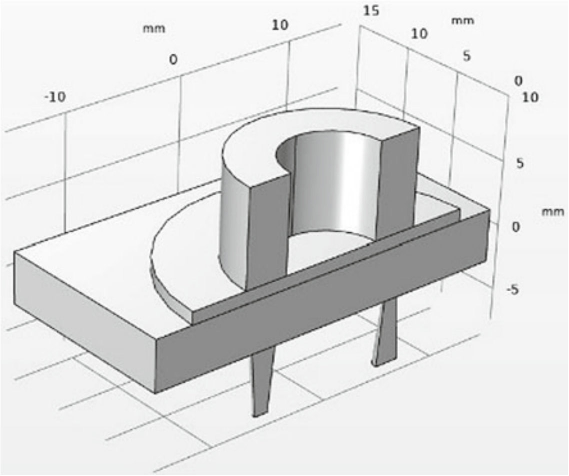

Fig. 32 Pump model with nozzle/diffusor valves

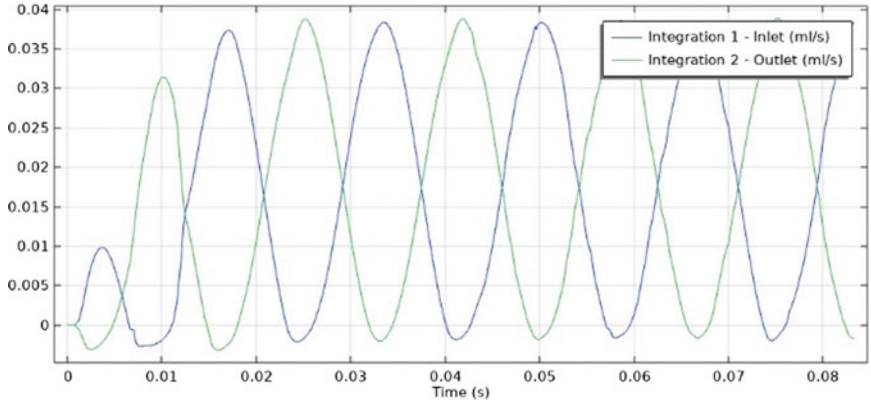

Fig. 33 Inlet flow rate (ml/s) and Outlet flow rate (ml/s) versus time

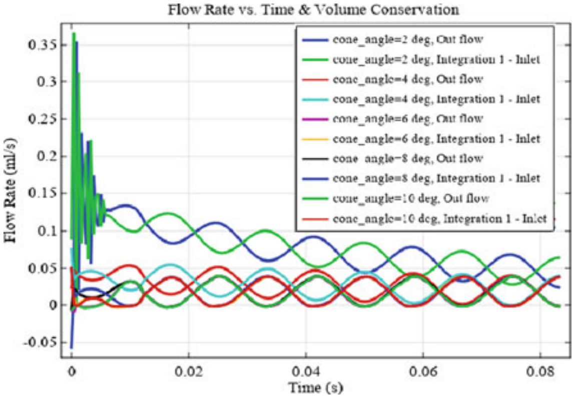

Fig. 34 Flow rate (ml/s) for different conical angles of valve

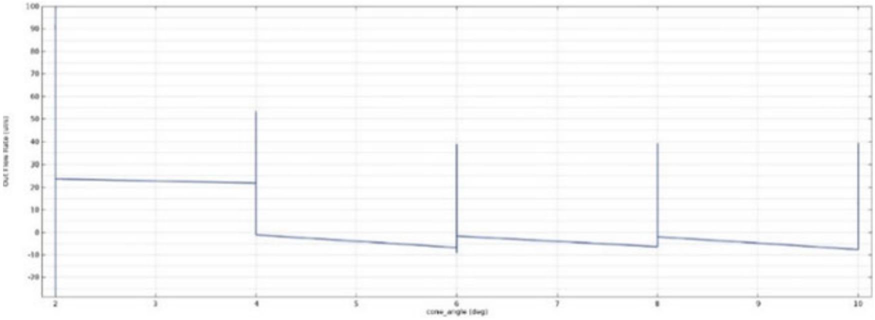

Fig. 35 Maximum outflow rate (ml/s) versus cone angle

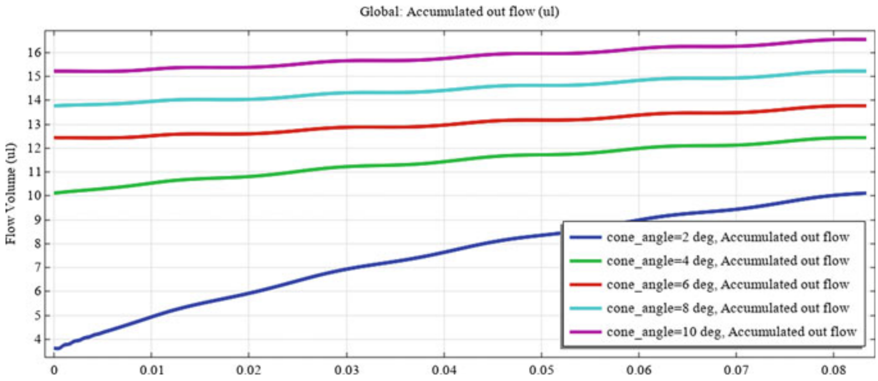

Fig. 36 Accumulated flow volume versus time for different cone angles

Figures 37, 38, 39, 40, 41 and 42 show the flow rate and pressure contours of a 10° angle conical valve in the direction opposite to the flow of regular valve operation. The negative pressure shown is due to the formation of eddies that create low-pressure areas and drastically reduce flow rates. There is a 30% increase in flow rate with increasing inlet pressure which settles to a nearly constant value at the inlet pressure of 130 Pa. The outlet pressure on the other hand shows a steady decrease with increasing inlet pressure with a 5% decrease across three different pressures. The maximum backflow rate observed is 3 ml/s.

Tesla valve under similar conditions exhibits a much lesser backflow rate as shown in Figs. 43, 44, 45, 46, 47 and 48. There is a maximum backflow rate of 240 μl/s at an inlet pressure of 130 Pa. The observed rise in back flow rate in 60% for every 60 Pa

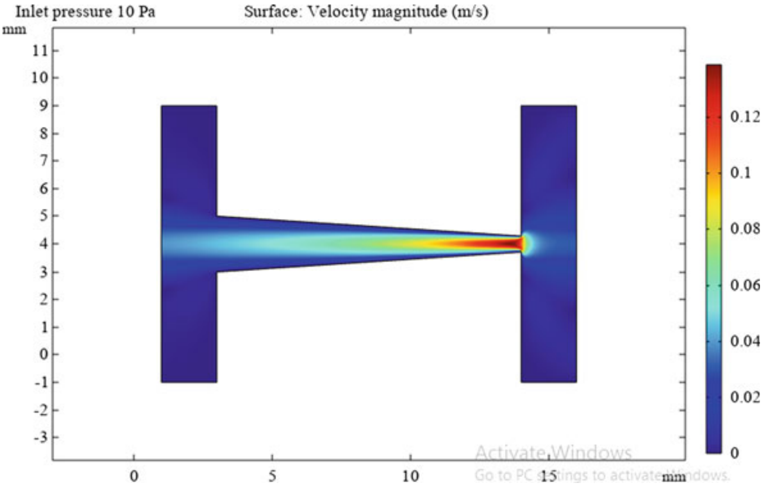

Fig. 37 Flow rate at 10 Pa inlet pressure for conical valve

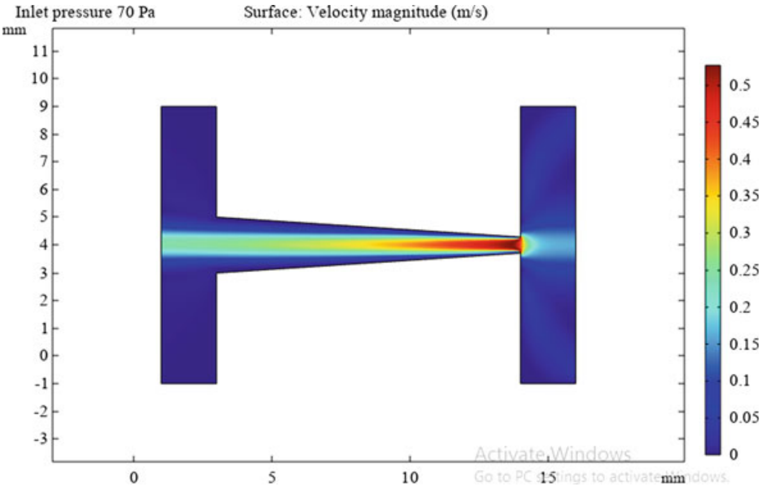

Fig. 38 Flow rate at 70 Pa inlet pressure for conical valve

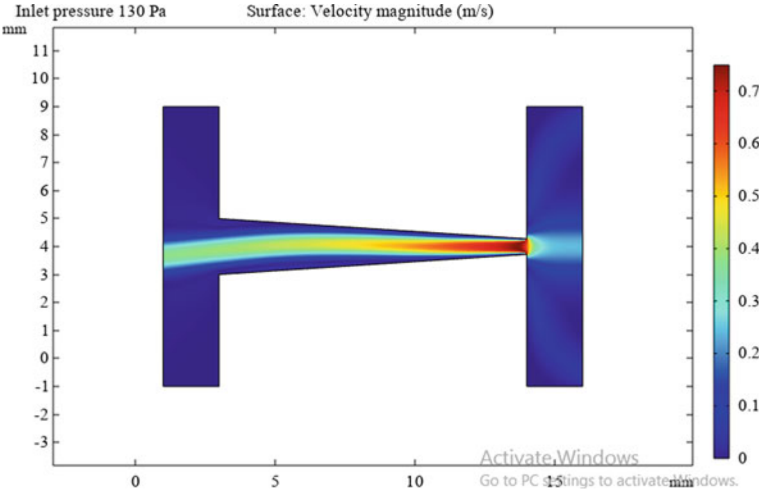

Fig. 39 Flow rate at 130 Pa inlet pressure for conical valve

raise in inlet pressure. The reduction in backflow rate can be attributed to the observed lack pressure variation at the inlet and outlet thus restricting backflow. The difference in pressure is hardly 1% as shown in the figures. The direction of flow is from right to left where it offers greater resistance to flow. The flow rate is calculated across a cross-sectional area of 1 mm cube as shown in proposed fabrication dimensions in Table 4.

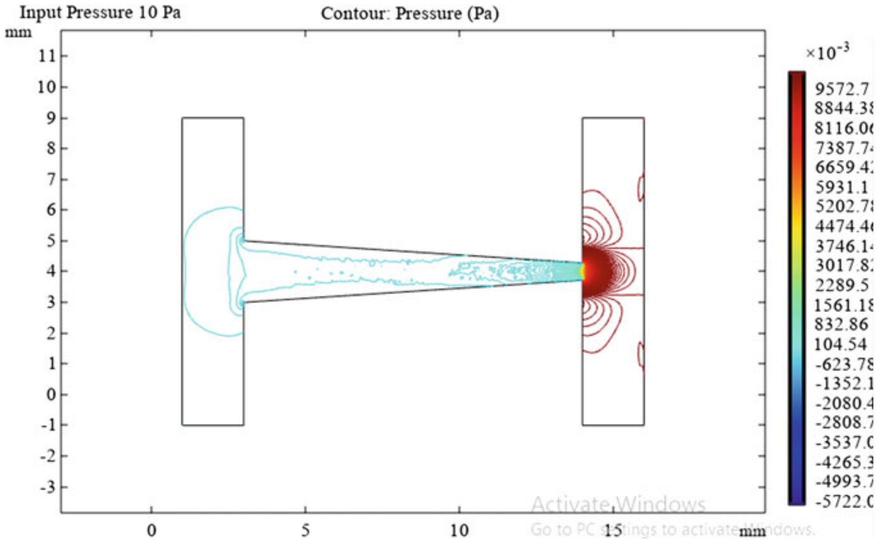

Fig. 40 Conical valve-Outlet pressure contours for 10 Pa inlet pressure

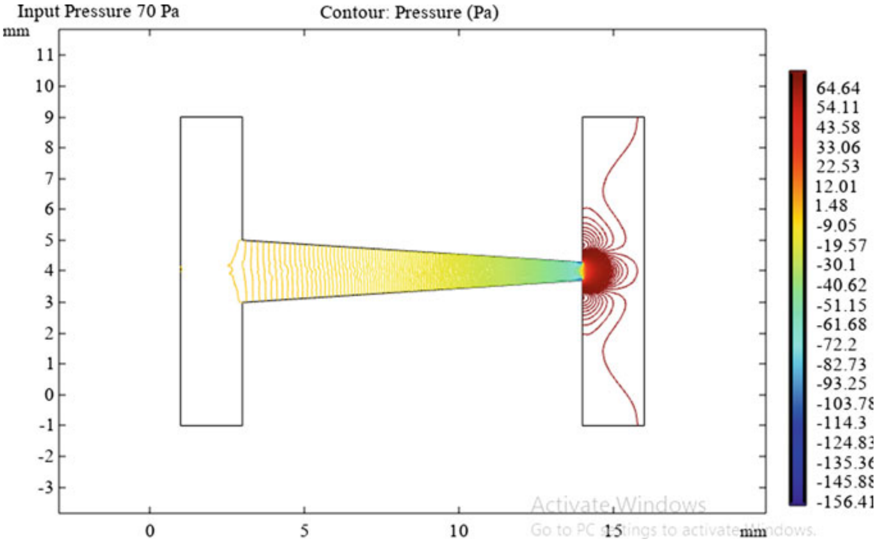

Fig. 41 Conical valve-Outlet pressure contours for 70 Pa inlet pressure

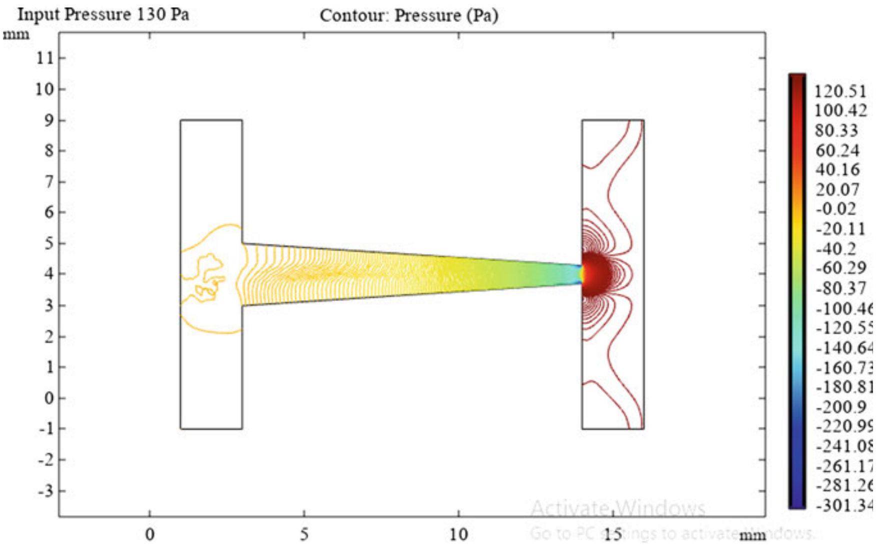

Fig. 42 Conical valve-Outlet pressure contours for 130 Pa inlet pressure

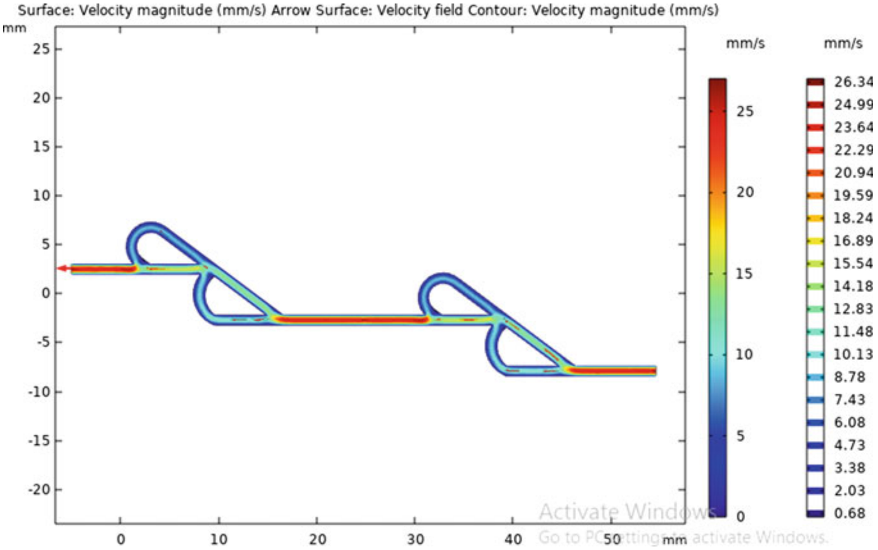

Fig. 43 Flow rate at 10 Pa inlet pressure for tesla valve

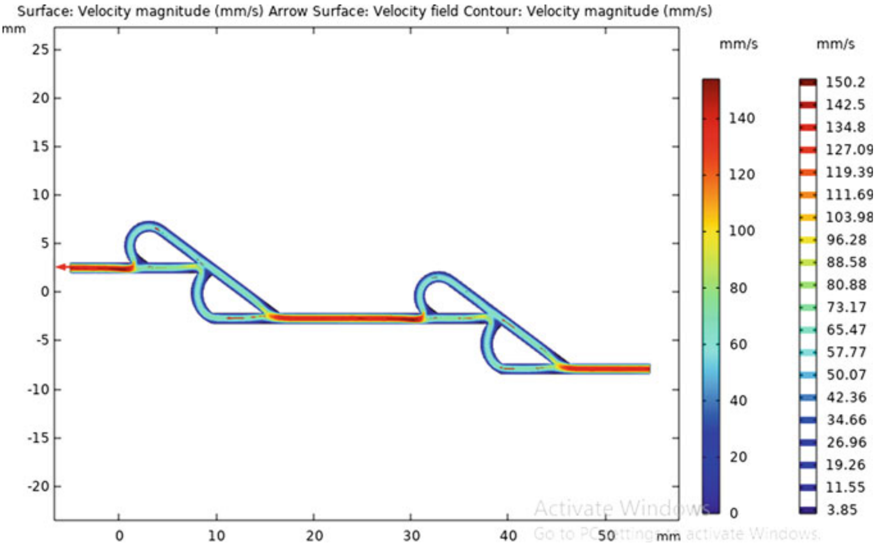

Fig. 44 Flow rate at 70 Pa inlet pressure for tesla valve

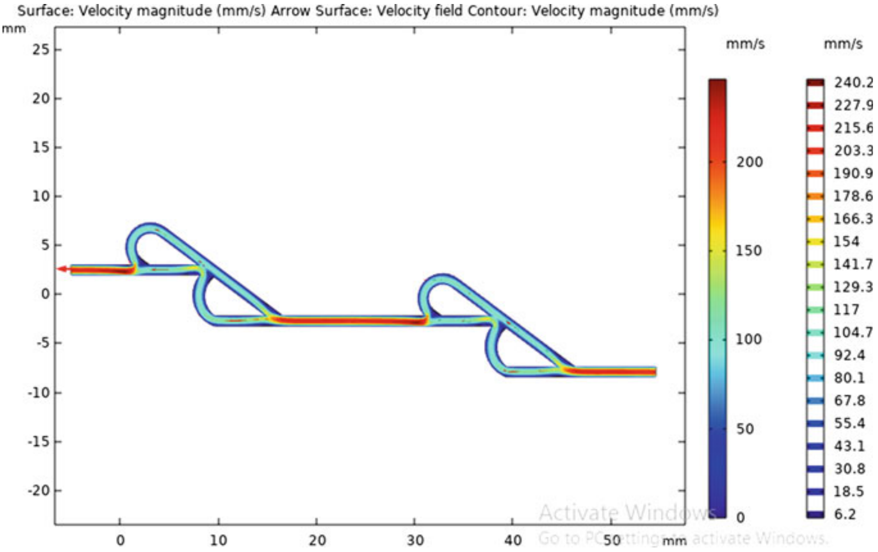

Fig. 45 Flow rate at 130 Pa inlet pressure for tesla valve

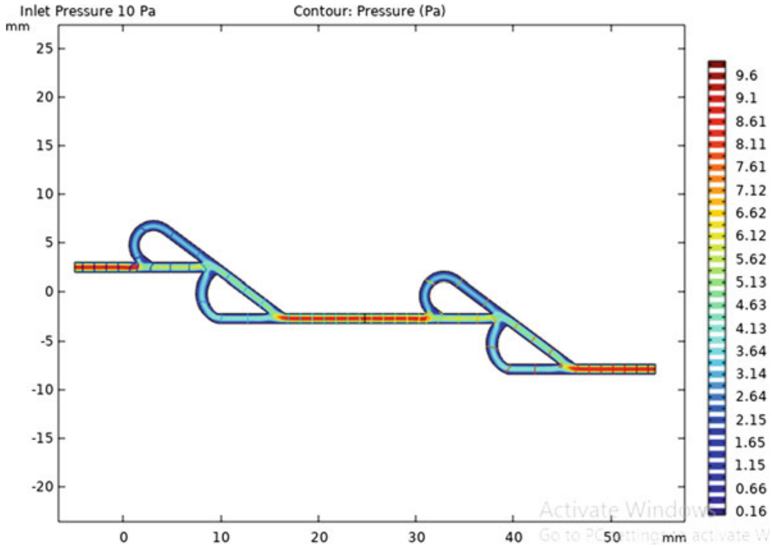

Fig. 46 Outlet pressure contours at 10 Pa inlet pressure for tesla valve

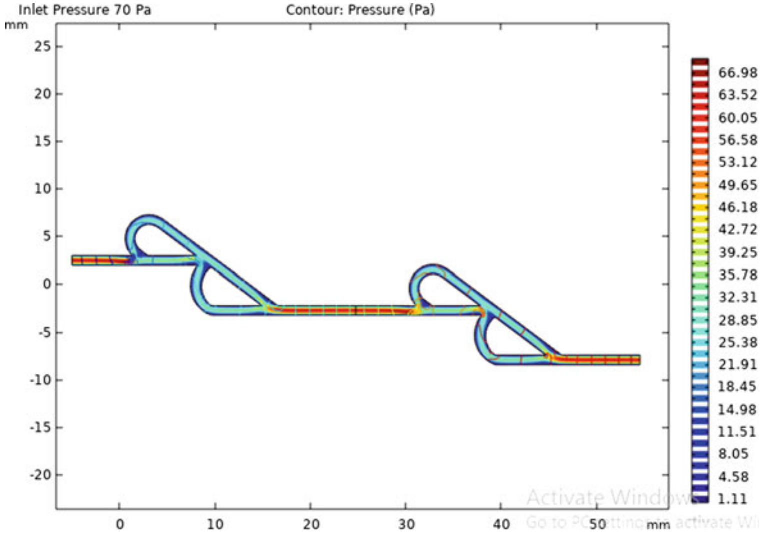

Fig. 47 Outlet pressure contours at 70 Pa inlet pressure for tesla valve

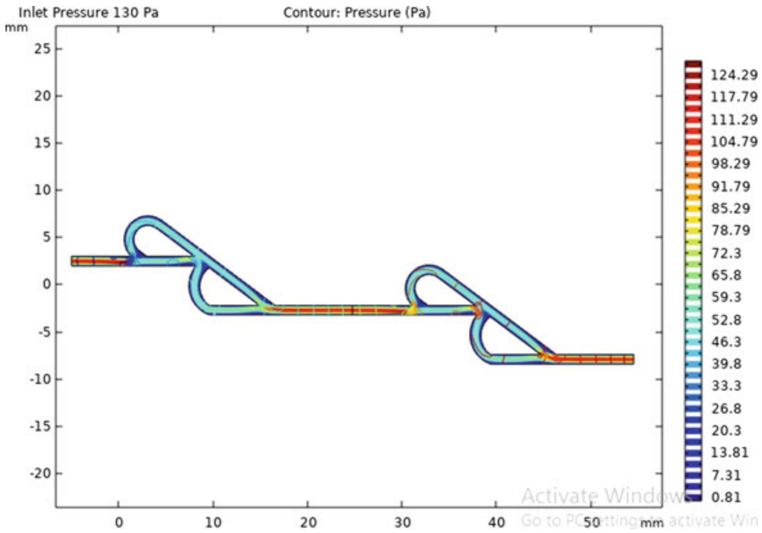

Fig. 48 Outlet pressure contours at 130 Pa inlet pressure for tesla valve

Table 4 Specifications of single chamber tesla valve-less micro-pump

Part	Dimensions
Main block	200 × 30 × 6 mm
Diaphragm holder radius	21 mm
Pumping chamber radius	19 mm
Tesla valve cross section	1 × 1 mm
Tesla valve length	60 mm
Angle of islands	53°
Fluid receiving chamber diameter	4 mm
Tube fitting pipe diameter	4.8 mm

5 Conclusion

This review article shows the comparison of various types of micro-pumps and majorly focused on IPMC-based micro-pumps. The IPMC micro-actuators consume less power, and hence it is possible to obtain low power operation. This is due to low voltage operation of IPMC actuator. The conical angles were analyzed for optimizing the performance with respect to flow rate. Using valve-less nozzle/diffuser setup with conical angle of 4–6°, the pump provides desired flow rate. However, the computational effort for the simulation of IPMC actuator is exceptionally large. Furthermore, there exists no concise methodology for modeling IPMC-based actuators. The simulation performed uses a white box model which is solved using approximation methods targeted at error reduction over several segregated iterations. The current model does not converge for 3D simulations in the electric current domain hence, direct characterization of pump in relation to actuator performance needs a different approach. Although the effectiveness of valve should be independent of type of diaphragm actuated micro-pump, a suitable methodology for relation of IPMC membrane displacement and flow rate across nozzle/diffuser type passive valves is required.

Fabrication designs were proposed for single chamber conical valve micro-pump, double chamber conical valve micro-pump functioning at 180° out of phase with each other and single chamber tesla valve micro-pump according to the specifications. The simulation results show the expected flow rates achievable for different fluid pressures that may arise giving rise to the desired flow rate. Future work would involve a suitable fabrication method that doesn't involve the difficulty faced in impression molding technique.

References

1. Bourouina T, Bossebuf A, Grandchamp J-P (1997) Design and simulation of an electrostatic micro pump for drug-delivery applications. J Micromech Microeng 7(3):186
2. Machauf A, Nemirovsky Y, Dinnar U (2005) A membrane micro pump electrostatically actuated across the working fluid. J Micromech Microeng 15(12):2309
3. Kaçar A, Özer MB, Taşcıoğlu Y (2020) A novel artificial pancreas: energy efficient valve less piezoelectric actuated closed-loop insulin pump for T1DM. Appl Sci 10(15):5294
4. Mohith S, Navin Karanth P, Kulkarni SM (2020) Performance analysis of valve less micro pump with disposable chamber actuated through Amplified Piezo Actuator (APA) for biomedical application, Mechatronics 67:102347. ISSN 0957–4158
5. He XH, Zhu JW, Zhang XT et al (2017) The analysis of internal transient flow and the performance of valve less piezoelectric micro pumps with planar diffuser/nozzles elements. Microsyst Technol 23(1):23–37
6. Zhang JH, Wang Y, Huang J (2017) Advances in valve less piezoelectric pump with cone-shaped tubes. Chin J Mech Eng 30:766–781
7. Bußmann A, Leistner H, Zhou D, Wackerle M, Congar Y, Richter M, Hubbuch J (2021) Piezoelectric silicon micro pump for drug delivery applications. Appl Sci 11:8008
8. Shan J et al (2022) Implantable double-layer pump chamber piezoelectric valve less micro pump with adjustable flow rate function. J Micromech Microeng
9. Asadi Dereshgi, Hamid, Huseyin Dal, and Mustafa Zahid Yildiz. "Piezoelectric micro pumps: State of the art review." Microsystem Technologies 27.12 (2021): 4127–4155.
10. Chia BT, Liao H, Yang Y (2010) A novel thermo-pneumatic peristaltic micro pump with low temperature elevation on working fluid. Sens Actuat A 165:86–93
11. Ha S-M, Cho W, Ahn Y (2009) Disposable thermo-pneumatic micro pump for bio lab-on-a-chip application. Microelectron Eng 86(4–6):1337–1339
12. Chee PS et al (2015) Wireless powered thermo-pneumatic micro pump using frequency-controlled heater. Sens Actuat A: Phys 233:1–8
13. Hamid NA et al (2017) A stack bonded thermo-pneumatic micro-pump utilizing polyimide based actuator membrane for biomedical applications. Microsyst Technol 23(9):4037–4043 (2017)
14. Setiawan MA (2008) The performance evaluation of SMA Spring as actuator for gripping manipulation. J Teknik Elektro 7:110–120

15. Bhandari B, Lee G-Y, Ahn S-H (2012) A review on IPMC material as actuators and sensors: fabrications, characteristics and applications. Int J Precis Eng Manuf 13(1):141–163
16. Jung K, Nam J, Choi H (2003) Investigations on actuation characteristics of IPMC artificial muscle actuator. Sens Actuat A 107(2):183–192
17. Chung C-K et al (2006) A novel fabrication of ionic polymer-metal composites (IPMC) actuator with silver nano-powders. Sens Actuat B: Chem 117(2):367–375 (2006)
18. Gareev KG et al (2021) Microfluidic system for drug delivery based on microneedle array and IPMC valve less pump. In: 2021 IEEE conference of russian young researchers in electrical and electronic engineering (ElConRus). IEEE
19. Olvera D, Monaghan MG (2021) Electroactive material-based biosensors for detection and drug delivery. Adv Drug Deliv Rev 170:396–424
20. Bußmann AB et al (2021) Microdosing for drug delivery application—A review. Sens Actuat A: Phys 330:112820 (2021)
21. Zhang Z et al (2022) Smart film actuators for biomedical applications. Small 2105116 (2022)
22. Ilami M et al (2021) Materials, actuators, and sensors for soft bioinspired robots. Adv Mater 33(19):2003139
23. Liu G, Shen C, Yang Z, Cai X, Zhang H (2010) A disposable piezoelectric micro pump with high performance for closed-loop insulin therapy system. Sens Actuat A 163:291–296
24. Lee S, Yee SY, Besharatian A, Kim H, Bernal LP, Najafi K (2009) Adaptive gas pumping by controlled timing of active micro valves in peristaltic micro pumps. In: Proceedings of transducers, Denver, CO, pp 21–25
25. Kim JH, Na KH, Kang CJ, Kim YS (2005) A disposable thermopneumatic actuated micro pump stacked with PDMS layers and ITO coated glass. Sens Actuat A 120:365–369
26. Fang T, Tan X (2010) A novel diaphragm micro pump actuated by conjugated polymer petals: Fabrication, modeling, and experimental results. Sens Actuat A 158:121–131
27. Al-Halhouli AT, Kilani MI, Büttgenbacha S (2010) Development of a novel electromagnetic pump for biomedical applications. Sens Actuat A 162:172–176
28. Zou JX, Ye YZ, Zhou Y, Yang Y (1997) A novel thermally actuated silicon micro pump. In: International symposium on micromechatronics and human science, Nagoya, Japan, pp 5–8
29. Yamahata C et al (2005) A PMMA valve less micro pump using electromagnetic actuation. Microfluidics Nanofluidics 1(3):197–207 (2005)
30. Pun AM, Lo JH, Louie DC et al (2007) Micro-fabrication of the non-moving part valve micro-pump by hot-embossing technology. World congress on medical physics and biomedical engineering. Springer, Berlin 1:242–245
31. Sim WY, Lee SW, Yang SS (2021) The fabrication and test of a phase-change type micro pump. In: IMECE2001/MEMS-23870, pp 479–484
32. Zhang HJ, Qiu CJ (2006) A TiNiCu thin film micro pump made by magnetron Co-sputtered method. Mat Trans 47:532–535
33. Pak JJ et al (2004) Fabrication of ionic-polymer-metal-composite (IPMC) micro pump using a commercial Nafion. In: Smart structures and materials, vol 5385. SPIE, p 9
34. Lee S, Kim KJ (2006) Design of IPMC actuator-driven valve-less micro pump and its flow rate estimation at low Reynolds numbers. Smart Mater Struct 15(4):1103
35. Nguyen TT, Nguyen VK, Yoo Y, Goo NS (2006) A novel polymeric micro pump based on a multilayered ionic polymer-metal composite. In: IECON 2006 - 32nd annual conference on IEEE industrial electronics, pp 4888–4893
36. Nguyen TT, Goo NS, Nguyen VK, Yoo Y, Park S (2008) Design, fabrication, and experimental characterization of a flap valve IPMC micro pump with a flexibly supported diaphragm. Sens Actuat A 141(2):640–648
37. Santos J, Lopes B, Branco PJC (2010) Ionic polymer–metal composite material as a diaphragm for micro pump devices. Sens Actuat A 161(1):225–233
38. Wei W, Guo S (2010) A novel PDMS diaphragm micro pump based on ICPF actuator. In: International conference on robotics and biomimetics, pp 1577–1583
39. McDaid J, Aw KC, Haemmerle E, Xie SQ (2012) Control of IPMC actuators for microfluidics with adaptive "online" iterative feedback tuning. IEEE/ASME Trans Mechatron 17(4):789–797

40. Rajapaksha CPH, Feng C, Piedrahita C, Cao J, Kaphle V, Lüssem B, Kyu T, Jákli A (2020) Poly(ethylene glycol) diacrylate based electro-active ionic elastomer. Macromolecul Rapid Commun J 41:1900636
41. Schabmueller CGJ, Koch M, Mokhtari ME et al (2002) Self-aligning gas/liquid micro pump. J Micromech Microeng 12(4):420
42. Huang XY, Wang SS, Yang (2009) Single-nozzle micro pumps. In: Proceedings of the ASME 2009 7th international conference on nanochannels, microchannels, and minichannels, Pohang, South Korea. June 22–24, pp 717–721
43. Annabestani M, Fardmanesh M (2019) Ionic electro active polymer-based soft actuators and their applications in microfluidic micro pumps, micro valves, and micromixers: a review. arXiv:1904.07149
44. Pugal D, Kim KJ, Aabloo A (2011) An explicit physics-based model of ionic polymer-metal composite actuators. J Appl Phys 110
45. Pugal D, Stalbaum T, Palmre V, Kim KJ (2016) Modelling ionic polymer metal composites with COMSOL. In: IPMCs smart multi-functional materials, and artificial muscles, vol 1, Chapter 5
46. Sangki L, Kwang JK (2006) Design of IPMC actuator-driven valve-less micro pump and its flow rate estimation at low Reynolds Numbers. Smart Mater Struct 15(4):1103
47. Ashraf MW, Tayyaba S, Afzulpurkar N (2011) Micro electromechanical systems (MEMS) based microfluidic devices for biomedical applications. Int J Mol Sci 12:3648–3704
48. Pawar SJ, Singh R (2017) Parametric simulation and flow visualization of micro-diffuser used in MEMS and microsystem devices. Int J Mech Product Eng. ISSN: 2320–2092
49. Tan HY, Loke WK, Nguyen N (2010) A reliable method for bonding polydimethylsiloxane (PDMS) to polymethylmethacrylate (PMMA) and its application in micro pumps. Sens Actuat B 151:133–139
50. Ziaie B, Baldi A, Lei M, Yuandong Gu (2004) Ronald A Siegel, Hard and soft micromachining for BioMEMS: review of techniques and examples of applications in microfluidics and drug delivery. Adv Drug Deliv Rev 56(2):145–172
51. Riahi R, Tamayol A, Shaegh SAM, Ghaemmaghami AM, Dokmeci MR, Khademhosseini A (2015) Microfluidics for advanced drug delivery systems. Current Opin Chem Eng 7: 101–112
52. Ahn J, Ko J, Lee S, James Yu, Kim YongTae (2018) Noo Li Jeon, Microfluidics in nanoparticle drug delivery. From synthesis to pre-clinical screening. Advanced drug delivery reviews 128:29–53
53. Amirouche F, Zhou Y, Johnson T (2009) Current micro pump technologies and their biomedical applications. Microsyst Technol 15:647–666
54. Aishan Y, Yalikun Y, Shen Y, Yuan Y, Amaya S, Okutaki T, Osaki A, Maeda S, Tanaka Y (2021) A chemical micro pump actuated by self-oscillating polymer gel. Sens Actuat B: Chem 337
55. Yamahata C, Lacharme F, Gijs MA (2005) Glass valve less micro pump using electromagnetic actuation. Microelectron Eng 78:132–137
56. Nisar A et al (2008) MEMS-based micro pumps in drug delivery and biomedical applications. Sens Actuat B: Chem 130(2):917–942
57. Lai H-Y, Kang J-H (2021) System modeling and characterization of enhanced valve less micro pumps. Mech Based Design Struct Mach 1–22
58. Kalyonov VE et al (2020) Valve less microfluidic pump based on IPMC actuator for drug delivery. In: 2020 IEEE conference of Russian young researchers in electrical and electronic engineering (EIConRus). IEEE
59. Chappel E, Dumont-Fillon D (2021) Micro pumps for drug delivery. Drug Delivery Devices Therapeut Syst 31–61

Fabrication Techniques and Materials for Bio-MEMS

Sudhanshu Dwivedi

Abstract Microelectromechanical systems (MEMS) based advanced point-of-care rapid diagnostic solutions with high degree of sensitivity along with high accuracy are required that can remain efficient even after a decrement in the form factor of the sensor. MEMS technology is at the forefront of development of miniaturized biosensor devices in bulk batches that offer a highly efficient, sensitive, accurate, precise and commercial platform. Arranged arrays of MEMS devices can be spatially covered in more than an area of 1000 mm^2. Bio-MEMS devices are fabricated by the conventional micromachining techniques employing oxidation, thin film deposition by sputtering, e-beam & thermal evaporation, and chemical vapor deposition (CVD). Photolithography is applied for patterning of the micrometre sized geometrical shapes, while electron beam lithography (EBL) patterns nanostructures down to few nanometres scale in reference to the nano-electromechanical-systems (NEMS) for advanced bio-detection applications including lab-on-a-chip technology. Bulk micromachining offers high commercially viable technology involving selective removal by etching of the bulk substrate materials that develop MEMS components, such as, cantilevers and beams. Wet or dry etching methods can be employed for the bulk substrate material removal by selective elimination of unmasked areas for the patterning of geometrical shapes and patterns. Faster etch rates are obtained by chemical wet etching while dry etching technique offers fabrication of anisotropic geometrical patterns with high aspect ratio. Lift-off is also a conventional commercial technique that develops patterns on the surface of the material. Stereo-lithography is an advanced 3D fabrication technology that has a commercial orientation focused on ultraviolet (UV) radiation-based curing of the polymer solution for fabrication of high aspect ratio structures in a layer-by-layer approach. Bio-MEMS/NEMS relies on different types of biomaterials, such as, DNA and RNA, that are used as biomimetic materials. The other categories are inorganic (Si, GaAs, Ge, SiC, Si_3N_4, SiO_2 and glass/quartz for biomedical applications) and organic materials (PMMA, SU-8, PDMS,) for use in MEMS/NEMS. Polymers and plastic substrates are more favourable because of ease of micromachining, faster prototyping along with higher mechanical bending characteristics, and low costs. Moreover, optically transparent

---

S. Dwivedi (✉)
S.S. Jain Subodh P.G. (Autonomous) College, Jaipur, India
e-mail: sudhanshu.dwivedi@gmail.com

K. Guha et al. (eds.), *MEMS and Microfluidics in Healthcare*, Lecture Notes in Electrical Engineering 989, https://doi.org/10.1007/978-981-19-8714-4_6

substrates can be used in optical detection techniques along with being biologically compatible. Paper microfluidics is another special variant of bio-MEMS due to its features of low-cost technology, biodegradable nature along with the normal wicking action. Paper microfluidics has been employed in paper immunoassays and electrophoresis. Microfluidic approaches in reference to bio-MEMS manipulates very small quantities of fluid over the microfabricated substrates and combines electronics for rapid testing device prototypes. There have also been efforts for the fabrication of microchannels in glass and/or fused quartz and other similar types of substrates using ultrafast lasers for microfluidics that combine optical detection techniques as well. This chapter is a concise effort to present an overview of various micro- and nanofabrication technologies for bio-MEM/NEMS device fabrication for sensing platforms. Technical nitty-gritties of photolithography and EBL have been presented in a critical manner along with different materials used in the advanced bio-MEMS/NEMS micro- and nanofabrication. A small portion is also devoted to the description of cleanroom technology including its classifications with a note on international standardization protocols. Apart from this, deposition techniques have also been discoursed in special reference to bio-MEMS/NEMS. Superhydrophobic feature or wetness property and its importance in the bio-MEMS/NEMS based sensing platforms have also been discussed.

1 Introduction

Microelectromechanical systems or MEMS entails the fabrication of micron-sized devices by the use of a host of fabrication techniques of thin film deposition, photolithography and wet- or mostly dry-etching techniques [1, 2]. Fabrication of nano-sized devices by the above techniques including electron beam lithography (EBL) for nano-patterning is termed as nanoelectromechanical systems or NEMS [1, 2]. This technology is a combination of microelectronics and μm- or nm-sized mechanical structures obtained by micromachining. This technology is referred to as microsystems technology (MST) in Europe while as micro-machines in Japan. MEMS is a word that pertains to a relevant technological platform stating that electrical circuits and correlated components are combined to form a mechanical device in form of a sensor or actuator. Microelectronics and micromachined structures can be integrated during or after the process of fabrication and for this a standard design process is extensively tested before the actual production of the device structure. MEMS is an established commercially viable technology that ensures production of micromachined architectural systems with enhanced performances. MEMS is decades old technology now widely used for the fabrication of accelerometers as navigational sensors, radiofrequency (RF) MEMS for automotive radar sensors in the operational frequency range of 76–81 GHz, MEMS based fabrication of 3D architectures, robust MEMS devices for ground aero-propulsion wind tunnels, MEMS based inertial measurement units (IMUs) for missile applications including applications in high speed re-entry spacecraft guidance, navigation as well as control (**GNC**) systems, fuel cell applications, applications in integrated circuitry (**IC**), geotechnical underground sensor including monitoring applications and also inclusive of bio-MEMS or even bio-NEMS based implantable devices [2, 3].

Bio-MEMS or bio-NEMS is a sub-branch of MEMS/NEMS that makes use of prevalent techniques in MEMS/NEMS for the fabrication of bio- or medical-devices [4–7]. In relation to bio-MEMS, the important ingredients are inclusive of microfabrication of devices on silicon (***Si***), glass and polymer substrates, microfluidics and the associated electrokinetics, physics of devices that include sensors as well as actuators, micro-total-analysis systems (**μTAS**), lab-on-a-chip or **LOC** device, detection as well as measuring and quantification systems, packaging of bio-MEMS systems, **RF** safety measures, power systems & effective transportation of data packages as well as a host of biological systems that include clinical medicines and correlated systems, deoxy-ribose nucleic acid (**DNA**), proteomics, genomics and protein microarrays.

Fabrication of bio-MEMS devices involves four different strategies that include photolithography-based patterning of the material, (ii) deposition of thin films over the substrates followed by patterning, (iii) selective etching of material to form uniform or shape-anisotropic structures and (iv) bonding in which two substrates are bonded with each other.

2 Fabrication Technology

The first and the foremost step in fabrication methodology on a substrate involves the meticulous cleaning process. Different types of substrates are silicon (***Si***), germanium (**Ge**), gallium arsenide (**GaAs**), sapphire ($\mathbf{Al_2O_3}$) or even glass substrates, such as, fused silica. Very often ***Si*** is used in the fabrication of MEMS, switching and memory devices for logic & memory operations. ***Si*** fabrication technology is highly developed device processing technology because of low cost of the raw material of $\mathbf{SiO_2}$ for ***Si*** wafer manufacturing along with being readily available. This is despite the fact that ***Si*** is an indirect bandgap semiconductor material [8], while **Ge** is a direct bandgap semiconductor material [9] and possesses much reduced electron mobilities in comparison to ***Ge***. Lin et al. has specifically worked on indirect to direct bandgap engineering in ultrathin Si semiconductor films [8]. Fadaly et al. reported on highly efficient light emission from direct bandgap Ge semiconductor materials [9]. Cleaning of ***Si*** substrates is performed by the **RCA** (Radio Corporation of America) method, Piranha cleaning methods, dipping in **HF** solution and/or even cleaning with acetone, methanol & isopropyl alcohol subsequently followed by cleaning with doubly deionized water (resistivity, $\boldsymbol{\rho} = 18.2\ \text{M}\Omega\text{-cm}$ at $\boldsymbol{T} = 25\ °\text{C}$). A dehydration bake is performed before application of photoresist (**PR**) over ***Si*** substrates for removal of residual $\mathbf{H_2O}$ molecules or water vapor molecules attached to the substrate. Wafer priming is the process of enhancement of adhesion by use of adhesion promoter, hexamethyldisiliazane [**linear formula:** $\mathbf{(CH_3)_3SiNHSi(CH)_3}$], or application of plasma based etching of the substrate surface to coarsen it. After cleaning of the substrate, an oxide layer of $\mathbf{SiO_2}$ is very often required. This $\mathbf{SiO_2}$ layer not only acts as an insulating layer but can also be used as a protective mask in the subsequent processing steps of etching, for example. Oxidation of ***Si*** wafers can be done both by wet and dry oxidation methods in a tube furnace at higher temperatures for dry oxidation (900–1150 °C) and at relatively temperatures in case of wet oxidation (700 °C). The first step in the photolithography process involves the application of a thin photosensitive organic polymer layer, i.e., of liquid **PR** over the oxidized substrate surfaces. ***Si*** substrate is held in a spin-coater with the help of a vacuum chuck so that it does not get thrown away during the spinning process, and to ensure formation of uniform layers of **PR** over the substrate surface. Spinning of ***Si*** substrate is performed at highly controlled speeds in one or even more steps. Usual spin speeds are in the range of 1500–8000 rpm causing liquid **PR** material to drive towards the edges of the substrate due to centrifugal forces. The material keeps on compiling at the edges where surface tension keeps on holding the material and is thrown out on exceeding this force. The generated **PR** thickness is the function of molecular weight, solution concentration and the spin speeds. Optimization of spinning process is highly desirable for effective transfer of the patterns in addition to the control of defect density in the spun polymer. Subsequently, the substrate is soft baked to remove remaining solvents in the spun **PR** to ensure that no built-in stresses are generated as a result of residual liquid. Prebaking or soft-baking is performed at $\boldsymbol{T} = 75\text{–}100\ ^{\circ}\mathrm{C}$ for removal of residual solvent and subsequent promotion of adhesion of **PR** to the substrate surface. After soft-baking, the pattern is transferred onto the **PR** by light exposure through a photomask consisting of a pattern to be replicated with desired geometrical features. Light sources can be a mercury lamp, ultraviolet (UV) light and even laser sources. Light radiation from mercury lamp can be of wavelengths 435 nm (***g*-line**) or even 365 nm (***i*-line**). UV light has the wavelength of 285 nm, while laser sources have typical wavelengths of 193 and 248 nm. The smallest feature that can be lithographed is almost proportional to the wavelength of the source that is implemented for exposure. The exposed **PR** becomes either soluble or insoluble in the developer solution depending on itself being a positive or negative PR. Profiling of side-walls of **PR** is of critical importance that can be better adjusted by appropriate control of exposure time and dosage, strength of the developer as well as the time of development. Post-exposure development and treatment is required for cessation of reactions initiated during the exposure and even inducing newer reactions. Post-exposure treatments are inclusive of post-exposure baking, vacuum reactions, interaction in an environment of a reactive gas and even flood exposure from different radiation sources. Aqueous alkaline solutions are generally used for the development of positive **PR**s while organic solvents are used for the development of negative **PR**s. After the development procedure, undesired residual **PR** is eliminated before further processing. This process is known as descumming that removes undesired **PR** with the help of mild plasma-based procedure typically known as plasma ashing. Highly energetic $\mathbf{O^{2-}}$ ions are generated in the plasma by use of $\mathbf{O_2}$ gas that strikes the undesired **PR** in a controlled manner to burn it out. Hard-baking or post-baking is performed to enhance adhesion qualities of **PR** over the substrate that has been rendered to be weak as a result of penetration of the developer solution into the **PR**-substrate interface or swelling mainly in case

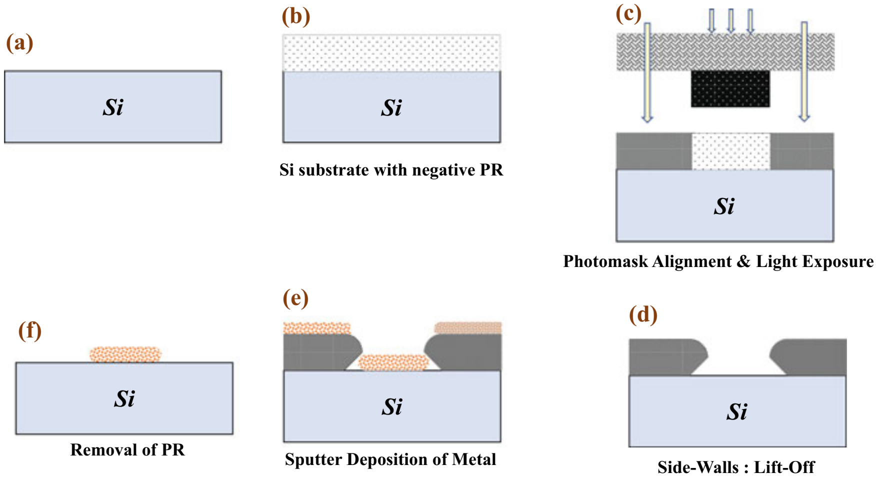

Fig. 1 Microfabrication technology process steps are shown with the help of a process flow diagram. As shown below (a) RCA cleaned wafer is taken, which is, (b) spun-coated with a negative PR followed by (c) proper photomask alignment and light exposure to develop PR for pattern formation. Lift-off generates non-uniform sidewalls as shown in (d) followed by (e) metal sputtering and (f) subsequent removal of PR, more specifically by plasma-ashing in case of a negative PR [10]

of negative **PR**s. Post-baking removes residual solvents from **PR** along with a proper heat-treatment or annealing to fill-up gaps between **PR** and the substrate. Post-baking is performed at higher temperatures of 120 °C to induce hardness in the thin **PR** layer to enhance tolerance level against etching as well as deposition steps. Sacrificial **PR** mask is used as a patterned covering layer in further processing steps involving etching and/or deposition. In the etching process, the masked **PR** layer is the protective layer against the etching solution that can be in a liquid form, gas or even plasma. After printing of the pattern, **PR** is ashed out for subsequent processing. In certain types of MEMS device architectures, **PR** is an integral part and it may not be essential to ash it out. Microfabrication process steps are shown schematically in Fig. 1.

2.1 Photolithography

Semiconductor technology relies on photolithography for the development of microstructures for the production of architectural systems for MEMS. Photolithography is an optical lithography technology employing mostly **UV** light for generation of the user-defined pattern by application of the photomask [10–13]. Photolithography technique has been discussed in a critical manner by Mahalik in his book on Micromanufacturing and Nanotechnology [10]. Hubenthal has given technical details on photolithography in the work titled as “Noble Metal Nanoparticles: Synthesis and

Optical Properties" [11]. Cirelli, Watson & Nalamasu have provided excellent technical knowhow about optical lithography in "Encyclopedia of Materials: Science and Technology" [12]. Similarly, May and Sze have discussed about principles of optical lithography in their book on "Fundamentals of Semiconductor Fabrication" [13]. Operative principle of optical lithography is based on the application of a photosensitive mask to fabricate the geometrical patterns by using a light-sensitive **PR** which has already been blanket-deposited over a substrate. The photosensitive mask is fabricated over special glass plates in the locality of a clean room that is typically designed with all the desired geometrical boundaries, sizes and shapes. The photoresist or **PR** is an organic liquid material with special photosensitive properties that is spun onto a substrate using a spin-coater followed by light exposure and baking [14–16]. Photoresist materials have been discussed in good amount by K. S. Gandhi [14] and Turner and Daly [15]. An important note is that photolithography is performed in a yellow or red-green lightened clean room to prevent initiation of photo-induced reactions in the photosensitive resist material. The technology is based on the fact that **PR**s are sensitive only to light radiations that have wavelengths shorter than those of yellow light. The wavelength of the yellow light usually lies in the range of 560–590 nm towards which the **PR** is not sensitive so that a photoreaction can never be induced, and bonds in the photosensitive PR material are not broken. Only high frequency or short wavelength light radiation can impart sufficient energy to cause photo-induced bond-breaking in **PR**s. However, with advancing technology day-by-day, there are efforts to develop highly efficient PRs along with processing of **PR**s in rather miniaturized machines with reduced processing steps to have lesser dependency on yellow light environment inside the clean room.

There are two types of **PR**, the positive **PR** and the negative **PR**. If the **PR** becomes soft bonded or bond-breaking happens in the material as a result of light exposure, and it becomes soluble in the **PR** developer solution in contrast to the unexposed part of the same **PR**, it is termed as a positive **PR**. On the other hand, if the **PR** gets hardened with bonds becoming stronger due to enhanced crosslinking on exposure to the light so that it becomes insoluble into the **PR** developer solution in comparison to the unexposed part, it is called as negative **PR**. Both positive and negative **PR**s have merits and demerits, and are applied according to the requirements. Negative **PR**s possess excellent adhesion over ***Si*** substrates in comparison to the positive **PR**s, are less expensive, have usually organic base, while positive **PR** have aqueous base, minimum feature size obtainable from positive **PR** is 0.5 μm while it is 2 μm from negative **PR**, and step coverage is better with a positive **PR** than with that obtained from a negative **PR**. Patterning with photolithography has been shown schematically in Fig. 2 given below which shows the use of a photomask-based pattern-generation procedure by the application of a positive **PR**.

As pointed out in the above schematic to generate patterns with a positive **PR**, initially a thin metal layer is deposited over the substrate. A host of techniques can be employed for the purpose that include chemical vapor deposition (**CVD**), thermal evaporation, e-beam evaporation, sputtering, molecular beam epitaxy (**MBE**) and/or pulsed laser deposition (**PLD**), and may be other clean-room physical vapor deposition (**PVD**) techniques, such as, atomic layer deposition (**ALD**). Licari and

Fig. 2 Photolithographic process with positive PR for pattern generation over a metal film in the form of a schematic

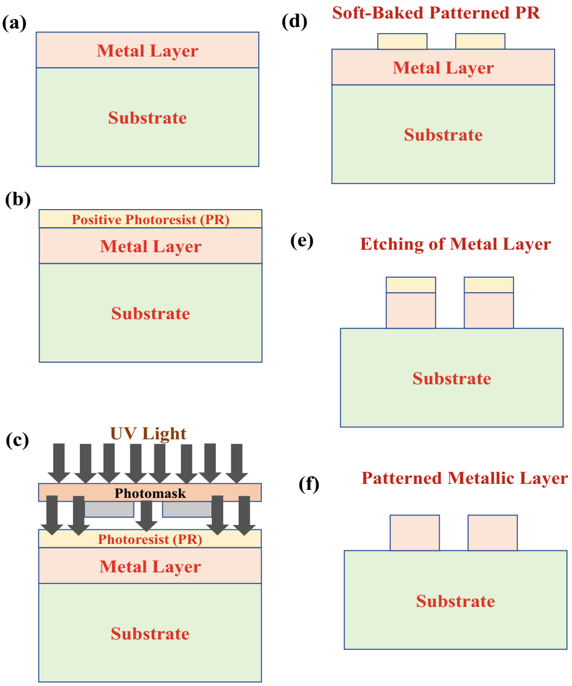

coworkers have given details of different thin film processes in "Hybrid Microcircuit Technology Handbook (Materials, Processes, Design, Testing and Production)" [16]. The choice of the deposition technique depends on the specific requirements of high through-put, congruent thin films, uniform with well-connected grain morphology, epitaxial or polycrystalline films, and single or multilayer deposition including the area of deposition for production of devices over large-sized wafers. For example, **CVD** can deposit large-area thin films over large-sized substrates (8 inches or 12 inches sizes), while **PLD** usually deposits uniform and congruent thin films in small areas of 1 × 1 cm^2 over the substrates. For commercial purposes, state-of-the-art highly automated and sophisticated large area deposition techniques are required. In the research domain, state-of-the-art techniques, such as, **PLD** are also useful. Now, for geometrical patterns generation on the deposited metallic layer, positive **PR** is spun over the deposited metallic film using a spin-coater that is subsequently exposed to **UV**-light. Geometrical patterns are transferred with the help of a photomask that needs to be produced as shown in Fig. 2(c). Before exposure to light, spun **PR**-coated substrate is soft-baked in a temperature range of 60–90 °C to evaporate any liquid phase and help facilitate normal bonding in the spun **PR** layer. Light exposure with the help of a photomask causes geometrical pattern generation over the positive **PR** as per its photosensitivity mechanism discussed above. Subsequently, positive **PR** is developed in the **PR** developer solution followed by hard-baking in the usual temperature range of 120–180 °C. The uncovered or open metal areas (those lying outside the coverage of **PR**) are etched away with the help of an etchant solution by wet or dry etching methods selectively as shown in Fig. 2(e) followed by removal of **PR** to expose the protected parts to get the finally patterned structures of the metallic film as shown in Fig. 2(f).

Patterns can also be generated over metallic films using a negative **PR** [17] as shown in the process flow given below in Fig. 3. In this approach, a negative **PR** is spun over the substrate using a spin-coater that is subsequently exposed to light with the help of a photomask after the process of soft-baking as shown in steps (a), (b) and (c) of Fig. 3. In the next steps, negative **PR** is subjected to the negative **PR** developer solution followed by hard-baking. Now, metal films are deposited over the structures obtained in step (c) of Fig. 3 to fill the voids and empty areas as shown in Fig. 3(d) followed by etching to get patterned films without **PR** as shown in Fig. 3(e). Ceyssens and Puers have discussed the technology of SU8 negative PRs in the "Encyclopedia of Nanotechnology" [17].

Photolithography is a parallel process technique that is applied for commercial level production of MEMS devices in addition to the device research. The main drawback associated with photolithography is that it is a diffraction-limited technique defined by the Abbe-Rayleigh criterion as follows [10–13],

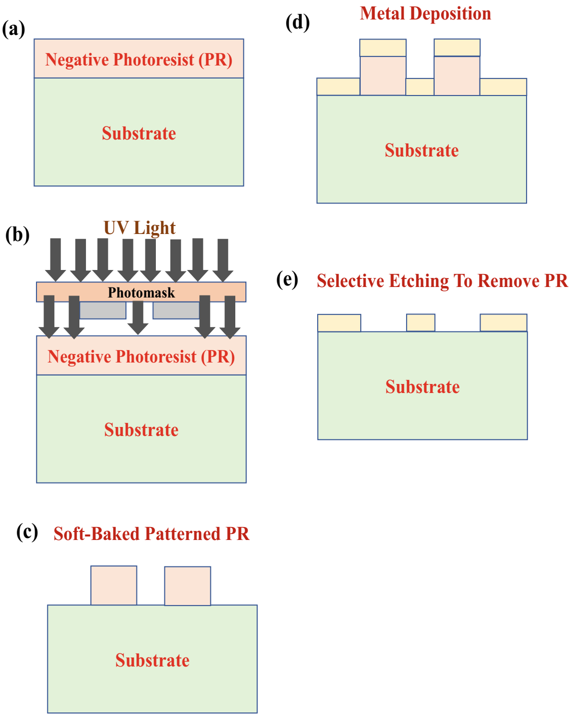

Fig. 3 Photolithographic process with negative PR for pattern generation over a metal film in the form of a schematic

$$\boldsymbol{d_{min}} = 0.61\frac{\boldsymbol{\lambda}}{\boldsymbol{nsin\alpha}} = 0.61\frac{\boldsymbol{\lambda}}{\boldsymbol{NA}} \tag{1}$$

Here, $\boldsymbol{\lambda}$ is the wavelength of the point source, $\boldsymbol{\alpha}$ is the angle of aperture, ***NA*** is numerical aperture, ***n*** is the refractive index of the surrounding medium and $\boldsymbol{d_{min}}$ entails the minimum size of structure that is illuminated with the point source of light. As the above criterion entails in Eq. (1), shorter wavelengths and high ***NA****s* are required to produce small-sized structures. A high-pressure mercury lamp is good-enough to write (word "litho" means to write) structures with features above 250 nm. Shorter wavelengths should be used for writing structures in the range of 150–250 nm. An excimer laser is the best one to produce wavelengths in the specified range. Different excimer laser sources produce lights of different wavelengths that includes **ArF** and **KrF** sources with wavelengths of 193 and 248 nm, respectively. Herve et al. have produced an effective comparison of the use of **ArF** and **KrF** laser sources-based microfabrication process [18]. For the production of structures with features below 100 nm, extreme ultraviolet (**EUV**) lithography uses much shorter wavelengths down to 13.4 nm. Endert et al. talked about a novel laser cavity combined with a line narrowing module for the deep ultraviolet (**DUV**) optical lithographic tool that utilized excimer laser steppers [19]. An important task is the reduction of minimum feature sizes and increment of aspect ratio of the geometrical features to be fabricated. In the contact exposure technique, the resolution limit for **UV** photolithography with wavelength of 365 nm is counted as follows in the manner expressed by Maalouf et al. [20] and Kumar et al. [21].

$$\textbf{Resolution Limit} \sim k(\textbf{Constant})\ \textbf{x}\ \sqrt{}(\lambda h) \tag{2}$$

Here, ***h*** is the thickness of the photoresist, ***k*** usually has a value of $\boldsymbol{\sqrt{}2}$ and $\boldsymbol{\lambda}$ is the wavelength of light that is exposed onto the sample. The value of constant ***k*** expresses the diffraction limitation that can be reduced by optimization of exposure to the **UV** light with desired intensity level. Several parameters have been tuned for reduction of the ***k***-value that include reducing the thickness of the **PR** and application of low wavelength light for improvement of the resolution. Bourdillon et al. was successful in generating features down to 16 nm with the help of **X**-ray lithography that reduced constant ***k*** to the value of 0.65 to improve the resolution [22]. DUV photolithography is a technique that can be performed with excimer laser sources of wavelengths 193 nm (ArF) or 248 nm (KrF) that fall on the lower side as demonstrated by Jain et al. [23]. Mojarad et al. successfully generated spatial line structures possessing periodicity of 14 nm along with a resolution of 7 nm [24]. In the next-generation lithographic methods, immersion lithography is extensively used in the latest times to produce feature sizes down to 25 nm [25]. In this lithography technology, the air-gap between the lens and the **PR**-spun substrate is filled with a liquid possessing refractive index greater than 1 ($\boldsymbol{\mu} > 1$). Owa and Nagasaka pointed out improvement in resolution as a result of increment in refractive index of the medium (perfluoropolyether or PFPE, $\boldsymbol{\mu} = 1.37$) and also in ***NA*** as defined by Eq. (1) [26].

Photolithography involves a chain of controlled processes that is performed strictly in a clean room environment. A cleanroom entails a highly cleaned room with controlled environment in which minute dust particles, aerosol particles, airborne microbes and even other much smaller contaminants not visible to the eye are filtered out using special types of high-class filters. Other important factors that need to be controlled in a cleanroom are inclusive of humidity inside the chamber, air-flow and temperature. Different types of cleanrooms are possible that depend on the quantity of contaminants present inside the room after filtration. High efficiency particulate air or **HEPA** filter is used for contamination removal to the tune of 99.97% that effectively removes minute dust particles, bacteria or other smaller particulates not generally visible to the eye. Another type of filter is ultra-low particulate air or **ULPA** that is used in commercial filters for the removal of particulate contaminants that are extremely smaller in size. Both types of filters generate efficiency of 99.97% of filtration with **HEPA** possessing the capability of removal of smaller particles of sizes 0.3 μm, while **ULPA** can filter particles as small as 0.12 μm. T. Sandle has discussed in detail about the cleanrooms, isolators and cleanroom technology [27]. International Organization For Standardization (ISO) 14,644–1 states the following formulae for the cleanroom classification possessing maximum concentration of particles per class and per particle size [28],

$$\boldsymbol{C}_{N} = 10^{N}\left(\frac{0.1}{\boldsymbol{D}}\right)^{2.08} \tag{3}$$

Here, $\mathbf{C_N}$ is the maximum concentration of particles present per unit volume (1 m^3) of airborne particles. These are considered to be equal to or higher in size in comparison to the particle size under consideration that has been approximated by rounding-off to the closest whole number upto three significant digits. Here, $\boldsymbol{N}$ expresses the ISO class number, $\boldsymbol{D}$ represents the particle size in microns and 0.1 is a constant that has been expressed in μm. As per ISO 3, **class 1** consists of 1000 particles per m^3 of sizes equal to or less than 0.1 μm, 237 particles per m^3 of sizes equal to or less than 0.2 μm, and 102 particles per m^3 of sizes equal to or less than 0.3 μm. Similarly, **class 10** is defined by ISO 4 and all the above counts are multiplied by 10 to get the number of particles per m^3 for different sizes of particles. Similarly, class 100 is defined by ISO 5 and all the above counts in case of **class 1** are multiplied by 100 to get the number of particles per m^3 for different sizes of particles. Similarly, **class 1000** is defined by ISO 5 and all the above counts in case of **class 1** are multiplied by 1000 to get the number of particles per m^3 for different sizes of particles. Usually, before processing of substrates, they are cleaned by acetone, methanol or preferably with non-reacting isopropyl alcohol followed by cleaning with deionized water (DI).

Exposure is the process of production of an imprint on the **PR** with the help of a photomask that restricts light in certain parts but letting it through in other parts. The different modes of exposures are inclusive of contact and proximity, and the projection types. In the contact mode of exposure, the photosensitive **PR** spun substrate is placed and pressed in “contact” mode below the photomask that consists of opaque chromium patterns, after which the sample is exposed followed by the developing steps. An important phenomenon is the near-field diffraction after passing through the interface of **PR**-photomask deep into the **PR** so that it causes diminishing contrast with increasing depth. This is owed to the speedy decline of the highest-order evanescent waves as a function of the increasing distance from the interface. This rapid decline of the highest-order evanescent waves can be shed-off in parts by application of thinner **PR**. There are technologies of plasmon resonances and lensing films that are applied for contrast enhancements. The advantages of contact photolithography include refraining away from the requirement of complicated projection optics between the object and its image. Further, it does not suffer from limitations as experienced by projection optics of capturing only a limited spatially confined spectrum originating out of the object, and restriction of the resolution limit originating from the finitely sized final imaging lens and its distance from the plane of the image. McNab et al. reported the resolution of the contact photolithography to be way ahead λ/20 periodicity [29]. Drawback associated with contact photolithography is due to the much smaller dust particles or ***Si*** specks entering forcefully into the mask and causing defects into the substrates as well. In order to avoid these pitfalls, proximity lithography can be adopted in which a small gap of typically 10–50 μm is introduced, which in turn, causes diffraction-limited phenomenon on the edges of the features so that the resolution gets typically limited in the range of 2–5 μm. Contact or proximity printing is also known as shadow printing and the minimum printable line-width ($\boldsymbol{l}_{\mathbf{m}}$) is given as follows,

$$l_m = (\lambda g)^{\mathbf{1/2}} \tag{4}$$

Here, $\boldsymbol{g}$ is the spacing that is constituted after the photomask and substrate are brought closer to each other including thickness of the **PR**, and $\boldsymbol{\lambda}$ is the wavelength of light radiation that is applied for exposure. Like before, the same conclusion is drawn from Eq. (3) that spatial separation of $\boldsymbol{l}_{\mathbf{m}}$ can be minimized significantly by reduction of $\boldsymbol{g}$ and $\boldsymbol{\lambda}$. Figure 4 given below shows the optics involved in the photolithography process.

Photolithography can be performed in different modes of (a) contact, (b) proximity and (c) projection optics as shown below in Fig. 5(a–c).

2.2 E-Beam Lithography (EBL)

In electron beam lithography (EBL), an electron beam scans the thin photosensitive material layer over a substrate for patterning of very small and precise feature sizes down to atomic scale [31–33]. *E*-beam is advantageous for patterning of very small feature sizes because of much smaller wavelengths of electron beam in contrast to the wavelength of light used in photolithography. EBL forms a potential alternate technique for **UV** photolithography on account of capabilities of higher resolution

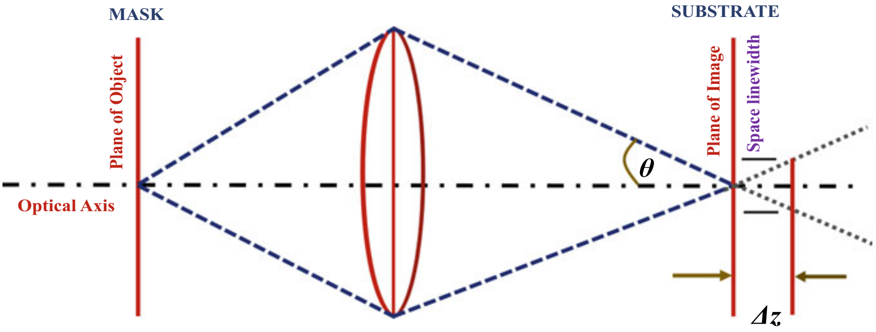

Fig. 4 Schematic of the optical phenomena happening during photolithography process where θ is the conic half-angle that converges in form of an image at the side of the substrate [30]

enabling smaller feature sizes and the costings involved. Photolithography systems are diffraction limited due to maximum resolution of the involved optics limited by the type of wavelength being used for patterning. Resolution enhancement methodologies, such as, immersion and phase shifting lithographies, result in increment of processing times of photomasks, pricing as well as increasing complicacy. In case of commercial production, the costs involved rose significantly even to few million dollars according to the node of technology applied for fabrication. In case of electrons, the *de* Broglie wavelength can be expressed as,

$$\boldsymbol{\lambda} = \frac{\boldsymbol{h}}{\sqrt{2\boldsymbol{m}\boldsymbol{E}_{\boldsymbol{Kinetic}}}} = \frac{1.23}{\sqrt{\boldsymbol{E}_{\boldsymbol{Kinetic}}}}\,\boldsymbol{nm} \tag{5}$$

Here, $\boldsymbol{\lambda}$ is the wavelength of electrons used and $\boldsymbol{E}_{\mathbf{Kinetic}}$ is the kinetic energy of electrons forming the beam which is expressed in terms of electron volts (eV).

From $\boldsymbol{\lambda} = \frac{\boldsymbol{h}}{\boldsymbol{p}} = \frac{\boldsymbol{h}}{\boldsymbol{m}.\boldsymbol{v}}$, the famous de Broglie equation, wavelengths are typically very small usually of the order of few angstroms with mass of electrons being, $\boldsymbol{m} = 9.1 \times 10^{-31}$ kg, $\boldsymbol{h}$ is Planck's constant, and $\boldsymbol{v}$ is the speed. Here, it is assumed that the electrons are moving effectively below the speed of light that is in negation of the special relativity effects. Electron wavelengths are typically a fraction of the unit angstrom for a few electron volts of energy imparted. This actually reduces the diffraction-limited patterning effects very significantly that happens in case of **UV** photolithography. EBL systems are highly advanced, such that, they do not require the use of photomasks and apply a projection system for patterning. Hence, resolutions are limited by the beam column system and not by the electron wavelengths. Diffraction-limitation by wavelength of electrons become effective only when very high-resolution systems possessing very low throughput are required. W.F.R Pease has reported a nice work on EBL [31]. On the other hand, Pala [32] and Wilson [33] have presented nice theoretical explanations on EBL.

An EBL system consists of different components of electron sources, electron lenses, apertures, beam blankers, stigmators, and stage. Electrons are ejected from

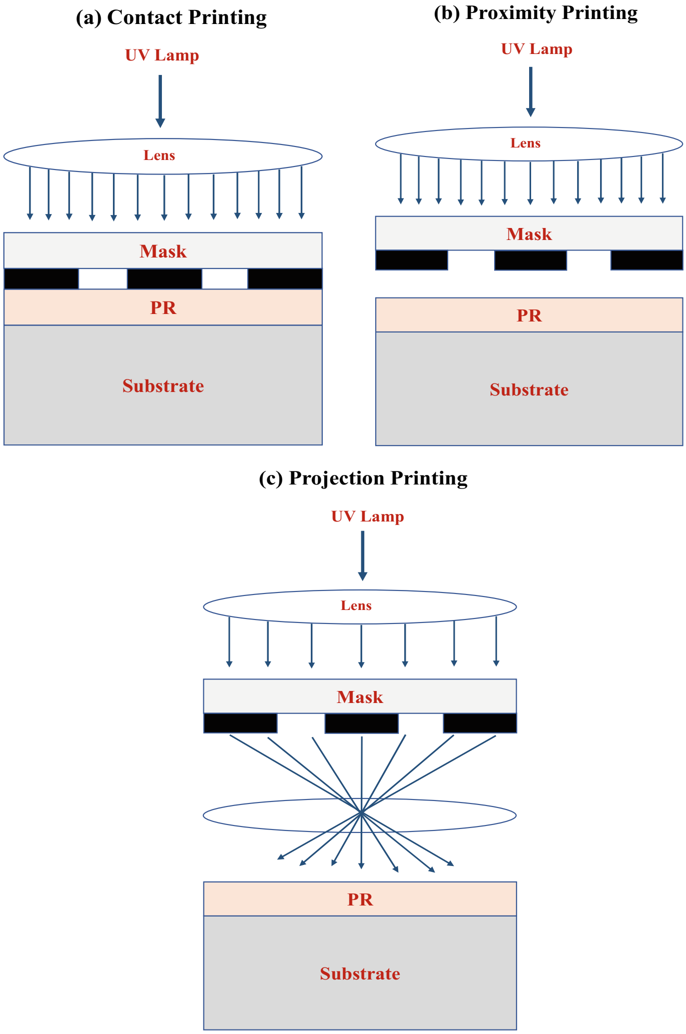

Fig. 5 Schematics of different modes of photolithography process that include **a** contact printing, **b** proximity printing and **c** projection printing. Projection lithography is diffraction limited and is taken care of by adjustment of the refractive index of the medium, thickness of the PR and the corresponding gap

the source by either thermionic emission or field emission techniques which rely on taking out electrons from the cathode either by thermal induced emission or by application of a large amount of electric field, respectively. Thermionic emission is generally attained by the use of tungsten (**W**) or tungsten thoriated filaments and lanthanum hexaboride (**LaB_6**) which is a better source for thermionic emission of electrons. However, thermionic emission sources are limited by crossover diameter or finite source size causing broader beam energy distribution profiles. Field emission relies on application of high potentials to surpass the surface potential acting as a barrier in case of emitter sources. Electron source generates the electrons that should be possessing brightness or high intensity, small electron beam spot sizes, higher levels of uniformities & stabilities. Higher brightness or intensity of the electron beam leads to faster rate of reaction with the organic photosensitive layer. This eventually results in shorter times of exposure as well as enhanced throughputs. Reduced brightness or intensities of the electron beam are needed in case of requirement of higher resolution or smaller feature sizes. Smaller virtual size of the electron source generates smaller spot sizes ensuring minimized application of lenses suitable for attainment of higher resolution and demagnification of the beam column as well. Electron beams with narrow energy distribution is another important feature in order to minimize chromatic aberration effects.

Electromagnetic lenses are used in EBL similar to that of the transmission electron microscope (TEM). Classical optics laws are applied in modulation of the electron motion under the effect of electromagnetic (EM) waves. Electrons in the form of classically charged particles are modulated through an external electric field or magnetic fields. The electric field force is denoted by $\boldsymbol{F}_{\mathbf{E}} = -\boldsymbol{eE}$ and the magnetic field force through $\boldsymbol{F}_{\mathbf{M}} = -\mathbf{ev} \times \mathbf{B}$. Magnetic lenses are usually suitable for application in beam column because they produce highly reduced aberrations in comparison to electrostatic lenses. Application of a radial magnetic field generates the rotation of electrons about the optical axis of the electromagnetic lens causing components of velocity in a tangential direction with reference to the optical axis. The velocity component of electrons now begins to have an interaction with the magnetic field along the axis. Electrons start experiencing a force along the direction of optical axis that brings them in vicinity of the axis. Beam deflectors perform the task of scanning the electron beam over an area called as scan field over target surfaces. The mechanism of beam deflection must be highly predictable for fabrication of high precision very small feature sizes, and hence is required to be perfectly linear along with minimized disruption in the beam spot size and showing non-hysteretic features. Magnetic deflectors are more effective in the generation of precise and accurate beam deflection in comparison to electrostatic beam deflectors. Two types of apertures are blanking and beam-splitting apertures that cause deflection of the beam at a distance away from the hole of the aperture, and by setting the beam convergence angle ($\boldsymbol{\alpha}$) that guides the lens aberration effects, resolution along with limiting the beam current, respectively. Stigmators are used to remove astigmatism that generates focusing conditions of different orders over spatially different positions.

2.3 Lift-Off Process

Lift-off is a typical patterning technique in MEMS used in case of noble metals or materials that are difficult to be processed by dry etching techniques based on plasma [34, 35]. It is a technique of micro- or nanostructuring to create patterns of a specific material or noble metals over the substrate surface by employing a sacrificial layer. García et al. used lift-off and etching technologies to fabricate magnetic microsensors and compared the two techniques in a critical manner in the experimental framework [34]. Negative PR was applied in case of the lift-off method followed by patterning before depositing the material. Lift-off of the unwanted parts of deposited films were removed effectively and highly efficient magnetoimpedance responses were recorded for the micron-sized geometrical structures. Positive PR was applied for patterning by the wet-etching method and the magnetoimpedance response was not even distant comparable to the architectures fabricated by lift-off technology [34]. Cheung et al. experimentally performed the polydimethylsiloxane (PDMS)-stamp-supported monolayers in bimetallic configuration by the chemical lift-off lithography (CLL) technology [35]. This technology makes patterns of self-assembled monolayers of functional molecules by the application of PDMS stamps. A schematic of the lift-off process has been shown below in Fig. 6.

Step coverage in the lift-off technique is poor as it involves the application of an intermediate layer along with a deposition process. Lift-off technique involves (***a***) deposition of an intermediate thick layer of oxide (**SiO_2**) or **PR** possessing a mild reentrant profile followed by patterning, (***b***) deposition of material that is to be in a specific patterned structure along with thickness to be only a part of the thickness

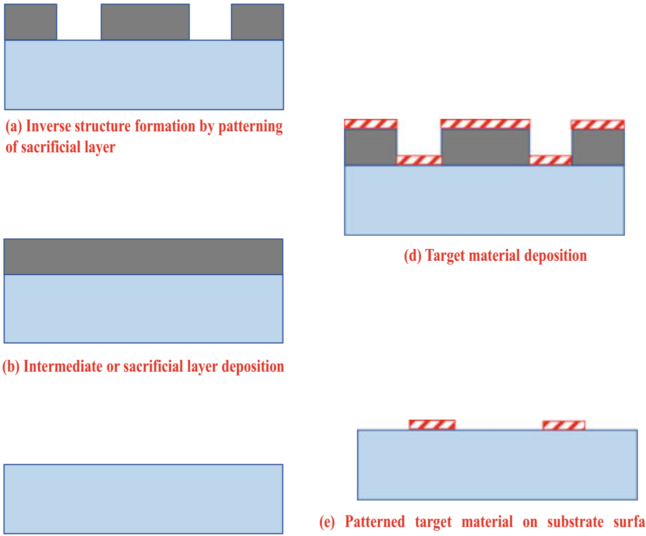

Fig. 6 Schematic representation of lift-off process in MEMS technology with the help of a sacrificial oxide or photoresist layer. First process, **a** involves usual RCA cleaning of the substrate surface so that no oxides remain on the surface, **b** second part involves the deposition of sacrificial or intermediate layer, **c** patterning of the sacrificial layer to create inverse structure patterns, **d**, deposition of the target material, and **e** creation of typically shaped & micro- or nanoengineered structures by washing-off the sacrificial layer followed by deposition of target material

of the intermediate layer, any technique that possess poor step-coverage offers an effective alternate e.g., evaporation, (*c*) final step is the lift-off of the intermediate oxide layer or **PR** that will be possible due to the higher degree of stress formation in portions possessing poor step-coverages made possible eventually by fracture of the metallic layer or material layer to generate patterns of the deposited metals or materials.

Generally, lift-off technique is applied to generate patterns for the formation of metal interconnects. Multiple sacrificial layers of different types of photosensitive materials can also be applied that possess the capability to produce architectural features to protect side-walls of the photosensitive material from getting covered with the metal during the metal deposition process. Lift-off presents an effective alternative technique in case of materials that cannot be etched-out directly and may lead to undesirable consequences on the material layer underneath. Disadvantages of the lift-off technique are retention, ears formation and redeposition. Retention is a problem in lift-off so that undesirable metal layer sections adhere to the substrate so that complete lift-off of the layer is prevented. Another reason is the non-dissolution of the photoresist in the dissolution solvent so that it becomes difficult to perform lift-off properly. "Ear" formation takes place when the depositing metal covers the side-walls of the photoresist and points upwards in the standing instruction. The possibility of these "ear structures" falling over the substrate surface equally exist forming undesirable structures over substrate surfaces and may cause undesirable connections. The third one is redeposition that entails re-attachment of the metal particles in a random manner at undesirable locations during the process of lift-off.

2.4 Etching Technology: Wet and Dry Etching Techniques

2.4.1 Wet or Chemical Etching

Wet or chemical etching is applied on a large scale in the semiconductor and microelectronics manufacturing industry [13, 14, 36]. Chemical etching is a high potential technique for the removal of blanket depositions of oxides, nitrides, metals and even III-V compound semiconductors. Here, blanket deposition means the depositions of materials that are performed over the whole substrate surface area. The substrates are immersed in the etchant solution under application of suitable temperature and mechanically controlled agitation to ensure uniform and faster etching rates. Etching rate denotes the amount of film peeled-off in a single unit of time. For optimization of the etching recipe, substrates consisting of layers of desired materials are immersed in the etchant solution and time is measured with a stop watch. The amount of minimum time consumed to peel-off a particular thickness of the deposited film attests to the etching rate, i.e., thickness etched per minute. In the wet chemical etching process, diffusion of the reactants takes place in a direction pointing towards the substrate surface followed by chemical reactions, and eventually removal of the substrate-based materials happens, such as, oxides or the deposited thin film material gets peeled-off by the process of diffusion. Chemical or wet etching produces etch rates that are generally isotropic which means that the etch rates along the plane, lateral etch rates as well as the etch rates perpendicular to the plane or vertical etch rates remain the same. In the microelectronics manufacturing production lines, an essential requirement is the uniformity of the etching rates to ensure consistency of removal across a series of wafers and in successive automated runs as well. Etch rate uniformity can be expressed as follows,

$$\textbf{Etch Rate Uniformity}\ (\%) = \frac{\textbf{Maximum Etch Rate} - \textbf{Minimum Ech Rate}}{\textbf{Maximum Etch Rate} + \textbf{Minimum Etch Rate}} \times \textbf{100}\%$$

Orientation-dependent etching can be performed using chemical etchants in which case specifically oriented crystal planes of single crystal ***Si*** can be etched preferably or comfortably. For example, the number of available bonds in a single unit of area for (110) and (100) crystal planes of ***Si*** are larger than in the case of (111) oriented single crystal ***Si***. Hence, etch rate is faster for (110) and (100) oriented crystal planes of singly crystalline ***Si*** than for (111) oriented crystal planes based single crystals of ***Si***. The lowest bond density happens in case of (111) oriented crystal planes and hence the slowest etch rate is obtained in this case. Etch rates for ***Si*** usually depend on the bond densities that are in the order of 1: 0.707: 0.557 for orientations of (100):(110):(111) of crystal planes. Such etching reactions do not produce sufficient amount of heat on account of being slow and, hence, are reaction-rate limited. The slowest etch rates for (111) orientations are owed to the faster oxidizing capabilities of (111) orientation at reduced temperatures that are generally encountered during the wet chemical etching process typically in the temperature range of 0–100 °C. Covering of surfaces with oxide layers facilitates hindering of the dissolution process in the etchant solution, thereby generating slower etch rates. ***Si*** etching is usually done by oxidation with $\mathbf{HNO_3}$ to form $\mathbf{SiO_2}$ followed by etching with hydrofluoric or **HF** acid so that it dissolves $\mathbf{SiO_2}$ to form $\mathbf{H_2SiF_6}$. For etching of $\mathbf{SiO_2}$, generally **HF** solution is mixed with ammonium fluoride ($\mathbf{NH_4F}$) that alters the ***p*****H** value to form a buffer **HF** solution or **BHF**. This has the effect of restoration of the depleting fluoride ($\mathbf{F^-}$) ions to ensure an overall highly stable etching mechanism. Important parameters are etchant concentration, etchant solution, temperature, agitation including microstructure, porous nature, density and impurities and, in addition, defects in oxide that have a bearing on the etch rate. In case of polysilicon, much faster etching rates can be achieved because of the occurrence of grain-boundaries in the polycrystalline materials. In case of $\mathbf{Si_3N_4}$ layers, a thin $\mathbf{SiO_2}$ layer is usually deposited over it followed by **PR** coating for effective patterning by etching in the boiling $\mathbf{H_3PO_4}$ solution.

Chemical etching suffers from the major drawback of undercut formation in the layer just below the masking layer that generates loss of resolution in geometrical patterns to be produced as a result of etching. Ideally, for better patterns having resolution much smaller in comparison to the thickness of the film, dry plasma-based etching must be applied to ensure the anisotropic etching pattern. Isotropic etching is favourable in cases when the thickness of the film is lesser than the resolution of the patterns. This can be expressed more precisely with the following condition as given below in the form of a mathematical equation,

$$\boldsymbol{A_f} \equiv 1 - \frac{\boldsymbol{l}}{\boldsymbol{h_f}} \tag{6}$$

Here, $\mathbf{A_f}$ is the degree of anisotropy, $\boldsymbol{l}$ is the lateral length covered as a result of etching below the **PR** mask layer and $\mathbf{h_f}$ denotes the thickness of the layer material. For anisotropic etching, the conditional equality of $1 \geq \mathbf{A_f} > 0$ holds well.

2.4.2 Dry Etching Technique

Dry etching techniques are basically plasma-assisted etching techniques that are actually very important in ultra-large-scale integration (**ULSI**) chip technology for transfer of patterns over the substrate surfaces with high-fidelity [13, 14, 36]. Different variants of dry etching techniques include reactive ion etching (**RIE**), plasma-assisted etching, reactive ion beam etching, magnetically enhanced reaction ion etching or magnetically **RIE**, and high-density plasma etching or **HDP** etching. In the dry etching technique, material removal is performed by physical bombardment of the substrate surfaces with chemically inert mobile projectile atoms or ions that are highly mobilized by gas discharges. This results in the transfer of momentum to the atoms of the deposited layer or of substrate surfaces in elastic collisions so that the imparted energy starts exceeding the binding energy of atoms of the surfaces. The maximum transferrable energy ($\boldsymbol{E_m}$) from the projectile atoms or ions of mass $\mathbf{M_1}$ and energy $\boldsymbol{E_0}$ to the substrate surface or surface layers of mass $\mathbf{M_2}$ is expressed as follows,

$$\boldsymbol{E_m} = \left[\frac{4\boldsymbol{M}_1\boldsymbol{M}_2}{(\boldsymbol{M}_1 + \boldsymbol{M}_2)^2}\right]\boldsymbol{E}_0 \tag{7}$$

The above equation shows that it is advisable to use heavy inert gases, such as, **Ar** as projectiles for the sputtering process to knock out the material atoms that are to be etched out. The process is performed at relatively high energies (usually below ~2 keV) so that atoms or ions are able to cause considerable damage in the surface layers as a result of penetration quite deeply inside the surfaces. At rather higher energies, all projectiles have the tendency to escape and are not able to reach the surfaces appropriately causing considerable losses in energy underneath the surface. Consequently, the yield of sputtering is not dependent on the energy imparted to the ions for most of the materials. Angle of incidence of the projectiles or atoms and ions onto the surfaces is also of paramount importance. For smaller angles of projections, penetration depth increases that generates poor dislodgement of atoms from the surfaces. Sputtering yield is found to increase with increment in the angle of incidence in case of polycrystalline targets with the maximum obtainable yield happening at an angle of incidence of 60°. Dry etching techniques are particularly useful for multi-layered thin film stacks ensuring minimized undercut formation in all the subsequent layers to be etched. A usual drawback is the extremely difficult removal of photoresist layers by chemical methods after ion-based etching.

Plasma etching relies on plasma formation by arcing the inert gas molecules kept at low pressures in a vacuum chamber. Two variants of plasma etching methodologies are physical etch and chemical etches. Physical etching methodology is typified by sputter etching in which the positive ions formed out of inert gas molecules strike the surfaces with high kinetic energies to knock out the material to be etched. Small amounts of negative ions are also formed in the plasma that do not possess sufficient kinetic energy to sputter out the material effectively and do not even reach closer to the surfaces. Thus, the physical method completely relies on sputtering the material out for etching purposes by heavy energetic bombardment of ions on the surfaces. The second variant of plasma etching relies on the generation of neutrally reactive species in the plasma that undergo chemical reaction with the materials on surfaces to be etched out and the formation of volatile products takes place. An advantage of this technique is the reduced damage as a result of heavy ion-bombardment caused damages. However, it yields isotropic etch profiles of the structures. A justified combination of physical and chemical etching methods produces anisotropically etched structures, significantly controlled damages due to ion-bombardment over surfaces along with high selectivity. Reactive ion etching or **RIE** is a variant of plasma-based etching in which reactive ions are generated and etching of the materials takes place which is a chemical process. In **RIE**, the wafer is placed on a substrate holder that forms the RF capacitively coupled electrode in the configuration of a parallel-plate integrated diode system. In this way, the substrate placed on the grounded bottom electrode experiences a negative self-bias at a lower operating pressure of typically less than 500 mTorr leading to heavy energetic ion-bombardments. Etch selectivity in **RIE** is usually improved by inducting an appropriate etch chemistry. Triode-configuration **RIE** systems are also possible in which ionic transport is differentiated from the plasma production process. Etch selectivity in such systems is maintained by control of the ion energy by application of a bias applied separately to the electrode holding the substrates.

Dry chemical etching processes involves the use of gaseous chemical reagents for the purpose of etching. Gaseous reagents $\mathbf{SF_6}$ and **HCl** have been employed for etching of ***Si***, while $\mathbf{AsCl_3}$ and **HCl** gases have been used for dry chemical etching of **GaAs**. Highly selective gaseous etching of $\mathbf{SiO_2}$ can be performed with interhalogenic compounds of $\mathbf{BrF_3}$, $\mathbf{ClF_3}$, $\mathbf{BrF_5}$ and $\mathbf{IF_5}$ with an etch rate of 0.5–5 $\mu m.min^{-1}$ in an isotropic pattern. A combination of **UV** radiation and ozone ($\mathbf{O_3}$) gas has been used for the stripping of **PR** layers with a high etching rate of 1400 $Å.min^{-1}$ at the processing temperature of 300 °C. Usually reactive gaseous reagents are fed into the chamber having pressures in the range of 0.001 to 10 Torr under a glow discharge for dry chemical etching. Free electrons receive energy from the glow discharge that is lost in successive collisions with gas molecules by both elastic and inelastic collisions. Inelastic collisions dominate the mechanism of energy transfer involving much larger magnitudes that is accompanied in the process of excitation of gaseous species. As a result, a plasma chemistry is involved that guides the reactions taking place in partially-ionized gases that consist of electrons, ions and free radicals. House et al. has nicely pointed-out about anisotropic etching in the article on dry etching [37]. Morozov et al. reported about the fabrication of shape-anisotropic vertically aligned ***Si*** nanostructures by the dry etching technique [38]. Ganjian et al. patterned biofunctional titanium nanostructures by the reactive ion etching technique [39].

Exposed photoresist removal is usually performed by plasma-ashing technique which is a dry chemical etching technique. In this technique, substrates consisting of patterned and exposed photoresist layers are placed inside the chamber in presence of a plasma formed out of arcing the oxygen ($\mathbf{O_2}$) gaseous molecules.

$$\boldsymbol{e + O_2 \rightarrow 2O^- + e^-}$$

$$\boldsymbol{\rightarrow O + O + e^-}$$

Free radicals induced oxidation or burning of the PR molecules takes place at temperatures of 40–50 °C. Different parameters controlling the process include pressure of the $\mathbf{O_2}$ gas, RF power, temperature of the exposed substrate, number of substrates and flow rate of the gas inside the chamber. Several closely spaced substrates can be cleaned off from the exposed **PR**s in a single run. The process is diffusion-controlled so that the etching rate depends on the diameter of the substrates, spacing between them, in addition to the etching rate being slower in the middle while faster at the perimeters of the substrates. $\mathbf{O_2}$ plasma has actually no or very little effect on the surfaces holding the exposed PRs, such as, ***Si*** substrate, **GaAs** substrates, **Au** etc. This is the most positive factor of this technique allowing to use it till complete removal of **PR** happens without any considerations of substrate or underlayer damages. In MEMS/NEMS, plasma-ashing is generally required very often for the removal of the exposed **PR** [36].

2.5 Stereolithography

Stereolithography is a versatile tool for additive manufacturing or **3D** printing of highly precise complex structures with reasonable expenditure. Stereolithography has been utilized for the fabrication of a wide variety of applications including microfluidic devices for biodevices, medical implants, sensors as well as energy storage devices. Stereolithographic process takes place in a container that consists of the oligomers, liquid monomers and photoinitiators so that a photopolymerization reaction induced by **UV** photons takes place. Epoxy-, acrylate- and vinyl-based polymers are mostly used as photocurable resins in stereolithography. Epoxy-based polymer materials have the tendency to get cured even when light radiation from the laser does not hit the material. Acrylates, on the other hand, tend to stop curing on cessation of **UV** light onto the material. In the stereolithography process, first of all, a **3D** image of the desired structure is designed on a computer. This is transformed into a set of sliced hundreds or thousands of layers of very thin cross-sections. A large container or bath has an attachment for moving upwards along with photocurable resins. A movable attachment further supports the portion under patterning by a thickness of the order that is normally ~0.1 mm per unit layer. Laser beam scans the unit layer of liquid solution contained into the bath as shown in Fig. 7. **UV** light induced photopolymerization takes place at the place where it hits the surface so that the photopolymer becomes hardened. The construction of the system consists of a platform that works as an attachment situated beneath the surface of the bath. **UV** laser source of low power orientation strikes the layer solidifying it from the middle cross-section but does not have an effect on other part that is in excess. **UV** laser is guided to move in ***x–y*** directions with the help of a galvanometer scanner that is subsequently followed by the elevator bringing down the platform to the liquid solution. Laser then starts scanning from the left side and the solidified layer is coated with the liquid followed by tracing of the second layer by the laser just upside next to this layer. This process keeps on repeating till the final prototype is fabricated. The solidified part is then eliminated from the bath followed by its cleaning to take out the excess liquid solution. In the final step, the model is kept in an ultraviolet oven for curing it completely. All these steps involved in stereolithography based fabrication have been shown below in Fig. 7 in the form of a schematic. Huang et al. has reviewed the stereolithography process with full technical knowhow in a detailed manner [40].

3 Paper Micro- and Nanofluidics

Paper microfluidics is the technology of fabrication of micro- and nanochannels on papers, paper-like materials or porous membranes that can absorb or drop-off liquid by capillary action [42–45]. Nishat et al. reviewed the technology and utility of paper microfluidics for the fabrication of devices in an easier manner [42]. Reboud et al. demonstrated the paper microfluidics technology that integrates vertical flow specimen-processing stages inculcating paper-folding for the preparation of whole-blood specimen [43]. This was combined with an identical thermal amplification along with a lateral flow detection. The technology provided for the quick and efficient malaria detection that combined origami for enabling sensitive and multiplexed assays. Noviana et al. has critically reviewed microfluidic paper-based analytical devices (μPADs) [44]. Ghosh et al. reports on the fabrication of laser-printed microfluidic paper-based analytical devices or LP-μPADs for point-of-care applications [45]. Paper microfluidics can be employed for many applications out of which the most important is the development of point-of-care health diagnostic devices. This technology has helped to do away with cumbersome, time-consuming and costly disease diagnosis analytical procedures. In this technology, hydrophobic boundaries are defined over paper-like substrates for fabrication of hydrophilic channels and

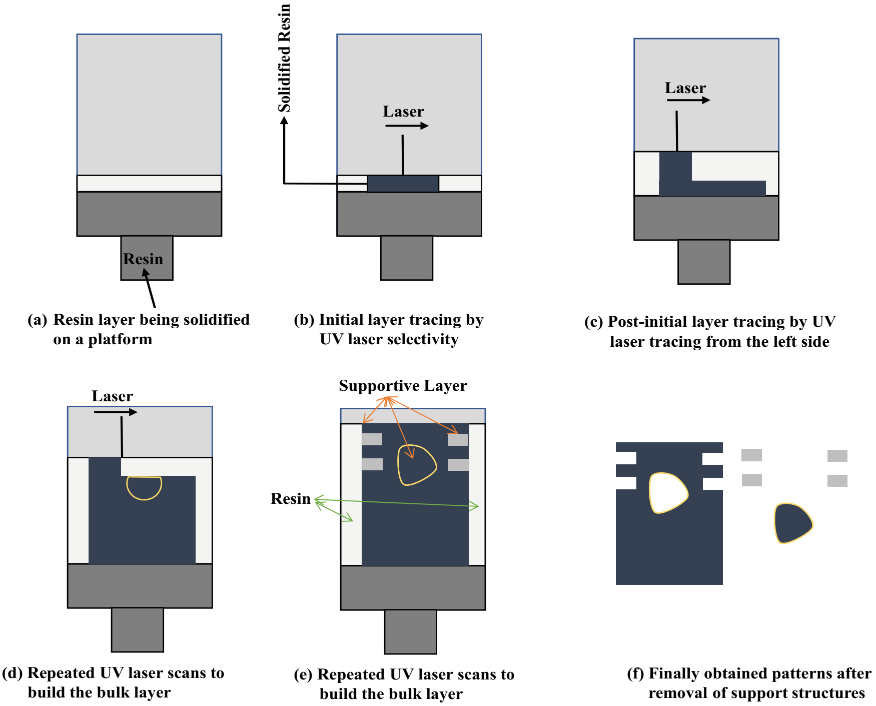

(a) Resin layer being solidified on a platform

(b) Initial layer tracing by UV laser selectivity

(c) Post-initial layer tracing by UV laser tracing from the left side

(d) Repeated UV laser scans to build the bulk layer

(e) Repeated UV laser scans to build the bulk layer

(f) Finally obtained patterns after removal of support structures

Fig. 7 Schematic of the stereolithography process [41]

regions. Very small volumes of fluids in the usual range of 10^{-6}–10^{-9} L are transported across these hydrophilic channels constituted by patterning of hydrophobic barriers. In addition, these devices are portable, possess the ability to carry out multiplexed assays, are generally cost-effective and do not require cleanroom facilities for fabrication. Cellulose fibres get pressed in the form of an interlaced network to form the paper and the corresponding capillary action. Some of the common materials for paper microfluidics is the cellulose-based paper, litmus paper, filter paper, nitrocellulose membranes and chromatography paper. Cellulose fibres possess a structural configuration in which large density of **−OH** groups and some of the **−COOH** functional groups are arranged to form the hydrophilic paper. Nitrating the cellulose, meaning replacement of **−OH** groups by $\mathbf{-NO_3}$ groups, produces the nitrocellulose polymer which is then casted in the form of membranes possessing controlled porosity. Such nitrated cellulose membranes have high degree of affinity to bind proteins finding sound applications in western blots and lateral-flow assays. Cellulose based papers are used mostly in the fabrication of microPADs and dipsticks. Lateral-flow assays consist of multiple porous membranes that are utilized for home pregnancy tests, detection of diseases, pollutants, toxins, pathogens, and are used even for the detection of Covid-19.

4 Thin Film Deposition Techniques

Thin film is the first and the foremost requirement in the state-of-the-art device fabrication technology, be it the CMOS scaling process or MEMS/NEMS. Thin films are usually defined as the layers having thickness less than 1 μm in a **2D** geometry. In the modern times, state-of-the-art deposition techniques are available that possess the capability to deposit layers down to near atomic level thicknesses. The deposited thin films may be epitaxial, polycrystalline or even amorphous depending on the deposition parameters and the nucleating surfaces present over the substrates or the substrate surfaces itself. Mostly employed deposition techniques in the clean room fabrication are the chemical vapor deposition (**CVD**) and physical vapor deposition (**PVD**) techniques that include sputtering, and possibly other techniques. For the simplistic MEMS/NEMS devices, metal sputter deposition, e-beam evaporation and thermal evaporation are sufficient to deposit normal metal layers. However, in case of complex material deposition at the commercial scale, **CVD** and sputtering are preferred over other techniques because of certain advantages attached to these techniques. **PVD** is a collective term used to define the techniques that involve vaporization of the solid-state material and subsequent condensation over top surfaces of the substrates held under the atmosphere of vacuum conditions. **PVD** can be more specifically defined as an atomistic procedure of deposition in which a wafer is held in the substrate-holder under usually high vacuum conditions or inert gases are flown at low rates to maintain low pressures in the vacuum chamber or even generation of a plasma or plasma-enhanced atmosphere [46–48]. Subsequently, the source material is broken down to eject atoms, molecules or even generation of plasma & plume can happen followed by cooling down of these energetically forced species over the substrate surfaces, and hence the nucleation. Reactive deposition happens when a reactive gas is introduced into the vacuum chamber for deposition. Abegunde et al. reviewed the different thin film deposition techniques in a critical manner [46]. Rossnagel et al. discussed about the various PVD based thin film fabrication techniques in detail [47]. In a previous work on fabrication of solar cells, I have presented a detailed account on sputtering and thermal evaporation techniques for thin film deposition in detail [48]. In a the previous work pertaining to spintronics, deposition techniques have been discussed in a special context to this topic [49]. In my previous works, pulsed laser deposition (PLD) has been used for the deposition of stable ferromagnetic chromium oxide thin films for enhanced room temperature magnetoresistance (MR) and for insulating TiO_2 thin films [50–53].

Different major steps involved in the **PVD** process are outlined below,

(i) All the target solid-state materials in the form of a solid disk of desired thickness are converted to vapor phase by evaporation as a result of temperature or *e*-beam exposure or ejection of materials by striking of the target surfaces by plasma in sputtering. Thus, the first step involves the formation of vapor phase of the target material that is to be deposited.

(ii) Vapor-phase species are transported towards the substrate under streamlined molecular flow environment. Temperature inside the chamber has a specific bearing over these produced vapor-phase species, and thermal scattering events can also happen. During the streamlined molecular transport of the vapor-phase material to the substrate, there will happen huge number of collisions if the partial pressure of gases or material vapours is high enough. Thus, the molecular transport from the source material towards the substrate surface forms the second step.

(iii) Molecular transport towards the substrate enforces nucleation over the surfaces in a manner controlled by distance between source and the substrate, temperature, reactive environment and surface modified substrates. Specific crystalline substrate surfaces can nucleate epitaxial, polycrystalline or even amorphous phase films that can eventually be controlled by changed thermodynamics by changes in temperature and possibly other parameters. Less mobile vapor-phase species may form an amorphous phase even over crystalline substrates. Similarly, substrate temperature can change the thermodynamics of nucleation of crystallites that alters surface mobilities of the depositing atoms and molecules. Substrate temperature is of paramount importance in the film formation physics. Thus, nucleation and thin film growth is the third and final step of the thin film growth.

In the current chapter, the focus is to shed light on sputtering, thermal and e-beam evaporation **PVD** processes in short.

4.1 Sputtering

Sputtering involves ejection of atoms and molecules from the target surfaces by atomic level collision induced cascades through ions present in the plasma formed by high electric discharge of inert gases [46, 49]. This methodology of ejection of atoms and molecules by atomic level collisions is known as “sputtering” or knocking out of the material atoms. Highly energetic gaseous ions from the plasma are accelerated towards the substrate surface that knock out the material by transfer of momentum. This is a completely different process from thermal evaporation whereby atoms and molecules are knocked out due to heavy strike of ions on the surfaces along with shorter target-to-substrate distance. Different variants of sputtering include magnetron sputtering, reactive sputtering, radiofrequency (**RF**) or diode or cathode sputtering and bias sputtering. **DC** sputtering is based on the twin planar electrodes whereby the source disk forms the cathode and substrate forms the anode. An inert gas is flown inside the vacuum chamber to form the plasma of energetic ions to initiate atomic level collisions at the substrate surface. Usually, argon (**Ar**, *at. wt.* = 39.95) is implemented for the purpose because of its higher mass as compared to other inert gases of neon (**Ne**, *at. wt.* = 20.18) and helium (**He**, *at. wt.* = 2). The reason is that **Ar** can impact the substrate surface more energetically in comparison to **Ne** and **He** (Fig. 8).

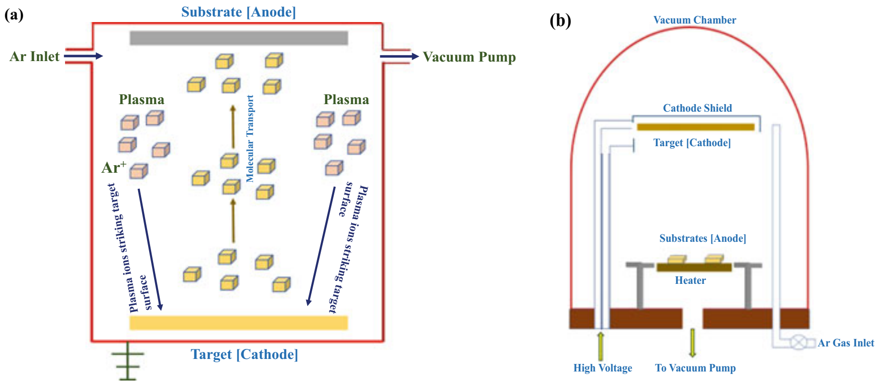

Fig. 8 **a** & **b** Schematics of a sputtering system portraying the substrate placed on an anode and the target placed over the cathode, formation of plasma ions (Ar^+) inside the vacuum chamber that strikes the target surface constituting the molecular transport towards the substrate

A direct current or DC voltage maintains the glow discharge that is applied between the source and the substrate. Due to sustained glow discharges or plasma formation, atoms and molecules are sputtered out of the substrate surface and start condensing on the substrate surface to enforce nucleation and growth of a thin film. Usually, the source disk material is a metal or a conducting material that possesses features to sustain glow discharge or current flow between the metallic electrodes. Reactive sputtering involves a process in which a reactive gas, e.g., $\mathbf{O_2}$ or $\mathbf{N_2}$ is flown into the vacuum chamber in a controlled manner so that they react with the atoms or molecules ejecting out of the target material that leads to the formation of a compound film over the substrate surface. An enhancement in the amount of the reactive gas transforms the upper layer of the target surface from a single phase to the compound type of phase formation that may cause alterations in the property of the material. Only **Ar** gas can be used for the purpose or in combination with the ionized non-inert gas or reactive gas or introduction of only the ionized non-reactive or reactive gas in the deposition chamber can also be performed. Stoichiometry of the compound film can be controlled by the regulation of percentage of the reactive gas to be introduced into the deposition chamber so that the produced thin film is different from the target material. In radiofrequency (**RF**) sputtering, current is applied at radio frequencies with alternating potentials to avoid piling of charges. Alternating current or periodically varying current thus mitigates the effect of accumulation of charges in each phase of the cycle when it is made to flow continuously along a single direction. Electrons are driven towards the target placed on the cathode during the positive cycle of the applied voltage resulting in generation of negative bias. On the other hand, during the negative cycles, knocking of target surfaces by plasma ions continues to eject atoms & molecules at an operational frequency of 13.56 MHz of **RF**. Accumulation of charges over specific target surfaces is a serious issue that can generate sparkling in the plasma resulting in droplets formation over produced thin films, and hence degrading the quality. Further, this can cease the sputtering of atoms & molecules from the target surfaces that eventually terminates the process. Thus, target surfaces are cleaned-up in each cycle in the **RF** sputtering so that charge build-up is protected that diminishes the unwanted arcing or sparkling. An advantage of **RF** sputtering is that it facilitates stable and sustained plasma formation at lower pressures of 1 mTorr to 15 mTorr resulting in highly reduced collisions of **Ar** gas ions so that a highly streamlined molecular transport of the target material happens towards the substrate. **RF** sputtering is also helpful in minimization of the formation of "race-track erosion" over the target surfaces. Due to the ***ac*** character of the **RF** discharge, height of depth along with the width of the race-track happens to be highly reduced in dimensions in addition to the minimized confinement of electrons in the applied magnetic field. This results in larger spread-outs of the plasma confined material so that shallower but larger & wider plasma spreads happen to produce better and highly uniform coatings.

Magnetron sputtering makes use of the magnetic field to accelerate the rate of ionization delivered by the current to the target material that eventually results in highly improved deposition rates. Another advantage of magnetron sputtering is that it restricts secondary electrons generally ejected from the target surface due to heavy ion-striking in the neighbourhood of the target. There is also another benefit attached to this specific technique of magnetron sputtering that it allows sputtering at a reduced pressure and voltages of 100 Pa and −500 V, respectively, in comparison to 10 Pa and 2–3 kV, respectively for the normal sputtering procedure. The two variants of magnetron sputtering are balanced and unbalanced magnetron sputtering. In the first variant, balanced magnetron sputtering, the plasma largely remains confined to the target region. On the other hand, in unbalanced magnetron sputtering, magnetic field lines are directed in parts towards the substrate in addition to the closed field lines. Kelly et al. has presented a nice review on magnetron sputtering and has discussed the details of the same [54]. Figure 9 given below shows the schematic of a DC magnetron sputtering mechanism and subsequent plasma-based knock-out of atoms or molecules from the target material to form thin deposition over substrates [55].

Pulsed magnetron sputtering or **PMS** is another variant of magnetron sputtering that is a short-pulse of magnetron discharge tuned to the orders of microseconds (***µs***) in a cycle of low duty operating in the medium frequency range of 10–200 kHz as shown in Fig. 10 [56]. In **PMS**, short or intermittent pulsing is used rather than the continuous mode of magnetic field applied in conventional magnetron sputtering. Collision of positive ions develops positive charges over the target surfaces resulting in a reduced drift of positive ions in a direction pointing towards the target. The two sub-variants of **PMS** are the unipolar and bipolar PMS.

In the unipolar **PMS**, pulsed voltage is applied to the target that lies between the standard operating voltage and the ground. Power waveform experiences positive voltages at a particular operational frequency in the unipolar **PMS** to clean target surfaces including the removal of charges accumulated over dielectric surfaces.

In the bipolar **PMS**, the voltage applied to the target is switched to positive voltages during the off-cycle of the intermittent pulse duration reflecting a reverse nature. Two pulses that are 180° out-of-phase are applied so that the magnetron can be swapped from the cathode to the anode and vice-a-versa for the mitigating effect of charge

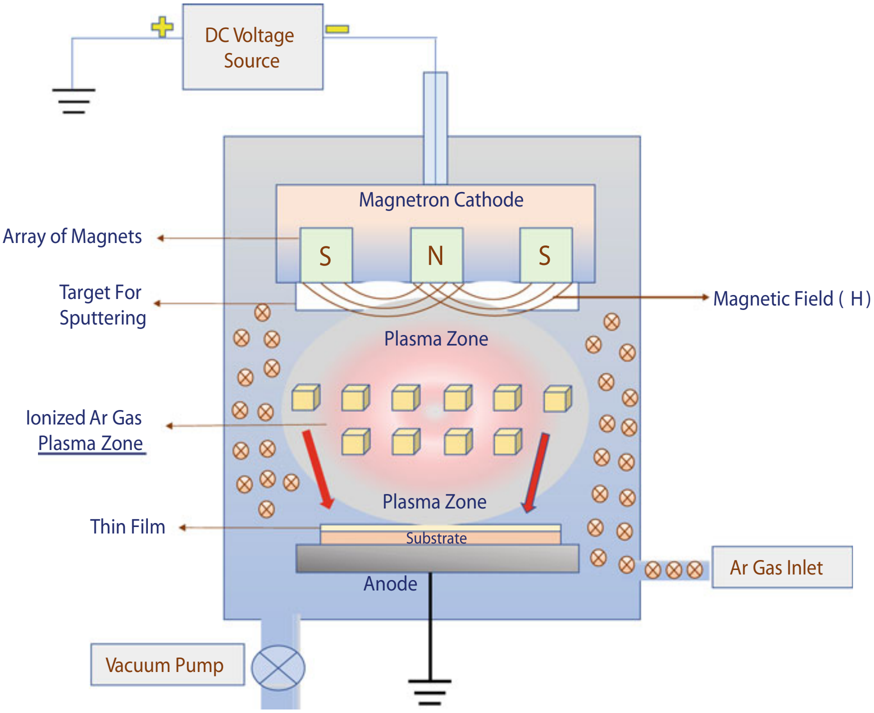

Fig. 9 Schematic of a DC magnetron sputtering system portraying substrate placed on an anode and target at the cathode [55]. A magnetic assembly is at the core of magnetron cathode providing acceleration to the charged ions. A high-density plasma of Ar gas (marked with crossed circles) takes place between the magnetron cathode and anode so that atoms and the molecules (shown in form of yellowish cubes) are ejected at a faster pace from the target surface at the cathode. Molecular transport towards the substrate takes place instantly so that nucleation starts happening and thin film growth is initiated

accumulation over dielectric surfaces. Super-dense plasma is created due to this specific short-pulsing process that results in the deposition of highly uniform thin films. Advantages associated with PMS as compared to conventional magnetron sputtering are the deposition of smoother layers even over irregular and complicated substrate surfaces, removal arc event attached to the reactive magnetron sputtering and exclusion of low rates of deposition as obtained in RF sputtering in addition to the target poisoning. Duplex sputtering is yet another variant of sputtering that combines two or more deposition techniques for the production of functional materials of high grading.

Power, pulse frequency, pulse duration including pressure are the common parameters that determine plasma formation process, time period and sustainability of the plasma as well as its stabilization. The PMS system can be operated in voltage & current modes.

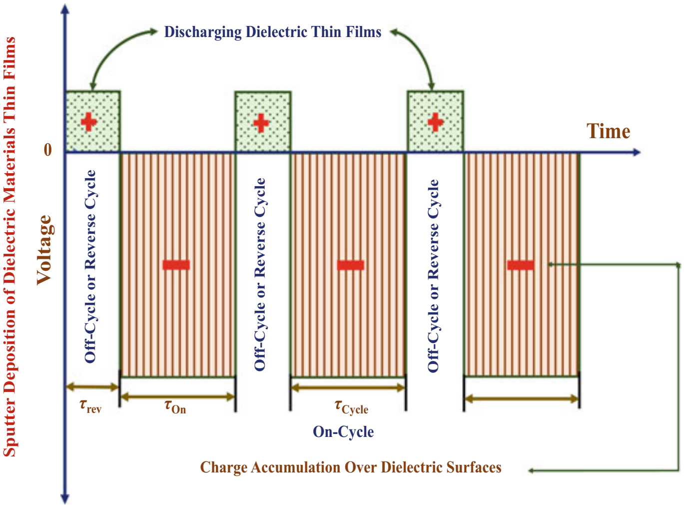

Fig. 10 Schematic of voltage as a function of time (τ) in a pulsed magnetron sputtering or PMS system for deposition of dielectric thin films showing off- and on-cycles during the process [56]. It reflects accumulation of charges over sputtered dielectric surfaces during the on-cycle and discharging the surfaces during off-cycle. Off-cycle is also called as the "reverse" cycle (τ_{rev}) during which polarity of the applied voltage inverts from negative to positive (typically 20 V) with smaller amplitudes. A negative voltage of a few hundred orders is applied to the target surface when a power is applied and this constitutes the "on-time (τ_{On})" of the process. During the on-cycle, dielectric surfaces are charged and are discharged during the off-cycle. The involved physics is that the on-cycle must be short in timescales so that the accumulated charges over dielectric surfaces do not result in a luminous discharge in this time period. On the contrary, off-cycle should be of sufficient timescales so that the collected charges can be cordoned-off completely. This helps in the prevention of accrual of charges in the subsequent repetitive on- and off-cycles

Shorter pulse durations but higher frequencies favour plasma accumulation to operate PMS in the constant voltage mode. In contrast, at longer pulse durations but lower frequencies, PMS operates in the constant current mode so that a high voltage accelerates the plasma ions highly energetically towards the target surfaces to reconfigure the current as well as the rate of deposition.

E-beam and thermal evaporation are other conventional techniques that are frequently used in MEMS/NEMS for metal deposition of nanometres thickness [46, 49]. *E*-beam deposited thin films are more uniform, congruent, continuous in a well-connected morphology in contrast to the thin films deposited by thermal evaporation. *E*-beam evaporation is a deposition technique in which an *e*-beam scans the surface of the material to impart a huge amount of energy onto the material's surface of which thin films are to be deposited so that it sublimates without undergoing melting. The solid material is placed in a crucible which is maintained at a lower temperature using a water-cooling circuit. This protects the diffusion of impurities from the crucible into the material that is eventually evaporated in the crucible for thin film formation. Crucibles should be restricted for the sublimation of one type of material only to avoid contamination. For example, if an *e*-beam system is used for gold (**Au**) deposition for metallization in MEMS/NEMS, the crucible and hence the system will be **Au**-contaminated for the deposition of other materials. Hence, **Au**-contaminated *e*-beam system can be used only for the **Au**-interconnects, contact pads or thin films in MEMS/NEMS or in CMOS technology. Contamination-free crucibles are highly costly and they can be used in a specific range of temperature only. For example, graphite-made crucibles can be used for *e*-beam sublimation at very high temperatures, but however, carbon may enter the thin films in ppm or ppb or even in few thousands range of concentration of the depositing material. An added advantage of *e*-beam evaporation is that the different source materials can be introduced into the path of the scanning electrons inside the vacuum chamber to generate multiple thin films in a single point of time. The disadvantages associated with *e*-beam evaporation include difficulty in controlled cleaning of source surfaces, potential **X**-ray based damages and rather difficult improvement of the step-coverage. In contrast to a thermal evaporator utilizing temperature based melting and subsequent evaporation for thin film deposition, *e*-beam evaporator can induct higher temperatures for material sublimation so as to ensure significantly higher rates of deposition, refractory materials (**W**, **Ta** etc.) and high temperature materials. Thermal evaporation is rather an old technique with lots of literature already available and hence I will restrict myself to *e*-beam evaporation only. Details about the thermal evaporation are available in my another chapter on "Spintronics: The Realm of Nanotechnology" [49]. In other report, I have outlined the importance of an important variant of **PVD**, the pulsed laser deposition (**PLD**) technique, to deposit even phases as metastable as half-metallic ferromagnetic $\mathbf{CrO_2}$ for room temperature spintronic applications [50–53].

4.2 Chemical Vapour Deposition (CVD)

Chemical vapor deposition or **CVD** is a technique for the development of solid thin films or coating over various substrates in semiconductor materials process technology. Creighton & Ho have pointed out that, mostly, it is used for the fabrication of high quality, congruous thin films of well-connected granular configuration over large area silicon (***Si***) substrates [55]. It is preferably not used for metallization purposes for the fabrication of interconnects and metal contact pads for which sputtering, and even e-beam & thermal evaporation techniques are used widely. In a previous work on nanoelectronics, field effect transistors including metal oxide field effect transistors (MOSFETs) have been discussed including metallization of contact pads and interconnects [57]. **CVD** consists of a process flow chamber in which precursor gases are made to flow over materials placed at a desired temperature so that chemical reactions take place to deposit thin films over the substrate surfaces. The resulting chemical by-products are vented out of the chamber in addition to the process gas left unreacted after the deposition. Control of various parameters including tailoring of pressures from sub-torr level total pressures to pressures higher than the atmospheric pressures, change of temperatures and cold-wall & hot-wall reactors that provide wider functionality to the **CVD** process. Various types of **CVD** processes are thermal **CVD**, hot-wire **CVD**, atmospheric **CVD**, metal–organic **CVD** (**MOCVD**), organo-metallic **CVD**, organometallic vapour phase epitaxy (**OMVPE**) and metalorganic vapour phase epitaxy (**MOVPE**) [46]. In the enhanced **CVD** processes, plasmas, photons, ions, combustion reactions, lasers and even hot filaments are applied for enhancement of the deposition rates and or lowering temperatures of deposition. Advantages of **CVD** are inclusive of deposition of thin films that are usually conformal to higher orders. Conformal means the deposited films have a thickness on the sidewalls that is quite comparable to the film thickness over the top side. A specific advantage of **CVD** is the deposition of thin films of very high purity that emerge out of the filtration techniques to remove impurities including elimination of a high vacuum environment and line-of-sight between the source and the substrate similar to sputtering, & evaporation techniques, and eventually the possibility of deposition of a wide variety of materials. Disadvantages of **CVD** are inclusive of non-volatility of precursors at or near-room temperatures typically, toxicity of chemical precursors including by-products, deposition of thin films at higher temperatures that produce stress in thin films leading to mechanical instabilities, and higher costs of precursors specially in case of metal–organic precursor materials. **CVD** plays a crucial role in the fabrication of **MEMS** devices since most of such devices are fabricated from polysilicon films deposited over ***Si*** substrates consisting of intermediate sacrificial $\mathbf{SiO_2}$ layers or masks that are subsequently removed by the etching process to expose the devices [58]. Polycrystalline ***Si*** and oxide layers of high quality can be fabricated using **CVD** or plasma-enhanced **CVD** (**PECVD**) so as to establish the device structure in a direction perpendicular to ***Si*** substrate [59]. On the other hand, various other steps involving lithographic & etching processes define device structure in rest of the two directions (***X*** and ***Y***). Current fabrication technology has aims to integrate microelectronics manufacturing with MEMS processing on a single unit of the substrate for enhanced multifunctional devices at the micro- and nanometre scale. Epitaxial heterostructures consist of **2D** quantum wells and superlattices that are made-up of 1–10 nm thick strained epitaxial layers. Additionally, vertical cavity surface emitting laser (VCSEL) consists of mirror stacks that are made-up of several alternating semiconductor layers of typical thickness in the range of 50–100 nm with a precision of more than 1 nm. **OMVPE** and atomic layer epitaxy (**ALE**) are the techniques that perform the task efficiently to the orders of subnanometer scale.

Hot wall reactors-based **CVD** consists of a chamber consisting of an enclosure of a furnace that induces temperature-based heating effects inside the chamber. After setting of temperatures to the desired levels, reactive gases are flown inside the chamber at lower pressures of the orders of torrs. Reactors can be of large sizes for large-area coating or may consist of shelves for coating of several parts in a single point of time. These reactors have the capacity to process large-batches of closely spaced ***Si*** substrates, generally over hundred, for semiconductor processing simultaneously. Usually, uniform substrate temperatures are generated without any thermal gradient that drives the formation of uniformly thick coatings. Hot wall reactors start possessing thicker coatings from inside on successive depositions requiring extensive cleaning procedures. In the cold wall reactors, walls are made to cool and substrate is kept at a suitable temperature. The walls are made-up of a quartz material with a chiller attached for water-cooling. ***Si*** or compound semiconductor substrates are placed on a rotating holder possessing a system for resistive heating from the bottom side. Relatively higher pressures are used in a cold-wall reactor along with a carrier gas flown into the reactor consisting of diluted precursors. In contrast to hot wall reactors, cold wall reactors do not suffer from the disadvantage of higher levels of cleaning due to lesser deposition on its walls and operational power of highly reduced energies including imposition of lesser thermal stresses due to substrates undergoing quicker heating and cooling cycles. Drawbacks attached to this technique are inclusive of non-uniformly deposited thin films because of generation of thermal gradients on the substrate, thermal stress imposition because of quicker heating and cooling cycles along with batch-production sizes that are not larger in number similar to hot wall reactors-based **CVD**.

Plasma enhanced **CVD** or **PECVD** is another variant of **CVD** in which an inert gas is ionized by the application of electric currents to form ionized gas environment to constitute plasma for initiating the reactions [60]. This is helpful in lowering down the higher temperatures of deposition generally used in a **CVD** process. A great advantage is the significant lowering of deposition temperatures in **PECVD**. Deposition can be performed even at room temperature so as to avoid temperature-based effects, and thus, it becomes possible to coat the organic polymer including other types of materials possessing low melting temperatures (M.P.). Hence, **PECVD** can be used for the deposition of both inorganic and organic materials based on highly reactive precursors. A herd of ionized inert gas particles, innumerable electrons and neutral atoms constitute the highly energetic plasma state that can be partially or completely ionized. However, it must be noted that plasma is a neutral state of matter so that the net charge is always zero. Two methods of plasma production are the heating of the gas to produce temperature-based ionization for which higher temperatures are required, and the other one is based on the application of an electrical current for ionizing the gas. The electrical energy can be imparted to the gas in various frequency ranges of audio frequency of 10–20 kHz, RF of 13.56 MHz and microwave frequency of 2.45 GHz that actually produce different types of plasmas. Plasma causes disintegration of the material to be deposited that generates free radicals, ions and sub-monomers. Further, the highly energetic plasma matter causes the monomers to undergo plasma or radical polymerization. Chemically reactive species are obtained when neutral molecules interact with the plasma species in addition to the generation of radicals, polymerization reactions, etching reactions or even generation of implantation reactions. In **PECVD**, monomers are generally taken in the liquid or gaseous states for comfortable vapour formation. In case of solid monomers, sublimation system is required to evaporate the material that allows the deposition of a range of materials. In the gaseous or liquid state with high vapour pressures, dissociation of the precursor material takes place followed by high mobilization of the dissociated species that makes the deposition happen at highly reduced temperatures. In the case of a polymer substrate, etching, deposition and cross-linking & functionalization take place that modify polymer substrate surfaces. Plasma polymerization adopts a random radical recombination approach in which a radical kick starts the polymerization reaction inducing radicalization that results in the generation of the polymer at the end of the reaction. Radicals are present in each of the series of the polymer produced to induce cross-linking of the polymer to produce a polymer of the cross-linked structure. Plasma produced polymer thin films do not resemble a traditional polymer because of highly branched and cross-linked structures along with "sub-units" of the plasma produced polymers not remaining to be same after plasma-processing. For preservation of "sub-units" of the plasma produced polymers, optimization of the internal and external plasma parameters is required.

5 Materials for Bio-MEMS

Both inorganic and organic materials are employed in the bio-MEMS/NEMS technology. ***Si*** and glass are widely used in the MEMS technology because of high developments in this field. ***Si*** is an indirect low bandgap semiconductor material, while glass is dielectric in nature and falls in the category of wide bandgap materials. ***Si*** and glass possess sound mechanical properties, while glass can be used for optical device fabrication as well. ***Si*** is transparent to the infrared radiation while remaining opaque to other wavelengths. Glass offers uniform surfaces for the fabrication of microfluidic devices, highly sensitive optical sensing platform in addition to the formation of hermetically sealed devices owing to the creation of covalent bond of high strengths. Glass based device processing is too costly and complicated. Etching is an integral part of the device fabrication technology. As is well known, glass is amorphous in nature and does not possess any crystalline character. Drawbacks associated with ***Si*** and glass include high brittleness of both the materials, costly and limited disposable bio-MEMS devices are possible only because of higher costs involved in the fabrication process [7]. Polymers offer an effective alternate as substrates for microfluidics and bio-MEMS device fabrication. In addition, polymer substrates are less brittle, dielectric in nature, possess sound thermal properties & high chemical stability, are glassy, optically transparent, existing in soft or hard states, offer elastic platform & the possibility of fabrication of disposable devices on account of being lesser expensive, and are applicable *in-vivo* drug delivery platforms. An added advantage is the ease of micromachining of these polymeric substrates by the routine etching techniques of VLSI technology or even by laser-based microfabrication to pattern microchannels. Ultrafast laser-based micro-patterning of thin films is possible for advanced MEMS and for even deposition processes. In a work on microfabrication, micro-patterning of indium thin films was performed for the generation of micron and submicron particles using femtosecond laser-induced forward transfer (LIFT) [61].

Laser based microfabricated channels can also act as optical waveguides for the fabrication of optical circuitry for quantum computers, and even light-sensitive microfluidic and bio-MEMS devices. Laser based microfabrication requires processing of optically transparent polymeric substrates by scanning of laser beam across the surface to create spatially separated microchannels at equal distances. Light can also be coupled from each of the ends of the microchannels to act as waveguides in the refractive index modified areas inside the microchannels. Basically, laser beam is focused at a specific distance deep inside the substrate to fabricate refractive index modified regions that act as a sort of optical cables. Such microfabricated channels can be used both in the form of microchannels and as optical waveguides as well. The drawback associated with laser-based microfabrication is the fabrication of uneven sidewalls of the deeply buried microstructures. Controlled energy should be imparted by the laser pulses otherwise cracks due to heated zones may happen on polymeric or glass substrates. Pulsed femtosecond oscillator lasers that can produce nanoenergy pulses are suitable for this type of fabrication that can modify the refractive index in a highly controlled manner. A train of pulses of the laser beam strikes deep inside the substrate focused by means of suitable optics. This modifies the refractive index inside the substrate in a highly controlled manner that is achieved by scanning the substrate placed over a 3D translation stage possessing the capability to make movements in three dimensions.

5.1 Inorganic Materials

Si is the most abundant material existing in compound form with other materials. Single crystal ***Si*** is highly suitable for microelectronics and bio-MEMS devices as it forms the platform for device fabrication and integration in the form of wafers or substrates. Pure single crystal ***Si*** wafers can be fabricated using the Czochralski (**CZ**) method. ***Si*** is mechanically stable, can be integrated easily onto substrates of the same materials, possesses Young's modulus of ~2×10^5 MPa similar to steel, has a density of ~2.3 gcm^{-3} which makes it as light as aluminium, an elevated melting point (M.P.) of 1400 °C makes it stable for use at higher temperatures, does not show any mechanical hysteresis making it ideal for actuators and sensors, possesses highly flat surfaces for coatings and subsequent multi-layered coatings, and overall availability of its raw material of $\mathbf{SiO_2}$ has made the processing technology advanced and even cost-effective. Single crystal ***Si*** structure is "face centered cubic or ***fcc***" in which eight atoms are placed at the corner while six atoms happen to occur on the faces. However, single crystal ***Si*** has four extra atoms in its interior that makes the total number of available atoms in a single crystal ***Si*** structure to be eighteen. Unsymmetrical or uneven distribution of atoms inside the single crystal ***Si*** develops anisotropic or directional mechanical properties in this semiconductor structure, but however, ***Si*** is normally treated as an isotropic material overall. Miller indices of the three distinct planes of a cubic crystal are inclusive of (001), (010), (100) for the top, right and front faces, (110) for the diagonal face and (111) for the inclined face. These crystal plane orientations possess their own intrinsic energies depending on the number of atoms forming that orientation. Hence, (100) offers least resistance and is the easiest to work with on account of the minimum number of atoms forming this specific crystal orientation. Similarly, (110) crystal orientation offers the ultraclean surfaces for microfabrication purposes. On the contrary, (111) consists of the shortest bonds formed between the atoms to form the strongest plane and hence the most difficult to work with. Other ***Si*** based materials used in bio-MEMS are silicon-*di*-oxide ($\mathbf{SiO_2}$), silicon carbide (**SiC**), silicon nitride ($\mathbf{Si_3N_4}$) and polysilicon or polycrystalline silicon as well. Polysilicon or polycrystalline ***Si*** can be deposited by various techniques that consist of ***Si*** crystals of different orientations and sizes that form grain boundaries and also induce resistance related to them. Polysilicon is usually highly doped and is deposited for the production of gates for transistors and localized resistors. Polysilicon crystals are stronger than the single crystal ***Si***.

$\mathbf{SiO_2}$ is the most readily available material that offers good thermal as well as electrical insulation protective layers, is also used in the form of oxide masks as replacement of **PRs** for device patterning, deep buried oxide layers, and the initial use in the form of device isolation layers decades ago. It forms a significant and cost-effective use as "oxidic masking layer" for deposition, diffusion and etching processes in microfabrication. It is also used as a "sacrificial layer" in surface micromachining [13, 14]. It can be produced by both dry and wet oxidation methods in a furnace. In wet oxidation, steam is made to flow at a specific temperature to oxidize the ***Si*** substrate surface, while in dry oxidation, $\mathbf{O_2}$ is flown over the high temperature heated substrates. Generally, $\mathbf{SiO_2}$ has the resistivity of $\geq 10^{16}$ Ω-cm and a dielectric constant of 3.9. **SiC** is used as a masking layer in microfabrication technology owed to its high M.P. and the capability to resist chemical reactions, along with a higher dimensional stability.

Silicon nitride ($\mathbf{Si_3N_4}$) possesses superior electrical insulation properties, and is used as a masking layer in the deep etching process owing to its highly powerful resistive nature against oxidation including several etchants [13, 14]. It is prepared by the following reaction,

$$\mathbf{3SiCl_2H_2 + 4NH_3 \rightarrow Si_3N_4 + 6HCl + 6H_2}$$

High quality $\mathbf{Si_3N_4}$ layers are grown by **LPCVD** and **PECVD** techniques. **LPCVD** grown $\mathbf{Si_3N_4}$ layers have a dielectric constant of 6–7 & resistivity of 10^{16} Ω-cm, while **PECVD** grown layers possess a dielectric constant of typically 6–9 & resistivity of typically ~10^{16} Ω-cm. The etch rates of **LPCVD** grown $\mathbf{Si_3N_4}$ layers in concentrated **HF** acid are 200 Å per minute, while the etch rate is 5–10 Å per minute in boiling **HF**.

Quartz is silicon-*di*-oxide or $\mathbf{SiO_2}$ in which the unit cell acquires the shape of a tetrahedron. It is highly applicable in microfluidics for biomedical purposes. Further, it offers a high degree of insulation in microsystems or MEMS. This material is rather difficult to etch out and is normally etched with a combined recipe of $\mathbf{HF\text{-}NH_4F}$ in the required geometries.

5.2 Organic Materials

Organic materials are inclusive of polymers that consist of plastics, plexiglass, lucite and adhesives. Polymer substrates can also be doped with suitable agents that can possess electrical conductivities as well. In MEMS and microsystems fabrication technology, organic substrates made-up of conductive polymers are frequently used [7, 60]. B. Bhushan has presented an account of bioMEMS and bioNEMS that gives details about biomimetics, and correlated materials & devices. Ferroelectric polymers are another interesting material behaving similar to piezoelectric crystals that can be manipulated as the actuation controller in a range of MEMS devices, such as, micro pumping. Polymers are also used in microfluidics for facilitation of effective electro-osmotic flow by coating polymers with specific properties over the capillary tubes. Maheshwari and Ramgopal Rao have pointed out various materials involved in the fabrication of bio-MEMS [7]. In this article, electronic materials, such as, **SU8** photopolymer, *poly*-dimethylsiloxane (**PDMS**) and *poly*-methyl meth acrylate (**PMMA**) have been discussed in special reference to bio-MEMS. **SU8** is an epoxy polymer which is negatively toned so that photo-induced cross-linking of 8-epoxy groups happens on exposure to **UV**-light [17]. **SU8** is made-up of Bisphenol A Novolac epoxy usually made to dissolve in gamma-butyrolactone (**GBL**) or cyclopentanone in which triarylsulfonium/hexafluoroantimonate is added in about 10 wt% of proportion to act as a photoacid generator. This photoacid generator is responsible for polymerization along with a unit photon triggering many polymerization reactions at a single time. In the next step, it is post-baked at a suitably high temperature for effective cross-linking of the epoxy groups in advanced configurations as a result of curing. **SU8** is a highly used negatively toned **PR** in MEMS applications owing to its compatibility in micromachining process, bio-compatibility features, higher degree of resistivity to chemicals, and generation of high aspect ratio micro- and nanostructures with high mechanical stabilities. However, surface chemistry reactions need to be performed on **SU8** before performing bio-applications of the cell sorter or microchannels. *Poly*-dimethyl-siloxane (**PDMS**) is a specific class of materials of silicones that belongs to the category of viscoelastic polymer of molecular formula of $[\text{-}(C_2H_6OSi)_n]$ [15, 21]. **PDMS** is widely used in microfluidic devices for biological sensing applications owing to capabilities to polymerize at rather low temperatures, capabilities to deform reversibly, optically transparent nature for wavelengths of 280 nm and higher, bio-compatible nature along with the capacity to regenerate micrometre-sized features certifying high degree of reproducibility. **PDMS** is highly compatible for the development of cell growth systems owing to its permeable characteristics towards carbon-*di*-oxide (CO_2) and oxygen (O_2). Pure **PDMS** possess hydrophobic surfaces along with highly reduced surface energies that can enforce the adsorption of hydrophobic compounds and bio-molecules over its surfaces subsequently lower the sensing capabilities of devices. Hence, specific surface chemistry led modifications are required for enhancing the functionality. An associated drawback is the huge difference between **PDMS** and metals pertaining to Young's modulus that causes stress generation including buckling of metallic bonds along with crack formation. This results in difficulty in the formation of electrical interconnects and contact pads in the form of thin films over the **PDMS** surfaces. *Poly*-methyl-meth-acrylate (**PMMA**) is a widely used, low-cost polymer with transparent features that can be applied in the form of a masking material in the fabrication technology along with use as a structural material [15, 21]. It is widely used in bio-MEMS applications in the form of microfluidic devices.

Polymer materials must undergo specific surface chemistry reactions for modification of polymer surfaces. Polymers used for optical sensing applications or devices must not suffer from auto-fluorescence in addition to coating with bio-fouling material for doing away with the adsorption of bio-molecule hydrophobic organic materials. Polymers selected for bio-MEMS should have temperature-tolerance characteristics along with a sense of wearability towards organic solvents. Different techniques for polymer materials processing for patterning of devices include hot embossing, photo- and electron beam lithographies (**EBL**) laser ablation and **X**-ray lithographies.

MEMS devices length scales are smaller than 1 mm but greater than 100 nm, while NEMS length scales are smaller than 100 nm. In that sense, quantum-dot transistor is usually at the scale of 300 nm. Biomaterials, such as, **DNA** molecules are typically ~2.5 nm wide in scales, biological cells are thousands of nanometres in diameter and molecular gears are typically ~10 nm in length scales. Hence, it can be realized that nature has already provided us with well structured, designed and patterned biomaterials that can eventually be utilized for bio-MEMS/NEMS devices. This will be actually helpful in the fabrication of devices that can be exploited at the human-interface consisting of highly advanced electronics at the micro- and nanoelectronics regime in form of an integrated circuitry. This is further coupled with advanced approaches of artificial intelligence (AI), machine learning and data analytics for next-generation commercial production of advanced devices for bio-, safety-, medical- and defence-applications. Machine learning is already integrated in research domain these days for the development of advanced, well-planned, structured and well-designed biomaterials. Microelectronics manufacturing technology is usually based on ***Si*** fabrication technology exploiting conventional surface and bulk micromachining techniques. ***Si*** as a substrate can have detrimental effects on the human body on application in form of microimplants. For elimination of this anomaly, ***Si*** substrate surfaces are passivated with protein coatings for mimicking a biological surface. In this way, ***Si*** based microimplants & devices are made compatible with the human body. Nanoscale **3D** structural conformation of the protein provides information about the function imparted by the protein as a biomaterial. Bio-MEMS exploits functional specificity of the polymers along with large-scale self-assembly of arranged molecules at the nanoscale for a rich variety of operations. Bio-MEMS can be applied for the development of biosensors consisting of specific protein antigens that bind to the specific protein antibodies. This is the particular bio-sensing mechanism driven by affinity towards specific moieties that is applicable in therapeutics. Proteins used in bio-MEMS should display higher degree of wear resistance in case of direct contact with the circulatory blood flow without getting eliminated and tissues as well. Adhesion of the mobile parts in polymer based micro-nanofluidic biodevices should be minimized. Biomolecules in the fluidic form get adhered to the walls of the microchannels restricting transport along the length of the channel, and hence, microchannel surfaces must be mobilized accordingly. Hence, hydrophobicity or wettability of a surface is of critical importance in bio-MEMS/NEMS as well [62, 63]. It is measured by the static contact angle made between the hydrophilic spherically shaped water droplet and the corresponding surface under study. The contact angle range is defined to be $90° < \theta \leq 180°$ for non-wetting of the surfaces by the liquid. Superhydrophobic surfaces are defined to be surfaces with contact angle in the range of 150–180°. Superhydrophobic surfaces must also possess very low hysteresis ($\boldsymbol{\theta}_{\mathbf{H}}$) of the water contact angle for self-cleaning purposes. Superhydrophobic surfaces have applications in energy conversion in addition to energy conservation, are good for fuel economies, while reversible superhydrophobicity provides novel routes for energy conversion, such as, microscale capillary engine. Self-cleaning capability is acquired by the specific feature of water droplets rolling off over the superhydrophobic surfaces with some degree of slip and taking away minute contaminants with them, hence the "**lotus effect**" [60, 61]. Contact angle hysteresis is a measure of the heterogenous character of the surfaces and roughness and portrays the difference occurring between forwarding and back-geared contact angles that are realistically two separate values being of highly stable nature. The removal of contaminant particles happens on the lower values of contact angle hysteresis so that rolling happens in addition to sliding. Self-cleaning surfaces can have a wide variety of applications that include solar panels, self-cleaning windows, textiles, roof tiles, paints, and in micro- and nanochannels in micro- and nanofluidics.

6 Future Scope

Bio-MEMS is at the forefront in development of biomedical sensing devices for various types of disease detection, point-of-care health applications. Bio-NEMS is all set to create a revolution in biomedical sensing devices in health monitoring with significantly enhanced efficiencies for non-invasive patient health monitoring. State-of-the-art diagnostic tools can be developed by applying micro- and nanofabrication technologies. Recently, outbreak of Covid-19 created a high degree of turbulence worldwide. However, with modern scientific advancements, rapid testing equipments were developed that had high sensing capabilities towards the novel coronavirus. MEMS/NEMS based biomedical sensors and diagnostic tools is a huge commercial technology that is expected have a global market of around 15 billion US dollars by the end of 2022. Bio-MEMS/NEMS based sensing devices can be used for detection of diseases, such as, malaria, cholera, Ebola, leprosy, schistosomiasis, and many other diseases. Diagnosis methodologies include culture techniques for microorganism detection, serological detection procedures in case of pathogenic markers, such as, proteins & antigens, and many other different ones. With the advent of bioweapons methodologies for modern warfare without directly hitting on a country, bio-MEMS/NEMS has become increasingly important for state-of-the-art rapid detection and sensing platforms. Modern viruses are continuously striking the society across the world. For example, Covid-19 proved to be highly fatal for humans across the world. Similarly, a new virus, named as lumpi skin disease virus, is striking the cows in a damaging manner. For agriculture dependent countries like India, it is extremely important to develop bio-MEMS/NEMS based rapid detection and sensing technologies so that administration of drugs, medicines & injections can be performed at an early stage. Hence, bio-MEMS/NEMS is the need of the hour not only to protect humans but animals as well, and all societies and countries must focus on it in an out-of-box manner.

7 Conclusion

Bio-MEMS/NEMS is currently at the forefront of technology for point-of-care health applications, fabrication of advanced biosensors, biodevices, drug-delivery systems, lab-on-a-chip technology for early diagnosis, and advanced microimplants that are biocompatible. Photolithography combined with wet- or dry-etching is a rather conventional method for the MEMS/NEMS based production of structures. The technology is well-established and commercial production of devices is already in place. Dry etching process can produce even anisotropic structures for advanced MEMS/NEMS fabrication. Superhydrophobic and self-cleaning surfaces with specific surface energies are important for micro- and nanofluidic systems. Stereolithography is a state-of-the-art additive manufacturing technique for the production of **3D** printed structures with many applications in consumer electronics, medical & surgical equipments, dental applications, and even defence applications. Stereolithography is a very stable, fully automatic process producing structures with high accuracy and precision. Once started, the process advances automatically without requirement of any attention. A drawback associated with stereolithography is the generation of warping and curling due to the inclusion of water in the resins over a period of time in thinner areas. Another is the non-curing of certain parts even after the exposure of laser due to energy imparted in form of conical shapes by the laser spot. Moreover, stereolithography is a costly system with costs of laser guns being very high along with costs of the photocurable resins also being high.

Micro- and nanofluidic are also in use for bio-MEMS/NEMS device fabrication by conventional lithographic technologies. Electron beam lithography (**EBL**) can be employed for device patterning at the nanometric level for NEMS fabrication. Both positively- and negatively toned photosensitive polymer solutions are used in NEMS as well. Nanochannels can be fabricated by both conventional lithography as well as by laser-based microfabrication in glasses and/or polymer substrates. Glass or polymer substrates are optically transparent to light offering the possibility of micro- and nanochannels fabrication for light-sensitive detection of biomolecules.

References

1. Crone WC (2008) A brief introduction to MEMS and NEMS. In: Sharpe W (eds) Springer handbook of experimental solid mechanics. Springer handbooks. Springer, Boston, MA. https://doi.org/10.1007/978-0-387-30877-7_9
2. Senthil Kumar PJ, Sankaranarayanan R, Jennifa Sujana AJ, Hynes JRN (2021) Advantages and disadvantages of nanodevices. In: Verpoort F, Ahmad I, Ahmad A, Khan A, Chee YC (eds) Nanomedicine manufacturing and applications. A vol. in micro and nano technologies. Elsevier https://doi.org/10.1016/C2019-0-02508-3
3. Young DJ, Zorman CA, Mehregany M (2004) MEMS/NEMS devices and applications. In: Bhushan B (ed) Springer handbook of nanotechnology. Springer handbooks. Springer Berlin, Heidelberg. https://doi.org/10.1007/3-540-29838-X_8
4. Katta M, Sandanalakshmi R (2018) A technology overview and future scope of bio-MEMS in tropical disease detection. Rev Int J Eng Technol **7**:648–651. https://doi.org/10.14419/ijet.v7i3.12.16446
5. Chircov C, Grumezescu MA (2022) Microelectromechanical (MEMS) systems for biomedical applications. Micromachines 13(1–31):164. https://doi.org/10.3390/mi13020164
6. Madou JM (2011) From MEMS to bio-MEMS and bio-NEMS (Manufacturing Techniques and Applications). CRC Press, Boca Raton. https://doi.org/10.1201/9781439895245
7. Maheshwari N, Chatterjee G, Rao RV (2014) A technology overview and applications of bio-MEMS. Smart Struct Syst 3:39–59
8. Lin L, Li Z, Feng J, Zhang Z (2013) Indirect to direct band gap transition in ultra-thin silicon films. Phys Chem Chem Phys 15:6063–6067. https://doi.org/10.1039/C3CP50429H
9. Fadaly TME, Dijkstra A, Suckert RJ, Ziss D, van Tilburg JAM, Mao C, Ren Y, van Lange TV, Korzun K, Kölling S, Verheijen AM, Busse D, Rödl C, Furthmüller J, Bechstedt F, Stangl J, Finley JJ, Botti S, Haverkort MEJ, Bakkers MAPE (2020) Direct-bandgap emission from hexagonal Ge and SiGe alloys. Nature 580:205–228. https://doi.org/10.1038/s41586-020-2150-y
10. Mahalik PN (2006) Micromanufacturing and nanotechnology. Springer Berlin, Heidelberg. https://doi.org/10.1007/3-540-29339-6
11. Hubenthal F (2011) Noble metal nanoparticles: synthesis and optical properties **1**, 375–435. In: Andrews LD, Scholes DG, Wiederrecht PG (eds) Comprehensive nanoscience and technology. Elsevier. https://doi.org/10.1016/B978-0-12-374396-1.00034-9
12. Cirelli AR, Watson PG, Nalamasu O (2001) In encyclopedia of materials: science and technology. Elsevier Science Ltd., pp 6441–6449
13. May SG, Sze SM (2004) Fundamentals of semiconductor fabrication. Wiley
14. Ghandhi KS (1994) VLSI fabrication principles. Wiley
15. Turner RS, Daly CR (1988) Polymers in microlithography. J Chem Edu 65:322–325. https://doi.org/10.1021/ed065p322
16. Licari JJ, Enlow RL (1998) Thin film processes. 63–103. In: Hybrid microcircuit technology handbook (materials, processes, design, testing and production). https://doi.org/10.1016/B978-081551423-7.50005-5
17. Ceyssens F, Puers R (2012) SU-8 photoresist. In: Bhushan B (ed) Encyclopedia of nanotechnology. Springer. https://doi.org/10.1007/978-90-481-9751-4
18. Besaucele H, Das PP, Duffey PT, Embree JT, Ershov IA, Fleurov BV, Grove LS, Melcher CP, Ness MR, Padmabandu GG (2000) Comparison of ArF and KrF laser performance at 2 kHz for microlithography. In: Proceedings of the SPIE 4000, optical microlithography XIII. https://doi.org/10.1117/12.388986
19. Endert H, Pätzel R, Powell M, Rehban U, Basting D (1995) New KrF and ArF excimer laser for advanced DUV lithography. Microelectronic Engg. 27:221–224. https://doi.org/10.1016/0167-9317(94)00093-A
20. Maalouf A, Gadonna M, Bose D (2009) An improvement in standard photolithography resolution based on Kirchhoff diffraction studies. J Phys D Appl Phys 42(1–11):015106. https://doi.org/10.1088/0022-3727/42/1/015106

21. Kumar V, Pallapa M, Rezai P, Selvaganapathy RP (2015) Polymers. In: Reference module in materials science materials engineering. Elsevier. https://doi.org/10.1016/B978-0-12-803581-8.00522-1
22. Bourdillon JA, Boothroyd BC, Kong RJ, Vladimirsky Y (2000) A critical condition in Fresnel diffraction used for ultra-high resolution lithographic printing. J Phys D Appl Phys 33:2133–2141. https://doi.org/10.1088/0022-3727/33/17/307
23. Jain K, Willson CG, Lin BJ (1982) Ultrafast high-resolution contact lithography with excimer lasers. IBM J Res Dev 26:151–159. https://doi.org/10.1147/rd.262.0151
24. Mojarad N, Hojeij M, Wang L, Gobrecht J, Ekinci Y (2015) Single-digit-resolution nanopatterning with extreme ultraviolet light for the 2.5 nm technology node and beyond. Nanoscale 7:4031–4037. https://doi.org/10.1039/C4NR07420C
25. French RH (2012) Immersion lithography. In: Bhushan B (ed) Encyclopedia of nanotechnology. Springer, Dordrecht. https://doi.org/10.1007/978-90-481-9751-4_354
26. Owa S, Nagasaka H (2003) Immersion lithography: its potential performance and issues. In: Proceedings of the SPIE 5040, optical microlithography XVI. https://doi.org/10.1117/12.504599
27. Sandle T (2013) Cleanrooms, isolators and cleanroom technology. In: Sterility, sterilization and sterility assurance for pharmaceuticals (technology, validation and current regulations). https://doi.org/10.1533/9781908818638.189
28. https://en.wikipedia.org/wiki/Cleanroom
29. Alkaisi MM, Blaikie JR, McNab JS (2000) 70 nm features on 140 nm period using evanescent near field optical lithography. Microelectronic Engg. 53:237–240. https://doi.org/10.1016/S0167-9317(00)00305-1
30. Naulleau P (2012) Optical lithography. Lawrence Berkeley National Laboratory, Berkeley, CA
31. Pease WFR (1981) Electron beam lithography. Contemp Phys 22:265–290. https://doi.org/10.1080/00107518108231531
32. Pala N, Karabiyik M (2016) Electron beam lithography. In: Bhushan B (ed) Encyclopedia of nanotechnology. Springer, Dordrecht. https://doi.org/10.1007/978-94-017-9780-1
33. Willson GC, Stewart DM (2001) Photoresists. In: Buschow JHK, Flemings CM, Kramer JE, Veyssiere P, Cahn WR, Ilschner B, Mahajan S (eds) Encyclopedia of materials: science and technology, 2nd edn. pp 6973–6977. https://doi.org/10.1016/B0-08-043152-6/01235-3
34. García-Arribas A, Fernandez E, Barrainkua A, Svalov AV, Kurlyandskaya GV, Barandiaran JM (2012) Comparison of microfabrication routes for magneto-impedance elements: Lift-off and wet-etching. IEEE Trans Magn 48:1601–1604. https://doi.org/10.1109/TMAG.2011.2173167
35. Cheung MK, Stemer MD, Zhao C, Young DT, Belling NJ, Andrews MA, Weiss SP (2019) Chemical lift-off lithography of metal and semiconductor surfaces. ACS Mater Lett 2:76–83. https://doi.org/10.1021/acsmaterialslett.9b00438
36. Sze S (1988) VLSI technology. McGraw-Hill Science. ISBN 0070627355 (ISBN13: 9780070627352)
37. House D, Li D (2008) Anisotropic etching. In: Li D (eds) Encyclopedia of microfluidics and nanofluidics. Springer, Boston, MA. https://doi.org/10.1007/978-0-387-48998-8_35
38. Morozov AI (2017) Influence of dry etching condition to geometry of vertically aligned silicon nanostructures. J Phys Conf Ser 917(1–5): 052030. https://doi.org/10.1088/1742-6596/917/5/052030
39. Ganjian M, Modaresifar K, Zhang H et al (2019) Reactive ion etching for fabrication of biofunctional titanium nanostructures. Sci Rep 9:18815. https://doi.org/10.1038/s41598-019-55093-y
40. Huang J, Qin Q, Wang J (2020) A review of stereolithography: processes and systems. Processes 8(1–16):1138. https://doi.org/10.3390/pr8091138
41. ebrary.net/158129/engineering/liquid_based_additive_manufacturing_systems#122202
42. Nishat S, Jafry TA, Martinez WA, Awan RF (2021) Paper-based microfluidics: simplified fabrication and assay methods. Sens Actuat B Chem 336:129681. https://doi.org/10.1016/j.snb.2021.129681

43. Reboud J, Xu G, Garrett A, Adriko M, Yang Z, Tukahebwa ME, Rowell C, Cooper MJ (2019) Paper-based microfluidics for DNA diagnostics of malaria in low resource underserved rural communities. Proc Natl Acad Sci USA 116:4834–4842. https://doi.org/10.1073/pnas.1812296116
44. Noviana E, Ozer T, Carrell SC, Link SJ, McMahon C, Jang I, Henry SC (2021) Microfluidic paper-based analytical devices: from design to applications. Chem Rev 121:11835–11885. https://doi.org/10.1021/acs.chemrev.0c01335
45. Ghosh R, Gopalakrishnan S, Savitha R (2019) Fabrication of laser printed microfluidic paper-based analytical devices (LP-μPADs) for point-of-care applications. Sci Rep 9(1–11):7896. https://doi.org/10.1038/s41598-019-44455-1
46. Abegunde OO, Akinlabi TE, Oladijo PO, Akinlabi S, Ude UA (2019) Overview of thin film deposition techniques. AIMS Mater Sci 6:174–199. https://doi.org/10.3934/matersci.2019.2.174
47. Rossnagel MS (2003) Thin film deposition with physical vapor deposition. J Vac Sci Technol A 21:S74–S87. https://doi.org/10.1116/1.1600450
48. Dwivedi S (2020) Fabrication and manufacturing process of solar cell: Part I. In: Tripathi LS, Padmanaban S (eds) Green energy: solar energy, photovoltaics, and smart cities. Wiley Online, pp 1–37. https://doi.org/10.1002/9781119760801.ch1
49. Dwivedi S (2014) Spintronics: the realm of nanotechnology. In: Islam N (ed) Nanotechnology: recent trends. Nova Publishers, USA, Emerging issues and future directions, pp 311–335
50. Dwivedi S, Biswas S (2018) Enhanced magnetoresistance in pulsed laser deposited stable chromium oxide thin films. Thin Solid Films 655:13–21. https://doi.org/10.1016/j.tsf.2018.03.093
51. Dwivedi S, Jadhav J, Sharma H, Biswas S (2014) Pulsed laser deposited ferromagnetic chromium dioxide thin films for applications in spintronics. Phys Proc 54:62–69. https://doi.org/10.1016/j.phpro.2014.10.037
52. Dwivedi S, Biswas S (2012) Pulsed laser deposition of half-metallic CrO_2 thin films for spintronic applications. Int Conf Emerg Electron 1–4. https://doi.org/10.1109/ICEmElec.2012.6636271
53. Dwivedi S, Biswas S (2013) Effects of annealing on pulsed laser deposited TiO_2 thin films. Appl Mech Mater 446–447:306–311. https://doi.org/10.4028/www.scientific.net/amm.446-447.306
54. Kelly PJ, Arnell RD (2000) Magnetron sputtering: a review of recent developments and applications. Vacuum 56:159–172
55. www.semicore.com/news/93-what-is-hipims
56. vaccoat.com/blog/pulsed-dc-magnetron-sputtering/#Pulsed_DC_Magnetron_Sputtering
57. Creighton JR, Ho P (2001) Introduction to chemical vapor deposition (CVD). Chem Vapor Depos 2:1–22. www.asminternational.org/documents/10192/1849770/ACFAA6E.pdf
58. Dwivedi S Nanoelectronics. In: Birla S, Singh N, Shukla KN (eds) Nanotechnology: device design and applications. CRC Press, Boca Raton. https://doi.org/10.1201/9781003220350
59. Jones CA, Hitchman LM (2009) Chemical vapor deposition: precursors, processes and applications. R Soc Chem 1–36. https://doi.org/10.1039/9781847558794
60. Hamedani Y, Macha P, Bunning JT, Naik RR, Vasudev CM (2016) Plasma-enhanced chemical vapor deposition: where we are and the outlook for the future. In: Neralla S (ed) Chemical vapor deposition—recent advances and applications in optical, solar cells and solid state devices. InTechOpen. https://doi.org/10.5772/61559
61. Alti K, Dwivedi S, Chidangil S, Mathur D, Khare A (2015) Micro-patterning of Indium thin film for generation of micron and submicron particles using femtosecond laser-induced forward transfer. Laser Part Beams 33:449–454. https://doi.org/10.1017/S0263034615000476
62. Bhushan B (2011) MEMS/NEMS and bioMEMS/bioNEMS: materials, devices and biomimetics. In: Bhushan B (ed) Nanotribology and nanomechanics, vol. 23, 833–945. https://doi.org/10.1007/978-3-642-15263-4_23
63. Yilbas SB, Al-Sharafi A, Ali H (2019) Surfaces for self-cleaning. In: Self-cleaning of surfaces and water droplet mobility. Elsevier, pp 45–98. https://doi.org/10.1016/B978-0-12-814776-4.00003-3

In-silico Analysis of Expandable Radiofrequency Electrode for Ablation of Hepatic Tumors

Shaik Sadikbasha and Ashish. B. Deoghare

Abstract The current study evaluates radiofrequency (RF) ablation of hepatic tumors with an expandable multi-prong RF applicator. To assess the localized cooling effect of blood flow on necrosis volume, a three-dimensional computational model of hepatic tissue, cancer tumor, blood vessel, and RF applicator was created. The finite element method is used to calculate the effect of blood vessel location, diameter, change in input voltage, and tumor property uncertainty on ablation volume. An increase in blood vessel diameter causes a 6.52% reduction in ablation volume, and a 10 mm diameter blood vessel located next to a tumor causes a 12.19% reduction in ablation volume.

Keywords Hepatic tumors · Bio-heat equation · Hepatocellular Carcinoma · Ablation volume

1 Introduction

Cancer kills millions of people worldwide each year, with Hepatocellular Carcinoma (HCC) being the third leading cause of death in Asia and Africa [1]. Surgical resection is the most commonly used treatment method for cancer tumors. However, open surgery removes part of tissue permanently which shortens the organ and tumor location restricts the use of surgical resection in some cases. To overcome these limitations, researchers were drawn to minimally invasive percutaneous techniques such as RF ablation, Laser, Microwave, and Cryoablation as an alternative to surgical resection. RF ablation is a clinically well-accepted hyperthermia technique that uses heat energy to effectively treat multifocal and surgically non-resectable tumors. Its ability to ablate targeted tissue while causing minimal normal tissue invasion and low cost made it an attractive alternative to open surgery. When compared to surgical resection, RF ablation as an initial treatment for HCC has better long-term outcomes and survival rates [2].

S. Sadikbasha · Ashish. B. Deoghare (✉)
Department of Mechanical Engineering, National Institute of Technology Silchar, Assam 788010, India
e-mail: abdeoghare@mech.nits.ac.in

K. Guha et al. (eds.), *MEMS and Microfluidics in Healthcare*, Lecture Notes in Electrical Engineering 989, https://doi.org/10.1007/978-981-19-8714-4_7

Large blood vessels cause localized cooling and reduce the efficacy of hyperthermia treatment, according to Roemer et al. [3]. Kolios et al. [4] developed a numerical model to investigate the cooling effect of large blood vessels in heated tissue. Chinn et al. [5] investigated the effect of vascular occlusion on hepatic tumor RF ablation. Jain and Wolf [6] presented a novel three-dimensional model to investigate the effect of blood flow on lesion volume in RF ablation using a single-tip electrode. Supan et al. [7], Haemmerich et al. [8], Suarez et al. [9], and Huang et al. [10] investigated the effect of a large blood vessel on ablation volume using isothermal and convective boundary conditions with an expandable electrode. However, assuming isothermal and convective boundary conditions at the tissue-blood vessel interface overestimate ablation volume, and results obtained under these conditions may not accurately predict temperature profiles. As a result, combining blood flow analysis with electrothermal analysis yields a more accurate estimate of ablation volume.

Haemmerich et al. [11] studied the variation of electrical conductivity in rat tumors in vivo and discovered that it was significantly different from normal tissue conductivity. Liu et al. [12] investigated the relationship between temperature and perfusion rate and discovered that increased blood flow decreases coagulation volume and time required to achieve thermal equilibrium. Schutt et al. [13] compared various perfusion models, their effect on temperature profiles, and confirmed that multi-tined electrodes are more susceptible to perfusion change. Hall et al. [14] validated the effect of perfusion, thermal, electrical conductivity, and cell death models on ablation volume, establishing that perfusion and cell death models are critical parameters for accurate ablation volume prediction. Various protocols for increasing ablation volume have been developed, including internally cooled electrodes [15], multiple electrodes [16], two-compartment models [17], expandable electrodes [7, 8, 10], and bipolar RF ablation [18]. These studies, however, show that taking into account the same properties for both tissue and tumor may not provide an accurate prediction of ablation volume and temperature profiles. As a result, a variation in tumor properties with temperature, as well as uncertainty in tumor properties, require more attention for accurate analysis. The purpose of this study is to determine the effect of blood flow velocity, blood vessel diameter, and the relative location of a blood vessel with a tumor on ablation volume. The impact of input voltage, tumor density, specific heat, thermal conductivity, electrical conductivity, and perfusion rate on ablation volume and temperature distribution is also investigated. This study aids the therapist in the effective pre-planning of RF ablation treatment for hepatic tumors.

2 Materials and Methods

A schematic diagram used for computational analysis is shown in Fig. 1. It shows liver tissue, the spherical tumor is located at the center, a blood vessel, and an RF applicator inserted in the tumor. A 15 gauge RITA Medical Systems Model30 umbrella-shaped expandable four-tined RF applicator [7] is used to destroy tumor by heating as shown in Fig. 1. The liver is a complex organ and its physical properties are inhomogeneous.

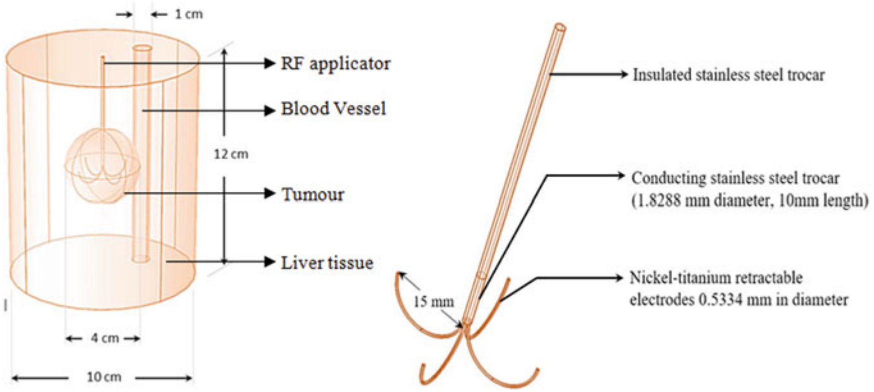

Fig. 1 Schematic of the computational domain for RF ablation

Therefore, investigations are carried out for tumor cells by varying density, specific heat, thermal conductivity, electrical conductivity, and perfusion rate to study the influence on temperature distribution and ablation volume. Blood vessels of diameter more than 6 mm cause localized cooling in heated tissue, hence a blood vessel is modeled in hepatic tissue and its diameter has been varied from 6 to 13 mm to evaluate the effect on ablation volume and temperature distribution. The influence of relative distance between tumor and blood vessel on temperature change and an ablation volume is studied by locating blood vessel at 21 and 26 mm from the tumor center. Analysis has been carried out at 30, 70, and 90 mm/s velocity of blood flow to evaluate the effect on ablation volume and temperature profiles [6].

In RF ablation procedure electrical potential is applied to RF applicator at 500 kHz frequency for the period of 8 min to destroy the targeted tissue. The electrical potential applied generates a flow of alternating current in conductive electrodes which causes ion agitation and produces localized heating. This results in resistive heating of liver and tumor tissue in the proximity of electrodes. Intercellular protein denaturation, cell membrane destruction occurs at the temperatures beyond 45 °C [7] and produces coagulative necrosis.

2.1 Governing Equations

The heat generated from the electrodes propagates to surrounding tissue through conduction mode. The maximum temperature reduces the fourth power as the distance from the electrode increases in tissue [4]. Tumor cells near to large blood vessels are more difficult to ablate because blood flow causes localized cooling effect and influences heat deposition in tissue. Hence, theoretical formulation of RF ablation procedure is necessary to evaluate the localized cooling effect for accurate prediction of ablation volume and to plan the treatment effectively.

Table 1 Properties of materials used for computational domains [7, 19, 20]

Domain	Material	$\rho\left(\frac{kg}{m^3}\right)$	$c\left(\frac{J}{kg.K}\right)$	$k\left(\frac{W}{m.K}\right)$	$\sigma\left(\frac{S}{m}\right)$	Other properties
Insulation	Polyurethane	70	1045	0.026	1×10^{-5}	
Trocar	Stainless steel	21,500	132	71	4×10^6	
Electrodes	Ni–Ti alloy	6450	840	18	1×10^8	
Tissue	Liver	1060	3600	0.512	0.333	0.0064 $\omega\left({}^1/_s\right)$
Tumor	Liver tumor	999	4200	0.552	0.117	0.0156 $\omega\left({}^1/_s\right)$
Blood	Blood	1050	4180	0.543	0.667	0.0035 $\mu[Pa.s]$

Modeling of heat transfer and temperature distribution in biological tissues is expressed using bioheat Eq. (1) [7].

$$\rho C\frac{\partial T}{\partial t} = \nabla.k\nabla T + \rho_b C_b \omega_b (T_b - T) + Q_e + Q_m \tag{1}$$

where ρ is the density of the medium(kg/m^3), C is the specific heat (J/kg.K), T is the temperature(K), t is the time(s), k is the thermal conductivity(W/m.K), subscript b denotes blood, and ω is the blood perfusion(1/s). The properties of materials used for computational domains are given in Table1.

The equation involves the metabolic heat energy $Q_m\left({}^W/_{m^3}\right)$ generated in the body which is negligible when compared to other terms in Eq. (1), source energy $Q_e\left({}^W/_{m^3}\right)$ generated by electrodes, $\rho_b C_b \omega_b (T_b - T)$ is the heat carried away due to the blood perfusion, $\nabla.k\nabla T$ is the heat energy propagated in tissue through conduction mode and $\rho C\frac{\partial T}{\partial t}$ is the energy deposited in the tissue over the period of time.

The source energy Q_e is evaluated from the distribution of current density and electrical field intensity in the computational domain. The distribution is expressed by generalised Laplace Eq. (2), from this equation voltage distribution is evaluated.

$$\nabla.[\sigma \nabla V] = 0 \tag{2}$$

where V is the voltage (V) and σ is the electrical conductivity (S/m).

The electrical field intensity and the current density are obtained from Eqs. (3) and (4) from the voltage distribution.

$$E = -\nabla V \tag{3}$$

$$J = \sigma.E \tag{4}$$

where E is the electric field intensity(V/m) and J is the current density(A/m^2). The resistive heat generated by current density is expressed by Eq. (5)

$$Q_e = J.E \tag{5}$$

The thermo-electrical system further needs to be coupled with a fluid flow field to determine the localized cooling effect caused by blood flow. The continuity (6), Navier Stokes (7), and energy Eqs. (8) are solved over the computational domains.

$$\vec{\nabla} \cdot \vec{V} = 0 \tag{6}$$

$$\frac{\partial \overrightarrow{V}}{\partial t} + \overrightarrow{\mathrm{V}}.\nabla \overrightarrow{V} = -\frac{1}{\rho_b} \nabla \overrightarrow{P} + \rho_b \overrightarrow{g} + \frac{\mu_b}{\rho_b} \nabla^2 \overrightarrow{V} \tag{7}$$

$$\rho \mathrm{C}\left(\frac{\partial T}{\partial t} + \overrightarrow{V}.\nabla T\right) = \nabla.k\nabla T + \rho_b C_b \omega_b (T_b - T) + Q_e \tag{8}$$

where $\overrightarrow{V}$ is the velocity vector, $\overrightarrow{P}$ is the pressure vector, $\overrightarrow{\mathrm{g}}$ is the gravitational acceleration vector, and μ is the viscosity of blood.

The sensitivity of electrical, thermal conductivity, and blood perfusion rate to the temperature [21] is evaluated using Eqs. (9), (10), and (11)

$$\sigma(T) = \sigma_0(1 + 0.02(T - T_b) \tag{9}$$

where σ_0 is the baseline conductivity, Eq. (9) considers 2% per °C variation in electrical conductivity for both tumor and tissue [21].

$$k(T) = k_0(1 + 0.013(T - 310.13) \tag{10}$$

where k_0 is the baseline thermal conductivity, Eq. (10) considers 1.3% per K variation in thermal conductivity for both tumour and tissue [21].

$$\omega_b = \left\{ \begin{array}{ll} \omega_{b0} & \Omega(t) \le 0 \\ \omega_{b0}\left[1 + 25\Omega(t) - 260\Omega(t)^2\right] & 0 < \Omega(t) \le 0.1 \\ \omega_{b0} e^{[-\Omega(t)]} & \Omega(t) > 0.1 \end{array} \right\} \tag{11}$$

where ω_{b0} is the baseline perfusion rate, $\Omega(t)$ is the thermal induced tissue damage. The destruction of cancer cells in RFA occurs due to direct and indirect heating mechanisms. At the end of the procedure of RFA, three zones of necroses tissue, sub-lethal damage tissue, and normal tissue can be observed. The tissue subjected to temperature more than 50 °C is considered necroses tissue because denaturation of protein, cell membrane collapses, metabolism, and enzymatic function halt occurs at 50 °C. The tissue with a temperature of 40–50 °C is considered sub-lethal damage and at a temperature less than 40 °C is considered normal tissue. However, necrosis depends on tissue type, temperature level, time duration, and heat energy accumulated. In this analysis damage integral Eq. (12)derived using the Arrhenius equation [21] is used to evaluate the ablation volume and results are compared with isothermal temperature contour of 50 °C. The thermal damage integral of tissue is calculated using Eq.(12).

$$\Omega(t) = \int_0^t A e^{\left[\frac{-E_a}{RT}\right]} \tag{12}$$

where $\Omega(t)$ is the tissue damage integral, E is the activation energy for irreversible tissue damage, A is the tissue frequency factor, T is the temperature, and R is the universal gas constant. For liver tissue E = 2.577×10^5 Jmol^{-1}, A = 7.39×10^{39} s^{-1}.

The fraction of tissue damage is expressed by Eq. (13),

$$\theta_d = 1 - e^{-\Omega(t)} \tag{13}$$

where θ_d is the fraction of tissue damage, its value lies between (0, 1). The value of tissue damage $\Omega(t)$ =1 and 4.6 corresponds to 63.2 and 99% probability of cell death respectively.

2.2 Boundary Conditions and Analysis

The boundary conditions employed on computational domains for this analysis are as follows:

The initial voltage in the computational domain is 0 V and an impedance of $Z = 60\Omega$ is maintained in the analysis. Grounded (V = 0) boundary condition is employed on the one of the outer surfaces of tissue, and analysis is carried out by changing electrical potential from 20–40 V which is given to the electrode. Stainless Steel (SS) trocar of the RF applicator is subjected to insulated boundary condition, $\boldsymbol{n}.\boldsymbol{J} = 0$.

For thermal analysis, the initial temperature employed in the computational domain is the same as body temperature, $T = T_b$. The outer boundaries of tissue which remains unaffected also subjected to temperature boundary condition of $T = T_b$. The electric energy applied generates heat in the tissue to necroses the tumor cells.

For the fluid domain at the inlet, the temperature boundary condition $T = T_b$ is employed with the pressure of $P = 3333.33(Pa)$. The inlet blood velocity considered in the analysis is $u(x) = u(y) = 0; u(z) = 35, 70, \text{and}\, 90\, mm/s$. At the liver–blood interface, blood velocity is $u = v = z = 0$. At the outlet of blood vessel, $P = 3333.33(Pa)$ is employed to carry out an investigation.

The prepared models are imported into COMSOL Multiphysics FEM software to perform coupled analysis of thermoelectric, fluid field problem. In this study, electric currents AC/DC module, biological heat transfer module, and laminar fluid flow module are used to simulate RF ablation of hepatic tumors. Multiphysics has been used to couple modules considered for analysis.

Physics-dependent meshing has been done on domains using tetrahedral elements of a minimum size 1 mm and a convergence test has been performed to find an optimum number of elements. The relative error obtained for the mesh with 189,385 elements and higher density mesh is <0.5%. Therefore, the analysis is carried out at this mesh size and solved for 545,255 degrees of freedom. The implicit time-dependent analysis is performed for 8 min with time step 0.01 to 5 s using Backward Differential Formula (BDF) of second order.

2.3 Validation

Validation of the model has been done with the experimental work of B. Chinn et al. (2000) [5]. Lesion volume by occlusion of the portal vein is $8.6 \pm 3.8cm^3$. Results obtained by placing simple hepatic artery at 21 and 26 mm from tumor centre produce 9.13 and 9.57 cm^3 respectively using 50 °C isothermal contours. Analysis shows $\leq$ 10% relative error with experiment results. The results also compared with the study performed by Tungjitkusulmon et al. (2003) [7]. Ablation volume obtained in his work with no blood vessel, 10 mm diameter blood located 5 mm and 1 mm away from the probe is 19.2, 18.6, and 17.2 cm^3 respectively. However, in the present work results are 21.8, 17.5, and 17.1 cm^3 respectively with a maximum difference of 13.54%.

3 Results and Discussion

The HCC cases diagnosed increased 115% from the year 2002 to 2012, in many cases using open surgery to eliminate cancer tumors is difficult due to the critical location of the tumor. Hence, percutaneous techniques like RF ablation evolved as a safe and efficient technique to destroy hepatic tumors without causing much damage to normal tissue. The necrosis volume in RF ablation primarily depends on applied voltage, duration of treatment, tumor physical properties, and relative location blood vessel with respect to the tumor.

The effect of voltage on temperature distribution and an ablation volume is evaluated by varying input voltage from 20–40 V at 500 kHz. Figures 2 and 3 show results obtained by locating a 10 mm diameter blood vessel at 26 mm from the tumor center with a blood flow velocity of 70 mm/s. Temperature-dependent property models are given in Eqs. (9), (10) and (11) are used in the analysis. The temperature increases with an increase in source voltage, temperature rises to the maximum value within 70 s for all voltages and remains almost constant for the remaining duration as shown in Fig. 2.

Maximum and minimum temperatures observed in the analysis are 119 °C at 40 V and 52 °C at 20 V respectively. Figure 3 shows a change in ablation volume with time for different input voltage conditions. Maximum and minimum ablation volumes obtained in the study are 12.3 cm^3 at 40 V and 1.44 cm^3 at 20 V respectively when calculated using volume integral of 50 °C isothermal contours. Figure 4 shows ablation volume obtained using tissue damage integral, 99% probability of cell death, 50 °C isothermal contours when a blood vessel of 10 mm diameter located at 21 and 26 mm.

Ablation volume decreases with a decrease in relative distance between tumor and blood vessel. The ablation volume corresponds to 50 °C isothermal contours and 99% cell death damage integral is 12.3, 13 cm^3, and 13.8, 14.5 cm^3 when a blood vessel is located at 21 and 26 mm respectively from tumor center. Results obtained using tissue damage integral and isothermal contours differ by 6% and ablation volume

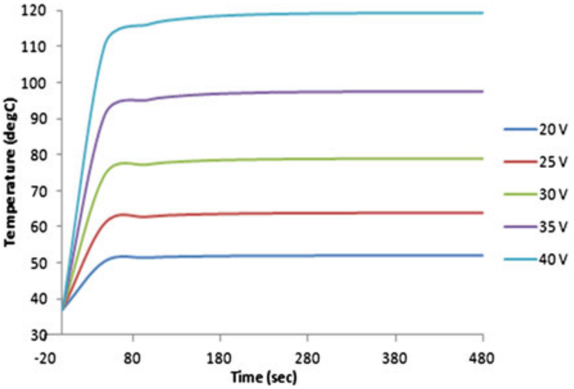

Fig. 2 Effect of volume on temperature distribution over time

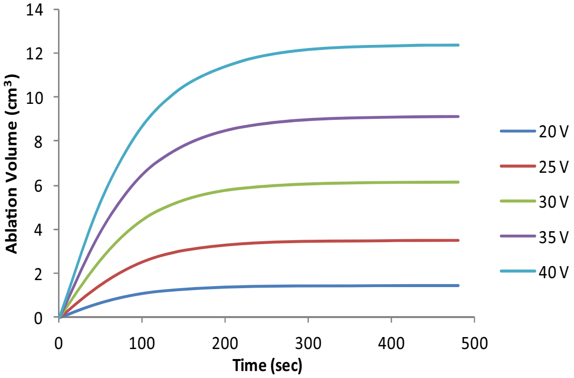

Fig. 3 Ablation volume observed with time at various voltages

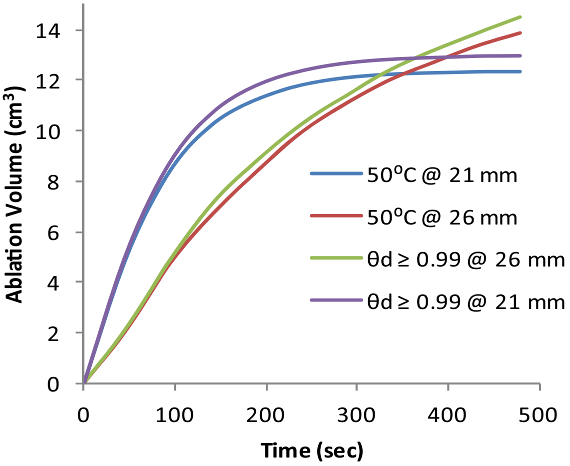

Fig. 4 Effect of blood vessel location and cell death models on ablation volume at 40 V

variation with blood vessel location is 12.19% as shown in Fig. 4. Maximum ablation volume for each condition is attained before 5 min, however; analysis is carried out for 8 min to make sure that the heat energy required for complete ablation is supplied. Figure 5 shows the effect of time on the ablation volume accumulated. Temperature above 100 °C causes tissue charring, carbonization, and increases impedance which further restricts the accumulation of necrosis volume. Hence source voltage is tuned to 35 V to keep the temperature below 100 °C.

Blood perfusion is another critical parameter which significantly affects lesion volume. Figure 6 shows temperature distribution and ablation volume with time considering different perfusion rates for tumor. The analysis is carried out at 35 V, locating 10 mm diameter blood vessel 26 mm away from the tumor center. The perfusion rate in normal tissue is significantly different from the tumor; hence perfusion

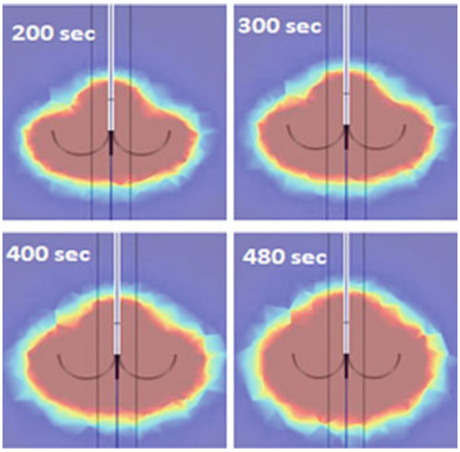

Fig. 5 Ablation accumulated over time in RF ablation at 40 V

Fig. 6 Effect of tumor perfusion variation on ablation volume and temperature at 35 V

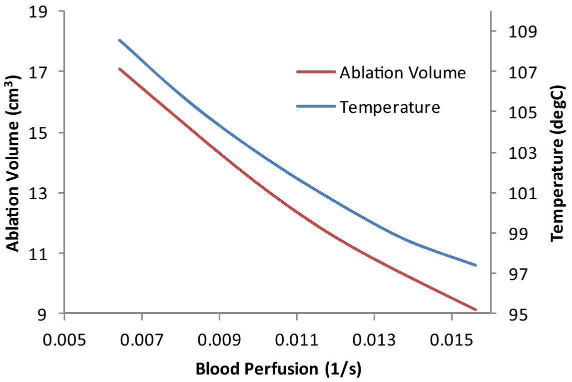

rate has been varied from normal tissue perfusion, 6.4×10^{-3} to tumor perfusion $0.1168\,s^{-1}$.

A maximum temperature of 108.5 °C is observed when tumor and normal tissue perfusion is considered to be the same and a minimum temperature of 97 °C is observed when actual perfusion rates given in Table 1 are considered. Ablation volume obtained is 17.8 and 9.13 cm^3 when tumor perfusion is 6.4×10^{-3} and $0.1168\,s^{-1}$ respectively. Maximum temperature and ablation volume decrease with an increase in perfusion rate as shown in Fig. 6. Therefore, any uncertainty in considering perfusion rate causes significant error in the estimation of temperature distribution and necrosis volume.

The thermal conductivity of the tumor is another critical parameter which can influence ablation volume. Therefore, the effect of thermal conductivity on temperature distribution and an ablation volume is evaluated at 35 V by locating the 10 mm diameter blood vessel at 26 mm from the tumor center. Results shown in Fig. 7 indicate the variation of ablation volume and temperature with thermal conductivity. Temperature reduces with increase in thermal conductivity whereas ablation volume increases as shown in Fig. 7. The error in the estimation of ablation volume is <2% by considering the same thermal conductivity for tumor and tissue. The electrical conductivity of tumor is another influencing characteristic of RF ablation procedure. Results in Fig. 6 show the effect of electrical conductivity on temperature distribution and ablation volume. Both temperature and ablation volume increases with an increase in electrical conductivity as shown in Fig. 8. Considering the same electrical conductivity for both tumor and tissue produces 126 °C temperature and necrosis volume of 16.8 cm^3, otherwise, temperature and volume are 97 °C and 9.13 cm^3 respectively. Therefore, uncertainty in the electrical conductivity of the tumor overestimates ablation volume.

Analysis has been carried out to evaluate the effect on ablation volume by locating a blood vessel of diameters 6, 10, and 13 mm at 21 and 26 mm from the tumor centre. Ablation volume is evaluated for 30, 70, and 90 mm/s as shown in Table 2. Changing velocity of blood flow from 30 to 90 mm/s reduced ablation volume by 3, 1.7, 3.8,

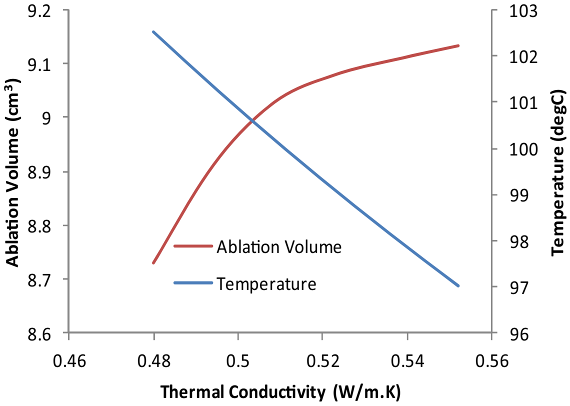

Fig. 7 Effect of variation in thermal conductivity on temperature and ablation volume with time

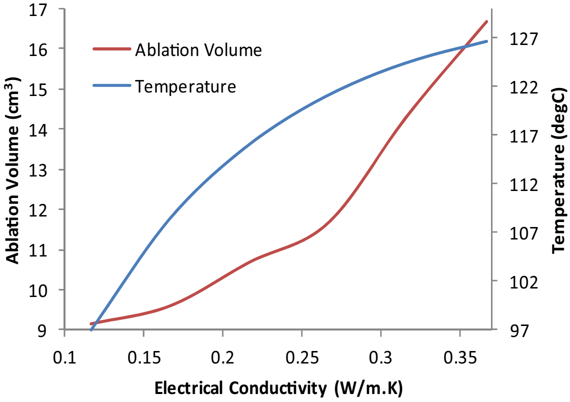

Fig. 8 Effect of variation in electrical conductivity on temperature and ablation volume with time

1.75, 2.59, and 1.89% when 6, 10 and 13 mm diameter blood vessel located at 21 and 26 mm distance from tumor respectively.

The results shown in Table 2 state that the increase in diameter of the vessel when located at 21 mm from the tumor center showed a significant decrease in ablation volume. But the increase in diameter of the blood vessel has no considerable change

Table 2 Results obtained for the ablation volume using tissue damage integral at 99% cell death after 8 min duration considering temperature dependent property models at 35 V

Blood vessel diameter (mm)	6	6	10	10	13	13
Location of blood vessel (mm)	21	26	21	26	21	26
Flow velocity (mm/s)	Ablation volume (cm^3)					
30	7.14	7.55	7.23	7.54	7.13	7.54
70	7.36	7.42	7.12	7.43	7.07	7.40
90	7.28	7.53	7.24	7.35	6.87	7.48

in ablation volume. Increase in velocity of blood flow reduces ablation volume as shown in Table 2. Variation of density and specific heat of tumor has no major effect on temperature distribution and ablation volume. Therefore, input voltage, perfusion rate, and electrical conductivity are the most important parameters along with cell death models.

4 Conclusions

RF ablation is an effective and safe method of treating surgically inoperable tumors in critical locations. Predicting lesion volume accurately prior to surgery allows for lower recurrence rates and more effective treatment planning. This study looked at the factors that influence lesion volume. Temperature and lesion volume increase significantly as voltage increases, but temperatures above 35 V exceed 100 °C, which is undesirable due to increased impedance and carbonization. The most influential parameter is blood perfusion; considering the same perfusion for tumor and tissue doubles the ablation volume, causing a prediction error. When thermal conductivity is changed, it causes a 2% change in temperature and ablation volume. Increasing the electrical conductivity of the tumor results in a 1.5-fold increase in ablation volume. When compared to blood vessels at 26 mm, large blood vessels located 21 mm from the tumor center cause localized cooling and reduce ablation volume by 12.19%. As a result, this study may be useful to medical practitioners in effectively planning RF ablation treatment.

References

1. White DL, Thrift AP, Kanwal F, Davila J, El-Serag HB (2017) Incidence of hepatocellular carcinoma in all 50 United States, from 2000 through 2012. Gastroenterology 152
2. Yamao T, Imai K, Yamashita Y-I, Kaida T, Nakagawa S, Mima K, Hashimoto D, Chikamoto A, Ishiko T, Baba H (2018) Surgical treatment strategy for hepatocellular carcinoma in patients with impaired liver function: hepatic resection or radiofrequency ablation? HPB 20
3. Chen ZP, Roemer RB (1992) The effects of large blood vessels on temperature distributions during simulated hyperthermia. J Biomech Eng 114
4. Kolios MC, Sherar MD, Hunt JW (1995) Large blood vessel cooling in heated tissues: a numerical study. Phys Med Biol 40
5. Chinn SB, Lee FT, Kennedy GD, Chinn C, Johnson CD, Winter TC, Warner TF, Mahvi MD (2001) Effect of vascular occlusion on radiofrequency ablation of the liver: Results in a porcine model. Am J Roentgenol 176
6. Jain MK, Wolf PD (2001) A three-dimensional finite element model of radiofrequency ablation with blood flow and its experimental validation. Ann Biomed Eng 28
7. Tungjitkusolmun S, Staelin TS, Haemmerich D, Tsai J-Z, Webster J, Lee FT, Mahvi MD, Vorperian VR (2002) Three-dimensional finite-element analyses for radio-frequency hepatic tumor ablation. IEEE Trans Bio-Med Eng 49

8. Haemmerich D, Tungjitkusolmun S, Staelin TS, Lee FT, Mahvi DM, Webster J (2002) Finite-element analysis of hepatic multiple probe radio-frequency ablation. IEEE Trans Bio-Med Eng 49
9. González-Suárez A., Trujillo M, Burdío F, Andaluz A, Berjano E (2014) Could the heat sink effect of blood flow inside large vessels protect the vessel wall from thermal damage during RF-assisted surgical resection? Med Phys 41
10. Huang H-W (2013) Influence of blood vessel on the thermal lesion formation during radiofrequency ablation for liver tumors. Med Phys 40
11. Haemmerich D, Staelin ST, Tsai JZ, Tungjitkusolmun S, Mahvi DM, Webster JG (2003) In vivo electrical conductivity of hepatic tumours. Physiol Meas 251
12. Liu Z, Ahmed M, Sabir A, Humphries S, Goldberg SN (2007) Computer modeling of the effect of perfusion on heating patterns in radiofrequency tumor ablation. Int J Hypertherm 23(1)
13. Schutt DJ, Haemmerich D (2008) Effects of variation in perfusion rates and of perfusion models in computational models of radio frequency tumor ablation. Med Phys 35
14. Hall SK, Ooi EH, Payne SJ (2015) Cell death, perfusion and electrical parameters are critical in models of hepatic radiofrequency ablation. Int J Hypertherm 31
15. Haemmerich D, Chachati L, Wright AS, Mahvi DM, Lee FT, Webster J (2007) Hepatic radiofrequency ablation with internally cooled probes: Effect of coolant temperature on lesion size. IEEE Trans Bio-Med Eng 50
16. Takaki H, Nakatsuka A, Uraki J, Yamanaka T, Fujimori M, Hasegawa T, Arima K, Sugimura Y, Yamakado K (2013) Renal cell carcinoma: radiofrequency ablation with a multiple-electrode switching system—a phase II clinical study. Radiology 267
17. Zhang B, Moser M, Zhang E, Luo Y, Zhang H, Zhang W (2014) Study of the relationship between the target tissue necrosis volume and the target tissue size in liver tumours using two-compartment finite element RFA modelling. Int J Hypertherm 30
18. Shao YL, Leo HL, Chua KJ (2017) Studying the thermal performance of a bipolar radiofrequency ablation with an improved electrode matrix system: in vitro experiments and modelling. Appl Therm Eng 116
19. Sheu TW, Chou CW, Tsai SF, Liang PC (2005) Three-dimensional analysis for radiofrequency ablation of liver tumor with blood perfusion effect. Comp Methods Biomech Biomed Eng 8(4)
20. Tsushima Y, Funabasama S, Aoki J, Sanada S, Endo K (2004) Quantitative perfusion map of malignant liver tumors, created from dynamic computed tomography data 1. Acad Radiol 11(2)
21. Shao YL, Arjun B, Leo HL, Chua KJ (2017) A computational theoretical model for radiofrequency ablation of tumor with complex vascularization. Comput Biol Med 1:89

Lab-On-Chip Electrochemical Biosensor for Rheumatoid Arthritis

Rahul Kumar Ram, Nirmita Dutta, Jai Shukla, and Gorachand Dutta

Abstract With the current prevalence rate of 0.5–1%, rheumatoid arthritis (RA) is the most common type of autoimmune arthritis. The chances of occurrence of this chronic multifactorial disease are more in females than males, significantly increasing with age (Crowson et al. in Arthritis Rheum 63:633–639, 2011;Eriksson et al. in Arthritis Care Res (Hoboken) 65:870–878, 2013; Smolen JS, Aletaha D, Barton A, et al. (2018) Rheumatoid arthritis. Nature Reviews Disease Primers 2018 4:1 4:1–23. 10.1038/nrdp.2018.1;Vollenhoven in BMC Med 7, 2009;). Rheumatoid arthritis primarily affects the lining of the synovial joints and can cause progressive disability, premature death, and socioeconomic burdens. Currently, there is no cure for RA. Hence the treatment strategy aims to speed up diagnosis and rapidly achieve a low disease activity state (LDAS) (Guo Q, Wang Y, Xu D, et al. (2018) Rheumatoid arthritis: pathological mechanisms and modern pharmacologic therapies. Bone Research 2018 6:1 6:1–14. 10.1038/s41413-018–0016-9). Presently, even though different techniques like ELISA (enzyme-linked immunosorbent assay), radioimmunoassay, fluorescence-based analysis, surface-enhanced Raman scattering, and chemiluminescence-based analysis are prevalent as reliable diagnostic tools for rheumatoid arthritis biomarker detection, they have their own shortcomings. The immediate need for rapid, accurate, cheap, and early diagnosis have urged scientists to develop new advanced technologies, of which biosensors are one of the most reliable platforms. This review discusses the clinical as well as pathophysiological features of rheumatoid arthritis along with the application of different electrochemical nanobiosensors for its rapid and early diagnosis.

Keywords Rheumatoid Arthritis · Electrochemical nanobiosensors · Biomarker · Diagnosis · Point of care

---

R. K. Ram · N. Dutta · J. Shukla · G. Dutta (✉)
NanoBiosensors and Biodevices Lab, School of Medical Sciences and Technology, Indian Institute of Technology, Kharagpur, West Bengal, India
e-mail: g.dutta@smst.iitkgp.ac.in

K. Guha et al. (eds.), *MEMS and Microfluidics in Healthcare*, Lecture Notes in Electrical Engineering 989, https://doi.org/10.1007/978-981-19-8714-4_8

1 Introduction

Rheumatoid arthritis (RA) is a chronic inflammatory autoimmune disorder that causes cartilage, bones, and joints to deteriorate over time [1–3]. It affects three times as many women as it does men [4–7]. Inadequate treatment leads to the accumulation of irreparable joint damage, putting patients at risk for the rest of their lives [3]. They have discomfort and deformity in their joints, and in severe cases of sickness, they may require assistance from family members or nurses to move around and complete daily duties. RA is a multifactorial disease [8] that advances rapidly in the first few days after the onset [9]. Lack of markers, signs, or symptoms to specifically diagnose RA causes a considerable delay in treatment administration, resulting in permanent joint degeneration within a few days after beginning. Furthermore, the presently utilized diagnostic processes have limits with regard to point-of-care applications and use in remote places, where patients have limited access to advanced healthcare facilities. To overcome the limits of traditional detection methods, a variety of physical diagnostic instruments have emerged in recent years, the majority of which are based on biosensors because of the advantages they present, such as high sensitivity, high specificity, cost-effectiveness, and ease of use. Biosensors are devices with both organic and inorganic components that analyze and offer qualitative and quantitative information about the type of analyte present in the sample. The necessity of biosensors is in high demand in the field of diagnostics, and they will be incredibly useful in the early diagnosis of rheumatoid arthritis and other chronic inflammatory disorders.

This review presents a broad insight into the pathophysiology of rheumatoid arthritis and significant diagnostic biomarkers associated with it. Different electrochemical nanobiosensors were reviewed, including enzymatic, non-enzymatic, and label-free nanobiosensors for rheumatoid arthritis diagnosis using several surface modification strategies. Besides, the conventional diagnostic techniques for rheumatoid arthritis biomarker detection and their drawbacks are also discussed. Furthermore, the advancement of recent technologies in the field of biosensors that have simplified the instrumentation system, sped up the diagnosis time, made it more specific and sensitive, have also been discussed briefly.

2 Rheumatoid Arthritis Pathophysiology

“Arthr”- means joints, “-it is” refers to inflammation, and “rheumatoid” derives from rheumatism, which refers to musculoskeletal illness in general. Rheumatoid arthritis is a chronic systemic inflammatory autoimmune condition that primarily affects the joints, although it can also affect the skin, lungs, and heart.

The etiology of rheumatoid arthritis is not well known. But it is believed that the interaction between some susceptible genes of the immune proteins like HLA-DR1 and HLA-DR4 with some environmental factors like smoke from cigarettes or a pathogen like a bacterium that resides inside the gut can trigger the development of the disease [10]. These environmental influences can cause alterations of a few proteins, namely vimentin or Type II collagen, and also IgG antibodies.

One of the processes involved in the modifications of these self-antigens is citrullination. Citrullination is a process in which the amino acid arginine in a protein changes to citrulline. These modified proteins are thought to be a threat to the body by the immune cells and therefore they gather these self-antigens up and take those to the lymph nodes. There, the self-antigens are presented to the CD4+ T-helper cells to activate them. Because of the T-helper cells, the neighboring B-cells which present these self-antigens are activated too and begin to multiply and differentiate into plasma cells that produce the required autoantibodies. T-helper cells along with the antibodies enter the circulation to reach the joints. Cytokines, for example, interferon-γ (IFN-γ) and interleukin-17 (IL-17), are released by T-cells that recruit macrophages in the joint area. Inflammatory cytokines, such as tumor necrosis factor-alpha (TNF-α), IL-6, and IL-1, are also produced from the macrophages which, combined with T-cell cytokines, encourage synovial cells to multiply. This rise in the number of immune cells along with synovial cells results in the formation of a pannus, which is a bulging and thick synovial membrane consisting of granulation or scar tissue composed of fibroblasts, inflammatory cells, and myofibroblasts. The pannus is capable of dissolving bone as well as destroying cartilage, along with other soft tissues over time. Activated synovial cells also secrete proteases that can disintegrate proteins present in the articular cartilage. This causes the bones to present underneath to be stripped off of their protective cartilage and rub against one another [2, 11].

Additionally, the level of receptor activator of nuclear factor kappa-B ligand (RANKL), on the surface of T-cells, is increased by inflammatory cytokines. RANKL is required to bind to RANK, a protein found on the surface of osteoclasts, and this association is needed to break down bone. High amounts of T-cells are responsible for carrying out this attachment between RANKL and RANK, and therefore affect more degradation of bone.

Furthermore, during the course of the disease, immune complexes are formed when antibodies like anti-cyclic citrullinated peptide antibodies or rheumatoid factor (RF) bind to their targets, and they fill the space inside the synovial fluid. On doing so, they turn on the complement system, which promotes inflammation in the joints and causes injury [2, 11].

Eventually, chronic inflammation results in angiogenesis, allowing the entry of additional inflammatory cells. Several joints get inflamed and damaged when the disease starts to advance. However, the inflammatory cytokines don’t merely linger in the confined joint region. Instead, they infiltrate the bloodstream and cause extra-articular disorders by reaching many organ systems. They accelerate the degradation of protein in the skeletal muscle and produce collections of round-shaped lymphocytes and macrophages with a core area of necrosis, in various parts of the skin and other internal organs. Inflammation of blood vessels may result in various kinds of vasculitis, creating a risk for coronary artery heart disease resulting from atherogenesis [2, 11].

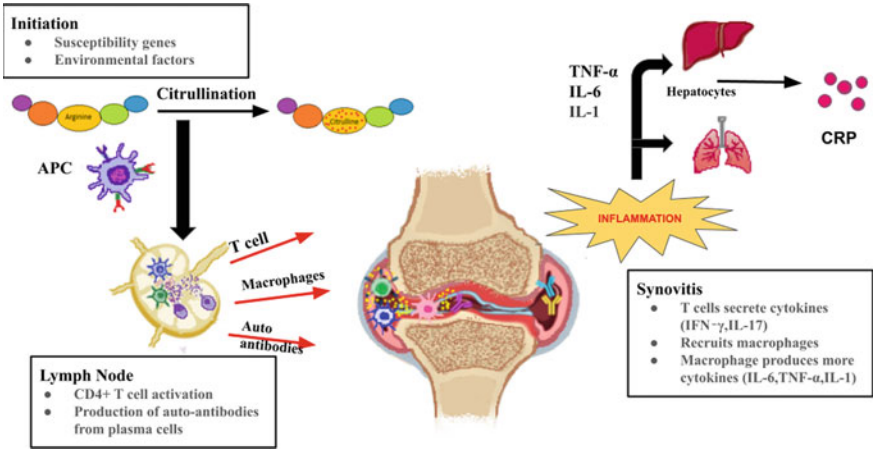

Fig. 1 Overview of Rheumatoid Arthritis pathophysiology

In reaction to inflammatory cytokines, the liver produces considerable amounts of CRP or ESR proteins, which are inflammatory markers, and a lot more hepcidin, a protein that causes anemia. In the meantime, the fibroblasts that are present in the lung interstitium get activated and multiply, producing a fibrotic tissue that hinders alveolar gas exchange. At later stages, inflammation of pleural cavities leading to pleural effusion can occur, which can further obstruct lung expansion (Fig. 1).

3 Diagnostic Biomarkers

The novel notion of "window of opportunity" demonstrates that early detection of RA is critical for preventing erosion and stopping the progression of radiologic abnormalities. In this context, the identification of biomarkers with diagnostic potential in the initial stages of the disease remains a hot topic [12, 13].

Rheumatoid factor (RF) and antibodies against cyclic citrullinated proteins (anti-CCP) are currently used in the ACR/EULAR 2010 criteria for RA diagnosis. Other diagnostic biomarkers that can aid in the early diagnosis of RA have also been discovered.

A reaction that is mediated by peptidyl arginine deiminase causes the citrullination of vimentin, which results in the generation of anti-vimentin antibodies. To increase the test's quality and to test the notion that additional alterations could affect vimentin antigenicity, a mutation where arginine residues were replaced with glycine, was performed, resulting in the creation of mutant citrullinated vimentin antibodies (anti-MCV) [14].

A 2010 meta-analysis indicated that there is no difference between anti-CCP and anti-MCV for the diagnosis of RA, based on 14 trials. Anti-MCV may thus be a line

2 test, performed in patients suspected of this autoimmune disease but negative for anti-CCP and RF [15].

Antibodies to carbamylated proteins (anti-CarP) were discovered in the blood of RA patients in 2011. Anti-CCP (generation II), RF (IgM), and anti-CarP were investigated in a study of 2086 patients with early RA. The anti-CarP test had a sensitivity of 44% and a specificity of 89%, compared to 54% sensitivity and 96% specificity for anti-CCP and RF who had 59 and 91%, respectively [16].

The 14-3-3 eta protein is a member of the 14-3-3 protein family. It is present intracellularly but becomes externalized during the inflammatory process, where it becomes citrullinated [17].

The specificity and sensitivity of 14-3-3 eta protein for rheumatoid arthritis were found to be 93 and 77%, respectively, in a trial of 619 individuals [18]. The presence of protein 14-3-3 eta, as well as RF and anti-CCP, enhances the diagnosis rate from 72% (RF + anti-CCP) to 78% (RF + anti-CCP + 14-3-3eta) in the preliminary stages of the disease.

C-reactive protein (CRP) is a sensitive marker of systemic inflammation that is elevated in people with RA. Therefore it could be another potential marker for increased RA risk [19]. It has been proposed to mediate part of the complement activation in RA. In a study, serial measurement in male and female blood donors showed an increase in CRP levels particularly within 2 years of RA diagnosis [19–21] (Fig. 2).

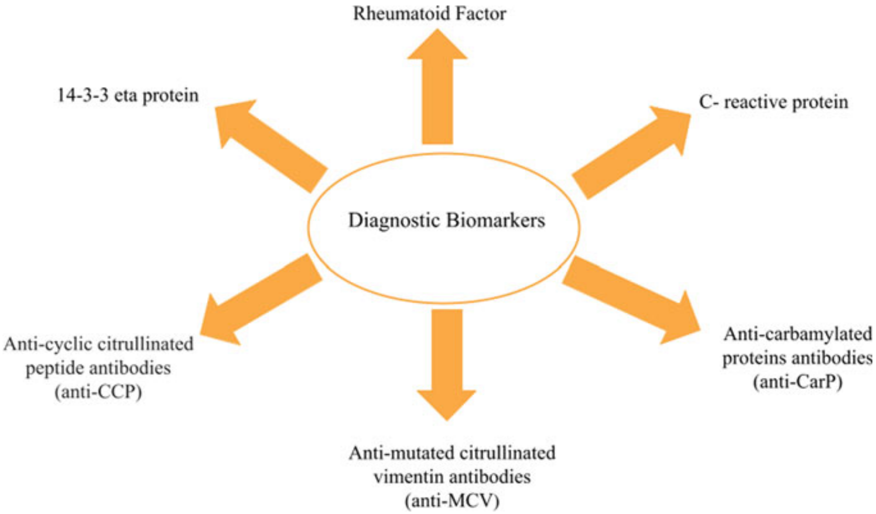

Fig. 2 Diagnostic biomarkers for Rheumatoid Arthritis

4 Conventional Diagnostic Techniques for Rheumatoid Arthritis Biomarker Detection and the Challenges Associated

4.1 Imaging

The standard method for determining the number of anatomic alterations in RA patients is plain radiography. At a later stage of the RA process, radiographic symptoms of RA such as joint space narrowing, erosions, and subluxation appear. Early signs of RA include synovitis, which is a good predictor of bone degradation [11]. In early-stage RA, soft-tissue edema and modest juxta-articular osteoporosis may be the first radiological findings of hand joints [22]. These abnormalities are characteristic of synovitis, although they cannot be seen in all patients on conventional radiographs, and they are not precise enough to be used in routine synovitis assessments [23]. Plain radiography is insensitive for detecting bone deterioration, which is a feature for the diagnosis of RA, due to the delayed onset of radiographic changes [24]. In the initial stages of RA, sonography is a reliable test that detects more erosions and in a greater population of patients than radiography [25]. The development of magnetic resonance imaging (MRI) imaging has increased the diagnostic capability for diagnosing RA sooner and distinguishing it from non-RA disorders. In one study, traditional radiography had a sensitivity of just 13% in detecting bone erosion, whereas MRI and ultrasonography had a sensitivity of 98 and 63%, respectively, in detecting bone erosion [26]. Furthermore, when it comes to detecting synovitis of the hands and wrists in RA, MRI is more sensitive than clinical examination. Sonography and MRI are more sensitive and appear promising, but they can only be performed in a few centers [12, 27].

4.2 ELISA-Based Detection

Antibodies against CCP (ACPA) had been detected using first-generation ELISAs, which had a specificity of about 85 percent for RA and a sensitivity of 65–70%. Synthetic peptides with a ring configuration due to the formation of disulfide bridge within molecules are used as antigens in second-generation ELISAs, with the citrulline epitope in a prominent position. The specificity of these CCPs has improved to 96–98% without affecting sensitivity [28].

Fibrinogen and fibrin are also considered as citrullinated antigens. Filaggrin and citrullinated fibrin exhibit a close cross-reactivity, according to studies using citrullinated peptide derivatives of the two proteins [29]. The identification of antibodies against citrullinated fibrinogen in patients with rheumatoid arthritis has been demonstrated to have high diagnostic specificity and sensitivity in several studies [30]. The sensitivity of ELISA for RA was around 75%, with a specificity of 98 %. For some time, an ELISA based on mutant citrullinated vimentin (MCV) has been commercially available for the detection of rheumatoid arthritis, with diagnostic sensitivity and specificity comparable to that for ACPA.

The challenges faced with ELISA-based methods are longer incubation time, a larger sample volume, and more intermediate sample preparation processes.

4.3 Chemiluminescence and Fluorescence-Based Detection

Sandwich detection techniques based on chemiluminescence have also been developed for the detection of CRP and RF. Optical biosensors based on fluorescence and chemiluminescence technologies have demonstrated their ability to detect biomarkers associated with RA with decreasing LODs, long dynamic ranges, and high specificity. They are becoming a significant technology that allows for the provision of a reliable, highly sensitive, reusable, and fully automated solution for the diagnosis of RA [31, 32].

Despite their advantages in the field of diagnosis, they have certainly added disadvantages too. These include high expenses, longer assay duration, less compatibility, and limitation to a certain application [33].

4.4 Radioimmunoassay-Based Detection (RIA)

CRP is a long-established acute phase reactant, whose serum levels can elevate following most types of tissue injury, infection, or inflammation. The serum CRP levels can be persistently elevated in chronic active inflammatory diseases such as RA [20]. Radioimmunoassay determines the concentration of an antigen in a sample based on the competitive binding between radiolabeled antigen and unlabeled antigen for its specific high-affinity antibody. Solid-phase RIAs had been developed for the quantification of CRP in body fluids such as human serum and cerebrospinal fluid. The findings showed that CRP exhibited the properties of an acute phase protein in infection or inflammation, and that it could be used to monitor the clinical course of the disease [34, 35].

There are numerous challenges while using RIA. The first is the unavoidable radiation hazard that comes along with it. This is why laboratories require a special license to handle radioactive materials used in this assay. Also, special storage arrangements for radioactive material are mandatory. Highly skilled and trained persons are required to run the assay, and proper radioactive waste disposal arrangements are necessary.

4.5 Surface-Enhanced Raman Scattering-Based Assay (SERS)

The use of SERS-based approaches in clinical diagnosis is gaining popularity. SERS-based immunoassays have already been used to quantify a number of biomarkers. A sandwich immunocomplex platform is a more frequently used detection approach using a surface-enhanced Raman scattering-based assay. Magnetic beads have recently been used to build a fast SERS-based test method. To aid in the early diagnosis of RA, a SERS-based immunoassay was built for the early diagnosis of RA in human serum. The assay was based on the formation of a sandwich-type immunocomplex involving CCP-conjugated magnetic beads, ACPA from the serum sample and anti-human IgG (or anti-ACPA)-conjugated SERS nanotags [36, 37].

This detection technique has the limitation of the requirement of a highly reliable system, and it is also an expensive one.

5 Importance of Early Diagnosis of Rheumatoid Arthritis

Early diagnosis of rheumatoid arthritis can have an impact on the disease's progression. If discovered during the first 2 years of disease development, it can help avoid articular damages and bone and joint degradation. When disease-modifying antirheumatic medicines (DMARDs) are prescribed early after a diagnosis, it is possible to achieve remission. The mechanism of action of DMARDs is unique, interfering with crucial pathways in the inflammatory cascade [38]. Early diagnosis of RA is critical for the beginning of treatment, otherwise, the disease may advance to severe forms, necessitating more vigorous therapy with potentially dangerous side effects [12].

6 Biosensor as a Device for "Rapid and Early Diagnosis"

According to IUPAC, the definition of biosensors encompasses "integrated receptor-transducer devices, which are able to provide selective quantitative or semi-quantitative analytical information using a biological recognition element" [39]. Biosensors are basically a type of an analytical cum sensing tool that combines organic i.e., the biological component, inorganic, i.e., the transducer, and the signal processing components to detect a specific analyte or molecule. A biosensor gives an amplified output and processed information about both the presence and the quantity of the analyte in the sample. It does so by integrating a recognition element which can be an antibody or aptamer, into a transducer which in turn generates the signal in the sensor [40, 41].

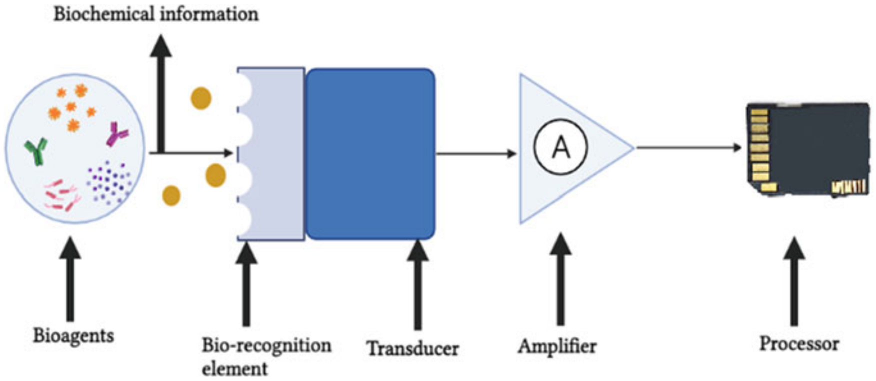

Fig. 3 Working principle of a biosensor

Recent advances in the fields of nanotechnology and microfluidics are opening up new avenues for the development of multidimensional biosensors, which is the next upcoming step to the world of biosensors [42, 43]. Some of these physicochemical-based biosensors have already been commercialized as rapid diagnostic tools; however, some are yet to be made available on the market as they are still in the stage of development. This is because some are based on the principle of CRISPR-based technology, isothermal amplification, microfluidics, microarray, and many others, which are quite modern technologies and would require further research but are predicted to be revolutionary technologies that would make the detection of analytes so much easier [44]. Various nanomaterials like silica-based nanoparticles, metallic nanoparticles, nanotubes, TiO_2, graphene, and ZnO show promising results in increasing sensitivity and selectivity even when there is an extremely low limit of detection (LOD), which suggests the better scope of enhancing biosensor efficiency in the future [45–47] (Fig. 3).

6.1 Working of a Biosensor

Biosensors are made up of three parts:

6.1.1 An Element for Recognition

It recognizes a specific analyte or multiple analytes present in the sample.

6.1.2 A Transducer

It is responsible for generating the electric signal. The receptor unit sends data to a transducer unit, which converts the data into an analytical form.

6.1.3 A Signal Processor

It analyzes the sample's chemical information. This information could have been derived from the system's physical properties or from any type of chemical reaction of a species present in our system [48].

Apart from this, the working electrode, a part of the transducing system, also plays a key role in the biosensor. The working electrode may be made up of diverse types of materials, from expensive metal electrodes, namely silver, gold, mercury, and platinum, to less expensive materials like carbon paste, screen-printed electrodes, and glassy carbon. The bioreceptor molecules can also be of several types like antibodies, enzymes, dyes, metal ions, and nucleic acids. These are made to attach to the electrodes for producing an efficient signal and for better detection of our desired biomarkers or analytes. The working electrode is applied with a potential with respect to the reference electrode (e.g., Ag/AgCl, saturated calomel, etc.), while the electrical circuit is completed by the counter electrode (e.g., platinum wire, carbon, etc.). When a negative potential is applied, the working electrode releases electrons into the solution, and the electroactive molecules get reduced. On the application of a positive potential, the electroactive molecules get oxidized on the working electrode [49].

Further analysis of the reaction is done through various electrochemical techniques like cyclic voltammetry, differential pulse voltammetry, chronoamperometry, square wave voltammetry, electrochemical impedance spectroscopy, etc.

6.2 Types of Biosensors

Based on the distinct types of systems for generating a signal, biosensors can be classified as:

6.2.1 Electrochemical Biosensors

An electrochemical sensor is a device that reads a sample's chemical information and converts it into an analytical signal. They involve the integration of a receptor and a transducer component in a single device that can be easily miniaturized and are mostly robust, sensitive, and can produce output signals rapidly. They have become a favorable platform for field analysis or point-of-care diagnosis [50].

6.2.2 Optical Biosensors

These are compact analytical devices that have an optical transducer integrated with a biorecognition element [51]. Its working principle is based on the fact that the intensity of adsorbed or emitted light can also change based on the physical quantity of the analyte that is provided. Molecular interaction between the analyte particles and substrate receptors will change the refractive index of the medium. The amount of analyte that is present in the sample can influence the amount of change in the RI, thus allowing us to measure the target analyte quantitatively. These biosensors are also used to determine association and dissociation kinetic interactions along with the affinity of the receptor [52].

6.2.3 Piezoelectric Biosensors

These are the biosensors that base their analysis on affinity-based interaction recording. The sensors in these devices are the piezoelectric platform or piezoelectric crystal, whose oscillations change when the desired analyte binds on its surface [53, 54]. The reduction in the oscillatory frequency is directly proportional to the amount of analyte in contact with the crystal, making it an efficient device for the detection of an analyte without the requirement of a label.

6.2.4 Thermometric Biosensors

These biosensors work on the principle of the amount of heat generation that arises in a medium due to a biochemical reaction. This generated heat change in the medium is then converted into an electric signal allowing quantitative measurement of the analyte [55].

7 Electrochemical Biosensors

Electrochemical sensors have recently grown to have enormous potential to be the best-suited platform for biomedical applications. Modifications with various nanomaterials have increased the efficiency of biosensors in identifying a wide range of biomolecules with high specificity and sensitivity. The biosensor consists of a transducer that helps in converting biological events into electrical signals. Amperometric and potentiometric parameters are two of the most commonly used parameters in electrochemical sensing. Potentiometric analysis converts the analytical data gathered after biorecognition processes into potential, whereas amperometric analysis is involved in monitoring the constant potential current generated from the reduction or oxidation of an electroactive species [49, 56]. As a result, they are widely used in diagnosing diseases to detect appropriate marker proteins, DNA sequences, or antibodies. Various electrode modifications have been made so that the surface compatibility of biological species is improved. Electrochemical sensors are made to be extremely sensitive and can be easily miniaturized and have a short analytical time. It is also necessary to have a simple instrumentation system in them [57].

An electrochemical sensor is a device that reads a sample's chemical information and converts it into an analytical signal. The sample information could have come from the system's physical properties or from reactions taking place in a species that is present in the system. The receptor unit sends data to the transducer unit, where it gets converted into an analytical form. In electrochemical biosensing for target analytes, a three-electrode system is typically used. Electrochemical sensing has been extensively studied in order to identify markers of various diseases such as cancer, hepatitis, acquired immunodeficiency syndrome, cardiac disease, and urinary infections [58–63]. Electrochemical biosensors that have been miniaturized and are implantable have now been regarded to be of immense importance for the detection of specific metabolites like triglycerides, cholesterol, blood glucose, and various other protein biomarkers without patient intervention or altering their physiological state like resting or sleeping or exercising [64–67].

7.1 Measurement Methods in Electrochemical Biosensors

7.1.1 Amperometry

This is a type of electrochemical technique that continuously measures the current generated from the oxidation or reduction in an electroactive species during a biochemical reaction [68, 69]. Clark oxygen electrodes may serve as the foundation for the most basic amperometric biosensors, in which the oxygen concentration available determines the amount of current that is produced. At a given potential, this is measured when the oxygen gets reduced at a platinum working electrode in comparison to an Ag/AgCl reference electrode. The current peak calculated over a linear potential range is proportional to the bulk concentration of the electroactive species, which is the analyte [39, 69, 70]. Since all protein analytes are not able to undergo redox reactions in electrochemical reactions, these devices rely heavily on mediated electrochemistry at the working electrode where the analyte undergoes electrochemical reaction [68, 69].

7.1.2 Potentiometry

This technique measures the charge potential accumulation at the working electrode in an electrochemical cell compared to the reference electrode when there is no or little current flowing between them [39, 69, 70]. Potentiometry, in other words, gives information about the electrochemical reaction and the ion activity in it [71].

The Nernst equation governs the relationship between potential and concentration in potentiometric measurements.

7.1.3 Conductometry

This technique assesses an analyte's (e.g., electrolyte solutions) or medium's (e.g., nanowires) ability to conduct electrical current between reference nodes or electrodes. Most conductometric devices are strongly associated with enzymes, where an enzymatic reaction between two electrodes changes the conductivity and the ionic strength of a solution. When the concentration of a charged species present in the solution changes, in a reaction involved with enzymes, that change can be measured using conductometric devices [72]. The variable ions in clinical samples, as well as the need to measure the change in small conductivity in a medium with high ionic strength, limits the application of conductometric tools [39, 73].

7.1.4 Voltammetry

Voltammetry is the study of currently produced by a system between two electrodes while applying controlled potential changes to the working electrode as a function of time. This is typically done with a potentiostat, which is capable of applying varying potentials to the working electrode with respect to a reference electrode while measuring the current that flows as a result of the electrode reaction. It is possible to use reducing and/or oxidizing potentials depending on the procedure. The current is referred to as a cathodic current when it undergoes a reduction. When there is an oxidation, the current is referred to as an anodic current. Voltammetry is a subset of ammeter technology [74].

7.1.5 Impedimetry [Electrochemical Impedance Spectroscopy (EIS)]

EIS can investigate particular processes that may affect the conductive or resistive properties in an electrochemical system. Hence, EIS is a helpful method in the examination of biosensor transduction substances, like polymer degradation studies. The current response (I) is measured by applying a small potential (U) that varies sinusoidally [75]. In other words, imaginary as well as real impedance components like resistance or reactance can be evaluated by EIS after their integration [73, 76, 77].

7.1.6 Field-Effect Transistor (FET)

The field-effect transistor is a form of transistor that controls the conductivity of a channel between two electrodes (source and drain) in a semiconducting material by using an electric field (at the gate). When the voltage from the drain to the source is lower than the voltage between the gate and the source, in linear mode, FET switches between conductive and non-conductive states similar to a variable resistor. However, FET acts as a source providing constant current and is frequently used to amplify the voltage, in saturation mode. The amount of constant current in this mode is determined by the voltage between the gate and the source. FET devices can work in low signals and also have high-impedance applications. This could be the reason they will be preferred more in the future when the field of electrochemical biosensors expands [69, 73].

Due to qualities such as easy instrumentation, requirement of low sample volume, easy miniaturization, portability, efficient analysis, high selectivity and sensitivity, electrochemical detection is anticipated to be used more in the future than other quantitative detection methods.

8 The Function of Nanostructures in a Sensor

Nanostructures involve nanoparticles, nanotubes, nanowires, nanopores, self-adhesive monolayers, and nanocomposites that share dimensions with biological molecules such as DNA and proteins [74]. By combining nanostructures and biomolecules, an interface composed of nanostructural and biological material with favorable characteristics and efficient performance is created [78, 79].

8.1 Biocompatibility of Nanoparticles

Nanomaterials have distinctive chemical, physical, and electronic properties by virtue of their small size, which distinguishes them from larger-scale materials. Nanoparticles tend to have a large surface area, as well as high surface energy, because of which they can adsorb biomolecules on their surface strongly. On the surface of the biosensor, this property goes a long way in biomolecule stabilization. When biomolecules are adsorbed onto the surface of nanomaterials, the biological potency of the biomolecules is retained, this is because of the biocompatibility property of nanoparticles [80]. Nanoparticles possess charge in them and hence they can electrically adsorb oppositely charged biomolecules [74].

8.2 Nanoparticles as Catalysts for Reactions

Compared to bulk materials, because of the high surface energy of nanoparticles, they tend to be more active. Nanoparticles, especially the ones that are metal in nature, are used as catalysts in most reactions since they have powerful catalytic effects. This is because they are efficient in surface activity [74, 81, 82].

8.3 Nanoparticles for Facilitating Better Electron Transfer

A critical step when constructing a biosensor would be when redox proteins, for example, enzymes, attach to the surface of the electrode. Redox proteins tend to have a protein shell on their active sites that don't conduct electricity. This makes it difficult for any type of electron exchange to take place from the active site of the protein to the surface of the electrode and vice versa. However, when nanoparticles, particularly metal nanoparticles come into the picture, the scenario gets altered, because these provide an effective way to transfer electrons between the electrode and the protein [74, 81, 82].

8.4 Labeling of Biomolecules With Nanoparticles

The use of nanoparticles to label biomolecules is becoming increasingly essential for the construction of electrochemical biosensors. Biomolecules that have been labeled with nanoparticles can retain their biological activity. The analyte binds with its receptor, and in doing so the analyte concentration can be determined with the help of nanoparticles electrochemically detecting the binding levels [74]. When biomolecules labeled with nanoparticles dissolve, the concentration of ions that get dissolved is estimated with the help of voltammetry stripping. This estimation allows us to calculate metal effects, that in turn facilitates the measurement of analytes in trace amounts [84].

8.5 Nanoparticles as Direct Reactants

Nanoparticles that have a high surface energy tend to be more active than bulk materials. They also tend to execute unique chemical properties [74]. This advantage can be exploited in several modern electrochemical devices.

9 Overview of Electrochemical Nanobiosensor for Rheumatoid Arthritis Detection

For the detection of biomarkers associated with rheumatoid arthritis, the application of electroanalytical-based immunodetection methods has played a significant role in the past few years. Among the discerning antigens for diagnosing rheumatoid arthritis like citrullinated fibrinogen, citrullinated α-enolase, citrullinated vimentin and CCPs have been the most commonly selected antigens for the capture and detection of ACPAs.

In the work shown by Selvam et al. [33], the use of a nanomatrix probe, namely, the polyaniline (PANI), nanowire-gold nanoparticle (AuNP), nanomatrix enhanced the capacity of loading of ACPA on the nanomatrix which further improved the sensitivity of the ACPA immunosensor. Also, an enhanced electrocatalytic performance was observed, which was attributed to the molybdenum disulfide-PANI matrix (MoS_2/PANI) modification on the screen-printed electrode (SPE). Additionally, the PANI base matrix made it easier to immobilize CCP on the electrode surface by forming stable amide bonds between CCP and PANI. Bovine serum albumin (BSA) was further used as a free-site blocking agent. ACPA detection was carried out in phosphate buffered saline and 10% human serum with an LOD of 0.16 and 0.22 IU/mL, respectively, and a logarithmic dynamic range of 0.25–1500.0 IU/mL using the BSA/CCP/PANI/MoS_2/SPE-based immunosensor. The acquired experimental results revealed increased LODs for a broad range of analytical dynamic ranges. Because CCP was immobilized, the ACPA immunosensor could discriminate ACPA from other human serum proteins and demonstrated high selectivity. With low storage stability, the ACPA immunosensor could be stored for three weeks at 4 °C. It was established that the total time required for ACPA detection, including CCP immobilization and the final addition of PANI-Au-ACPA, was less than 2 hours. The constructed sensor has many advantages as compared to other reports.

According to Pruijn et al. [85], ACPAs are the most specific serological indicators for diagnosing RA, and their presence in patient serum supports clinicians in making initial treatment decisions. According to research conducted recently, the ACPA response in RA patients is polyclonal and heterogeneous [86]. An artificial chimeric peptide synthesized using filaggrin and fibrin was adsorbed to the surface and used as a biorecognition element on an electrochemical transducer composed of multiwalled carbon nanotubes and polystyrene (MWCNT-PS) in the research presented by de Gracia Villa et al. [87]. According to the amperometric response, the transducer construction process demonstrated good repeatability and reproducibility from an electrochemical standpoint. The resulting immunosensor was first tested in rabbit sera that had been injected with the synthetic peptide before being used in human sera.

In a work conducted by Ma et al. [88], an electrochemical immunosensor without the use of any label was prepared for the capture of ACPA, where they used nitrogen-doped graphene modified with AuNPs, as an electrode substrate material and CCP as the biological recognition material. The negatively charged gold nanoparticles (AuNPs) electrostatically interacted with the positively charged amine groups of CCP to immobilize CCP on the electrode surface. CCP was used as a probe to capture ACPA on the surface through affinity binding. The combination of antigen and antibody created an insulating barrier that prevented the transfer of electrons. As a result, the square wave voltammetry response of the sensor decreased with the increase in ACPA concentration. The proposed ACPA immunosensor has a wider linear range of 0.125–2000 pg mL^{-1} and a lower LOD of 0.0125 pg mL^{-1} owing to the strong conductivity of nitrogen-doped graphene and the favorable biocompatibility of AuNPs. It can also be employed in human serum samples with satisfying test

Table 1 Comparison of electrochemical nanobiosensor for the detection of ACPA with other reported works

Detection assay	Linear range	Detection limit	References
Surface-enhanced Raman scattering	0–100 pgmL^{-1}	13 pgmL^{-1}	[35]
Electrogenerated chemiluminescence immunosensor	1–15,000 pgmL^{-1}	0.2 pgmL^{-1}	[86]
Electrochemical immunosensor (BSA/anti-CCP/AuNPs/N-G/GCE	0.125–2000 pgmL^{-1}	0.0125 pgmL^{-1}	[85]
Electrochemical square wave voltammetry	0.25–1500.0 IU/mL	0.16 IU/mL	[32]

results making it a worldwide applicable platform in the field of biological analysis (Table 1).

CRP is a well-known hallmark of inflammation. A conductive hybrid nanomaterial made of AuNPs and ionic liquid functionalized MoS_2 (IL-MoS_2) with a large specific surface area was developed and used to adsorb capture antibodies against CRP in a study conducted by Ma et al. [88]. Subsequently, using π- π stacking, 1,5-diaminonaphthalene (DN) was attached onto GO, where iridium nanoparticles (IrNPs) were loaded next. This hybrid has been described to mimic catalase and peroxidase activity, and therefore, was used as a tag to label secondary antibodies against CRP. The combination of a large surface area provided by AuNPs/IL-MoS_2 and enhanced electrocatalytic properties of IrNPs/GO-DN toward H_2O_2 reduction caused an extremely sensitive detection. The linear range of this immunosensor was 0.01 to 100 ng mL^{-1}, with an LOD of 3.3 pg mL^{-1}. Low cost, great sensitivity, low interference, and low LOD were all features of this sensor. This CRP immunosensor can be used to analyze real serum samples and produce excellent findings, demonstrating that the immunosensor has biomedical detection capacity.

In a study conducted by Tang et al. [91], one-pot biomimetic mineralization was used to create a novel nanoflower composed of BSA-anti-CRP antibodies-copper phosphate hybrid (BSA-Ab_2-$Cu_3(PO_4)_2$) as a signal amplifier for an electrochemical non-enzymatic immunoassay for the detection of CRP. Inorganic phosphate ions were first used for electrochemical transduction in this study, in the form of the nanoflower composite BSA-Ab_2-$Cu_3(PO_4)_2$, as mentioned by the authors. The composite had a 3D hierarchical porous nanoflower structure with a large specific surface area that could immobilize more antibodies and BSA for non-specific site blocking, significantly raising the sensitivity of the developed biosensor. $Cu_3(PO_4)_2$ hybrid nanoflowers can provide a large amount of PO_4^{3-} for molybdate reactions, resulting in molybdophosphate precipitates and the generation of redox currents for much more robust electrochemical signal readout without the requirement of the enzyme. The fabricated immunosensor performed well in terms of detection, with a linear range of 5 pg/mL^{-1} ng/mL and an LOD of 1.26 pg/mL. Furthermore, this technique has shown great feasibility for clinical sample analysis (Table 2).

Table 2 Comparison of electrochemical nanobiosensor for the detection of CRP with other reported works

Detection assay	Linear range	Detection limit	References
Label-free immunoassay	0.2–80 ngmL^{-1}	0.04 ngmL^{-1}	[89]
Fluorescent aptasensor	0.05–100 ng mL^{-1}	0.01 ngmL^{-1}	[90]
Molecularly imprinted	0.0625–1 mg L^{-1}	0.0625 mg L^{-1}	[91]
Surface plasmon resonance-based immunoassay	1.2–80 ng mL^{-1}	1.2 ngmL^{-1}	[92]
Enzyme-free electrochemical immunoassay	5 pg/mL–1 ng/mL	1.26 pgmL^{-1}	[88]
Electrochemical immunosensor	0.01–100 ng mL^{-1}	3.3 pgmL^{-1}	[87]

10 Real Sample Detection

Sample obtained from the patient, for instance, blood and urine have several surface fouling components and this component tends to foul the surface of the detector and show interference. Due to surface fouling noises are introduced in the signal given by the sensor and results into reduces sensitivity. To overcome this microfluidic and mems-based devices are incorporated for preprocessing of the sample.

Blood plasma separation: Blood tends to clot outside the human body resulting in surface blocking of the analytical surface of the sensor. To overcome this blood and plasma are separated using microfluidic or mems devices. This can be demonstrated by the application of capillary forces in a microfluidic channel. (https://link.springer.com/article/10.1007/s10404-017-1907-6). Furthermore with a single junction design by Tripathi et al. (https://www.nature.com/articles/srep26749) efficient blood plasma separation can be obtained by varying the flow rate at the bifurcation exploiting Zweifach-Fung bifurcation law at elevated dimensions. Another approach to separate blood from the plasma could be using the di-electrophoresis. Dielectrophoresis force is experienced by a polarized body when it is subjugated to the electric field. Using these techniques mems devices can be designed. One of the examples is C-MEMS devices developed by Pramanick et al. (https://iopscience.iop.org/article/10.1149/MA2018-01/13/1030). In this device, a microchannel was made between a carbon and ITO electrode. These two electrodes were in capacitive coupling and on the application of voltage varying at 1 MHz resulted in different velocities of blood and plasma. Similarly adding a hydrophobic patch in the microchannel results in the formation of a self-build filter that results in the separation of plasma from blood (https://www.mdpi.com/2306-5354/8/7/94).

Surface Fouling: Surface fouling affects the sensor surface greatly that causes the sensor to reduce its effectiveness and results in decreased sensitivity. To sensur

11 Conclusion

Early detection of rheumatoid arthritis can have an impact on the disease’s progression. Early diagnosis is critical for achieving recovery, where medications can have a much more significant effect on reducing disease severity. Also, more aggressive therapy could be avoided, hence lowering the risk of therapy-induced side effects [12].

Biosensors are considered to be immensely potential diagnostic and decision-making tools that could aid in improving health monitoring at both the individual and community levels. The incorporation of nanostructures in the fabrication of electrochemical sensors has resulted in the construction of a highly efficient platform that makes use of both nanotechnology and electrochemical-based techniques. Metal nanostructures increase the loading capacity of the bioreceptors in electrochemical nanobiosensors, enhancing the sensor’s sensitivity. The electrocatalytic effect of metal nanoparticles, on the other hand, aids in quicker electron transfer. Rapid transfer of electrons minimizes response time and increases the sensor’s productivity. As a result, detections at the attomolar levels are feasible. Nanotechnology and microfluidics tools and advancements can contribute to the creation of numerous biosensors that will provide us with the advantage of rapid diagnosis with extremely low LOD and more precision at the point-of-care, letting us take a multidimensional approach in solving various health-related issues [42, 43].

12 Futuristic Strategy for the Detection of Rheumatoid Arthritis

The first electrochemical dual biosensor was recently developed for the simultaneous determination of RF and ACPA based on sandwich-type bioassays for the target compounds captured between Fc (IgG) or biotin-CCP attached to carboxylated MBs or neutravidin-functionalized MBs, respectively, and HRP-labeled detector antibodies [96]. Since there have been no other such demonstrations of electrochemical biosensors based on a multiplex system for the detection of rheumatoid arthritis, therefore there is a scope for building a novel one. The biosensor can use the benefit of the simultaneous diagnosis of multiple biomarkers to increase the specificity and sensitivity and therefore increase the diagnostic rate to a higher level. Also, the use of nanoparticles will open many advantageous possibilities that will make the biosensor more efficient.

While fabricating these sensor platforms, the real emphasis is given to the rapid and cost-effective point-of-care testing (POCT) of rheumatoid arthritis markers with real samples. Therefore, there has been a high demand to upgrade such systems for their implementation in bench-to-bedside applications. Multiple strategies which have been evolved in the area of biosensor development research can be incorporated to enhance and modify the parameters of these biosensors by either changing the electrochemical properties, the surface properties or the biorecognition element of the sensor [97].

Dutta and Lillehoj developed a novel label-free and wash-free electrochemical biosensor for the one-step detection of *Pf*HRP2 biomarker in a whole blood sample without any pretreatment, using a signal amplification step based on electrochemical-chemical (EC) redox cycling [98]. This innovative sensing platform has not only simplified the protocol for detection but also decreased the detection time to 5 mins. A similar strategy can be applied while fabricating the nanobiosensors for the detection of rheumatoid arthritis biomarkers and thus can be implemented in rapid and user-friendly point-of-care testing.

Acknowledgements Authors gratefully acknowledge the Start-Up Research Grant (SRG) funded by the Science & Engineering Research Board (SERB) (SRG/2020/000712), Department of Science and Technology (DST) (Government of India, Ministry of Science and Technology), (Technology Development and Transfer, TDP/BDTD/12/2021/General), Indo-German Science & Technology Centre (IGSTC) (IGSTC/Call 2019/NOMIS/22/2020-21/164), and Institute Scheme for Innovative Research and Development (ISIRD) (IIT/SRIC/ISIRD/2019–2020/17), Indian Institute of Technology Kharagpur (IIT Kharagpur), India for the financial support.

References

1. López-Mejías R, Carmona FD, Genre F et al (2019) Identification of a 3’-untranslated genetic variant of RARB associated with carotid intima-media thickness in rheumatoid arthritis: a genome-wide association study. Arthrit Rheumatol 71:351–360. https://doi.org/10.1002/ART.40734
2. Ostrowska M, Maśliński W, Prochorec-Sobieszek M et al (2018) Cartilage and bone damage in rheumatoid arthritis. Reumatologia 56:111–120. https://doi.org/10.5114/REUM.2018.75523
3. Smolen JS, Aletaha D, Barton A, et al (2018) Rheumatoid arthritis. Nat Rev Dis Prim 4(1):1–23. https://doi.org/10.1038/nrdp.2018.1
4. Crowson CS, Matteson EL, Myasoedova E et al (2011) The lifetime risk of adult-onset rheumatoid arthritis and other inflammatory autoimmune rheumatic diseases. Arthritis Rheum 63:633–639. https://doi.org/10.1002/ART.30155
5. Eriksson JK, Neovius M, Ernestam S et al (2013) Incidence of rheumatoid arthritis in Sweden: a nationwide population-based assessment of incidence, its determinants, and treatment penetration. Arthritis Care Res (Hoboken) 65:870–878. https://doi.org/10.1002/ACR.21900
6. Kumar B, Das MP, Misra AK (2017) A cross-sectional study of association of Rheumatoid arthritis with sero-positivity and anaemia in a tertiary care teaching hospital. J Med Res 3:280–283
7. van Vollenhoven RF (2009) Sex differences in rheumatoid arthritis: more than meets the eye. BMC Med 7. https://doi.org/10.1186/1741-7015-7-12
8. Jirholt J, Lindqvist AKB, Holmdahl R (2001) The genetics of rheumatoid arthritis and the need for animal models to find and understand the underlying genes. Arthritis Res 3:87–97. https://doi.org/10.1186/AR145
9. Barhamain AS, Magliah RF, Shaheen MH et al (2017) The journey of rheumatoid arthritis patients: a review of reported lag times from the onset of symptoms. Open Access Rheumatol 9:139. https://doi.org/10.2147/OARRR.S138830

10. Sugiyama D, Nishimura K, Tamaki K et al (2010) Impact of smoking as a risk factor for developing rheumatoid arthritis: a meta-analysis of observational studies. Ann Rheum Dis 69:70–81. https://doi.org/10.1136/ARD.2008.096487
11. Guo Q, Wang Y, Xu D, et al (2018) Rheumatoid arthritis: pathological mechanisms and modern pharmacologic therapies. Bone Res 6(1):1–14. https://doi.org/10.1038/s41413-018-0016-9
12. Heidari B (2011) Rheumatoid Arthritis: early diagnosis and treatment outcomes. Caspian J Intern Med 2:161
13. Schneider M, Krüger K (2013) Rheumatoid Arthritis—early diagnosis and disease management. Dtsch Arztebl Int 110:477. https://doi.org/10.3238/ARZTEBL.2013.0477
14. Gavrilă BI, Ciofu C, Stoica V (2016) Biomarkers in Rheumatoid Arthritis, what is new? J Med Life 9:144
15. Luime JJ, Colin EM, Hazes JMW, Lubberts E (2010) Does anti-mutated citrullinated vimentin have additional value as a serological marker in the diagnostic and prognostic investigation of patients with rheumatoid arthritis? A systematic review. Ann Rheum Dis 69:337–344. https://doi.org/10.1136/ARD.2008.103283
16. Shi J, van Steenbergen HW, van Nies JAB, et al (2015) The specificity of anti-carbamylated protein antibodies for rheumatoid arthritis in a setting of early arthritis. Arthritis Res Ther 17. https://doi.org/10.1186/S13075-015-0860-6
17. Maksymowych WP, Marotta A (2014) 14-3-3η: a novel biomarker platform for rheumatoid arthritis. Clin Exp Rheumatol 32:S35–S39
18. Maksymowych WP, Naides SJ, Bykerk V et al (2014) Serum 14–3-3η is a novel marker that complements current serological measurements to enhance detection of patients with rheumatoid arthritis. J Rheumatol 41:2104–2113. https://doi.org/10.3899/JRHEUM.131446
19. Tishler M, Caspi D, Yaron M (1985) C-reactive protein levels in patients with rheumatoid arthritis: the impact of therapy. Clin Rheumatol 4:321–324. https://doi.org/10.1007/BF02031616
20. Nielen MMJ, van Schaardenburg D, Reesink HW et al (2004) Increased levels of C-reactive protein in serum from blood donors before the onset of rheumatoid arthritis. Arthritis Rheum 50:2423–2427. https://doi.org/10.1002/ART.20431
21. Otterness IG (1994) The value of C-reactive protein measurement in rheumatoid arthritis. Semin Arthritis Rheum 24:91–104. https://doi.org/10.1016/S0049-0172(05)80003-4
22. Grassi W, de Angelis R, Lamanna G, Cervini C (1998) The clinical features of rheumatoid arthritis. Eur J Radiol 27(Suppl 1). https://doi.org/10.1016/S0720-048X(98)00038-2
23. Farrant JM, O'Connor PJ, Grainger AJ (2007) Advanced imaging in rheumatoid arthritis. Part 1: synovitis. Skeletal Radiol 36:269–279. https://doi.org/10.1007/S00256-006-0219-9
24. Devauchelle-Pensec V, Saraux A, Alapetite S et al (2002) Diagnostic value of radiographs of the hands and feet in early rheumatoid arthritis. Joint Bone Spine 69:434–441. https://doi.org/10.1016/S1297-319X(02)00427-X
25. Graudal N (2004) The natural history and prognosis of rheumatoid arthritis: association of radiographic outcome with process variables, joint motion and immune proteins. Scand J Rheumatol Suppl 118:1–37. https://doi.org/10.1080/03009740310004847
26. Rahmani M, Chegini H, Najafizadeh SR et al (2010) Detection of bone erosion in early rheumatoid arthritis: ultrasonography and conventional radiography versus non-contrast magnetic resonance imaging. Clin Rheumatol 29:883–891. https://doi.org/10.1007/S10067-010-1423-5
27. Goupille P, Roulot B, Akoka S et al (2001) Magnetic resonance imaging: a valuable method for the detection of synovial inflammation in rheumatoid arthritis. J Rheumatol 28:35–40
28. van Venrooij WJ, Zendman AJW, Pruijn GJM (2006) Autoantibodies to citrullinated antigens in (early) rheumatoid arthritis. Autoimmun Rev 6:37–41. https://doi.org/10.1016/J.AUTREV.2006.03.008
29. Sebbag M, Moinard N, Auger I et al (2006) Epitopes of human fibrin recognized by the rheumatoid arthritis-specific autoantibodies to citrullinated proteins. Eur J Immunol 36:2250–2263. https://doi.org/10.1002/EJI.200535790
30. vander Cruyssen B, Cantaert T, Nogueira L, et al (2006) Diagnostic value of anti-human citrullinated fibrinogen ELISA and comparison with four other anti-citrullinated protein assays. Arthritis Res Ther 8:R122. https://doi.org/10.1186/AR2011

31. Cinquanta L, Fontana DE, Bizzaro N (2017) Chemiluminescent immunoassay technology: what does it change in autoantibody detection? Autoimmun Highlights 8:1–8. https://doi.org/10.1007/S13317-017-0097-2/FIGURES/1
32. Imas JJ, Zamarreño CR, Zubiate P et al (2020) Optical biosensors for the detection of rheumatoid arthritis (RA) biomarkers: a comprehensive review. Sensors (Basel) 20:1–51. https://doi.org/10.3390/S20216289
33. Selvam SP, Chinnadayyala SR, Cho S (2021) Electrochemical nanobiosensor for early detection of rheumatoid arthritis biomarker: anti- cyclic citrullinated peptide antibodies based on polyaniline (PANI)/MoS2-modified screen-printed electrode with PANI-Au nanomatrix-based signal amplification. Sens Actuat B Chem 333. https://doi.org/10.1016/J.SNB.2021.129570
34. Chen XH (1991) Detection of C-reactive protein in patients with epidemic cerebrospinal meningitis by solid phase radioimmunoassay. Zhonghua Liu Xing Bing Xue Za Zhi 12:44–46
35. Goldsmith SJ (1975) Radioimmunoassay: review of basic principles. Semin Nucl Med 5:125–152. https://doi.org/10.1016/S0001-2998(75)80028-6
36. Chon H, Lee S, Wang R et al (2014) SERS-based immunoassay of anti-cyclic citrullinated peptide for early diagnosis of rheumatoid arthritis. RSC Adv 4:32924–32927. https://doi.org/10.1039/C4RA05149A
37. Chon H, Wang R, Lee S, et al (2015) Clinical validation of surface-enhanced Raman scattering-based immunoassays in the early diagnosis of rheumatoid arthritis. Anal Bioanal Chem 407. https://doi.org/10.1007/S00216-015-9020-8
38. Benjamin O, Bansal P, Goyal A, Lappin SL (2021) Disease modifying anti-rheumatic drugs (DMARD). StatPearls
39. Thévenot DR, Toth K, Durst RA, Wilson GS (2001) Electrochemical biosensors: recommended definitions and classification. Biosens Bioelectron 16:121–131. https://doi.org/10.1016/S0956-5663(01)00115-4
40. Bhalla N, Jolly P, Formisano N, Estrela P (2016) Introduction to biosensors. Essays Biochem 60:1–8. https://doi.org/10.1042/EBC20150001
41. Mobed A, Sepehri Shafigh E (2021) Biosensors promising bio-device for pandemic screening "COVID-19". Microchem J 164. https://doi.org/10.1016/J.MICROC.2021.106094
42. Dutta G, Regoutz A, Moschou D (2020) Enzyme-assisted glucose quantification for a painless Lab-on-PCB patch implementation. Biosens Bioelectron 167. https://doi.org/10.1016/J.BIOS.2020.112484
43. Park S, Kim J, Ock H et al (2015) Sensitive electrochemical detection of vaccinia virus in a solution containing a high concentration of L-ascorbic acid. Analyst 140:5481–5487. https://doi.org/10.1039/C5AN01086A
44. Nguyen T, Bang DD, Wolff A (2020) 2019 novel Coronavirus Disease (COVID-19): Paving the road for rapid detection and point-of-care diagnostics. Micromachines (Basel) 11:1–7. https://doi.org/10.3390/MI11030306
45. Chen X, Wang Y, Zhou J et al (2008) Electrochemical impedance immunosensor based on three-dimensionally ordered macroporous gold film. Anal Chem 80:2133–2140. https://doi.org/10.1021/AC7021376
46. Kailashiya J, Singh N, Singh SK et al (2015) Graphene oxide-based biosensor for detection of platelet-derived microparticles: a potential tool for thrombus risk identification. Biosens Bioelectron 65:274–280. https://doi.org/10.1016/J.BIOS.2014.10.056
47. Pividori MI, Alegret S (2010) Micro and nanoparticles in biosensing systems for food safety and environmental monitoring. An example of converging technologies. Microchim Acta 170:227–242. https://doi.org/10.1007/S00604-010-0347-8
48. Hussain KK, Malavia D, Johnson EM et al (2020) Biosensors and diagnostics for fungal detection. J Fungi (Basel) 6:1–26. https://doi.org/10.3390/JOF6040349
49. Singh P, Pandey SK, Singh J et al (2016) Biomedical perspective of electrochemical nanobiosensor. Nano-Micro Lett 8:193–203. https://doi.org/10.1007/S40820-015-0077-X/TABLES/2
50. Cosnier S (2014) Electrochemical biosensors. Electrochem Biosens 1–398. https://doi.org/10.1081/e-eafe2-120051918

51. Damborský P, Švitel J, Katrlík J (2016) Optical biosensors. Essays Biochem 60:91–100. https://doi.org/10.1042/EBC20150010
52. Chen C, Wang J (2020) Optical biosensors: an exhaustive and comprehensive review. Analyst 145:1605–1628. https://doi.org/10.1039/C9AN01998G
53. Chorsi MT, Curry EJ, Chorsi HT et al (2019) Piezoelectric biomaterials for sensors and actuators. Adv Mater 31:1802084. https://doi.org/10.1002/ADMA.201802084
54. Pohanka M (2018) Overview of piezoelectric biosensors, immunosensors and DNA sensors and their applications. Materials 11. https://doi.org/10.3390/MA11030448
55. Kopparthy VL, Tangutooru SM, Guilbeau EJ (2015) Label free detection of L-glutamate using microfluidic based thermal biosensor. Bioengineering 2:2. https://doi.org/10.3390/BIOENGINEERING2010002
56. Wang J (1999) Sol–gel materials for electrochemical biosensors. Anal Chim Acta 399:21–27. https://doi.org/10.1016/S0003-2670(99)00572-3
57. Kimmel DW, Leblanc G, Meschievitz ME, Cliffel DE (2012) Electrochemical sensors and biosensors. Anal Chem 84:685–707. https://doi.org/10.1021/AC202878Q
58. Babuin L, Vasile VC, Rio Perez JA et al (2008) Elevated cardiac troponin is an independent risk factor for short- and long-term mortality in medical intensive care unit patients. Crit Care Med 36:759–765. https://doi.org/10.1097/CCM.0B013E318164E2E4
59. Kumar A, Mazinder Boruah B, Liang XJ (2011) Gold nanoparticles: promising nanomaterials for the diagnosis of cancer and HIV/AIDS. J Nanomater https://doi.org/10.1155/2011/202187
60. Pan Y, Sonn GA, Sin MLY et al (2010) Electrochemical immunosensor detection of urinary lactoferrin in clinical samples for urinary tract infection diagnosis. Biosens Bioelectron 26:649–654. https://doi.org/10.1016/J.BIOS.2010.07.002
61. Tang D, Yuan R, Chai Y et al (2005) New amperometric and potentiometric immunosensors based on gold nanoparticles/tris(2,2'-bipyridyl)cobalt(III) multilayer films for hepatitis B surface antigen determinations. Biosens Bioelectron 21:539–548. https://doi.org/10.1016/J.BIOS.2004.11.024
62. Wang J (2006) Electrochemical biosensors: towards point-of-care cancer diagnostics. Biosens Bioelectron 21:1887–1892. https://doi.org/10.1016/J.BIOS.2005.10.027
63. Zani A, Laschi S, Mascini M, Marrazza G (2011) A new electrochemical multiplexed assay for PSA cancer marker detection. Electroanalysis 23:91–99. https://doi.org/10.1002/ELAN.201000486
64. Cai X, Gao X, Wang L, et al (2013) A layer-by-layer assembled and carbon nanotubes/gold nanoparticles-based bienzyme biosensor for cholesterol detection. Sens Actuat B Chem Complete 575–583. https://doi.org/10.1016/J.SNB.2013.02.050
65. Luo X, Davis JJ (2013) Electrical biosensors and the label free detection of protein disease biomarkers. Chem Soc Rev 42:5944–5962. https://doi.org/10.1039/C3CS60077G
66. Tang J, Wang Y, Li J et al (2014) Sensitive enzymatic glucose detection by TiO2 nanowire photoelectrochemical biosensors. J Mater Chem A 2:6153–6157. https://doi.org/10.1039/C3TA14173J
67. Veeramani MS, Shyam KP, Ratchagar NP et al (2014) Miniaturised silicon biosensors for the detection of triglyceride in blood serum. Anal Methods 6:1728–1735. https://doi.org/10.1039/C3AY42274G
68. Eggins B (2007) Chemical sensors and biosensors. Chem Sens Biosens 1–273. https://doi.org/10.1002/9780470511305
69. Luppa PB, Sokoll LJ, Chan DW (2001) Immunosensors–principles and applications to clinical chemistry. Clin Chim Acta 314:1–26. https://doi.org/10.1016/S0009-8981(01)00629-5
70. Chaubey A, Malhotra BD (2002) Mediated biosensors. Biosens Bioelectron 17:441–456. https://doi.org/10.1016/S0956-5663(01)00313-X
71. Bakker E, Pretsch E (2005) Potentiometric sensors for trace-level analysis. Trends Analyt Chem 24:199. https://doi.org/10.1016/J.TRAC.2005.01.003
72. D'Orazio P (2003) Biosensors in clinical chemistry. Clin Chim Acta 334:41–69. https://doi.org/10.1016/S0009-8981(03)00241-9

73. Grieshaber D, MacKenzie R, Vörös J, Reimhult E (2008) Electrochemical biosensors–sensor principles and architectures. Sensors (Basel) 8:1400. https://doi.org/10.3390/S80314000
74. Huang X, Zhu Y, Kianfar E (2021) Nano biosensors: properties, applications and electrochemical techniques. J Market Res 12:1649–1672. https://doi.org/10.1016/J.JMRT.2021.03.048
75. Katz E, Willner I (2003) Probing biomolecular interactions at conductive and semiconductive surfaces by impedance spectroscopy: routes to impedimetric immunosensors, DNA-sensors, and enzyme biosensors. Electroanalysis 15:913–947. https://doi.org/10.1002/ELAN.200390114
76. Patolsky F, Zayats M, Katz E, Willner I (1999) Precipitation of an insoluble product on enzyme monolayer electrodes for biosensor applications: characterization by Faradaic impedance spectroscopy, cyclic voltammetry, and microgravimetric quartz crystal microbalance analyses. Anal Chem 71:3171–3180. https://doi.org/10.1021/AC9901541
77. Tlili A, Abdelghani A, Ameur S, Jaffrezic-Renault N (2006) Impedance spectroscopy and affinity measurement of specific antibody–antigen interaction. Mater Sci Eng C 2–3:546–550. https://doi.org/10.1016/J.MSEC.2005.10.007
78. Wang H, Li S, Si Y et al (2014) Platinum nanocatalysts loaded on graphene oxide-dispersed carbon nanotubes with greatly enhanced peroxidase-like catalysis and electrocatalysis activities. Nanoscale 6:8107–8116. https://doi.org/10.1039/C4NR00983E
79. Yang GH, Zhou YH, Wu JJ et al (2013) Microwave-assisted synthesis of nitrogen and boron co-doped graphene and its application for enhanced electrochemical detection of hydrogen peroxide. RSC Adv 3:22597–22604. https://doi.org/10.1039/C3RA44284E
80. Auría-Soro C, Nesma T, Juanes-Velasco P, et al (2019) Interactions of nanoparticles and biosystems: microenvironment of nanoparticles and biomolecules in nanomedicine. Nanomaterials 9. https://doi.org/10.3390/NANO9101365
81. Miao Y, Ouyang L, Zhou S et al (2014) Electrocatalysis and electroanalysis of nickel, its oxides, hydroxides and oxyhydroxides toward small molecules. Biosens Bioelectron 53:428–439. https://doi.org/10.1016/J.BIOS.2013.10.008
82. Wang X, Wang J, Sun X et al (2018) Hierarchical coral-like NiMOS nanohybrids as highly efficient bifunctional electrocatalysts for overall urea electrolysis. Nano Res 11:988–996. https://doi.org/10.1007/S12274-017-1711-3
83. Chen X, Wu G, Cai Z, et al (2013) Advances in enzyme-free electrochemical sensors for hydrogen peroxide, glucose, and uric acid. Microchimica Acta 181(7):689–705. https://doi.org/10.1007/S00604-013-1098-0
84. Rajapaksha RDAA, Hashim U, Gopinath SCB, et al (2021) Nanoparticles in electrochemical bioanalytical analysis. Nanopart Analyt Med Dev 83–112. https://doi.org/10.1016/B978-0-12-821163-2.00006-6
85. Pruijn GJM, Wiik A, van Venrooij WJ (2010) The use of citrullinated peptides and proteins for the diagnosis of rheumatoid arthritis. Arthritis Res Ther 12:1–8. https://doi.org/10.1186/AR2903/TABLES/3
86. Verpoort KN, Jol-Van Der Zijde CM, Papendrecht-Van Der Voort EAM et al (2006) Isotype distribution of anti-cyclic citrullinated peptide antibodies in undifferentiated arthritis and rheumatoid arthritis reflects an ongoing immune response. Arthritis Rheum 54:3799–3808. https://doi.org/10.1002/ART.22279
87. de Gracia VM, Jiménez-Jorquera C, Haro I et al (2011) Carbon nanotube composite peptide-based biosensors as putative diagnostic tools for rheumatoid arthritis. Biosens Bioelectron 27:113–118. https://doi.org/10.1016/J.BIOS.2011.06.026
88. Ma J, Li D, Sun B et al (2022) Label-free electrochemical immunosensor for sensitive detection of Rheumatoid Arthritis biomarker Anti-CCP-ab. Electroanalysis 34:761–771. https://doi.org/10.1002/ELAN.202100045
89. Zhao Y, Liu Y, Li X et al (2018) Label-free ECL immunosensor for the early diagnosis of rheumatoid arthritis based on asymmetric heterogeneous polyaniline-gold nanomaterial. Sens Actuat B Chem 257:354–361. https://doi.org/10.1016/J.SNB.2017.10.184

90. Ma Y, Yang J, Yang T et al (2020) Electrochemical detection of C-reactive protein using functionalized iridium nanoparticles/graphene oxide as a tag. RSC Adv 10:9723–9729. https://doi.org/10.1039/C9RA10386D
91. Tang Q, Zhang L, Tan X et al (2019) Bioinspired synthesis of organic–inorganic hybrid nanoflowers for robust enzyme-free electrochemical immunoassay. Biosens Bioelectron 133:94–99. https://doi.org/10.1016/J.BIOS.2019.03.032
92. Zhang X, Hu R, Zhang K et al (2016) An ultrasensitive label-free immunoassay for C-reactive protein detection in human serum based on electron transfer. Anal Methods 8:6202–6207. https://doi.org/10.1039/C6AY01464J
93. Chen Q, Liu Z, Luo D et al (2019) Ultrasensitive fluorescent aptasensor for CRP detection based on the RNase H assisted DNA recycling signal amplification strategy. RSC Adv 9:11960–11967. https://doi.org/10.1039/C9RA01352K
94. Zubiate P, Zamarreño CR, Sánchez P et al (2017) High sensitive and selective C-reactive protein detection by means of lossy mode resonance based optical fiber devices. Biosens Bioelectron 93:176–181. https://doi.org/10.1016/J.BIOS.2016.09.020
95. Vashist SK, Schneider EM, Luong JHT (2015) Surface plasmon resonance-based immunoassay for human C-reactive protein. Analyst 140:4445–4452. https://doi.org/10.1039/C5AN00690B
96. Guerrero S, Sánchez-Tirado E, Martínez-García G et al (2020) Electrochemical biosensor for the simultaneous determination of rheumatoid factor and anti-cyclic citrullinated peptide antibodies in human serum. Analyst 145:4680–4687. https://doi.org/10.1039/D0AN00481B
97. Singh B, Datta B, Ashish A, Dutta G (2021) A comprehensive review on current COVID-19 detection methods: from lab care to point of care diagnosis. Sens Int 2:100119. https://doi.org/10.1016/J.SINTL.2021.100119
98. Dutta G, Lillehoj PB (2018) Wash-free, label-free immunoassay for rapid electrochemical detection of PfHRP2 in whole blood samples. Sci Rep 8. https://doi.org/10.1038/S41598-018-35471-8

Transdermal Injection with Microneedle Devices in Healthcare Sector: Materials, Challenging Fabrication Methodologies, and its Limitations

A. Gowthami, B. S. Sreeja, and S. Radha

Abstract In recent years, the management of many health disorders takes place at home either by community nurses or by patients independently. However, the medication management inside domestic healthcare situations may be difficult, mainly while therapy is administered via injection. The large percentage of transcutaneous injuries during needle handling has become a hazard in healthcare settings. The proper incineration of needle waste disposal after treatment is a major concern in the medical field. The cost-effective, biocompatible, portable, microfluidic devices are a promising technology for monitoring and diagnosing health conditions. One of the microfluidic device systems is a Microneedle (MN), which is an alternative method of an oral and conventional hypodermic needle for biomedical applications. The development of microminiaturized needles with scale dimensions in the order of 1 mm or less with a biocompatible material is a challenging aspect of today's scenario. Microneedle-based devices are customized for a wide range of applications, including disease detection, drug delivery mechanisms, and metabolic pathway monitoring. The different types of microneedles are developed based on the applications and their fabrication methodologies are selected based on the material and geometrical structure. Numerous fabrication processes of these microneedle devices from small-scale to large-scale production, with regulatory approval for commercialization, is a challenging perspective. This chapter mainly focuses on the various types of microneedles and the selection of materials for the microneedle type, the benefits of microneedle technology in various health sectors, along with a critical assessment of its possible impact on healthcare being investigated and discussed. It also elaborates on the different challenging microfabrication technologies and their limitations for various types of microneedle devices.

Keywords Transdermal delivery · Microneedles · Fabrication · Applications · Types

---

A. Gowthami (✉) · B. S. Sreeja · S. Radha
Materials and MEMS Laboratory, Department of Electronics and Communication Engineering,
Sri Sivasubramaniya Nadar College of Engineering, Chennai, Tamilnadu 603110, India
e-mail: gowthamia@ssn.edu.in

K. Guha et al. (eds.), *MEMS and Microfluidics in Healthcare*, Lecture Notes
in Electrical Engineering 989, https://doi.org/10.1007/978-981-19-8714-4_9

1 Introduction

An effective pharmaceutical depends not only on its active component but also on the delivery mechanism to the body. Therefore, it is important to consider an appropriate delivery method based on the drug characteristics. In general, the most convenient and simple way of drug delivery is through oral administration, but it can be difficult to use it with a complex pharmaceutical drug. This challenge can be overcome by the use of injections and it is a rapid start of pharmaceutical action. However, the injection with a hypodermic needle requires specialization, and patient compliance is limited. The future best drug delivery strategy should therefore be as straightforward as oral administration and have a high solubility and great health benefits as a like injection.

The transdermal administration of a drug has the benefit of continuous pharmaceutical release to the exact site of action without any alteration in drug concentration. Yet, the skin outermost layer called stratum corneum acts as barrier and makes drug delivery challenging [1]. Microneedles (MNs) serve as a delivery system for transdermal medication; they are simple to use on oneself and have a high level of medication bioavailability. Additionally, it is a non-invasive and painless approach that aids in the quick passage of drug through the stratum corneum. This technology has unique features such as safety, patient compliance, self-administration, increased permeability, and better performance [2]. Although it has numerous benefits, it also has some drawbacks. The sensitive skin may subject to irritation or allergy. In some cases, the tips of microneedles may break and causes issues inside the skin. These limitations are solved by using excellent microneedle material selection. The microneedles are produced in such a way that it bypasses the stratum corneum and deliver the entire dose of loaded drug directly into the epidermis layer [3]. Moreover, the medication dosage, delivery rate, and effectiveness of drug passage can be controlled by geometry and drug composition. Studies have been done so far on microneedles designed to deliver drugs and cosmetics that were made with a variety of fabrication techniques [4].

2 Patient Monitoring: Limitations and Challenges of Therapeutic Monitoring in the Health Sector

In most countries, chronic diseases are associated with high healthcare costs and lower societal productivity. Modern technology tools should be exploited to their full potential in an effort to minimize healthcare costs, improve patient monitoring through continuous assessment of symptoms and indicators of disease, and ensure compliance with self-management initiatives and chronic disease prevention. Because of the inability to notice difficulties linked with the drug therapy, inadequate monitoring might result in the emergence of Adverse Drug Events [5].

In general, oral delivery is still the most preferred method for the administration of active pharmaceutical ingredients because of the advantages such as self, pain free administration, more safe, and better patient compliance. Even though oral administration has many benefits, it has some drawbacks, such as the possibility of first-pass effect, the drug concentration may be reduced [6]. In addition, drug absorption may be limited by intestinal permeability and solubility, which may naturally limit the bioavailability of medications. These problems repeatedly appear during the delivery of biopharmaceuticals. As a result, intravenous (IV) injection is one of the most promising drug delivery systems, as it can accomplish precise dosing with the balance of high bioavailability. This system can cause some discomfort, and sometimes skin-pricking leads to blood drawing. One of the major problems is the sharp biomedical waste generated after usage of injection. The transdermal route has been investigated as another potential route for improving peptide medication delivery in order to potentially overcome some of these drawbacks [7].

Transdermal drug administration has gained popularity during the past ten years as a result of its advantages over traditional oral dosing forms. By 2025, the market for transdermal medication delivery is anticipated to increase and reach around $95.57 billion [8]. The different approaches of drug administration are depicted in Fig. 1. Transdermal Drug Delivery (TDD) is a painless method of injecting the drug into the stratum corneum layer and the drug reaches into the dermis layer without any skin damage. TDD is superior to other traditional drug delivery methods in several ways. By offering a non-invasive alternative to parenteral routes, it can get around problems like needle fear. Numerous placement choices on the skin for transdermal absorption are possible due to the skin's enormous surface area and ease of access. It keeps medication concentrations consistent despite repeated dosage administration, and plasma level instability brought on by oral dosing and injections, and it makes it simple to administer drugs with short half-lives. TDD bypasses pre-systemic metabolism, resulting in increased bioavailability [9]. In general, transdermal systems are economical and affordable, and the market available patches are used for the medication for up to 7 days. These patches are cost-effective when compared to other therapies. With little risk of systemic toxicity, the transdermal route allows the use of powerful drugs [10].

Furthermore, the World Economic Forum has named this distribution platform as one of the "Top 10 Emerging Technologies of 2020." The World Economic Forum's support for the quick commercialization of MN products presently through regulatory evaluation and development strengthens that position. To guarantee that MN technology may have a favorable influence on patients and doctors across the whole medical profession, it is crucial that regulatory oversight for this growing technology is thorough and that all aspects of commercialization are thoroughly handled [11].

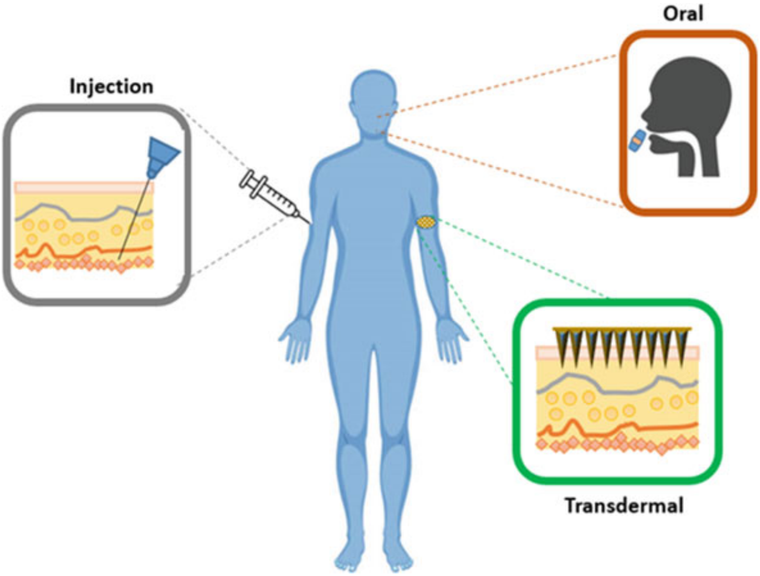

Fig. 1 Different approaches of drug administration

3 Evolution of Microneedle

Direct drug administration through the skin is referred to as transdermal delivery. The most popular method involves using hypodermic needles, which can cause pain to patients, needle aversion, and even the potential for infectious disease transmission [12]. These conventional injections can be substituted by microneedle technology, which is described as the non-invasive delivery of drugs through the skin surface. This technology has received interest from various research organizations and businesses. Microneedle delivery system is an appealing substitute for drug delivery technique to overcome the drawbacks of current traditional approaches [13]. The microneedle technology eliminates the needle phobia and more attracted the attention of the healthcare community. This technology also ensures the proper safe needle disposal is an added factor.

Microneedle patches are considered as minimally invasive devices that pierces the stratum corneum layer of the skin without pain and drawing blood. Microneedle devices are made to pierce the epidermis and deliver a medicine directly to the microcirculation beneath. These typically feature a variety of 50–900 μm long micron-sized projections. Needle length increment leads to more pain incredibly. Normally the needles have at least a certain length to overcome any deformation in the epidermis layer [14]. As compared to traditional needles, it attracts the industry with benefits such as non-hazardous, patient comforts, less painful, and cost-effective. Various designs of microneedles are progressed under research for efficient drug delivery

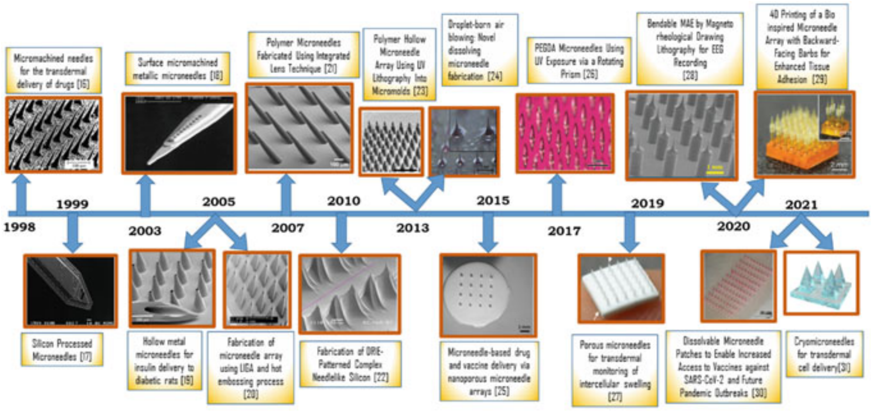

Fig. 2 Important developments in microneedle devices. Reproduced with permission from [16–31]

to avoid breakage of the needle. Many researchers reported that the sharpness and strength of the needle were decided by the proper material composition [15].

It is still challenging and difficult to exhibit the research idea at industry level. Some important problems and difficulties should be swiftly taken into account in order to move this novel technology from the lab level to practical products in the pertinent markets. Few of the innovative and significant advancements in MN research have been outlined in Fig. 2 [16–31].

4 Microneedle Classification

Based on fabrication, microneedles are generally divided into two categories, In-plane and Out-of-plane microneedles. In-plane MNs, needles are placed parallel to the substrate surface, and for out-of-plane MNs, needles are protruded out of the substrate surface. Out-of-plane MNs are ideal for two-dimensional geometry creation through wafer-level processing, but In-plane MNs are very difficult to produce with two-dimensional geometry [32].

Based on design, microneedles are classified as Solid, Hollow, Coated, Dissolving, and Hydrogel forming MN. The different types of microneedle representation are displayed in Fig. 3.

Solid Microneedles

Solid MNs are normally work in the principle of Poke with patch approach, it punctures a hole in the skin of the stratum corneum. They provide passage for the drugs to enter into the epidermis layer. The drug penetration or drug delivery rate depends on the depth of the opened pores. The micropores created on the skin that remain open for a week may cause infections. It is a major drawback for these types of microneedles

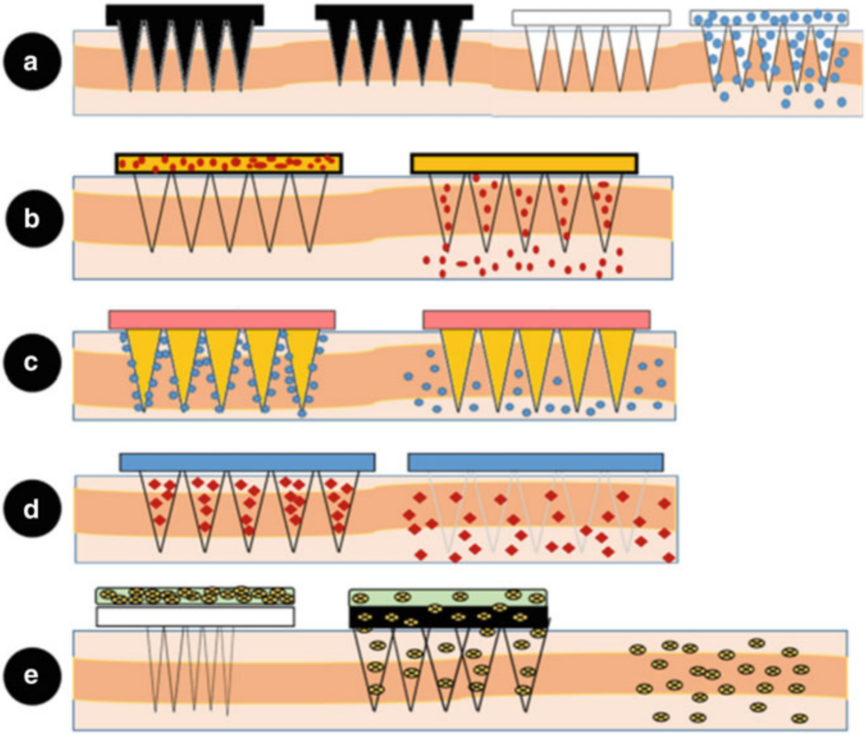

Fig. 3 Representation of Microneedle types **a**—Solid MNs; **b**—Hollow MNs; **c**—Coated MNs; **d**—Dissolving MNs; **e**—Hydrogel forming MNs [33]. Reproduced with permission from Sharma et al., Materials Science and Engineering C, (2019). Copyright © 2019 Elsevier

[34]. The materials used for developing solid MNs are typically silicon, metals, and polymers. Silicon is a fragile material and may break in the skin from an extended-release patch. The fabrication process for silicon-based solid MNs is very costly. The first silicon-based solid microneedles were manufactured using microfabrication technology. Some other fabrication methodologies are wet etching technology using mixtures of chemicals called HNA (Hydrofluoric acid, Nitric acid, Acetic acid) and reactive ion etching [36]. Some advantages of metal-based solid MNs are cost-effective and they have good mechanical strength. The frequently used materials for the fabrication of metal-based solid MNs such as stainless steel [35], titanium, and nickel. Polymer MNs are fabricated based on a mold-based method and usually made up of biocompatible polymers such as polyvinyl pyrrolidone, poly-lactic acid, poly-glycolic acid, and their copolymers. The fabrication method of polymer-based solid MNs is very inexpensive and easy for mass production.

Coated Microneedles

Based on the "coat and poke" strategy, these MNs are fabricated and the drug solution is applied to the microneedles before they are punctured into the skin. The coated drug will be dissolved and deposited into the skin surface by entering into the dermis layer. The amount of drug penetration into the skin mainly depends on the needle size and thickness of the drug-coated layer. But the important constraint is only a limited amount of drug can be coated on the body of the microneedle. Recent innovations in coating methods are developed for efficient Coated MNs in the field of drug delivery, biopharmaceuticals, and disease diagnosis [37]. It follows a single-step process of the fabrication either by dipping or micromolding techniques, with the use of materials such as stainless steel, titanium, and polymer.

Dissolving Microneedles

Dissolving microneedles are created using biocompatible (or) bio-degradable polymer (e.g., sugar, polyvinyl-pyrrolic (PVP), polyvinyl alcohol (PVA), poly-lactic acid (PLA), and poly-glycolic acid (PGA). They are fabricated based on the “poke and release” principle. The microneedle patch is loaded with the drug and it is inserted into the skin. The drug enters into the dermis layer and the dissolution of the drug takes place and it is released after a period of time. The dissolution of the drug depends on the polymer composition and the fabrication of the molding process. The preferred fabrication process for the dissolving microneedles such as micromolding fabrication, which is a one-step process always convenient for patients [15]. It involves a polymer solution poured into mold structures and allowing the mold to dry under ambient conditions. A less expensive fabrication process with better patient compliance is the major benefit of dissolving MNs. The stability can be improved by processing the polymer under high temperature and extreme pH. The hazard of polymers deposition into the skin can be avoided by the proper selection of biocompatible polymers for drug delivery. Water-soluble polymers are preferably used for eliminating biohazardous sharp waste in the skin layers [38]. Some literature works with the solid microneedle developed as coated or dissolving patches are displayed in Fig. 4.

Hollow Microneedles

Hollow MNs are designed with hollow holes or lumens in the middle of the needles [39]. These empty spaces are filled with a drug solution. Some designs of hollow MNS have holes at the tip of the needles to deliver the drug into the inner layers of the skin using methods like diffusion, pressure, electrical assistance, or mechanical vibration. These hollow microneedles can bypass the stratum corneum and directly enters into the epidermis and deeper dermis layer. The principle called “Poke and flow” is suitable for the hollow microneedle to deliver the drug into the skin [3, 40].

Based on internal bores or lumens, the hollow microneedles can be classified as side opened single lumen, tip opened single lumen, side opened double lumen and tip opened double lumen. Preferably, side opened double-lumen-based hollow microneedles are more suitable for drug transport. Hollow MNs occupy larger doses

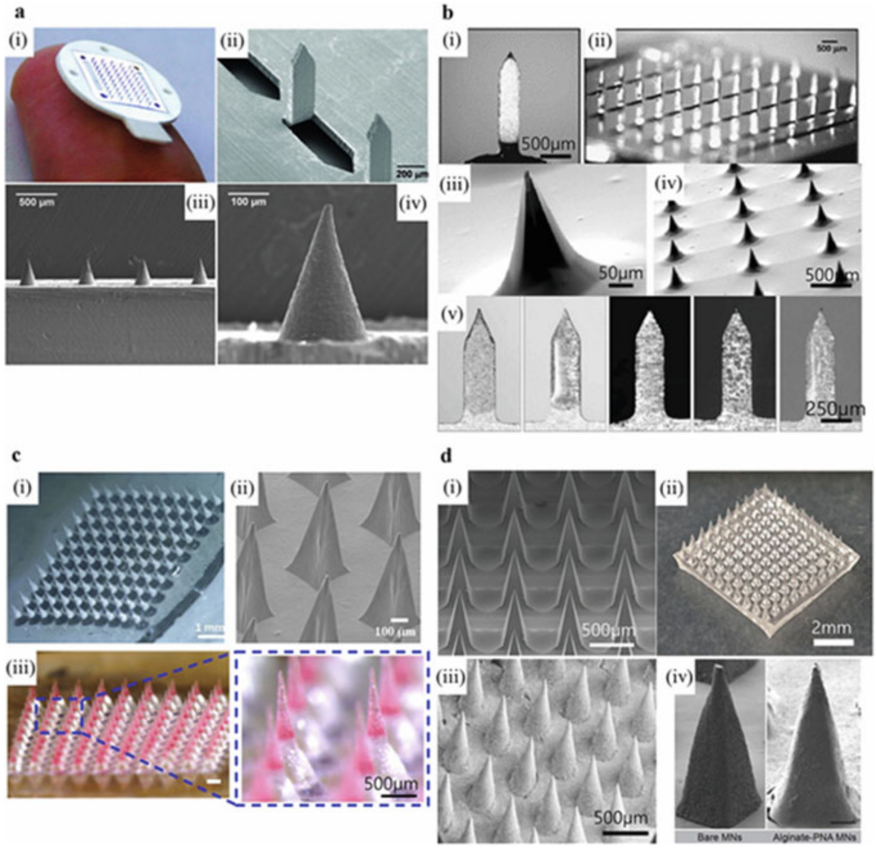

Fig. 4 Solid microneedles composed of stainless steel (i and ii) and titanium (iii and iv) b Coated microneedles composed of stainless steel (i and ii), silicon (iii and iv) and titanium (v) c Dissolving microneedles composed of CMC (i), HPMC (ii) and PLGA (iii) d Hydrogel microneedles composed of HA (i and ii), PVA (iii) and alginate (iv) [1]. Reproduced with permission from Jung, J.H., Jin, S.G. J. Pharm. Investig. 51, 503–517 (2021). Copyright © 2021 Springer

of the drug as compared to solid MNs, as it carries more amount of drug in the space inside the needle. The benefits of the hollow microneedle are that the diffusion of a drug is deeper into the skin, closer to blood vessels. Generally, it is preferred for high molecular weight substances like peptide or proteins, DNA or RNA molecules, and vaccines [41]. Continuous flow rate to be maintained with the adjustment of microneedle bore [42]. The major restrictions with the hollow type needles are flow resistance and clogging of the solution in the needle tip. Change in the hollow bore will increase the flow rate but it leads to a decrease in the strength and sharpness of the needle. To increase the needle strength, at times a metal coat is applied at the needle tip. The ongoing research studies with these limitations led to the innovative design of hollow microneedles. Side-opened sharp-tip hollow microneedles [43] are

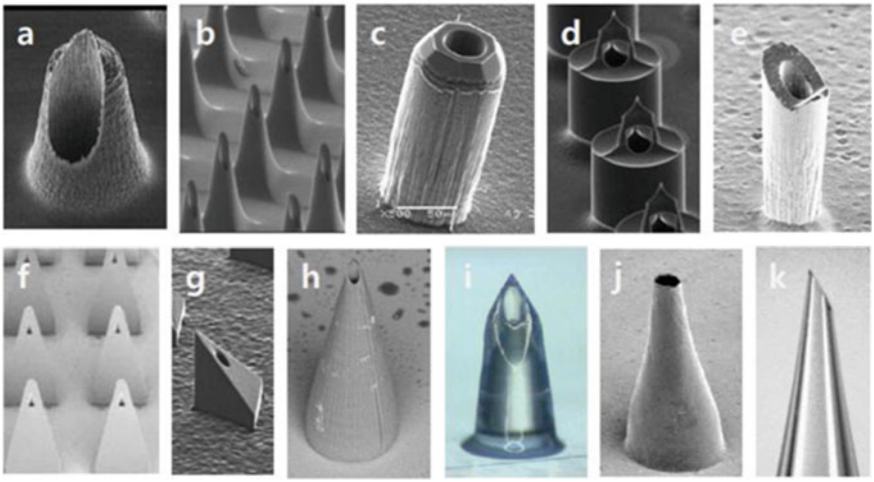

Fig. 5 Hollow microneedles made of silicon and polymers [44]. Reproduced with permission from Yeu-ChunKim et al., Advanced Drug Delivery Reviews, (2012). Copyright © 2012 Elsevier

repeatedly investigated as it leads to less prone of clogging and tranquil to insert. Predominantly used materials for the fabrication of hollow MNs are silicon, metals, polymers, glass, and ceramic. These microneedles are fabricated using processes like deep X-ray photolithography, laser micromachining, deep reactive ion etching, metal electroplating, two-photon polymerization, and a unified molding technique. The different types of the fabricated hollow microneedle are shown in Fig. 5.

Hydrogel forming Microneedles

This type of microneedle is made up of super-swelling polymers and these materials have a better capacity for water absorption. When the MN is injected into the skin, these polymers absorb the water and get swelled due to the presence of body fluid. This result in the development of conduits and these allow the discharge of drugs into the microcirculation from the reservoir. After injection, needles quickly absorb interstitial fluid from the tissue, causing the medication to diffuse from the patch through enlarged MNs. Specific polymeric components, such as poly methyl vinyl ether-co-maleic acid (PMVE/MA), carboxymethylcellulose (CMC), and amylopectin, are combined in aqueous solutions to create these types of microneedles [45].

5 Existing Methods: For Microneedle Fabrication

In the past few decades, the field of MN manufacturing technologies has experienced a steady flow of research and invention, with both conventional and cutting-edge methods being researched. The selection of an appropriate manufacturing method for microneedles depends on drug type and dose, targets for use, optimized geometry and material. Most of the existing fabrication methodologies are very costly, comprise tedious procedures, and are challenging to implement for batch production. Most of the future research focuses on the cost-effective, repeatable fabrication process to enhance the usage of microneedle usage in the market. In the case of the financial side, micromolding or solvent casting methodology is more preferred [46]. However, MEMS-based metal or silicon microneedles are manufactured to obtain better precision and to ensure the repeatability of needle production. The various MN fabrication techniques are summarized in Table 1 [47–65].

Table. 1 Available microneedle manufacturing techniques

References	Fabrication method	Material used for fabrication	Type of MN	Geometry
[47]	3D microlens mask Lithography	Glass	Solid	Pyramidal
[48–50]	Deep Ion reactive etching, wet or dry etching	Silicon	Solid, Hollow	Conical, Bevel
[51, 52]	Laser ablation, etching, and micromolding	Polyhydroxyalkanoate, PMMA	Solid, Hollow	Conical
[53, 54]	Sacrificial Micromolding and Selective Electrodeposition	PLA mold, Metal	Hollow	Conical, Pyramidal
[55, 56]	Photolithography	PEGDA	Solid, Hollow, Dissolving	Cylindrical, conic, Pyramid
[57–59]	3D Printing (microstereolithography, Two-photon polymerization)	PEGDA, PVP, PEGDMA, PLA	Hollow, Solid, Coated	Square Pyramidal, Conical
[60, 61]	Soft Lithography	Polycarbonate MN master mold, thermoplastic polyurethane (TPU), PDMS	Solid, Hollow	Square Pyramid
[62, 63]	Atomized spraying process	Polyvinyl alcohol, polyvinylpyrrolidone, carboxymethylcellulose, hydroxypropylmethylcellulose, sodium alginate	Dissolvable, Hydrogel	Pyramidal
[64, 65]	Pulling pipette	Glass	Hollow, Solid	Conical

6 Benefits of Microneedle Technology in Various Health Sectors

In recent years, the use of needle-free transdermal administration methods moved closer to reality. Particularly, microneedle technologies came into reality and gained an attention of the healthcare community because it eliminates the issue of needle phobia. In addition, the usage of many biocompatible material made needles ensures the safety issues typically connected with needle disposal. Due to the small size of the needles, physical harm to the skin is low and the pores close within a few hours of the initial treatment. However, numerous studies have shown that as compared to conventional injection systems, the risk of infection from the use of microneedles is significantly lower. The introduction of needles made up of biocompatible polymer can further lessen the risk of infection from germs that may have unintentionally been pulled into the channel during patch administration [14]. Currently, the usage of microneedles is being expanded into new domains, such as disease diagnostics, immunobiological administration, and cosmetic applications as described in Fig. 6.

Immunobiological administration

Due to the COVID-19 pandemic, there has been a huge surge in research into microneedles and their wide benefits for the vaccine delivery and medications. Microneedles as a method of transdermal administration were created in 1976, but this idea was only recently applied to vaccination. Becton, Dickinson, and Company created Soluvia^{TM} as the first intradermal vaccine. The vaccination antigen can be delivered into the dermis layer of the skin using the microneedle patch, which consists of a 30-gauge metallic microneedle implanted 1.5 mm into the skin. This

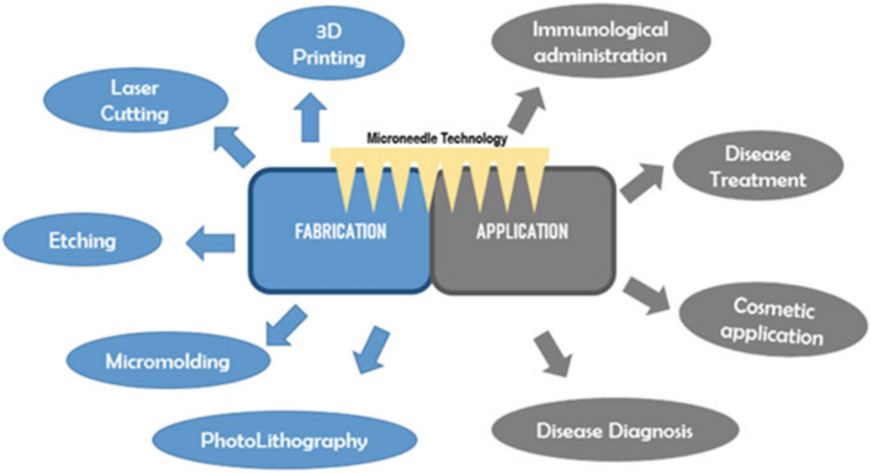

Fig. 6 Various microneedle fabrication methodologies and their applications

method was used to provide the influenza vaccine [66]. Cassie Caudill et al fabricated the microneedle patch using 3D printing and the transdermal vaccination provides many benefits over conventional vaccination such as less skin damage, self-implementation, minimally invasive, the potential to reduce cold chain dependency and there is no need of professional administration as like hypodermic needle [58].

Transdermal vaccination using biodegradable microneedles is a rapidly emerging area of research and application [67]. Dissolving microneedle patches made up of polymer material is very effective for vaccine delivery as they dissolve quickly in the skin and will not leave any biomedical waste [68].

Disease Treatment and Diagnosis

The most popular use for microneedles is still the transdermal drug delivery for disease therapy. In case of cancer disease, the effect of chemotherapy or surgery can cause serious side effects and in some anticancer therapy, only lesser amount of drug reaches the tumor site. The development of MNs offers a practical and minimally invasive method for administering drugs topically to treat surface malignancies. In general, MNs can lessen the effects of systemic toxicity as well as enhance drug distribution in the diseased position. Through MNs, the antigens enter the body and set off a generalized response that stimulates the immune cells, killing cancer cells [55]. Lan et al reported a method to cure cancer by developing a dissolving MN patch for the transdermal delivery of cisplatin to kill cancer cells. The cancer cells are killed by the dissolving patch loaded with pH responsive lipid nanoparticles by injecting directly into the tumor site. The author ensures the safety after administration and this method exhibits minimal side effects and less systemic toxicity [69]. In another study, researchers developed polymer-based dissolving microneedle patches for the treatment of breast cancer. The PVA and PVP microneedles are loaded with the combination of doxorubicin and docetaxel in aid for the photothermal and chemotherapy and increase the efficiency of cancer treatment [70].

For diabetes patient, the complex and multiple daily injections will reduce the patient compliance and increases the risk of hypo glycemia. The use of hypodermic needles in conventional ways has been discovered to cause tissue trauma and extremely discomfort. Nowadays, microneedle patches are used promisingly for diabetes management, which is an added benefit for patients with uncontrolled glucose levels or those at high risk of hypo glycemia. MN patches will release the medication when the blood glucose level raises and acts as an emerging drug delivery system that is being used to treat diabetic patients successfully [5]. Yu et al. developed insulin loaded biodegradable dissolving microneedle patch for the management of diabetes. The MN patch is made up of alginate and hyaluronate, these are non-cytotoxic and also improve the mechanical functionality. The system exhibits a more sustained release of insulin and avoids steep fall in glucose levels [71]. Chang et al developed a swellable microneedle patch for the diabetes management and insulin delivery. Additionally, the technology is capable of extracting ISF instantly to detect both cholesterol and glucose levels and this value is observed to be the same as that measured using a traditional glucometer [72].

Microneedle patches were also applied in the treatment of other diseases. For illustration, Alzheimer disease is treated with tip-loaded dissolving microneedles encapsulated with a Donepezil hydrochloride (DPH) drug, resulting in efficient treatment when compared to oral administration. Problems such as neuropathic disorder are treated with analgesic microneedle patches as an alternative to clinical treatments. It was reported that the MN patches transdermally distribute anti-calcitonin gene-related peptide (A-CGRP) to reduce localized neuropathic pain by blocking CGRP receptors [73].

Cosmetic applications

Since 2005, when microneedles were first employed in the cosmetics business, a number of new products have been created, greatly increasing the usage of these tiny needles to treat skin disorders like wrinkles, scars, seborrheic keratosis, depigmentation, reducing fat, and other uses [74, 75].

The skin pigmentation is called seborrheic keratosis or lentigo and is usually observed in elder adults of age >50 and these can be cured by injection of retinoic acid into the skin. Hibrobe et al. created an all-Trans retinoic acid (ATRA) loaded microneedle patch (ATRA-MNs) and the patch was applied on the wound site for once in a week and continuously monitored for the next 4 weeks. This study has demonstrated that microneedles are used as a safe and effective treatment for senile lentigo and seborrheic keratosis [76].

A microneedle can deliver active cosmetic molecules straight into the skin by forming microchannels that do not enter the nerve with better effectiveness and safety. An innovative cosmetic patch loaded with retinyl retinoate and ascorbic acid is fabricated for anti-wrinkle purposes. The best example of a microneedle-based equipment is “Dermaroller,” and other approved microneedle devices for cosmetic procedures are “Derma Pen” [77]. These microneedles assisted equipments are utilized in home environments, and they are easily sterilizable for repeated usage. This area is still in a wide range of research with innovations for the delivery of cosmeceutical agents [78].

7 Microneedles: Challenges Involved in Their Development

Although various uses for microneedles have been proposed, only a small number of items have actually hit the market. When creating microneedles for the transport of both small and large molecules, safety and efficacy must be taken into account. Metallic microneedles may cause irritation, erythema, discoloration, or other negative side effects because metal traces are left behind beneath the skin. The above issues could arise if the microneedle is used repeatedly at the same location. The variation in skin thickness or use of microneedles at different sites may differ in bioavailability, which should be taken into consideration when developing the microneedles [4, 79, 80].

Currently, research is focused on developing new technologies for the safe administration of existing molecules, thereby reducing development time and increasing success rates. For this reason, many in the pharmaceutical industry strive for the successful development of microneedles as transdermal drug delivery systems [79].

The fabrication of various microneedle types encounters a variety of difficulties. The use of solid microneedles made up of metal may irritate the skin or cause metallic particles to remain in the skin. Additionally, after usage, they could leave behind biohazardous sharp waste, thus careful destruction is required. Dissolving microneedles dissolve completely into the skin and do not leave any waste. The major challenges in the development will be effective needle penetration, drug interaction into the skin, and loading the drug abundantly at the tip. Researchers are also becoming interested in the usage of hollow microneedles because they have the ability to administer a wider variety of molecules than other types of devices. However, this particular sort of microneedle lacks sufficient strength, so the researcher needs to emphasize overcoming this issue.

8 Conclusion and Future Perspectives

MNs provide numerous chances for the intradermal delivery of a variety of medications, including biopharmaceuticals. MN approach is a painless, efficient, secure form of drug delivery when compared to other intravenous methods. Moreover, this method can be useful for medications with low oral bioavailability. MNs come in a variety of types and can be created from a vast range of materials. They can be customized to treat particular diseases because of this feature. Since the academic and patent literature has accumulated mounting evidence showing that microneedles of many different designs can be successfully used to deliver drugs, vaccines, and active substances, the industrial effort to develop microneedle devices is likely to intensify. It is expected that newer applications of microneedle technology will become more popular. As the number of novel pharmaceuticals with biological origins keeps increasing, microneedles will significantly increase the transdermal delivery market value and become more significant during the succeeding years.

References

1. Jung JH, Jin SG (2021) Microneedle for transdermal drug delivery: current trends and fabrication. J Pharmaceut Invest 51(5):503–517. https://doi.org/10.1007/s40005-021-00512-4
2. Prausnitz MR, Langer R (2008) Transdermal drug delivery. Nat Biotechnol 26(11):1261–1268. https://doi.org/10.1038/nbt.1504
3. Waghule T, et al (2019) Microneedles: a smart approach and increasing potential for transdermal drug delivery system. In: Biomedicine and pharmacotherapy, vol. 109. Elsevier, Masson, SAS, pp 1249–1258. https://doi.org/10.1016/j.biopha.2018.10.078

4. Donnelly RF, Raj Singh TR, Woolfson AD (2010) Microneedle-based drug delivery systems: Microfabrication, drug delivery, and safety. Drug Deliv 17(4):187–207. https://doi.org/10.3109/10717541003667798
5. Ng LC, Gupta M (2020) Transdermal drug delivery systems in diabetes management: a review. Asian J Pharmaceut Sci 15(1):13–25. Shenyang Pharmaceutical University. https://doi.org/10.1016/j.ajps.2019.04.006
6. Sahoo D, et al (2021) Oral drug delivery of nanomedicine. In: Theory and applications of nonparenteral nanomedicines. Elsevier, pp 181–207. https://doi.org/10.1016/b978-0-12-820466-5.00009-0
7. Alkilani AZ, McCrudden MTC, Donnelly RF (2015) Transdermal drug delivery: Innovative pharmaceutical developments based on disruption of the barrier properties of the stratum corneum. Pharmaceutics 7(4):438–470. MDPI AG. https://doi.org/10.3390/pharmaceutics7040438
8. Ramadon D, McCrudden MTC, Courtenay AJ, Donnelly RF (2022) Enhancement strategies for transdermal drug delivery systems: current trends and applications. Drug Deliv Transl Res 12(4):758–791. https://doi.org/10.1007/s13346-021-00909-6
9. Parhi R (2018) Nanocomposite for transdermal drug delivery. In: Applications of nanocomposite materials in drug delivery. Elsevier, pp 353–389. https://doi.org/10.1016/B978-0-12-813741-3.00016-9
10. Sengar V, Jyoti K, Jain UK, Katare OP, Chandra R, Madan J (2018) Lipid nanoparticles for topical and transdermal delivery of pharmaceuticals and cosmeceuticals: a glorious victory. In: Lipid nanocarriers for drug targeting. Elsevier, pp 413–436. https://doi.org/10.1016/B978-0-12-813687-4.00010-4
11. Detamornrat U, McAlister E, Hutton ARJ, Larrañeta E, Donnelly RF (2022) The role of 3D printing technology in microengineering of microneedles. Small 18(18). John Wiley and Sons Inc. https://doi.org/10.1002/smll.202106392
12. Bajaj S, Whiteman A, Brandner B (2011) Transdermal drug delivery in pain management. Contin Educ Anaesth Crit Care Pain 11(2):39–43. https://doi.org/10.1093/bjaceaccp/mkq054
13. Ita K (2015) Transdermal delivery of drugs with microneedles—potential and challenges. Pharmaceutics 7(3):90–105. https://doi.org/10.3390/pharmaceutics7030090
14. McConville A, Hegarty C, Davis J (2018) Mini-review: assessing the potential impact of microneedle technologies on home healthcare applications. Medicines 5(2):50. https://doi.org/10.3390/medicines5020050
15. Sharma DM (2017) Microneedles: an approach in transdermal drug delivery: a Review Review on Moisture activated Dry Granulation Process View project an updated review on medicated gum as a potential tool for novel drug delivery system view project. https://doi.org/10.29161/PT.v6.i1.2017.7
16. Henry S, McAllister DV, Allen MG, Prausnitz MR (1998) Micromachined needles for the transdermal delivery of drugs. In: Proceedings of the IEEE Micro Electro Mechanical Systems (MEMS), pp 494–498. https://doi.org/10.1109/memsys.1998.659807
17. Lin L, Pisano AP (1999) Silicon-processed microneedles. J Microelectromech Syst 8(1):78–84. https://doi.org/10.1109/84.749406
18. Chandrasekaran S, Brazzle JD, Frazier AB (2003) Surface micromachined metallic microneedles. J Microelectromech Syst 12(3):281–288. https://doi.org/10.1109/JMEMS.2003.809951
19. Davis SP, Martanto W, Allen MG, Prausnitz MR (2005) Hollow metal microneedles for insulin delivery to diabetic rats. IEEE Trans Biomed Eng 52(5):909–915. https://doi.org/10.1109/TBME.2005.845240
20. Moon SJ, Lee SS, Lee HS, Kwon TH (2005) Fabrication of microneedle array using LIGA and hot embossing process. Microsyst Technol 11(4–5):311–318. https://doi.org/10.1007/s00542-004-0446-8
21. Park JH, Yoon YK, Choi SO, Prausnitz MR, Allen MG (2007) Tapered conical polymer microneedles fabricated using an integrated lens technique for transdermal drug delivery. IEEE Trans Biomed Eng 54(5):903–913. https://doi.org/10.1109/TBME.2006.889173

22. Gassend BLP, Velásquez-García LF, Akinwande AI (2010) Design and fabrication of DRIE-patterned complex needlelike silicon structures. J Microelectromech Syst 19(3):589–598. https://doi.org/10.1109/JMEMS.2010.2042680
23. Wang PC, Paik SJ, Chen S, Rajaraman S, Kim SH, Allen MG (2013) Fabrication and characterization of polymer hollow microneedle array using UV lithography into micromolds. J Microelectromech Syst 22(5):1041–1053. https://doi.org/10.1109/JMEMS.2013.2262587
24. Kim JD, Kim M, Yang H, Lee K, Jung H (2013) Droplet-born air blowing: Novel dissolving microneedle fabrication. J Control Release 170(3):430–436. https://doi.org/10.1016/j.jconrel.2013.05.026
25. van der Maaden K, Luttge R, Vos PJ, Bouwstra J, Kersten G, Ploemen I (2015) Microneedle-based drug and vaccine delivery via nanoporous microneedle arrays. Drug Deliv Transl Res 5(4):397–406. https://doi.org/10.1007/s13346-015-0238-y
26. Takahashi H, Heo YJ, Shimoyama I (2017) Scalable fabrication of PEGDA microneedles using UV exposure via a rotating prism. J Microelectromech Syst 26(5):990–992. https://doi.org/10.1109/JMEMS.2017.2740177
27. Nagamine K, Kubota J, Kai H, Ono Y, Nishizawa M (2017) An array of porous microneedles for transdermal monitoring of intercellular swelling. Biomed Microdev 19(3). https://doi.org/10.1007/s10544-017-0207-y
28. Ren L, Chen Z, Wang H, Dou Z, Liu B, Jiang L (2020) Fabrication of bendable microneedle-array electrode by magnetorheological drawing lithography for electroencephalogram recording. IEEE Trans Instrum Meas 69(10):8328–8334. https://doi.org/10.1109/TIM.2020.2990523
29. Han D, et al (2020) 4D printing of a bioinspired microneedle array with backward-facing barbs for enhanced tissue adhesion. Adv Funct Mater 30(11). https://doi.org/10.1002/adfm.201909197
30. O'shea J, Prausnitz MR, Rouphael N (2021) Dissolvable microneedle patches to enable increased access to vaccines against SARS-CoV-2 and future pandemic outbreaks. https://doi.org/10.3390/vaccines
31. Chang H et al (2021) Cryomicroneedles for transdermal cell delivery. Nat Biomed Eng 5(9):1008–1018. https://doi.org/10.1038/s41551-021-00720-1
32. Sawon MA, Samad MF (2021) Design and optimization of a microneedle with skin insertion analysis for transdermal drug delivery applications. J Drug Deliv Sci Technol 63. https://doi.org/10.1016/j.jddst.2021.102477
33. Sharma S, Hatware K, Bhadane P, Sindhikar S, Mishra DK (2019) Recent advances in microneedle composites for biomedical applications: advanced drug delivery technologies. Mater Sci Eng C 103. Elsevier Ltd. https://doi.org/10.1016/j.msec.2019.05.002
34. Wei-Ze L et al (2010) Super-short solid silicon microneedles for transdermal drug delivery applications. Int J Pharm 389(1–2):122–129. https://doi.org/10.1016/j.ijpharm.2010.01.024
35. Rajabi M, et al (2016) Flexible and stretchable microneedle patches with integrated rigid stainless steel microneedles for transdermal biointerfacing. PLoS One 11(12). https://doi.org/10.1371/journal.pone.0166330
36. Aziz NA, Majlis BY (2006) Fabrication study of solid microneedles array using HNA. In: *IEEE International Conference on Semiconductor Electronics, Proceedings, ICSE*, pp. 20–24. https://doi.org/10.1109/SMELEC.2006.381012
37. Gill HS, Prausnitz MR, Coulter H Coated microneedles for transdermal delivery
38. Larrañeta E, Lutton REM, Woolfson AD, Donnelly RF (2016) Microneedle arrays as transdermal and intradermal drug delivery systems: Materials science, manufacture and commercial development. Mater Sci Eng R Rep 104:1–32. Elsevier Ltd. https://doi.org/10.1016/j.mser.2016.03.001
39. Vinayakumar KB, Hegde GM, Nayak MM, Dinesh NS, Rajanna K (2014) Fabrication and characterization of gold coated hollow silicon microneedle array for drug delivery. Microelectron Eng 128:12–18. https://doi.org/10.1016/j.mee.2014.05.039

40. Vinayakumar KB, et al (2016) A hollow stainless steel microneedle array to deliver insulin to a diabetic rat. J Micromech Microeng 26(6). https://doi.org/10.1088/0960-1317/26/6/065013
41. Mcallister DV, et al (2003) Microfabricated needles for transdermal delivery of macromolecules and nanoparticles: fabrication methods and transport studies. https://www.pnas.org/doi/10.1073/pnas.2331316100
42. Iliescu FS, Iliescu FS, Dumitrescu-Ionescu D, Petrescu M, Iliescu C (2014) A review on transdermal drug delivery using microneedles: current research and perspective microfluidics view project advanced techniques and increasing performance in the early detection of SARS-CoV-2 virus view project a review on transdermal drug delivery using microneedles: current research and perspective. Ann Acad Roman Sci Ser Sci Technol Inform https://www.researchgate.net/publication/268221237
43. Zhang P, Dalton C, Jullien GA (2009) Design and fabrication of MEMS-based microneedle arrays for medical applications. Microsyst Technol 15(7):1073–1082. https://doi.org/10.1007/s00542-009-0883-5
44. Kim YC, Park JH, Prausnitz MR (2012) Microneedles for drug and vaccine delivery. Adv Drug Deliv Rev 64(14):1547–1568. https://doi.org/10.1016/j.addr.2012.04.005
45. Tucak A, et al (2020) Microneedles: characteristics, materials, production methods and commercial development. Micromachines 11(11). MDPI AG. https://doi.org/10.3390/mi11110961
46. Mansoor I, Hafeli UO, Stoeber B (2012) Hollow out-of-plane polymer microneedles made by solvent casting for transdermal drug delivery. J Microelectromech Syst 21(1):44–52. https://doi.org/10.1109/JMEMS.2011.2174429
47. Lin TH, Jiang JM (2019) Fabrication of a pyramidal micro-needle array structure using 3D micro-lens mask lithography. Microsyst Technol 25(12):4637–4643. https://doi.org/10.1007/s00542-019-04610-0
48. Li Y, et al. (2019) Fabrication of sharp silicon hollow microneedles by deep-reactive ion etching towards minimally invasive diagnostics. Microsyst Nanoeng 5(1). https://doi.org/10.1038/s41378-019-0077-y
49. Bolton CJW et al (2020) Hollow silicon microneedle fabrication using advanced plasma etch technologies for applications in transdermal drug delivery. Lab Chip 20(15):2788–2795. https://doi.org/10.1039/d0lc00567c
50. Pradeep Narayanan S, Raghavan S (2017) Solid silicon microneedles for drug delivery applications. Int J Adv Manuf Technol 93(1–4):407–422. https://doi.org/10.1007/s00170-016-9698-6
51. Silvestre SL et al (2020) Microneedle arrays of polyhydroxyalkanoate by laser-based micro-molding technique. ACS Appl Bio Mater 3(9):5856–5864. https://doi.org/10.1021/acsabm.0c00570
52. Evens T, et al (2021) Producing hollow polymer microneedles using laser ablated molds in an injection molding process. J Micro Nano-Manuf 9(3). https://doi.org/10.1115/1.4051456
53. Norman JJ et al (2013) Hollow microneedles for intradermal injection fabricated by sacrificial micromolding and selective electrodeposition. Biomed Microdev 15(2):203–210. https://doi.org/10.1007/s10544-012-9717-9
54. Miller PR et al (2019) Fabrication of hollow metal microneedle arrays using a molding and electroplating method. MRS Adv 4(24):1417–1426. https://doi.org/10.1557/adv.2019.147
55. Dardano P, Caliò A, di Palma V, Bevilacqua MF, di Matteo AD, Stefano L (2015) A photolithographic approach to polymeric microneedles array fabrication. Materials 8(12):8661–8673. https://doi.org/10.3390/ma8125484
56. Kathuria H, Kang K, Cai J, Kang L (2020) Rapid microneedle fabrication by heating and photolithography. Int J Pharmaceut 575. https://doi.org/10.1016/j.ijpharm.2019.118992
57. Lim SH et al (2021) High resolution photopolymer for 3D printing of personalised microneedle for transdermal delivery of anti-wrinkle small peptide. J Control Release 329:907–918. https://doi.org/10.1016/j.jconrel.2020.10.021
58. Caudill C, et al Transdermal vaccination via 3D-printed microneedles induces potent humoral and cellular immunity. https://doi.org/10.1073/pnas.2102595118/-/DCSupplemental

59. Luzuriaga MA, Berry DR, Reagan JC, Smaldone RA, Gassensmith JJ (2018) Biodegradable 3D printed polymer microneedles for transdermal drug delivery. Lab Chip 18(8):1223–1230. https://doi.org/10.1039/c8lc00098k
60. Jang SJ, et al (2019) Microneedle patterning of 3D nonplanar surfaces on implantable medical devices using soft lithography. Micromachines 10(10). https://doi.org/10.3390/mi10100705
61. Ami Y (2011) Formation of polymer microneedle arrays using soft lithography. J Micro/Nanolithogr MEMS MOEMS 10(1):011503. https://doi.org/10.1117/1.3553393
62. McGrath MG et al (2014) Production of dissolvable microneedles using an atomised spray process: effect of microneedle composition on skin penetration. Eur J Pharm Biopharm 86(2):200–211. https://doi.org/10.1016/j.ejpb.2013.04.023
63. Kim MJ, Park SC, Choi SO (2017) Dual-nozzle spray deposition process for improving the stability of proteins in polymer microneedles. RSC Adv 7(87):55350–55359. https://doi.org/10.1039/c7ra10928h
64. Wang PM, Cornwell M, Hill J, Prausnitz MR (2006) Precise microinjection into skin using hollow microneedles. J Investig Dermatol 126(5):1080–1087. https://doi.org/10.1038/sj.jid.5700150
65. Römgens AM, Bader DL, Bouwstra JA, Baaijens FPT, Oomens CWJ (2014) Monitoring the penetration process of single microneedles with varying tip diameters. J Mech Behav Biomed Mater 40:397–405. https://doi.org/10.1016/j.jmbbm.2014.09.015
66. Ellison TJ, Talbott GC, Henderson DR (2020) VaxiPatch$^{\mathrm{TM}}$, a novel vaccination system comprised of subunit antigens, adjuvants and microneedle skin delivery: an application to influenza B/Colorado/06/2017. Vaccine 38(43):6839–6848. https://doi.org/10.1016/j.vaccine.2020.07.040
67. Menon I, et al (2021) Microneedles: a new generation vaccine delivery system. Micromachines 12(4). MDPI AG. https://doi.org/10.3390/mi12040435
68. Zaric M et al (2013) Skin dendritic cell targeting via microneedle arrays laden with antigen-encapsulated poly- D, l -Lactide- Co -Glycolide nanoparticles induces efficient antitumor and antiviral immune responses. ACS Nano 7(3):2042–2055. https://doi.org/10.1021/nn304235j
69. Yang D, et al (2021) Microneedle-mediated transdermal drug delivery for treating diverse skin diseases. Acta Biomater 121:119–133. https://doi.org/10.1016/j.actbio.2020.12.004
70. Bhatnagar S, Reddy Gadeela P, Thathireddy P, Vamsi Krishna Venuganti V (2019) Microneedle-based drug delivery: materials of construction. 2039. https://doi.org/10.1007/s12039-019-1666-xS
71. Yu W, Jiang G, Zhang Y, Liu D, Xu B, Zhou J (2017) Polymer microneedles fabricated from alginate and hyaluronate for transdermal delivery of insulin. Mater Sci Eng C 80:187–196. https://doi.org/10.1016/j.msec.2017.05.143
72. Chang H, et al (2017) A swellable microneedle patch to rapidly extract skin interstitial fluid for timely metabolic analysis. Adv Mater 29(37). https://doi.org/10.1002/adma.201702243
73. Xie X et al (2017) Analgesic microneedle patch for neuropathic pain therapy. ACS Nano 11(1):395–406. https://doi.org/10.1021/acsnano.6b06104
74. Hong JY et al (2018) Efficacy and safety of a novel, soluble microneedle patch for the improvement of facial wrinkle. J Cosmet Dermatol 17(2):235–241. https://doi.org/10.1111/jocd.12426
75. Kulkarni D et al (2022) Recent advancements in microneedle technology for multifaceted biomedical applications. Pharmaceutics 14(5):1097. https://doi.org/10.3390/pharmaceutics14051097
76. Hirobe S et al (2017) Clinical study of a retinoic acid-loaded microneedle patch for seborrheic keratosis or senile lentigo. Life Sci 168:24–27. https://doi.org/10.1016/j.lfs.2015.12.051
77. Yang J, Liu X, Fu Y, Song Y (2019) Recent advances of microneedles for biomedical applications: drug delivery and beyond. Acta Pharmaceut Sin B 9(3): 469–483. Chinese Academy of Medical Sciences. https://doi.org/10.1016/j.apsb.2019.03.007
78. Mccrudden MTC, Mcalister E, Courtenay AJ, González-Vázquez P, Raj Singh TR, Donnelly RF (2015) Microneedle applications in improving skin appearance. Exp Dermatol 24(8):561–566. Blackwell Publishing Ltd. https://doi.org/10.1111/exd.12723

79. Bariya SH, Gohel MC, Mehta TA, Sharma OP (2012) Microneedles: an emerging transdermal drug delivery system. J Pharm Pharmacol 64(1):11–29. https://doi.org/10.1111/j.2042-7158.2011.01369.x
80. Godin B, Touitou E (2007) Transdermal skin delivery: Predictions for humans from in vivo, ex vivo and animal models. Adv Drug Deliv Rev 59(11):1152–1161. https://doi.org/10.1016/j.addr.2007.07.004

An Economical and Efficient Method for the Fabrication of Spiral Micromixer

Ekta Tripathi, Pallab Sarmah, Promod Kumar Patowari, and Sukumar Pati

Abstract Micromixers have been widely used due to its vast applications in biological, chemical, electronics, and mechanical fields. Micromachining through common fabrication methods is a challenging issue, therefore it is emerging as the latest research area. This work presents the rapid and cost-effective method of micromixer fabrication. It includes two steps of fabrication. Initially, a mold of spiral micromixer is fabricated on an aluminum workpiece using wire electrical discharge machining (Wire-EDM). In the Wire-EDM process, molybdenum wire of diameter 180 μm is used as a tool electrode. Pulse-on-time (T_{on}) of 15 μs, pulse-off-time (T_{off}) of 6 μs, peak current (I_P) of 4 A and table feed (S) of 55.6 m/s are set as the cutting parameters. After machining the mold, in the second step final micromixer is fabricated using soft lithography technique with poly-di-methyl-siloxane (PDMS). It is confirmed by visualizing the flow inside the fabricated micromixer that a spiral micromixer may be used for mixing for various applications.

Keywords Spiral · Micromixer · WIRE EDM · PDMS · Soft lithography

1 Introduction

Micromixing has grown rapidly during the past few decades due to the developments in the MEMS and microfluidics fields. Microfluidic chips have gained popularity due to the growing demand for automatic and rapid agricultural, biomedical, and environmental screening. These chips demand micromixing to carry out lab-on-chip biomedical tests [1]. Active micromixers use an external source, such as an electric field, magnetic field, acoustic field, etc., to initiate the mixing of two fluids, whereas passive micromixer does not require external means for mixing. It utilizes pressure energy to

---

E. Tripathi (✉) · P. Sarmah · P. K. Patowari · S. Pati
Department of Mechanical Engineering, National Institute of Technology Silchar, Silchar, Assam, India
e-mail: ekta_rs@mech.nits.ac.in

K. Guha et al. (eds.), *MEMS and Microfluidics in Healthcare*, Lecture Notes in Electrical Engineering 989, https://doi.org/10.1007/978-981-19-8714-4_10

mix the fluids in the microchannel [2–4]. Fabrication of passive micromixers is easy because they are less sophisticated and require only the introduction of grooves or modification of the curvature, which can enhance mixing [5–9]. To increase mixing efficiency, chaotic advection or secondary flows are generated in various innovative designs of micromixers such as sinusoidal, square wave, zigzag, spiral, split, and recombine micromixers [10–14]. Regardless of the Reynolds number, spiral micromixers offer superior mixing than serpentine and straight channels [15].

The ever increasing demand for these microchannel devices has shifted the focus of the researchers towards developing less time-consuming, accurate, and precise microchannels. Microfluidic devices are generally fabricated on glass, metals, polymers, or silicon-based materials as per the need for biomedical, electronic, and mechanical-related applications. However, it is a difficult task to fabricate these micromixers because of the required precision. Many fabrication techniques have been developed to fabricate the channel, such as laser ablation, 3D printing, photolithography, and etching [16–19].

Wangikar et al. fabricated microchannel molds having obstacles using photochemical machining on copper and brass. First, control parameters such as etchant concentration, etching temperature, and time are optimized to get high material removal rate, low surface roughness, and low edge deviation. The mold is fabricated with the optimized value of the control parameters [19]. Arockiam et al. [20] fabricated serpentine micromixers having a width of 700 μm on the glass slide. The microchannel design was cut from the double-sided polymer-based adhesive tape which was sandwiched between two glass slides. Tarlet et al. [21] used laser stereolithography for mold fabrication having a width of 1.1 mm and soft lithography for channel fabrication. Mondal et al. [22] also fabricated serpentine microchannel using wire electric discharge machining (Wire-EDM) and soft lithography technique and suggested that WEDM could be useful for fabricating the channel with accurate dimensions.

It is established from the literature study that various attempts have been made to fabricate the micromixer using the non-traditional machining process. However, no significant work has yet been presented for the fabrication of a micromixer with a spiral shape. It motivates the authors to fabricate the spiral micromixer using CNC Wire-EDM mold. Wire-EDM is a non-traditional machining process that provides higher accuracy with a faster production rate [22]. It is a commonly used machine for cutting, so it can be easily accessed in any manufacturing laboratory to cut mold. Thus, in this work, an attempt has been made to fabricate the PDMS micromixer by soft lithography technique using a mold machined by Wire-EDM. A computational study on a spiral micromixer is first presented at $\mathrm{Re} = 100$, and then the detailed methodology of fabrication of the spiral micromixer using the Wire-EDM process and soft lithography technique is suggested. Wire-EDM is used to fabricate the mold, whereas the soft lithography process is used to fabricate the PDMS micromixer.

2 Design and Computational Study

The schematic design for the spiral micromixer is presented in Fig. 1. Two fluids (water and water-dye) enter into the main channel through Y joining. The width and depth of the channel are kept at 0.6 mm each. Fluids flow through a straight section of 3 mm and then through spiral sections of different radii of curvatures. The minimum and maximum radii of curvature of the spiral sections are 1 mm and 4.1 mm, respectively.

To observe the efficiency of the desired micromixer at higher Reynolds numbers, a computational study is performed in ANSYS-fluent software at Re = 100. N-S and mass transfer equations are solved by considering various boundary conditions for obtaining the velocity and concentration field continuity. Laminar and species transport model is selected. At the mixer wall, outlet, and inlets, no-slip boundary conditions, atmospheric pressure, and uniform velocities are applied respectively. The mass fractions of water in inlet 1 is 1, and in inlet 2 is 0. The SIMPLE algorithm is utilized for the pressure and velocity coupling for the simulation. The relative convergence criteria are selected as 10^{-5}. The mixing index (M) is calculated as follows [11–13],

$$M = 1 - \sqrt{\frac{1}{N}\sum_{J=1}^{N}\left(\frac{C_J - \overline{C}}{\overline{C}}\right)^2} \tag{1}$$

where N is the number of sampling points, C_J and $\overline{C}$ are normalized concentration and expected normalized concentration, respectively.

After performing the mesh independent test, 2,733,430 elements are selected to perform numeric simulations. Mixing characteristics are analyzed in the spiral micromixer through computational study. Figure 2 shows the concentration contours of water in the micromixer. The blue color denotes water (concentration = 1), whereas

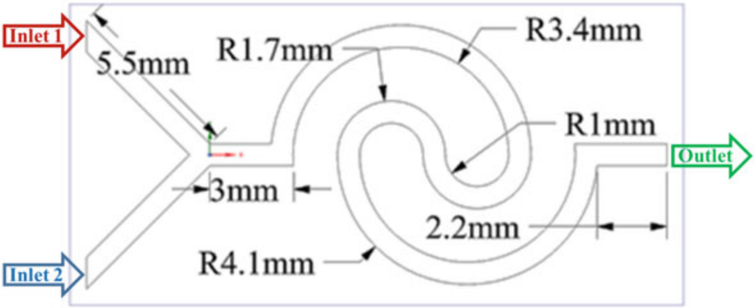

Fig. 1 Schematic diagram of spiral micromixer

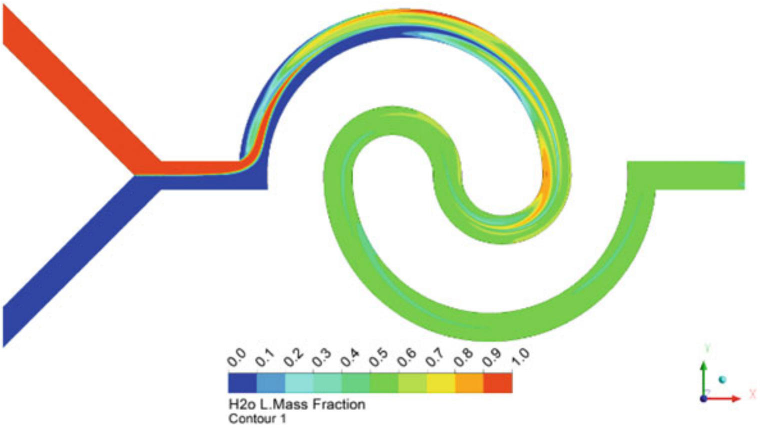

Fig. 2 Representation of concentration contour of water in spiral micromixer

red denotes water dye (concentration = 0). Green color (concentration = 0.5) represents the complete mixing. When fluid flows through any curve trajectory, it experiences the centrifugal force, leading to the generation of transverse dean flows. The dimensionless Dean number ($De = x^{0.5} Re$, where x is the ratio of the hydraulic radius of the channel and radius of curvature; Re is Reynolds number) is used as a measurement parameter for these flows. Due to these centrifugal forces, induced secondary forces generate a vortex in the fluid flow, promoting the mixing. Hence, from Fig. 2, 86.7% mixing of fluids at the outlet is observed at Re = 100. Microchannels providing more than 85% mixing can be used for practical applications [7].

3 Experimental Procedure

After confirming the mixing effectiveness of the micromixer, it is fabricated using Wire-EDM and soft lithography techniques. The fabrication of the micromixer is done in the order of: (i) mold fabrication using Wire-EDM and (ii) micromixer fabrication using soft lithography technique.

3.1 Mold Fabrication Using Wire-EDM

Wire-EDM is used to create the mold for the proposed micromixer. To create the profile, the design is first created with the required dimensions in the RR CAM plug-in software of CNC unit of the Wire-EDM machine. It is then converted into a machine file (.rrw) for profile cutting. Aluminum (Al) is chosen as the material for the workpiece, while a molybdenum wire of a diameter of 180 µm is used as a

Table 1 Set of process parameters

Parameter	Pulse-on-time (T_{on})	Pulse-off-time (T_{off})	Peak current (I_P)	Table feed (S)	Wire diameter
Value	15 μs	6 μs	4 A	55.6 μm/s	180 μm

tool electrode. Based on the different pilot experiments, the process parameters are chosen to cut the spiral profile as tabulated in Table 1. The photographic image of the mold for spiral micromixer cut by Wire-EDM machine is shown in Fig. 3. The dimensions of the fabricated mold are observed using an optical microscope. The average width of the spiral channel after machining is 603.32 μm, whereas the other measured dimensions are shown in Table 2. The obtained dimensions show less than a 3% average deviation from the required dimensions (Fig. 4).

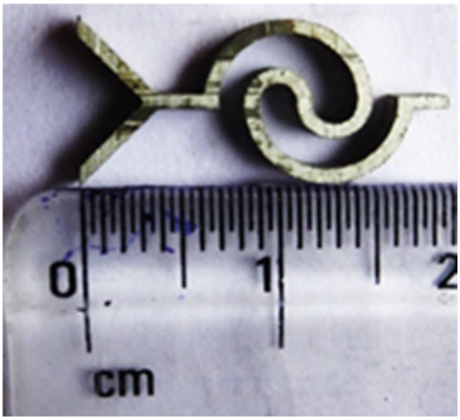

Fig. 3 Photographic image of spiral mold fabricated in Wire-EDM

Table 2 Comparison of required and obtained dimensions with percentage deviation

	Desired dimensions (μm)	Obtained dimensions (μm)	% deviation
L1	5500	5378.45	2.2
L2	3000	2890.604	3.6
R1	3400	3508.419	3.1
R2	1100	1104.77	0.4
R3	1700	1646.78	3.1
R4	4100	4153.994	1.3
L3	2000	1906.687	4.6

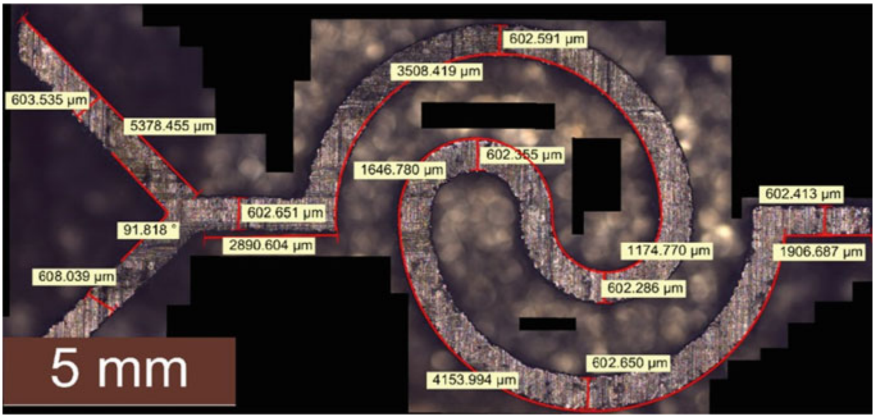

Fig. 4 Microscopic image of mold fabricated in Wire-EDM

3.2 Spiral Micromixer Fabrication Through Soft Lithography Technique

After fabricating the mold, it is the time to fabricate the micromixer by casting it with PDMS in the following steps. PDMS mixture is initially prepared in a beaker by combining Silicone Elastomer base and curing agent in a mass proportion of 1:10. Weight of these two materials is measured in precision analytical balance. Manual stirring of the mixture is done for about 10–15 min for proper mixing. While mixing, air bubbles get trapped inside the mixture. It is necessary to remove these bubbles. For this purpose, the mixture is held in a vacuum desiccator for almost an hour. The mold is kept inside the small square glass container where the mixed solution is poured. After that, it is kept in an open atmosphere for 24−30 h to let the mixture solidify. The PDMS microchannel is then removed from the master mold. A continuous microchannel with fine edges and accurate dimensions is obtained as shown in Fig. 5a. Then, inlet and outlet holes are punched through the PDMS microchannel using biopsy punch. However, it is open from one side. A closed microchannel is essential to observe the fluid flow inside the mixer. So, one more sheet of PDMS is needed to be prepared to cover it. Therefore, a fine sheet of PDMS solution is prepared and left in an open atmosphere for 8–10 h. The prepared one-sided open PDMS microchannel is glued to it when it is in semi-solidified condition. It is again put in an open atmosphere for 20–24 h for drying. After bonding, the final spiral PDMS micromixer is ready for use and which is shown in Fig. 5b. Thus, the spiral micromixer is successfully fabricated using mold fabricated by wire-EDM.

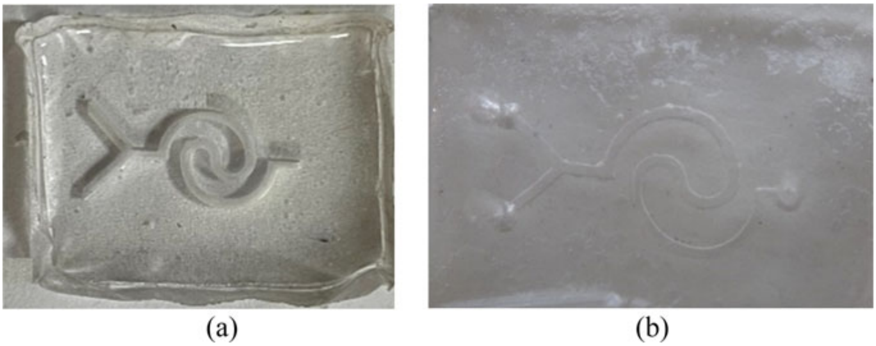

Fig. 5 **a** Open-sided spiral micromixer, **b** Final spiral PDMS micromixer

3.3 *Flow Visualization in the Fabricated Spiral Micromixer*

To check the functionality of the fabricated PDMS micromixer, fluid flow is visualized in it, as shown in Fig. 6. A twin syringe pump is used for delivering the fluids inside the channel. To conduct the experiment, water is used as an inlet fluid. As it is a colorless fluid, blue and red colors are added to it for better visualization. Water with red and blue colors is injected from the syringe into the micromixer. As seen from the inset of Fig. 6, red and blue color fluids are observed in the inlets whereas, in the outlet, dark violet color is seen. The dark violet color at the outlet depicts the proper mixing of fluids which is also depicted through computational analysis as observed in Fig. 2.

Fig. 6 Experimental arrangement for flow visualization

4 Conclusion

In this work, the spiral micromixer of PDMS is successfully fabricated using the soft lithography method with the mold machined by Wire-EDM. The mold is machined on an aluminum workpiece using a molybdenum wire of 180 μm at the parametric conditions as T_{on} of 15 μs, T_{off} of 6 μs, I_P of 4 A, and S of 55.6 m/s. The observed machining time is 4.2 min. The average deviation between obtained and desirable dimensions is less than 3%. The precision of the mold determines the accuracy of the micromixer. So, through Wire-EDM, it is possible to manufacture mold with accurate dimensions. Finally, in the fabricated PDMS micromixer, flow is visualized, confirming the micromixer's functionality in various applications.

References

1. Prakash S, Kumar S (2015) Fabrication of microchannels: a review. Proceedings of the Institution of Mechanical Engineers, Part B: Journal of Engineering Manufacture 229(8):1273–1288
2. Bayareh M, Ashani MN, Usefian A (2020) Active and passive micromixers: A comprehensive review. Chem Eng Process-Process Intensif 147:107771
3. Mondal B, Mehta SK, Pati S, Patowari PK (2021) Numerical analysis of electroosmotic mixing in a heterogeneous charged micromixer with obstacles. Chem Eng Process-Process Intensif 168:108585
4. Mehta SK, Pati S, Mondal PK (2021) Numerical study of the vortex-induced electroosmotic mixing of non-Newtonian biofluids in a nonuniformly charged wavy microchannel: Effect of finite ion size. Electrophoresis 42(23):2498–2510
5. Qin Y (2010) Micromanufacturing engineering and technology. William Andrew. The fabrication of micromixers is challenging task using conventional manufacturing processes
6. Sarma P, Patowari PK (2016) Design and analysis of passive Y-type micromixers for enhanced mixing performance for biomedical and microreactor application. J Adv Manuf Syst 15:161–172
7. Das SS, Patawari BK, Patowari PK, Halder S (2014) Computational analysis for mixing of fluids flowing through micro-channels of different geometries. In: 5th international & 26th all India manuf
8. Mondal B, Pati S, Patowari PK (2019) Analysis of mixing performances in microchannel with obstacles of different aspect ratios. Proceedings of the Institution of Mechanical Engineers, Part E: Journal of Process Mechanical Engineering 233(5):1045–1051
9. Tripathi E, Patowari PK (2020) Design and computational analysis of spiral microchannel for mixing of fluids. In: Techno-Societal 2018. Springer, Cham, pp. 305–313
10. Mondal B, Mehta SK, Patowari PK, Pati S (2019) Numerical study of mixing in wavy micromixers: comparison between raccoon and serpentine mixer. Chem Eng Process-Process Intensif 136:44–61
11. Tripathi E, Patowari PK, Pati S (2021) Numerical investigation of mixing performance in spiral micromixers based on Dean flows and chaotic advection. Chem Eng Process-Process Intensif 169:108609
12. Tripathi E, Patowari PK, Pati S (2022) Mixing characteristics and pressure drop analysis in a spiral micromixer. In: Proceedings of the institution of mechanical engineers, Part E: Journal of process mechanical engineering, p.09544089221095636
13. Bahrami D, Bayareh M (2022) Experimental and numerical investigation of a novel spiral micromixer with sinusoidal channel walls. Chem Eng Technol 45(1):100–109

14. Tripathi E, Patowari PK, Pati S (2022) Numerical investigations of mixing performance in split and recombine micromixer. In: Recent advances in manufacturing modelling and optimization. Springer, Singapore, pp121–129
15. Tripathi E, Patowari PK, Pati S (2021) Comparative assessment of mixing characteristics and pressure drop in spiral and serpentine micromixers. Chem Eng Process-Process Intensif 162:108335
16. Tripathi E, Patowari PK, Pati S (2019) December. Fabrication of spiral micromixer using mold machined by CO2 assisted laser machine. In: 11th international conference on precision, meso, micro and nano engineering (COPEN 11). IIT Indore, pp. 12–14
17. Tachibana D, Matsubara K, Matsuda R, Furukawa T, Maruo S, Tanaka Y, Fuchiwaki O, Ota H (2020) 3D helical micromixer fabricated by micro lost-wax casting. Advanced Materials Technologies 5(1):1900794
18. Mondal B, Pati S, Patowari PK (2020) Fabrication of wavy micromixer using soft lithography technique. Materials Today: Proceedings 26:1271–1278
19. Das SS, Patowari PK (2018) Fabrication of serpentine micro-channels on the glass by ultrasonic machining using developed micro-tool by wire-cut electric discharge machining. Int J Adv Manuf Technol 95:3013–3028
20. Arockiam S, Cheng YH, Armenante PM, Basuray S (2021) Experimental determination and computational prediction of the mixing efficiency of a simple, continuous, serpentine-channel microdevice. Chem Eng Res Des 167:303–317
21. Tarlet D, Fan Y, Luo L (2020) Design and mixing performance characterization of a mini-channel mixer with nature-inspired geometries. Chem Eng Res Des 164:230–239
22. Mondal B, Pati S, Patowari PK (2021) Serpentine square wave microchannel fabrication with WEDM and soft lithography. Materials Today: Proceedings 46:8513–8518
23. Debnath T, Patowari PK (2019) Fabrication of an array of micro-fins using Wire-EDM and its parametric analysis. Mater Manuf Processes 34(5):580–589

Damping Estimation and Analysis for High Performance Inertial MEMS for Early Detection of Neurological Disorders During Pregnancy

Sonali Biswas, Anup Kumar Gogoi, and Moushumi Biswas

Abstract High performance inertial MEMS require appropriate damping estimation and control. In any MEMS device, the ratio of the surface area to volume is large for which we need to do dynamic performance analysis. Inertial MEMS sensors find its suitability in varied applications and bio-motion sensors are no exception. One of such low frequency applications is the early detection of neurological disorders, targeted specially for pregnant women suffering from tremors, epilepsy and seizures. It becomes very important to capture the most feeble tremor (0 g) to a sudden jerk (±6 g) where the person usually falls. During Pregnancy, most of the drugs for curing neuro-disorders are not suitable to be consumed. Therefore, high performance micro-sensors are required for early detection of tremors (2−12 Hz) and seizure (0.5−29 Hz). An attempt has been made to design a micro sensor with adequate damping estimation by comparing it with the existing models. The proposed MEMS sensor simulated for the target application has an air gap of 23.5 μ which produces around 0.7 damping ratio. Finally, time dependent analysis is done by comparing both with intended damping and very low damping value. We obtain smooth characteristics for the intended damping and overriding oscillations appear for very low damping. Hence, the proposed inertial MEMS sensor has a dynamic range of ±6 g, frequency range of 0−25 Hz and damping ratio of 0.7. Therefore, the proposed microsensor makes it suitable for early detection of neurological disorders especially during pregnancy addressing maternal health care.

Keywords Inertial MEMS · Dynamic · Damping · Neurological · Tremor · Seizures

---

S. Biswas (✉)
Jorhat Engineering College, Assam Science and Technology University, Jorhat, India
e-mail: sonali.vclass@gmail.com

A. K. Gogoi
Indian Institute of Technology Guwahati, Amingaon, Guwahati, India
e-mail: akg@iitg.ac.in

M. Biswas
Silchar Medical College and Hospital, Silchar, India
e-mail: moushumidr@gmail.com

K. Guha et al. (eds.), *MEMS and Microfluidics in Healthcare*, Lecture Notes in Electrical Engineering 989, https://doi.org/10.1007/978-981-19-8714-4_11

1 Introduction

Inertial MEMS require adequate damping control for high performance applications [1]. The performance enhancement of inertial sensors is of utmost importance for diagnosing neurological disorders especially during pregnancy. Pregnancy is the most important and beautiful phase in the life of every woman. This crucial period can however be critical if some of the neurological disorders of the mother, which need urgent attention remain undetected. Therefore, early diagnosis of some of the deadliest neurological disorders becomes very essential to preserve the health of both the mother and the baby which can be fatal during this period. The focus of this research is early detection of some neurological disorders like epilepsy, parkinsons, etc. where tremor of very low frequency occurs. Tremor is basically roughly sinusoidal in nature. It may be mentioned that tremor occurs in frequency from 0.5 to 12 Hz and its causes may be many [2]. During pregnancy, the tremor action can occur at almost 0−6 g signifying jerks. Moreover, during this period some women have convulsions for the first time. There may be many factors which can trigger seizure, out of which hormonal changes, water retention and stress are the most common. The combination of any neurological disorder and pregnancy is very risky and fatal. There are certain drugs available for neuro-degenerative disorders for balancing the hormone levels but such doses are rarely preferred both by patients and medical practitioners to avoid risks. This is mainly because the physical health does not support all types of medications. Also, the EEG procedure requires a longer time with a large number of electrodes on the skull which adds to one’s discomfort. Thus, early diagnosis requires continuous monitoring. Such wearable sensors must be small and light weight and can measure low frequency range and must have high performance w.r.t sensitivity and resolution [3].

There may be several aspects of design modification to cater to a particular application, out of which adequate damping control is very important for high performance applications. In fact, damping is the most critical aspect one has to investigate for high performance device design [4, 5]. It is very important for micro-sensors to have a fine control of gap dimensions. Many Researchers have been working on several aspects of Squeeze film damping. Blech has studied adiabatic processes [4, 5]. Starr was the first to suggest damping control in solid-state inertial sensors [6]. The squeeze film detail was given by Bao [1]. Renolds equation is mainly used for the analysis [4, 7]. Different Researchers have proposed various Mathematical models for determining damping [7–9]. Investigations are focussed mainly onthe assumption of correct damping coefficient and damping ratio, for high performance MEMS applications.

Therefore, estimation of correct damping ratio becomes very important. Hence an attempt has been made to design an inertial micro sensor of low frequency range from 0.1 to 25 Hz and ±6 g by estimating its damping for appropriate dynamic behaviour.

2 Theoretical Background

Acceleration can be determined by Inertial MEMS sensor in terms of displacement. Thus, the equation of motion can be written in terms of Eq. 1 [11]. Here m is the mass, z is the displacement, ζ is the damping ratio, ω_n is the natural frequency. It is the damping ratio and natural frequency which determines the dynamic behavior [11].

$$\ddot{z} + 2\varsigma\omega_n\dot{z} + \omega_n^2 z = -a \tag{1}$$

$$\omega n = \sqrt{\frac{k}{m}} \tag{2}$$

$$\varsigma = \frac{c}{c_c} \tag{3}$$

Here C and Cc are the damping coefficient and the critical damping coefficient respectively.

We have the transfer function that can be written as

$$H(s) = \frac{\omega_n^2}{s^2 + 2\varsigma\omega_n s + \omega_n^2} \tag{4}$$

In this system underdamped means $\zeta < 1$ and Fig. 1 shows the settling time and overshoot.

The time history of the step response of a second-order system found from the inverse Laplace transform of H(s)/s is given as [1]

Fig. 1 Underdamped second-order response with settling time and overshoot [11]

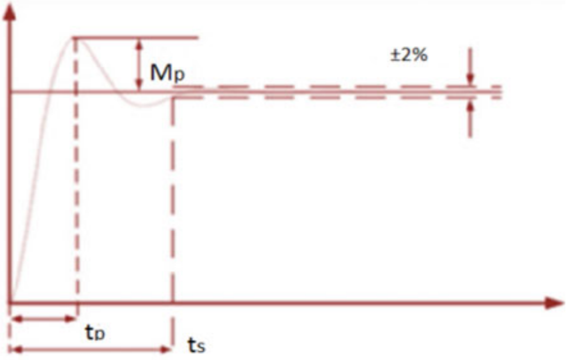

$$z(t) = 1 - \frac{1}{\sqrt{1-\varsigma^2}} e^{-\varsigma \omega_n t} \mathrm{Sin}(\omega_d t + \beta) \tag{5}$$

where ω_d and β are the damped frequency of oscillation and phase lag respectively.

By taking the derivative of Eq. (5) and equating to zero we obtain Mp, the Maximum Overshoot [11].

$$Mp = e^{-\frac{\pi\zeta}{\sqrt{1-\zeta^2}}} \tag{6}$$

Taking logarithm on both sides of Eq. (6) we obtain the damping ratio [11]

$$\zeta = \frac{|\ln Mp|}{\pi^2 + |\ln(Mp)|^2} \tag{7}$$

The peak time is given by [11]

$$tp = \frac{\pi}{\omega_d} \tag{8}$$

2.1 Damping Ratio Estimation for High Performance MEMS Device

The damping ratio is one of the most important parameters of inertial sensors. The device geometry, pressure, density and fluid viscosity decide the damping. The damping ratio should limit its value such that the device should not collapse nor the system becomes too slow and sluggish. Appropriate damping gives a very good frequency response.

The basic mechanism of air damping for micromechanical devices mainly are of two types viz. (1) squeeze film (2) slide film.

2.2 Squeeze Film Damping

When the thin film of air which is trapped in the gap interacts with the proof mass, then the squeeze damping occurs as shown in Fig. 2 [10].

The prediction of damping coefficient is based on some theoretical models for a given geometry and other related parameters. Different models provide damping coefficients of different levels of precision [4, 7, 9].

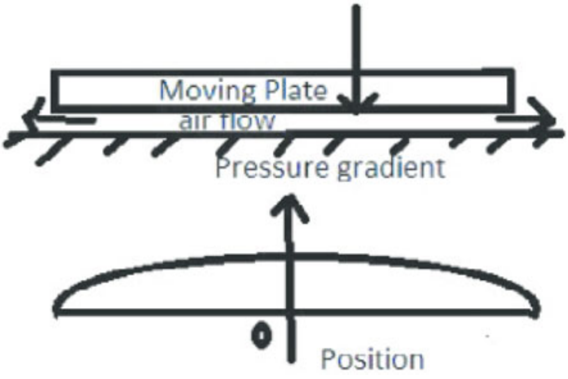

Fig. 2 Squeeze film damping phenomenon

3 Damping Analysis of the Proposed Structure

3.1 Estimation of the Damping Ratio

In any micro inertial sensor, the necessary damping is provided by the gas in the gap between mass and encapsulation. Mostly the intended value of the damping ratio which gives stability is 0.6−0.7. Here, the gap is designed to obtain the value of damping ratio of 0.7. For different models proposed in literature, the degree of accuracy varies. The geometry chosen was of area 3200 × 3200 μm, with a height of 250 μm.

3.2 Time Domain Analysis of the Microstructure

The Time Domain Analysis was done for sinusoidal input for different types of damping. The total response characteristic is the summation of both steady state and transient response.

4 Results and Discussion

The damping estimation and analysis are carried out by simulating the proposed quad geometry having a proof mass height of 250 μm using software COMSOL. The specifications and boundary conditions when given as input and simulated squeeze film damping results in a pressure distribution which gives an air gap dimension of 18.6 μm. Then with this gap height, the damping coefficient is obtained using the models proposed by Blech [4], Veijola [7] and Andrew [9] and also obtained by

Table 1 Damping ratio for different air gap heights

Height of the air gap(μm)	From simulations
18.6	≥1
23.5	0.69
30	0.31

simulation. It was observed that for the air gap height of 18.6 μm, the damping ratio obtained was greater than 1 which was not desirable. This is because we know for an almost flat and stable response characteristic damping ratio should be around 0.7. We then tried to simulate by increasing the thickness of gap height in steps as shown in Table 1 and finally obtained the desired damping ratio near to 0.7 for a gap height dimension of 23.5 μm. We, therefore, propose the air gap height design dimension of 23.5 μm as it gives the desired damping ratio. Thus, we can conclude that damping is controlled by the dimension of the air gap height chosen in the design and we need to design the air gap height for obtaining the necessary damping.

Also, as we know that Squeeze film damping effect is the interaction of the silicon proofmass and the air gap, so an attempt was made to obtain the air gap height by doubling the height of the proofmass (500 μm). In this case, the simulated air gap obtained was 16.6 μm for which we got a damping ratio of 0.7. From which we can conclude that by varying the height of the proofmass the air gap can be controlled to achieve the desired damping ratio.

The simulation results of displacements versus time and total force versus time are obtained for different air gap heights.

The simulation when done for the air gap height of 18.6 μm, we obtain the displacement time graph as shown in Fig. 3 and the total force versus time is shown in Fig. 4. From the response characteristic, we observe that for the chosen dimension of air gap height, the damping ratio obtained was greater than 1. This shows an overdamped behaviour where the response very slowly tries to reach the equilibrium.

So, we can conclude that we need to lower the damping ratio in our case and for this, we need to make necessary design modifications.

Next, we increase the height of the air gap to 23.5 μm and simulate it to obtain the displacement time graph as shown in Fig. 5 and the total force versus time is shown in Fig. 6. In this case, we obtain a damping ratio of almost 0.7 which is desirable as it offers a higher response time, fast settling time and good stability. The response clearly shows that there is initially some overshoot and then slowly it settles down. Therefore, we conclude that the air gap height in the proposed sensor should be designed as 23.5 μm in order to have a control over the damping and maintain the damping ratio as 0.7.

On further increasing the air gap height to 30 μm we obtain the displacement time graph as shown in Fig. 7 and the total force versus time characteristic is plotted in Fig. 8. The response characteristic shows that there is a higher amplitude and after two overshoots it settles down. Therefore, the damping ratio of 0.31 is not suitable for the design as the amplitude is very high and will not produce a flat response.

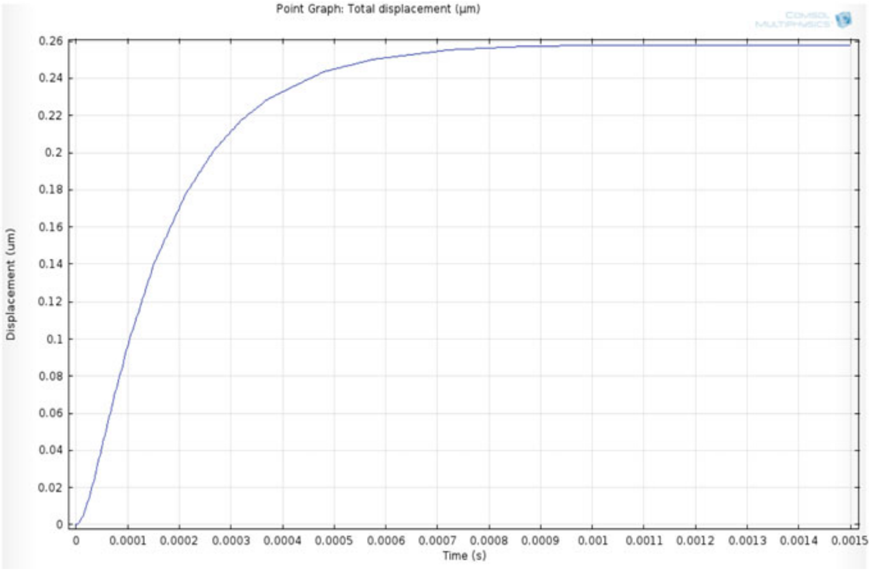

Fig. 3 The characteristic graph for displacement obtained with air gap height of 18.6 µm

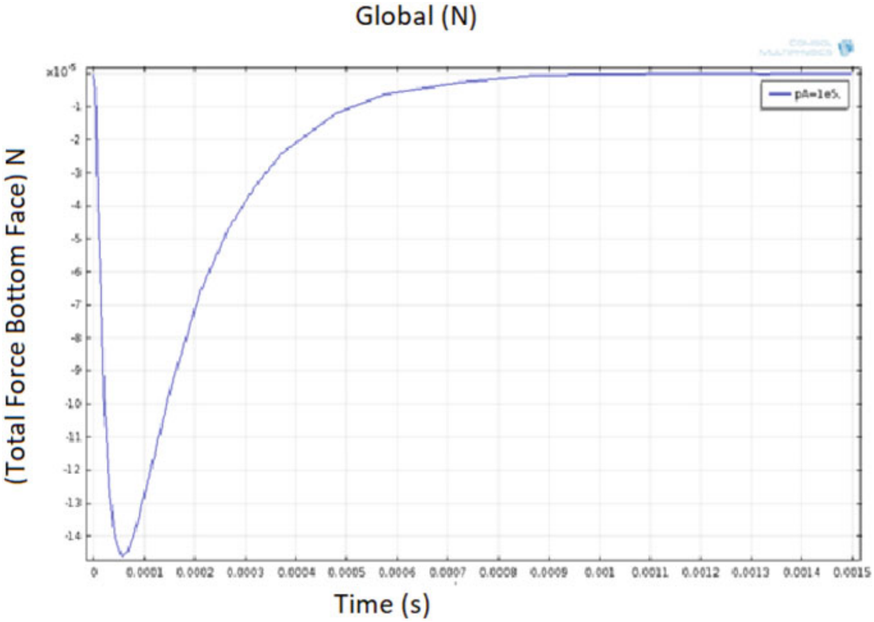

Fig. 4 Dynamic characteristics with air gap dimension of 18.6 µm

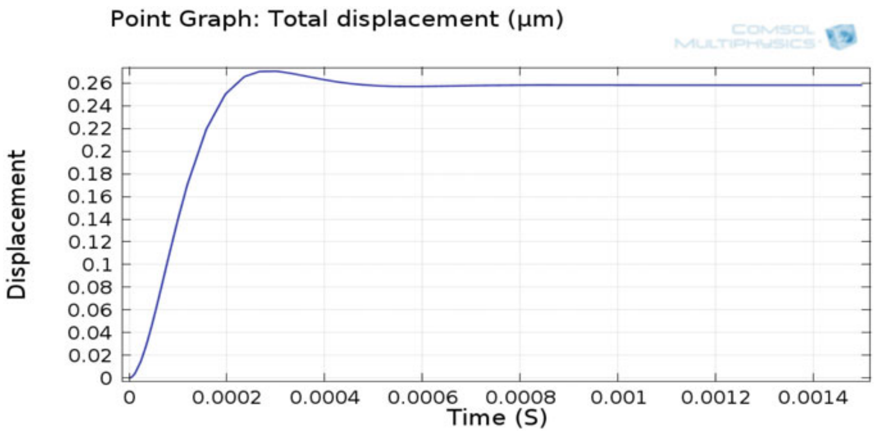

Fig. 5 The characteristic graph for displacement obtained with air gap height of 23.5 µm

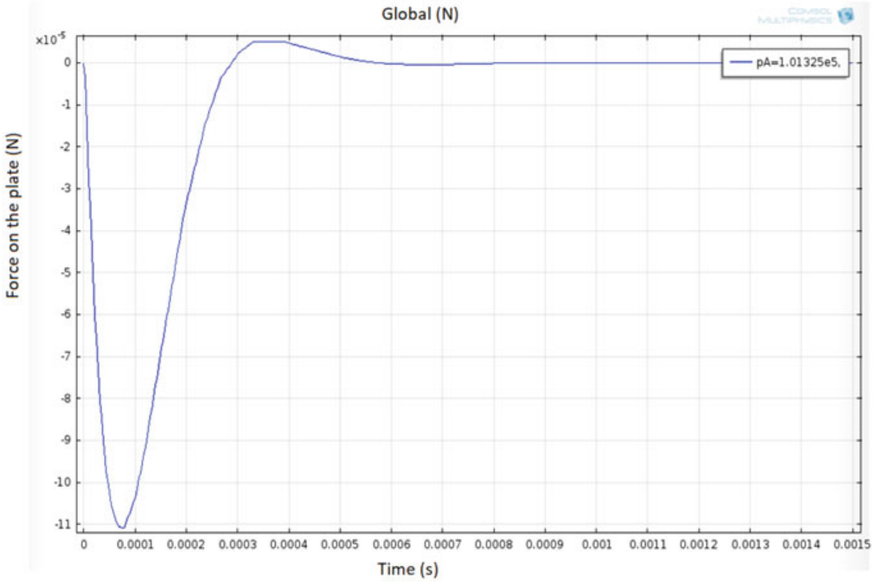

Fig. 6 Dynamic characteristics with air gap dimension of 23.5 µm

Finally, the dynamic characteristic is obtained for both low damping value and the estimated damping value as shown in Fig. 9 and Fig. 10. It is observed that a smooth response is obtained with the estimated damping as shown in Fig. 10, as compared to the one obtained with the very low damping as shown in Fig. 9.

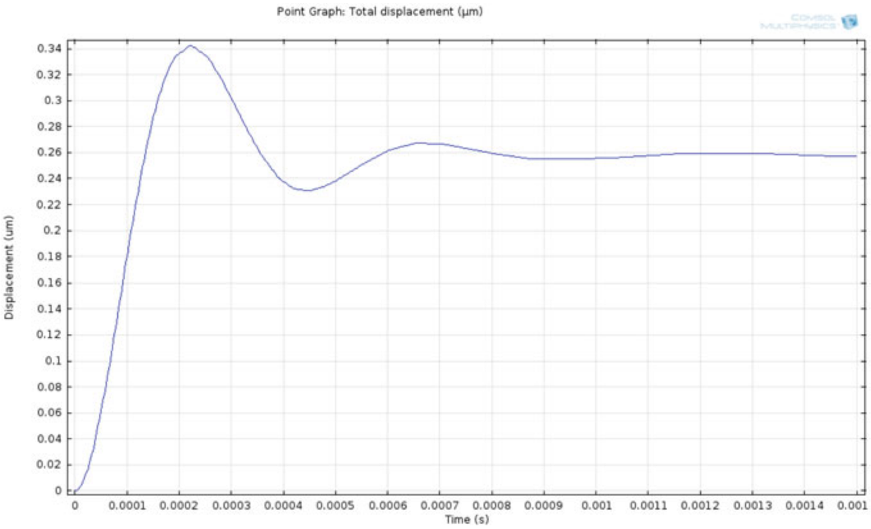

Fig. 7 The characteristic graph for displacement obtained with air gap height of 30 µm

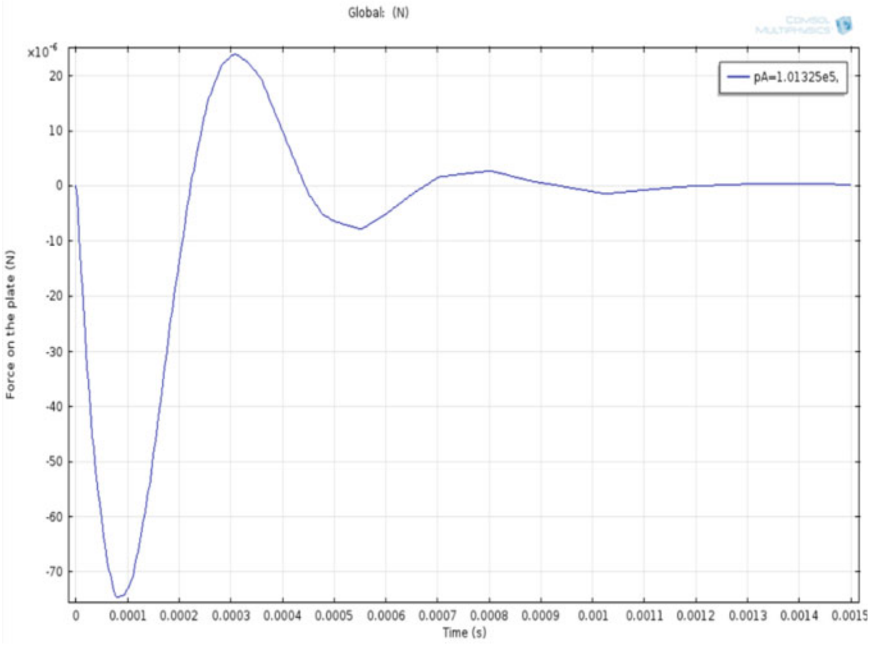

Fig. 8 Dynamic characteristics with air gap dimension of 30 µm

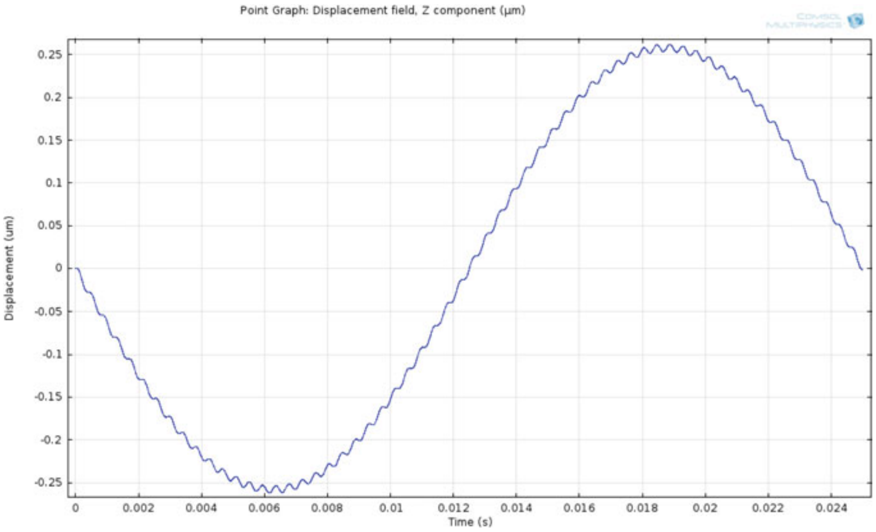

Fig. 9 Dynamic characteristic for very low damping value

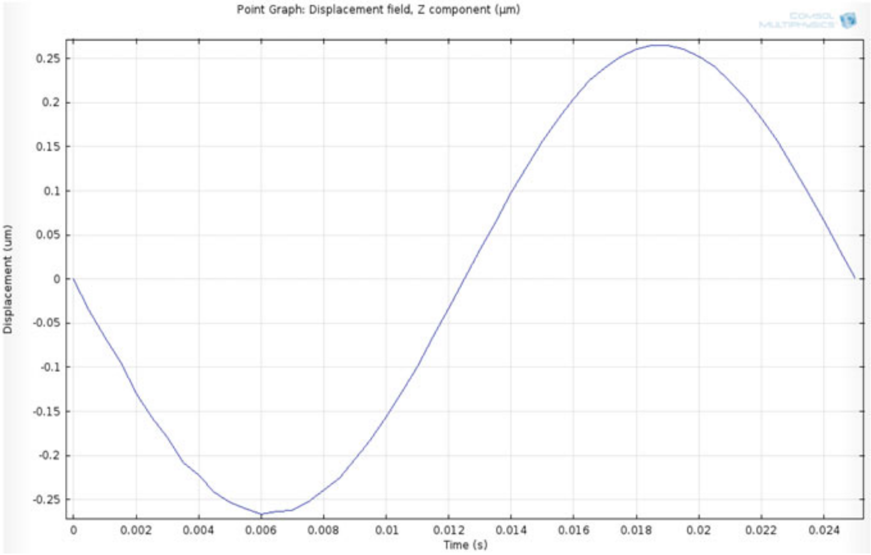

Fig. 10 Dynamic characteristic for estimated damping value

5 Conclusion

A detailed analysis of the damping aspects for the proposed MEMS inertial sensor for a low frequency range of 0−25 Hz has been carried out. It has been shown that for a thin film height of 23.5μ, the desired damping ratio of around 0.7 is achieved. The time domain analysis obtained through simulation reveals very smooth characteristics for sinusoidal input with the intended damping value whereas it shows overriding oscillations for very low damping. Thus, high performance design of MEMS sensors can be achieved by appropriate damping control.

From simulations, we also conclude that the air gap height can be varied by changing the height of the proof mass. Thus, by varying the height of the proofmass, the air gap can be controlled to achieve the desired damping.

Therefore, the proposed design with appropriate damping can be suitably used for sensing low g acceleration value (0 to ± 6 g), diagnosing feeble tremors to sudden jerks in case of neurological disorders especially during pregnancy. Thus, early diagnosis of such disorders with the help of high performing micro inertial sensors ensures safety for both the mother and the baby.

Acknowledgements I would like to thank IIT Guwahati for providing the research facilities and the doctors/Associate Professors from Silchar Medical College, Assam India, namely Dr. Moushumi Biswas and Dr. Debajit Das for helping me with medical related works. I got to know more on pathological tremor and other neurological disorders specially for Pregnant woman. Dr. Biswas is an expert in Community medicine and has immense contribution towards society specially in rural areas. I would like to thank her specially for arranging my visit to Guwahati Medical and Silchar Medical for case studies.

References

1. Bao M, Yang H (2007) Squeeze film air damping in mems. Sens Actuators, A 136:3–27
2. Marsden C, McAuley J (2000) Physiological and pathological tremors and rhythmic central motor control. J Neurology, Brain 123 (8), 1545–1567
3. Biswas S, Gogoi AK (2018) Design of a Piezoresistive Microaccelerometer with High Sensitivity for Medical Diagnostic, In proc. Advances in Systems, Control and Automation, Lecture Notes in Electrical Engineering, Singapore: Springer 442:481–490
4. Blech JJ (1983) On isothermal squeeze films, vol105. p 615
5. Lu Q, Fang W, Wang C et al (2021) Investigation of a complete squeeze-film damping model for MEMS devices. MicrosystNanoeng 7:54. https://doi.org/10.1038/s41378-021-00279-6
6. Starr JB (1990) Squeeze-film damping in solid-state accelerometers. In: 4th Technical digest on solid-state sensor and actuator workshop. pp. 44–47
7. Veijola T (2006) Analytic damping model for an mem perforation cell, vol 2. pp 249–260
8. Griffin WS, Richardson HH, Yamanami (1966) A study of fluid squeeze-film damping, vol 88.
9. Sumali H (2007) An experiment to determine the accuracy of squeeze-film damping models in the free molecule regime. In: ASME International mechanical engineering congress and exposition. J Micro Nano systems, Parts A and B 11

10. Biswas S, Gogoi AK (2018) Squeeze film damping control of a piezoresistive micro accelerometer for neurological disease diagnosis. In: Proceedings of Euromech conference of dynamics of micro and nano electromechanical systems multifield modelling and analysis
11. Chang L (2006) Piezoresistive sensors, Foundation of MEMS. NG Prentice Hall

Affinity Biosensing: Modeling of Adsorption Kinetics and Fluctuation Dynamics

Olga Jakšić

Abstract A vast number of processes that are crucial for biosensing in microfluidic MEMS devices for health applications are based on affinity bonding between analyte biomolecules and functionalized adsorption sites. Whether it is applied for the development of new drug discovery or new sensors for point of care devices, the final design relies greatly on modeling these interactions. This chapter aims to present a compendium of models used for the representation of these interactions. It addresses modeling in time and frequency domain, from a deterministic and from a stochastic point of view, with respect to monocomponent and multicomponent monolayer adsorption in microfluidic MEMS devices with or without direct flow-through and mass transfer effects. The goal is to contribute to sequential and concurrent multiscale modeling by offering a collection of theoretical kinetic models like pseudo first order and pseudo second order kinetic models. The text includes the criteria for the domains of viability of the presented models, stochastic simulation algorithms and comparative analysis of analytical vs numerical modeling with artificial intelligence-assisted approach complementing these methods.

Keywords Adsorption kinetics · Fluctuation dynamics · Immunosensing · MEMS · Microfluidics · Neural network fitting · Protein-Peptide Binding · Stochastic analysis · Surface Plasmon Resonance (SPR)

1 Introduction

Generally speaking, affinity-based biological or biochemical sensing may relate to interactions between biomolecules from a biological material (microorganisms, cells of multicellular organisms, their organelles, tissues, extracellular and intracellular targets–receptors, enzymes and transporters, antibodies, nucleic acids), a biologically derived material (engineered proteins and aptamers) or a biomimetic analogue

---

O. Jakšić (✉)
Center of Microelectronic Technologies, Institute of Chemistry, Technology and Metallurgy, National Institute of the Republic of Serbia, University of Belgrade, Beograd, Serbia
e-mail: olga@nanosys.ihtm.bg.ac.rs

K. Guha et al. (eds.), *MEMS and Microfluidics in Healthcare*, Lecture Notes in Electrical Engineering 989, https://doi.org/10.1007/978-981-19-8714-4_12

(synthetic receptors, biomimetic catalysts, combinatorial ligands, imprinted polymers). The MEMS devices investigating these interactions are the focus of research directed to multitudinous applications, for instance, the development of lab-on-a-chip devices for high throughput screening and identifying compounds of clinical interest for therapeutics [1, 2], the development of organ on chip MEMS devices such as a liver or kidney on a chip [3–9] or the development of lab on a disc MEMS microfluidic devices [10]. Microfluidic chips allow for food safety sensing, peptide analysis, medical diagnosis, DNA purification, PCR activity, pregnancy, glucose estimation [11] and many more. For all of these applications, the insight into the biomolecular interactions is of prime importance.

Surface plasmon resonance (SPR), localized SPR and SPR imaging have proven themselves as prominent techniques in optical biosensing and screening of biomolecular interactions [12, 13]. Mechanisms that ensure high quality readout of SPR-based refractometric biosensors are related to surface phenomena. The establishing, propagation and extinction of surface plasmon polaritons at a conductor–dielectric interface are greatly affected by every, even tiny, change on the interface between the plasmonic material of the sensor surface and the surrounding medium with targeted analytes. Thus the presence of analyte molecules on the sensor's active surface is detectable with an extremely high precision. Compared to a majority of other detection techniques, SPR-based biosensing proved superior in terms of the dynamic range and the detection limit (even reaching single-molecule sensitivity) [14, 15]. In pharmacology, SPR-based biosensing is the technique of choice for the drug profiling and screening, antibody characterization, proteomics, and immunogenicity, for different kinds of pharmaceutical analysis, ADMET studies (Absorption, Distribution, Metabolism and Excretion of chemicals processed by a living organism, accompanied by Toxicology tests), to name just a few [16].

SPR-based refractometric biosensing allows for the rapid detection, with high specificity, high-throughput analysis of biomolecular interactions, in real time, on the label-free assays, in compact, lightweight devices. As such, it allows for quality laboratory testing, but also for lab-on-a-chip testing in point of care (PoC) or bedside testing and patient treatment [17, 18]. Preventive measures and therapeutic recommendations in healthcare are often related to oral supplements and food. SPR-based refractometric biosensing also allows for food and feed quality analysis, by allowing a fast and accurate detection of the presence of antibiotics, microbes, toxins, pesticides and biomolecules in food, but also of food adulteration and genetically modified food [19]. In addition, the substrates that support the formation and propagation of surface plasmon polariton plasmonic waves and the technique of light manipulation by structures whose parts are significantly smaller than the light's wavelength bring benefits and magnify the signal in other sensing techniques such as surface enhanced Raman scattering (SERS). The development of microfluidic MEMS devices for healthcare applications is a multidisciplinary meeting point for scientists involved in engineering, biotechnology, medicine, physics, chemistry, material science, etc. Although the advancement in such a multidisciplinary field is already noticeable, there is ample room for further improvements posed by ever growing needs.

In a chemical sense, for screenings and analyses related to human health, the interactions between proteins and/or peptides plays a great role, for instance in pharmacology, preventive medicine and sports medicine, but also in everyday life, for the digestion of food and food supplements and the design of health-promoting foods [20]. Real-time surface plasmon resonance imaging of protein adsorption–desorption kinetics is not new, the studies of surface enzymatic reactions on peptide microarrays date back to 2004 [21]. However, the topic still remains a subject of vivid research scrutiny. The current research has new foci of interest, like monitoring and preventing unwanted adsorption of proteins on walls of microfluidic chips [22]. Once released from the parent protein, depending on the sequence of amino acids they consist of, bioactive peptides are able to alter the physiological systems in the human body. Among others, there are anti-obesity and satiety peptides, antihypertensive, antithrombotic, antioxidant, hypocholesterolemic, antimicrobial, cytomodulatory, immune-modulatory peptides, opioid peptides, to name just a few, and screening for new bioactive peptides is one of the attractive research goals [23]. Previous modeling of enzymatic reactions on peptide microarrays has been often based on linear, first order kinetic models. However, the domain of validity of these models is limited [24]. This is especially so when it comes to the detection of extremely low concentrations such as the detection by the use of nanobiosensors capable of detecting a single molecule [25].

In a mathematical sense, for mathematical modeling, scaling down to nanoscale dimensions and to extremely low concentrations makes a great difference. The calculation apparatus valid for moderate analyte concentrations is usually based on the Lagergren model of adsorption. It allows for an easy estimate of all figures of merit in time and frequency domain (sensor response, sensitivity, linearity, and selectivity), no matter whether we use a deterministic or a stochastic approach in our analysis. Models valid for extremely low concentrations are generally analytically unsolvable and one must resort to extensive numerical computations instead. Apart from the deterministic analytical or numerical approach, the stochastic approach, which takes into account the true nature of the binding process, is needed, for modeling the fluctuation kinetics in transient states and fluctuation dynamics in equilibrium. Artificial neural network fitting also complements these methods [26].

Subsequent sections are devoted to modeling. First, in Sect. 2, a general introduction to the system used for modeling biomolecular interactions, along with the notation and surmises, is given. Then, Sect. 3 outlines modeling in time domain. The possibility for emerging oscillations in a binding process is discussed in Sect. 4. Afterwards, in Sect. 5, an overview of the modeling of equilibrium fluctuations in frequency domain is given. Section 6 gives a summary of the text, along with conclusions and comments on future prospects.

2 Affinity Binding and Biosensing: Preamble

When speaking of a biosensor, we refer to a self-contained integrated device capable of providing specific quantitative or semi-quantitative analytical information using a biological recognition element which is in direct spatial contact with a transduction element (IUPAC definition, 1996). In a modern sense, it is a sensor that integrates a biological element with a physicochemical transducer to produce an output signal (e.g. electronic or optical) proportional to the amount of an analyte. This signal is then conveyed to a processing block which is often capable of conditioning and exhibiting other complex functionalities like sending data to cloud, etc. The specific biochemical reaction that we focus on here is physisorption, a reversible stochastic process of binding and unbinding between bioreceptor molecules positioned at the sensing surface (adsorbent) and freely moving adsorbate particles (target analyte molecules) in a surrounding fluid. Most often, the readout mechanism of such affinity devices is based on reversible adsorption. The one that we address here is electromagnetic (through surface plasmon resonance, SPR), however, it can be electrical (e.g. piezoelectric), electrochemical, mechanical, etc., as shown in Fig. 1.

Figure 1 is a schematic representation of the side view of a microfluidic channel with monocomponent target analyte and sensing surface functionalized with linker molecules in order to support bioreceptor adsorption sites.

Depending on the readout mechanism, the transducer part in the block diagram and the measured signal are different. Recent advancement in refractometric transducers is presented in a review of optical biosensing schemes in [27] and in works [28–30] alongside other transducer techniques. The focus here is on modeling the binding mechanisms. The target analyte concentration in a microfluidic channel or chamber may be modeled and considered a constant, as in Fig. 1, but more realistically, it has some spatial distribution, as shown in Fig. 2, where flow is depicted with horizontal arrows, their lengths being proportional to the velocity of the fluid.

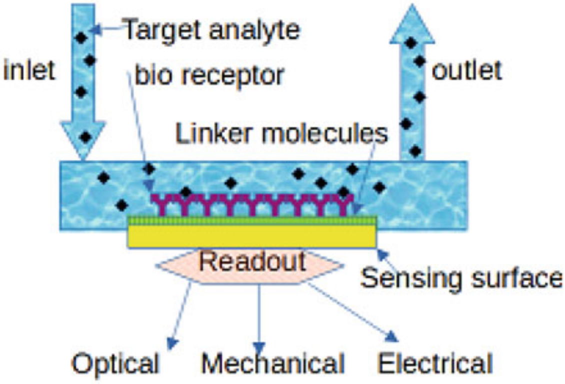

Fig. 1 Side view of a microfluidic channel with monocomponent target analyte and sensing surface functionalized with linker molecules in order to support bioreceptor adsorption sites

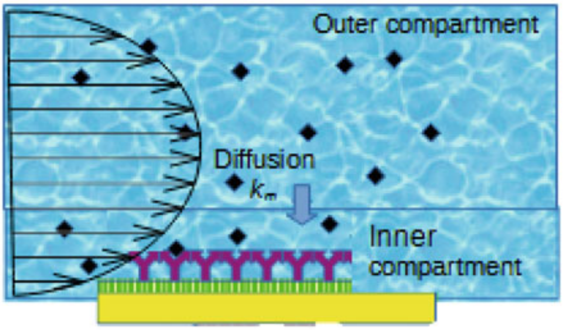

Fig. 2 Side view of a microfluidic channel magnified and denoted in accord with two compartment model, showing inhomogeneous spatial distribution of target analytes

In microchannels and microreactors, binding and unbinding of target analyte molecules to and from bioreceptor molecules positioned on the surface is additionally affected with mass transfer in the flow direction along separate compartments (convection), and mass transfer between the compartments (diffusion). In modeling of binding kinetics in the flow-through chamber, by using the two compartment models, target analyte concentrations in the outer compartment, far from the sensing surface and the inner compartment, adjacent to the sensing surface, are modeled differently. However, the general stoichiometric equation is the same for all models discussed here.

The general stoichiometric equation, (1), represents multicomponent adsorption of r_a different target analytes in a fluid, whose molecules are denoted with A_g on a multimodal surface with r_c different classes of adsorption centers with bioreceptors, denoted with A_f. After binding to a bioreceptor, target analyte molecule forms an occupied adsorption center A_a. k_a and k_d are the association rate constant and the dissociation rate constant respectively. The process takes place without dissociation or mutual interaction of target analyte molecules.

$$A_{g,i} + A_{f,j} \underset{k_{d,i}}{\overset{k_{a,i}}{\rightleftarrows}} A_{a,i} i = 1, ...r_a j = 1, ...r_c \tag{1}$$

Based on the interpretation of this system of stoichiometric equations one gets different systems of differential equations, *i.e.* different analytical models, different reaction rate equations and different propensity functions in chemical master equations. Next sections address these models and some of their solutions.

3 Time Domain: Transients and Steady States

3.1 Monocomponent Case

Lagergren pseudo first order (PFO) equation. Written in terms of the number of adsorbed target analyte molecules N, this reaction rate equation, (2) refers to the adsorption on homogeneously functionalized surface, meaning there is one type of adsorption center with bioreceptors. The rate Eq. (2) depicts a process whose transient response, (3) for initial condition equal to zero, exhibits an exponential relaxation towards the steady state N_s, with a time constant τ [31].

$$\frac{dN}{dt} = k_a N_0 (M - N) - k_d N \tag{2}$$

$$N(t) = N_s\left(1 - e^{-t/\tau}\right) = M k_a N_0 \tau \left(1 - e^{-(k_a N_0 + k_d)t}\right) \tag{3}$$

M is the number of adsorption centers with bioreceptors when the surface is fully populated and N_0 is the overall number of target analyte molecules in a microfluidic chamber. Adsorption rate in this model is modeled as greater than it truly is.

Riccati pseudo second order (PSO) equation. This more correct model takes into account the depletion of the overall number of target molecules due to adsorption, as shown in (4). It is still the process with exponential relaxation towards the steady state, denoted with β, (5), except that the number of transients is infinite (6).

$$\frac{dN}{dt} = k_a (N_0 - N)(M - N) - k_d N = k_a (N - \beta)(N - \gamma) \tag{4}$$

$$\begin{gathered} \beta = \left[k_a (N_0 + M) + k_d - \sqrt{(k_a (N_0 + M) + k_d)^2 - 4k_a^2 N_0 M} \right] / 2k_a \\ \beta = [k_a (N_0 + M) + k_d - k] / 2k_a \end{gathered} \tag{5}$$

$$N(t) = \beta \frac{\left(1 - e^{-kt}\right)}{1 - (\beta/\gamma)\left(1 - e^{-kt}\right)} = \beta + \sum_{i=1}^{\infty} (\beta - \gamma)(\beta/\gamma)^i e^{-ikt} \tag{6}$$

The drawback of this model is that it assumes a uniform concentration distribution of the analyte target molecules in the microfluidic channel and assumes that the mass transfer effects are negligible, which is usually not the case.

Two compartment model. Again, the reaction rate equation relates the change in the number of bound (adsorbed) target analyte molecules on its left hand side with the difference in adsorption and desorption rates on its right hand side. The analyte concentration in the vicinity of the sensing surface, C_s, does not equal the analyte concentration in the rest of the microfluidic chamber, C_0. Its change is caused by the adsorption and the mass transport between the compartments as shown in Fig. 2 [32–36].

$$\frac{dN}{dt} = k_a' \frac{C_0 + \frac{k_d}{k_m A} N}{1 + \frac{k_a'}{k_m A}(M - N)}(M - N) - k_d N \tag{7}$$

$$k_m = 1.467\sqrt[3]{\frac{D^2 \mathrm{v}}{Lh}}[m/s] \tag{8}$$

Rate constant of adsorption is now denoted with apostrophe in order to mind different units (now m^3/s) and k_m is the mass transfer coefficient, assumingly constant too (8). D is the diffusion coefficient of the target analyte molecules, v mean convection velocity, L is the length of the sensing area and h is the height of the sensing microchamber.

However, whether modeled as a process with pseudo first order kinetics (described with linear first order differential equations, first proposed by Lagergren) or modeled as a process with second order kinetics (described with nonlinear Riccati equations), adsorption is genuinely a stochastic process.

Analytical stochastic approach. By setting and solving the Chemical Master Equation in terms of the probability generating function one gets insight into all properties of the system, all its moments. Adsorption process with PFO kinetics has binomial probability distribution function PDF (11), its mean value of the number of adsorbed molecules $\overline{N}$ equals the deterministic solution N (3) and its probability generating function PGF, $F(s,t)$, (9) can be written in terms of the surface coverage, G, (10), (the number of adsorbed molecules normalized with the overall number of adsorption centers on the surface M) [37].

$$F(s,t) = [(1 - G) + sG]^M = \sum_{N=0}^{M} \binom{M}{N} (1 - G)^{(M-N)} G^N s^N |s| \le 1 \tag{9}$$

$$G(t) = k_a N_0 \tau \left(1 - e^{-(k_a N_0 + k_d)t}\right) \tag{10}$$

$$P_N(t) = \binom{M}{N} (1 - G)^{(M-N)} G^N \tag{11}$$

For adsorption process with PSO kinetics such an analysis partial differential equation stemming from the Chemical Master equation is generally not solvable, so one must resort to the numerical stochastic approach.

Numerical stochastic approach. Once set and coded, the stochastic simulation algorithm SSA [38], may serve successfully for simulation of adsorption processes with PFO as well as ones with PSO. In SSA, the time instances of transitions due to adsorption or desorption are also stochastic, not equally spaced in time. SSA is based on the use of built-in numerical routines for generating random numbers with exponential distribution (which is related here to the mean residential time of the adsorbed molecules on adsorption centers), applied with different parameters (which are here related to instantaneous sorption rates).

The algorithm has the following steps [39]

- set initial number of adsorbate particles and use the reciprocal value of the initial rate of adsorption ($1/k_a N_0 M$ in case all adsorption centers are initially empty) as a parameter for calculation of the first time step towards the first transition (in case of zero initial condition, the adsorption is only possible) and update the corresponding number of the adsorbed molecules in the next time step accordingly.
- for every next time step and every next update of the instantaneous number of adsorbed molecules, the random number with exponential PDF is calculated twice, for both sorption constants, once using the reciprocal value of the instantaneous adsorption rate as a parameter, and also using the reciprocal value of the instantaneous desorption rate as a parameter. Whichever number is smaller, it determines the next transition and the next transition update.

The adsorption process, as all natural processes, is ergodic, the mean value of multiple iterations of SSA (averaging over an ensemble), is in accord with time average, and for adsorption process with PFO, it is also in accord with the deterministic solution (3).

The approaches presented so far can be scaled up to multicomponent adsorption.

3.2 *Binary Analyte Mixture*

Lagergren pseudo first order (PFO) equation. The system of differential Eq. (12), has a characteristic polynomial (13) whose roots represent the time constants in the transient response (14)

$$\frac{dN_i}{dt} = k_{a,i} N_{0,i} \left(M - \sum_{j=1}^{2} N_j \right) - k_{d,i} N_i i = 1, 2 \tag{12}$$

$$\begin{gathered} P_2(s) = s^2 + bs + c = (s - z_1)(s - z_2) \\ b = k_1 + k_2 = \left(k_{a,1} N_{0,1} + k_{d,1}\right) + \left(k_{a,2} N_{0,2} + k_{d,2}\right) \\ c = k_1 k_2 - k_{a,1} N_{0,1} k_{a,2} N_{0,2} = k_1 k_2 - k_{l,1} k_{l,2} \end{gathered} \tag{13}$$

$$\begin{aligned} N_i &= N_{s,i} + N_{t1,i} e^{z_1 t} + N_{t2,i} e^{z_2 t} i = 1, 2 \\ N_{s,i} &= \tfrac{M k_{l,i} k_{d,j}}{z_1 z_2} j = 3 - i \\ N_{ti,j} &= (-1)^{(i+1)} \tfrac{k_{l,j} \left(k_{d,3-j} + z_i\right)}{z_i (z_1 - z_2)} \end{aligned} \tag{14}$$

Riccati pseudo second order (PSO) equation. The set of two nonlinear Riccati differential Eq. (15) is conveniently solved numerically for determining the full time response. The solution to stationary states in analytical form is calculated by

$$\frac{dN_i}{dt} = k_{a,i}\left(N_{0,i} - N_i\right)\left(M - \sum_{j=1}^{2} N_j\right) - k_{d,i}N_i i = 1, 2 \tag{15}$$

$$\begin{aligned} P_3(N_{1s}) &= N_{1s}^3 + b_2 N_{1s}^2 + b_1 N_{1s} + b_0 \\ N_{2s} &= N_{1s}\frac{k_{d,1}k_{l,2}}{k_{d,2}k_{l,1}+N_{1s}\left(k_{d,1}k_{a,2}-k_{d,2}k_{a,1}\right)} \end{aligned} \tag{16}$$

$$\begin{aligned} b_2 &= \frac{k_{l,1}k_{d,2}+k_{l,2}k_{d,1}}{k_{a,2}k_{d,1}-k_{a,1}k_{d,2}} - M - N_{01} - \frac{k_{d,1}}{k_{a,1}} \\ b_1 &= N_{01}\left(M - \frac{k_{l,1}k_{d,2}+k_{l,2}k_{d,1}+k_{a,1}k_{d,2}M+k_{d,1}k_{d,2}}{k_{a,2}k_{d,1}-k_{a,1}k_{d,2}}\right) \\ b_0 &= N_{01}^2 M \frac{k_{a,1}k_{d,2}}{k_{a,2}k_{d,1}-k_{a,1}k_{d,2}} \end{aligned} \tag{17}$$

Two compartment model. Mass transfer in microfluidic flow-through devices with binary mixture of analyte target molecules, with concentrations C_1 and C_2, competitively fighting for same adsorption centers on the surface with the overall capacity M is modeled with the set of Eq. (18) [40, 41].

$$\frac{dN_i}{dt} = k_{a,i}^{\prime\,\frac{k_{m,i}AC_i+k_{d,i}N_i}{k_{m,i}A+k'_{a,i}\left(M-\sum_{j=1}^{2}N_j\right)}\left(M-\sum\limits_{j=1}^{2}N_j\right)} - k_{d,i}N_i, i = 1, 2 \tag{18}$$

Analytical stochastic approach. Knowing that (12)–(14) refer to the mean values of the number of bound target analyte molecules in adsorption process with PFO kinetics, we can normalize N_1 and N_2 with M and calculate expectation E (19), variance *i.e.* dispersion D (20) and relative fluctuations δ (21) in terms of the surface coverages G_1 and G_2. (19)–(21) are given here for a general response where readout signal is linearly proportional to the numbers N_1 and N_2, like the refractive index change where $RIC = w_1N_1 + w_2N_2$, [37].

$$E_{RIC} = \mathrm{w}_1 M G_1(1 - G_1) + \mathrm{w}_2 M G_2(1 - G_2) \tag{19}$$

$$D_{RIC} = M\left[\mathrm{w}_1^2 G_1 + \mathrm{w}_2^2 G_2 - (\mathrm{w}_1 G_1 + \mathrm{w}_2 G_2)^2\right] \tag{20}$$

$$\delta_{RIC} = \frac{\sqrt{\mathrm{w}_1^2 G_1 + \mathrm{w}_2^2 G_2 - (\mathrm{w}_1 G_1 + \mathrm{w}_2 G_2)^2}}{\sqrt{M}(\mathrm{w}_1 G_1(1 - G_1) + \mathrm{w}_2 G_2(1 - G_2))} \tag{21}$$

Numerical stochastic approach. The SSA outlined for the case of monocomponent adsorption can be scaled up for estimations of the response of adsorption of multicomponent mixtures [26]. These calculations, however, depend on the specific numerical values used in simulations, and may be CPU and time consuming.

ANN assisted approach. Artificial neural network ANN fitting provides us with the tool that harnesses advantages of both worlds, analytical and numerical. In [26] the time response of the binary adsorption has been prioritized over numerical solutions. After training an ANN with examples obtained from a pool of experimental data or numerical simulations, we can use the generated ANN fitting function without concerns regarding calculations over a vast parameter space where differential equations may unexpectedly become stiff.

3.3 Ternary Analyte Mixture

Lagergren pseudo first order (PFO) equation. The system of differential Eq. (22), has a characteristic polynomial (23) whose roots represent the time constants in the transient response given by (24)-(28)

$$\frac{dN_i}{dt} = k_{a,i} N_{0,i}\left(M - \sum_{j=1}^{3} N_j\right) - k_{d,i} N_i i = 1, 2, 3 \tag{22}$$

$$\begin{aligned} P_3(s) &= s^3 + c_2 s^2 +_1 s + c_0 = (s - z_1)(s - z_2)(s - z_3) \\ c_2 &= \sum_{j=1}^{3} k_j = \sum_{j=1}^{3} k_{l,j} + \sum_{j=1}^{3} k_{d,j} c_0 = k_{d,1} k_{d,2} k_{d,3}\left(1 + \sum_{j=1}^{3} \frac{k_{l,j}}{k_{d,j}}\right) \\ c_1 &= \sum_{j=1}^{3}\left(k_{l,i} \sum_{\substack{y = 1 \\ y \neq j}}^{3} k_{d,y}\right) + k_{d,1} k_{d,2} k_{d,3} \sum_{j=1}^{3} \frac{1}{k_{d,j}} \end{aligned} \tag{23}$$

$$N_i(t) = M k_{l,i}\left[A_i + B_i e^{-z_1 t} + C_i e^{-z_2 t} + D_i e^{-z_3 t}\right] i = 1, 2, 3 \tag{24}$$

$$A_i = \frac{-k_{d,(i+1)mod3} k_{d,(i+2)mod3}}{z_1 z_2 z_3} i = 1, 2, 3 \tag{25}$$

$$B_i = \frac{\left(z_1 + k_{d,(i+1)mod3}\right)\left(z_1 + k_{d,(i+2)mod3}\right)}{z_1(z_1 - z_2)(z_1 - z_3)} i = 1, 2, 3 \tag{26}$$

$$C_i = \frac{\left(z_2 + k_{d,(i+1)mod3}\right)\left(z_2 + k_{d,(i+2)mod3}\right)}{z_2(z_2 - z_1)(z_2 - z_3)} i = 1, 2, 3 \tag{27}$$

$$D_i = \frac{\left(z_3 + k_{d,(i+1)mod3}\right)\left(z_3 + k_{d,(i+2)mod3}\right)}{z_3(z_3 - z_1)(z_3 - z_2)} i = 1, 2, 3 \tag{28}$$

Two compartment model. Mass transfer in microfluidic flow-through devices with ternary mixture of analyte target molecules, with concentrations C_1, C_2 and C_3, competitively fighting for same adsorption centers on the surface with the overall capacity M, is modeled with the set of Eq. (29) [42].

$$\frac{dN_i}{dt} = k'_{a,i} \frac{k_{m,i} AC_i + k_{d,i} N_i}{k_{m,i} A + k'_{a,i}\left(M - \sum_{j=1}^{3} N_j\right)} \left(M - \sum_{j=1}^{3} N_j\right) - k_{d,i} N_i i = 1, 2, 3 \tag{29}$$

Analytical stochastic approach. We know that (24)-(28) refer to the mean values of the number of bound target analyte molecules in the adsorption process with PFO kinetics. Thus we can normalize N_1, N_2 and N_3 with M and calculate expectation E (19), variance *i.e.* dispersion D (20) and relative fluctuations δ (21) in terms of the surface coverages G_1, G_2.and G_3. (30)-(32) here are given for general response where readout signal is linearly proportional to the numbers N_1, N_2 and N_3, like the refractive index change where $RIC = w_1N_1 + w_2N_2 + w_3N_3$ [37].

$$E_{RIC} = M \sum_{i=1}^{3} w_i G_i (1 - G_i) i = 1, 2, 3 \tag{30}$$

$$D_{RIC} = M\left[w_1^2 G_1 + w_2^2 G_2 - (w_1 G_1 + w_2 G_2)^2\right] \tag{31}$$

$$\delta_{RIC} = \frac{\sqrt{\left[\sum_{i=1}^{3} w_i^2 G_i - \left(\sum_{i=1}^{3} w_i G_i\right)^2\right]}}{\sqrt{M} \sum_{i=1}^{3} w_i G_i (1 - G_i)} \tag{32}$$

3.4 Mixture with Arbitrary Number of Analytes

Lagergren pseudo first order (PFO) equation. The general solution to Chemical Master Equation implemented on the stochastic analysis of adsorption of a mixture of an arbitrary number of analytes, derived in [37], provides the tool for complete insight into the system behavior, its means and all its higher moments. If we denote with r the number of components in a mixture of adsorbates and with N_f the number of free bioreceptors or alternatively the number of unoccupied adsorption centers on the surface, then consequently the fraction of bioreceptors which is free or the fraction of the surface would be G_f:

$$N_f = M - \sum_{i=1}^{r} N_i G_f = 1 - \sum_{i=1}^{r} G_i \tag{33}$$

The general solution to the probability generating function F implies that the process of multicomponent adsorption of analytes with pseudo first order kinetics has multinomial probability distribution function:

$$F_{s_1,\ldots s_r,t} = [1 + G_1(s_1 - 1) + \ldots + G_r(s_r - 1)]^M = \left[G_f + \sum_{i=1}^{r} G_i s_i\right]^M \tag{34}$$

$$F_{s_1,\ldots s_r,t} = \sum_{N_1+\ldots+N_r+N_f=M} \binom{M}{N_1,\ldots,N_r,N_f} G_f^{N_f} \prod_{i=1}^{r} (G_i s_i)^{N_i} \tag{35}$$

It is in accord with the conditions

$$F(s_1, \ldots s_r, t = 0) = 1F(1, \ldots 1, t) = 1 \tag{36}$$

The corresponding probability distribution function is

$$P_{N_1,\ldots N_r}(t) = \frac{M!}{N_f! \prod_{i=1}^{r} N_i!} G_f^{N_f} \prod_{i=1}^{r} G_i^{N_i} \tag{37}$$

Hence, the expectation, variance and all higher moments are known.

Riccati pseudo second order (PSO) equation. The solution to the matrix Riccati equation relevant for modeling of the process of multicomponent adsorption of analytes with pseudo second order kinetics, in an analytical form, is not derived yet. What is easily feasible is the determination of number of adsorbed molecules in the stationary state, for each component in the mixture. In order to calculate the number of adsorbed molecules in the stationary state for one component in the mixture with r components, one has to solve a polynomial with the rank $r + 1$. The set of the differential equations is such that for the mixture of r components, there are $r + 1$ solutions, $r + 1$ sets of r numbers that correspond to the stationary state of each component.

4 Multiple Steady States and Stability

The possibility of multiple solutions when determining stationary states in the adsorption process needs to be critically considered from a physical point of view. If the adsorption process is stable by its nature, there is only one stationary solution and all others, although present in mathematical models, are rejected as physically impossible. If multiple stationary states are physically possible, then it is necessary to determine the conditions for transitions between them. For that, it is necessary to apply a stochastic approach.

Many natural processes are truly stochastic and, due to inherent random mechanisms, fluctuate around some stationary state. In experiments and practical applications, these fluctuations can appear reproducible and resemble chemical or biological reactions that actually exhibit oscillatory behavior. Population dynamics in general can be oscillatory. Since the interest in oscillatory reactions is still growing in many areas, the results of the analysis of the stability of the adsorption process, carried out in the paper [43], are also summarized here.

In [43], stability was tested in several ways:

- By analyzing the Jacobian in Taylor expansion of a set of deterministic equations,
- By applying a stochastic approach, analyzing random perturbations around the stationary state,
- By applying the Langevin method with special attention to the correct modeling of the Langevin forces and the relationship between the reaction flux and the cross-correlation function,
- Using stochastic analysis, based on the basic chemical equation, and
- Using stochastic simulation algorithms.

The conclusion of the comparative analysis of those results is that the process of monocomponent adsorption and the process of binary adsorption with pseudo second order kinetics both have one stationary state which is a stable focus. Hence, monocomponent adsorption, as well as binary adsorption, is a stable process.

A generalization of this conclusion to the stability of adsorption of a mixture of an arbitrary number of analytes is possible. It is based on the fact that an arbitrary mixture can be viewed as a binary mixture by extracting one analyte from it. For the rest of the mixture, positive real numbers, which represent fictitious rate constants, can be defined, and, in a mathematical sense, satisfy the conditions that apply to a binary mixture.

Figure 3 shows monocomponent adsorption with zero initial conditions in time domain, obtained in three different ways. The first one is by the use of SSA, stochastic numerical approach, where multiple iterations are shown by green lines. Then, the mean value of these multiple iterations is calculated (magenta line) and compared with the deterministic solution (blue circles). In this case, they coincide with the solution of the chemical master equation as obtained by the stochastic analytical approach.

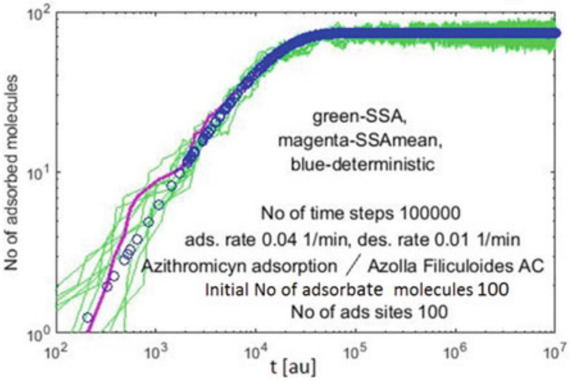

Fig. 3 Monocomponent adsorption with zero initial conditions (no adsorbed analyte at the beginning of the process) in time domain calculated in three different ways

5 Frequency Domain: Equilibrium Fluctuations

All models developed for the time domain are not informative enough when it comes to the fluctuation dynamics in equilibrium. In equilibrium, random processes fluctuate around the steady state and the dynamics of those fluctuations greatly affects the operation of the whole device. Next subsections present a collection of related results.

It will be shown that all natural processes with the exponential relaxation towards the stationary state have the power spectral density of intrinsic fluctuations in a form of typical Lorentzian curve, which, presented graphically, exhibits a flat region at low frequencies, LFNM (low frequency noise magnitude), and a slope after some distinctive knee related to the cut off frequency. Time constants and stationary states calculated for temporal response are the key data for the determination of power spectral densities of intrinsic fluctuations in the number of adsorbed molecules in the frequency domain.

5.1 Monocomponent Case

One compartment model. The analytical expression for the power spectral density of the fluctuations in the number of adsorbed molecules is [44–46]

$$PSD(\omega) = \frac{PSD_0}{1+\omega^2\tau^2} = \frac{4k_d N_s \tau^2}{1+\omega^2\tau^2} = \frac{4v_{des,(N=N_s)}\tau^2}{1+\omega^2\tau^2} \tag{38}$$

It has the same form for adsorption processes with PFO and PSO, and for the adsorption processes in flow through microchannels with mass transfer due to the convection and the diffusion, but the numerical values for the time constants and the stationary states are calculated in accord with the models developed for the time domain, as presented previously.

Two compartment model. The laminar flow of analyte solutions in microchannels and mass transfer caused by it, affect the fluctuation dynamics in equilibrium so that the system needs more time to reach the equilibrium once it has been drawn from it. The expression for the power spectral density of the fluctuations in the number of adsorbed molecules also has the form written in (38) but the time constant is greater than the time constant for systems with PFO [48].

$$\tau = \frac{1}{k_a' C_0 + k_d} + \frac{k_d k_a' M}{\left(k_a' C_0 + k_d\right)^2 A k_m} \tag{39}$$

The reasoning for calculating the low frequency noise magnitude is the same as in (38). It is the quadruple of the product of desorption rate in equilibrium and the squared time constant, but desorption rate in equilibrium is calculated in accordance with the models presented previously.

5.2 Binary Analyte Mixture

The analytical expression for the power spectral density of the fluctuations in the number of adsorbed molecules, in case of adsorption processes with PFO and PSO, has two important time constants and three changes of slope after the LFNM flat region, one zero and two poles [47]:

$$PSD(\omega) = \frac{PSD_0\left(1 + \omega^2 \tau_{III}^2\right)}{\left(1 + \omega^2 \tau_I^2\right)\left(1 + \omega^2 \tau_{II}^2\right)} \tag{40}$$

$$PSD_0 = 4\left(w_1^2 k_{d,1} N_{1s} + w_2^2 k_{d,2} N_{2s}\right) \frac{\tau_I^2 \tau_{II}^2}{\tau_{III}^2} \tag{41}$$

For transducer elements whose signals are proportional to the number of adsorbed analyte molecules, a scaling factor w_i is used, as before $RIC = w_1 N_1 + w_2 N_2$.

The expression for the third time constant, τ_{III}, is also the same for adsorption processes with pseudo first order kinetics and processes with pseudo second order kinetics:

$$\tau_{III} = \sqrt{\frac{w_1^2 k_{d,1} N_{1s} + w_2^2 k_{d,2} N_{2s}}{(w_1 M_{22} - w_2 M_{21})^2 k_{d,1} N_{1s} + (w_2 M_{11} - w_1 M_{12})^2 k_{d,2} N_{2s}}} \tag{42}$$

However, the expressions for the stationary states and the expressions for the time constants are calculated differently.

Lagergren pseudo first order (PFO) equation. Stationary states in expressions for the power spectral density (41)–(43) are calculated by using the expressions developed for the analysis in time domain for that case, that is expressions (13), (14). The same expressions (13), (14) are also used for calculations of time constants

$$\tau_I = z_1^{-1}, \tau_{II} = z_2^{-1} \tag{43}$$

Riccati pseudo second order (PSO) equation. For the determination of the stationary states expressions (16), (17) are used and for the determination of the time constants, the following expressions are valid:

$$\tau_{I,II} = 2\left[M_{11} + M_{22} \pm \sqrt{(M_{11} - M_{22})^2 + 4M_{12}M_{21}}\right]^{-1} \tag{44}$$

Constants M_{ij} are calculated after following expressions

$$M_{11} = k_1 + k_{a,1}(M - 2N_{1s} - N_{2s}), \tag{45}$$

$$M_{22} = k_2 + k_{a,2}(M - 2N_{2s} - N_{1s}), \tag{46}$$

$$M_{12} = k_{a,1}(N_{01} - N_{1s}), \tag{47}$$

$$M_{21} = k_{a,2}(N_{02} - N_{2s}), \tag{48}$$

6 Conclusions and Future Prospects

In this Chapter, a survey of modeling methods of adsorption kinetics and fluctuation dynamics in affinity-based biosensors is presented which are applicable for the design and application of healthcare microfluidic devices and systems. Various cases are considered regarding the number of analytes in the fluid (one, two, three or an arbitrary number). Different approaches to the analysis are presented (deterministic, stochastic, artificial neural networks-assisted) in time domain and frequency domain.

New advancements with respect to enriched functionalities, novel adsorbate materials and multi-functional sensing surfaces, new integrations in digital healthcare systems, novel design of microfluidic systems with independent but interconnected customizable microfluidic chips and new regulations regarding personal data protections are on their way too [48–50]. New advancements in modeling can be expected in the domain of stronger implementations of artificial intelligence and neural network fitting for optimal experiment design, optimal methodology design, and integrations of existing models into more complex sequential and concurrent multiscale models.

Acknowledgements This research was funded by the Ministry of Education, Science, and Technological Development of Republic of Serbia, grant number 451-03-68/2022-14/200026.

References

1. Christoffersson J et al (2021) Review on bio-inspired materials with nanotechnology applications in medical devices. J Phys Conf Ser 1948(1):012227. https://doi.org/10.1088/1742-6596/1948/1/012227
2. Onbas R, Bilginer R, Arslan Yildiz A (2021) On-chip drug screening technologies for nanopharmaceutical and nanomedicine applications, pp 311–346. https://doi.org/10.1007/978-3-030-44925-4_8
3. Theobald J et al (2018) Liver-kidney-on-chip to study toxicity of drug metabolites. ACS Biomater Sci Eng 4(1):78–89. https://doi.org/10.1021/ACSBIOMATERIALS.7B00417/SUPPL_FILE/AB7B00417_SI_001.PDF
4. Sateesh J, Guha K, Dutta A, Sengupta P, Srinivasa Rao K (2019) Design and analysis of microfluidic kidney-on-chip model: fluid shear stress based study with temperature effect. Microsyst. Technol 25 (7):2553–2560. https://doi.org/10.1007/S00542-018-4261-Z/FIGURES/11
5. Sateesh J, Guha K, Dutta A, Sengupta P, Srinivasa Rao K (2020) Regenerating re-absorption function of proximal convoluted tubule using microfluidics for kidney-on-chip applications. SN Appl Sci 2 (1): 1–11. https://doi.org/10.1007/S42452-019-1840-2/TABLES/2
6. Guha K, Sateesh J, Dutta A, Sengupta P, Srinivasa Rao K, Agarwal A (2020) Mimicking kidney re-absorption using microfluidics by considering hydrostatic pressure inside kidney tubules: structural and analytical study. Microsyst. Technol 26 (6):1769–1776. https://doi.org/10.1007/S00542-019-04720-9/FIGURES/9.
7. Sateesh J et al (2022) A comprehensive review on advancements in tissue engineering and microfluidics toward kidney-on-chip. Biomicrofluidics 16(4):041501. https://doi.org/10.1063/5.0087852
8. Sateesh J, Guha K, Dutta A, Sengupta P, Agarwal A, Srinivasa Rao K (2020) Recreating the size-dependent reabsorption function of proximal convoluted tubule towards artificial kidney applications: Structural analysis and computational study. Artif. Organs 44(8):E369–E381. https://doi.org/10.1111/AOR.13683
9. J. Sateesh, K. Guha, A. Dutta, P. Sengupta, and K. Srinivasa Rao, "Design and Modeling of Bioreactor Utilizing Electrophoresis and Di-electrophoresis Techniques for Regenerating Reabsorption Function of Human Kidney PCT in Microfluidics Environment," *IEEE Trans. Nanobioscience*, 2021, doi: https://doi.org/10.1109/TNB.2021.3131351.
10. Huo X et al (2022) A lab-on-a-disc platform based on nickel nanowire net and smartphone imaging for rapid and automatic detection of foodborne bacteria. Chinese Chem Lett 33(4):2091–2095. https://doi.org/10.1016/J.CCLET.2021.08.027
11. Pattanayak P et al (2021) Microfluidic chips: recent advances, critical strategies in design, applications and future perspectives. Microfluid Nanofluidics 25(12):1–28. https://doi.org/10.1007/S10404-021-02502-2/FIGURES/17
12. Breault-Turcot J, Poirier-Richard HP, Couture M, Pelechacz D, Masson JF (2015) Single chip SPR and fluorescent ELISA assay of prostate specific antigen. Lab Chip 15(23):4433–4440. https://doi.org/10.1039/C5LC01045D
13. Vaisocherová H, Faca VM, Taylor AD, Hanash S, Jiang S (2009) Comparative study of SPR and ELISA methods based on analysis of CD166/ALCAM levels in cancer and control human sera. Biosens Bioelectron 24(7):2143–2148. https://doi.org/10.1016/J.BIOS.2008.11.015

14. Nivedha S, Babu PR, Senthilnathan K (2018) Surface plasmon resonance: physics and technology. Curr. Sci 115(1):56–63 [Online]. Available http://search.ebscohost.com.proxy.kobson.nb.rs:2048/login.aspx?direct=true&db=aph&AN=130595119&site=eds-live
15. Iqbal MA, Malik M, Shahid W, Ahmad W, Min-Dianey KAA, Pham PV (2021) Plasmonic 2D materials: Overview, advancements, future prospects and functional applications. https://doi.org/10.5772/INTECHOPEN.101580
16. Nys G, Fillet M (2018) Microfluidics contribution to pharmaceutical sciences: From drug discovery to post marketing product management. J Pharm Biomed Anal 159:348–362. https://doi.org/10.1016/J.JPBA.2018.07.011
17. Haghayegh F, Salahandish R, Zare A, Khalghollah M, Sanati-Nezhad A (2021) Immuno-biosensor on a chip: a self-powered microfluidic-based electrochemical biosensing platform for point-of-care quantification of proteins. Lab Chip 22(1):108–120. https://doi.org/10.1039/D1LC00879J
18. Yaman G (2023) A suggestion of standard and optimized steps in the LOC (Lab on a Chip), LOD (Lab on a Disc), and POC (Point of Care) development process for biomedical applications: A case study about ESR. J Comput Appl Math 417:114626. https://doi.org/10.1016/J.CAM.2022.114626
19. Manessis G, Gelasakis AI, Bossis I (2022) Point-of-care diagnostics for farm animal diseases: From biosensors to integrated lab-on-chip devices. Biosens 12(7):455. https://doi.org/10.3390/BIOS12070455
20. Konoplev G et al (2022) Label-free physical techniques and methodologies for proteins detection in microfluidic biosensor structures. Biomed 10(2):207. https://doi.org/10.3390/BIOMEDICINES10020207.
21. Wegner GJ et al (2004) Real-time surface plasmon resonance imaging measurements for the multiplexed determination of protein adsorption/desorption kinetics and surface enzymatic reactions on peptide microarrays. Anal Chem 76(19):5677–5684. https://doi.org/10.1021/AC0494275
22. Klatt JN et al (2021) Blocking protein adsorption in microfluidic chips by a hydrophobin coating. ACS Appl Polym Mater 3(7):3278–3286. https://doi.org/10.1021/ACSAPM.0C01301/SUPPL_FILE/AP0C01301_SI_001.PDF
23. Canabady-Rochelle LLS, Selmeczi K, Collin S, Pasc A, Muhr L, Boschi-Muller S (2018) SPR screening of metal chelating peptides in a hydrolysate for their antioxidant properties. Food Chem 239:478–485. https://doi.org/10.1016/J.FOODCHEM.2017.06.116
24. Jokić I, Jakšić O, Frantlović M, Jakšić Z, Radulović K (2021) Modelling of plasmonic biosensor temporal response influenced by competitive adsorption and analyte depletion. Meas Sci Technol 32(9):95701. https://doi.org/10.1088/1361-6501/abfe85
25. Zhang Y et al (2018) Single-molecule analysis of microRNA and logic operations using a smart plasmonic nanobiosensor. J Am Chem Soc 140(11):3988–3993. https://doi.org/10.1021/JACS.7B12772/SUPPL_FILE/JA7B12772_SI_001.PDF
26. Jakšić O, Jokić I, Jakšić Z, Mladenović I, Radulović K, Frantlović M (2020) The time response of plasmonic sensors due to binary adsorption: analytical versus numerical modeling. Appl Phys A Mater Sci Process 126(5):342. https://doi.org/10.1007/s00339-020-03524-3
27. Chen Y, Liu J, Yang Z, Wilkinson JS, Zhou X (2019) Optical biosensors based on refractometric sensing schemes: A review. Biosens Bioelectron 144:111693. https://doi.org/10.1016/J.BIOS.2019.111693
28. Mishra S, Deshmukh R (2022) Overview on advancement in biosensing technology including its applications in healthcare. Curr Pharm Biotechnol 23. https://doi.org/10.2174/1389201023666220610163343.
29. Karimi-Maleh H et al (2021) A critical review on the use of potentiometric based biosensors for biomarkers detection. Biosens Bioelectron 184:113252. https://doi.org/10.1016/J.BIOS.2021.113252
30. Saha TK, Mukherjee M, Dhar RS (2022) A comparative study on label-free detection of biomolecules using various biosensing techniques. Lect Notes Networks Syst 426:325–331. https://doi.org/10.1007/978-981-19-0745-6_35/COVER

31. Jakšić O, Čupić Ž, Jakšić Z, Randjelović D, Kolar-Anić L (2013) Monolayer gas adsorption in plasmonic sensors: Comparative analysis of kinetic models. Russ J Phys Chem A 87(13):2134–2139. https://doi.org/10.1134/S0036024413130128
32. Jokić I, Djurić Z, Frantlović M, Radulović K, Krstajić P (2012) Fluctuations of the mass adsorbed on microcantilever sensor surface in liquid-phase chemical and biochemical detection. Microelectron Eng 97:396–399. https://doi.org/10.1016/J.MEE.2012.03.038
33. Jokić I, Djurić Z, Frantlović M, Radulović K, Krstajić P, Jokić Z (2012) Fluctuations of the number of adsorbed molecules in biosensors due to stochastic adsorption–desorption processes coupled with mass transfer. Sensors Actuators B Chem. 166–167:535–543. https://doi.org/10.1016/J.SNB.2012.03.004
34. Djurić Z, Jokić I, Peleš A (2014) Fluctuations of the number of adsorbed molecules due to adsorption–desorption processes coupled with mass transfer and surface diffusion in bio/chemical MEMS sensors. Microelectron Eng 124:81–85. https://doi.org/10.1016/J.MEE.2014.06.001
35. Jokić I, Djurić Z, Radulović K, Frantlović M, Milovanović GV, Krstajić PM (2021) Stochastic time response and ultimate noise performance of adsorption-based microfluidic biosensors. Biosens 11(6):194. https://doi.org/10.3390/BIOS11060194
36. Jokić I (2021) Microfluidic adsorption-based biosensors: Mathematical models of time response and noise, considering mass transfer and surface heterogeneity. Biosens—Curr Nov Strateg Biosensing. https://doi.org/10.5772/INTECHOPEN.97070
37. Jakšić OM, Jakšić ZS, Čupić ŽD, Randjelović DV, Kolar-Anić LZ (2014) Fluctuations in transient response of adsorption-based plasmonic sensors. Sensors Actuators B Chem. 190:419–428. https://doi.org/10.1016/j.snb.2013.08.084
38. Gillespie DT, Hellander A, Petzold LR (2013) Perspective: Stochastic algorithms for chemical kinetics. J Chem Phys 138(17). https://doi.org/10.1063/1.4801941
39. Jakšić O, Jakšić Z, Guha K, Jokić I, Frantlović M (2021) Equilibrium fluctuations in chemical reactions: a viable source of random data (numbers, maps and sequences). Microsyst Technol 27(9):3447–3456. https://doi.org/10.1007/s00542-020-05137-5
40. Frantlović M, Jokić I, Djurić Z, Radulović K (2013) Analysis of the competitive adsorption and mass transfer influence on equilibrium mass fluctuations in affinity-based biosensors. Sensors Actuators B Chem. 189:71–79. https://doi.org/10.1016/J.SNB.2012.12.080
41. Jokić I, Djurić Z, Radulović K, Frantlović M (2018) Analysis of stochastic time response of microfluidic biosensors in the case of competitive adsorption of two analytes. Proc 2(13):991. https://doi.org/10.3390/PROCEEDINGS2130991.
42. Jokić I, Frantlović M, Djurić Z, Radulović K, Jokić Z (2015) Adsorption–desorption noise in microfluidic biosensors operating in multianalyte environments. Microelectron Eng 144:32–36. https://doi.org/10.1016/J.MEE.2015.02.032
43. Jakšić OM, Jakšić Z, Rašljić MB, Kolar-Anić LZ (2019) On oscillations and noise in multi-component adsorption: The nature of multiple stationary states. Adv Math Phys 2019: 1–12. https://doi.org/10.1155/2019/7687643
44. Djurić Z, Jakšić O, Randjelović D (2002) Adsorption–desorption noise in micromechanical resonant structures. Sensors Actuators, A Phys. 96(2–3):244–251. https://doi.org/10.1016/S0924-4247(01)00834-2
45. Jokić I, Jakšić O (2016) A second-order nonlinear model of monolayer adsorption in refractometric chemical sensors and biosensors case of equilibrium fluctuations. Opt Quantum Electron. 48(353):1–7. https://doi.org/10.1007/s11082-016-0620-0
46. Jakšić Z, Jakšić O, Matović J (2009) Performance limits to the operation of nanoplasmonic chemical sensors: noise-equivalent refractive index and detectivity. J Nanophotonics 3(1):31770. https://doi.org/10.1117/1.3124792
47. Djurić Z, Jokić I, Frantlović M, Jakšić O (2007) Fluctuations of the number of particles and mass adsorbed on the sensor surface surrounded by a mixture of an arbitrary number of gases. Sens Actuators, B 127(2):625–631. https://doi.org/10.1016/j.snb.2007.05.025
48. Inci F, Saylan Y, Kojouri AM, Ogut MG, Denizli A, Demirci U (2020) A disposable microfluidic-integrated hand-held plasmonic platform for protein detection. Appl Mater Today 18:100478. https://doi.org/10.1016/J.APMT.2019.100478

49. Mejía-Salazar JR, Cruz KR, Vásques EMM, de Oliveira ON (2020) Microfluidic point-of-care devices: New trends and future prospects for eHealth diagnostics. Sensors 20(7):1951. https://doi.org/10.3390/S20071951
50. Lai X, Yang M, Wu H, Li D (2022) Modular microfluidics: Current status and future prospects. Micromachines 13(8), 1363. https://doi.org/10.3390/MI13081363